Impact de l'acidification et du réchauffement sur les communautés planctoniques de l'estuaire du Saint-Laurent et la production de diméthylsulfure

Thèse

Robin Bénard

Doctorat interuniversitaire en océanographie
Philosophiæ doctor (Ph. D.)

Québec, Canada

Impact de l’acidification et du réchauffement sur les communautés planctoniques de l’estuaire du Saint-Laurent et la production de diméthylsulfure

Thèse

Robin Bénard

Sous la direction de :

Maurice Levasseur, directeur de recherche
Michael Scarratt, codirecteur de recherche

Résumé

Les émissions anthropiques de dioxyde de carbone (CO_2) ont augmenté depuis la révolution industrielle, entraînant des modifications dans les teneurs atmosphériques en CO_2 et un accroissement de la pression partielle de CO_2 (pCO_2) océanique. L'absorption du CO_2 par les océans a entraîné une baisse du pH des eaux de surface, correspondant à une augmentation de l'acidité d'environ 30 % par rapport aux valeurs préindustrielles. D'autre part, l'accumulation de CO_2 anthropique dans l'atmosphère a également induit un réchauffement des eaux de surface depuis le milieu du 20^{e} siècle. Le devenir des communautés planctoniques face à ces altérations actuelles et futures de leur environnement demeure incertain. On ignore également comment l'acidification et le réchauffement affecteront la production du diméthylsulfure (DMS), un gaz sulfuré d'origine planctonique impliqué dans la régulation du climat. Le but de cette thèse est de déterminer l'impact d'une augmentation de la pCO_2 sur le développement des floraisons phytoplanctoniques de l'estuaire maritime du Saint-Laurent (EMSL) et la production de DMS, ainsi que d'évaluer dans quelle mesure le réchauffement des eaux de surface modulera l'effet de l'acidification. Deux grandes expériences ont été menées au cours de la thèse. Une première expérience en microcosmes (~20 L) a été conduite à l'été 2013 afin d'étudier les effets de la pCO_2 sur la floraison printanière des diatomées dans L'EMSL, en portant une attention particulière aux processus microbiens régissant la production de DMS. Une seconde expérience de type multifactorielle en mésocosmes (~2600 L) a été conduite à l'automne 2014 afin de déterminer l'impact combiné de l'augmentation de la pCO_2 et du réchauffement sur le développement de la floraison automnale de l'EMSL et la production du DMS.

Les résultats de l'expérience en microcosmes montrent que les communautés phytoplanctoniques responsables de la floraison printanière dans l'EMSL sont résistantes à des augmentations de la pCO_2 supérieures aux valeurs attendues pour 2100. Cette résistance reflète vraisemblablement leur adaptation au milieu estuarien, environnement connu pour ses variations de pCO_2 importantes et rapides. Cette première expérience a également mis en évidence une diminution de 15 et de 40 % des concentrations moyennes de DMS chez les communautés respectivement soumises à des pCO_2 de 1850 µatm et 2700 µatm par rapport au contrôle (~775 µatm). Des incubations menées en parallèle ont permis de montrer, au moyen de ^{35}S-$DMSP_d$, que l'effet négatif de l'acidification sur le DMS résultait en grande partie d'une diminution de l'efficacité de conversion du DMSP en DMS par les bactéries.

La deuxième expérience a également mis en évidence une forte résistance de la diatomée *Skeletonema costatum* à une large gamme de pH (~8.0–7.2) et de pCO_2 (~90–3000 µatm). Lors de cette étude, un réchauffement des eaux de 5 °C a accéléré le développement et le déclin de la

floraison, mais n'a pas eu d'effet sur la production primaire intégrée pendant l'expérience. À l'instar de l'expérience en microcosmes, l'augmentation de la pCO_2 a provoqué une diminution des concentrations moyennes de DMS de ~66 % dans les mésocosmes les plus acidifiés par rapport aux traitements les moins acidifiés à température in situ (10 °C). L'effet négatif d'une augmentation de la pCO_2 sur la production nette de DMS pourrait cependant être annulé par le réchauffement des eaux de surface. En effet, mes résultats révèlent que la production nette de DMS était plus élevée à 15 °C par rapport à 10 °C et ce à toutes les pCO_2 testées. Ces résultats inédits suggèrent que le réchauffement attendu des eaux de surface pourrait contrer en partie l'effet négatif de l'acidification sur la production nette de DMS dans l'EMSL et possiblement dans l'océan mondial.

Abstract

Anthropogenic carbon dioxide (CO_2) emissions have increased since the industrial revolution, leading to modifications in atmospheric CO_2 content and an increase in oceanic CO_2 partial pressures (pCO_2). The uptake of CO_2 by the oceans has resulted in a lowering of surface water pH, corresponding to an increase in the acidity of the oceans by ~30 % compared with pre-industrial times. Furthermore, climate change resulting from the accumulation of anthropogenic CO_2 in the atmosphere is responsible for the observed warming of sea surface temperatures since the mid 20th century. The fate of planktonic communities in the face of these changes in the marine environment over the next century remains uncertain. Even less understood are the possible interactions of acidification and warming on the production of dimethylsulfide (DMS), a sulfur-containing gas produced by planktonic communities and involved in climate regulation. The aim of this thesis is to determine the impact of heightened pCO_2 on the development of the phytoplanktonic blooms in the Lower St. Lawrence Estuary (LSLE), and their production of DMS, as well as to evaluate how concomitant warming could modulate the effects of acidification. Two intricate experiments were carried out during this study. First, a microcosm experiment (~20 L) was conducted in the summer of 2013 to assess the effects of pCO_2 on the development of the LSLE spring diatom bloom, paying special attention to the microbial processes governing the production of DMS. Second, a multifactorial mesocosm experiment (~2600 L) was carried out in the fall of 2014 to investigate the combined effects of pCO_2 and temperature on the development of the fall bloom in the LSLE and the production of DMS.

Results from our microcosm experiment show that the blooming phytoplankton community of the LSLE during spring is resistant to pCO_2 increases superior to the expected values for 2100. This resistance likely reflects its adaptation to the estuarine setting, an environment known for rapid and intense fluctuations of pCO_2. This first experiment has also highlighted a reduction of the average concentrations of DMS by 15 and 40 % in planktonic assemblages respectively subjected to pCO_2 of ~1850 µatm and ~2700 µatm compared to the control (~775 µatm). Parallel incubations have shown, using ^{35}S-DMSP$_d$, that the negative effect of acidification on DMS mostly stemmed from a decrease in the conversion efficiency of DMSP to DMS by bacteria.

The second experiment has also highlighted a strong resistance of the diatom *Skeletonema costatum* to a wide range of pH (~8.0–7.2), and corresponding pCO_2 (~90–3000 µatm). In this study, a warming of 5 °C accelerated the development and decline of the bloom, but did not affect the integrated primary production over the duration of the experiment. As in the first experiment, heightened pCO_2 resulted in a decrease of average concentrations of DMS of ~66 % in the most acidified mesocosms compared to the least acidified mesocosms at in situ temperature (10 °C).

However, the negative effect of an increase in pCO_2 on the net production of DMS could be mitigated by a warming of surface waters. Indeed, my results reveal that the net production of DMS was higher at 15 °C compared to 10 °C over the whole pCO_2 gradient in our mesocosm study. These novel results suggest that warming of surface waters could mitigate, at least partly, the negative effect of acidification on DMS net production in the LSLE and perhaps in the world's oceans.

Table des matières

Résumé ... **iii**

Abstract ... **v**

Table des matières ... **vii**

Liste des tableaux ... **ix**

Liste des figures ... **x**

Liste des abréviations et des sigles ... **xii**

Remerciements ... **xv**

Avant-propos ... **xvi**

Chapitre 1 Introduction ... **1**

1.1 L'océan en changement ... 1
1.1.1 Acidification des océans ... 1
1.1.2 Variations attendues des concentrations atmosphériques de CO_2 ... 5
1.1.3 Impacts de l'acidification océanique sur les organismes marins ... 6
1.1.4 Influence de la température sur l'effet de l'acidification ... 7
1.2 La production océanique de DMS et son impact sur le climat ... 8
1.2.1 Impacts de l'acidification océanique sur le DMS ... 10
1.2.2 Effets combinés de l'acidification océanique et du réchauffement sur la production de DMS ... 11
1.3 Approche scientifique ... 12
1.3.1 Objectifs ... 12
1.4 Région d'étude ... 13
1.4.1 L'estuaire maritime du Saint-Laurent ... 13

Chapitre 2 Impact of ocean acidification on dimethylsulfide cycling: a peek into the microbial black box ... **15**

Résumé ... 15
Abstract ... 16
2.1 Introduction ... 17
2.2 Materials and methods ... 19
2.2.1 Water collection and experimental setting ... 19
2.2.2 Treatments and acidification protocol ... 20
2.2.3 Microcosm subsampling of chemical and biological parameters ... 21
2.2.4 Statistical analyses ... 27
2.3 Results ... 27
2.3.1 Physical and chemical conditions during the experiment ... 27
2.3.2 Phytoplankton, bacterial abundance, and primary production ... 30
2.3.3 $DMSP_t$ and DMS ... 33
2.3.4 Microbial DMSP cycling ... 35
2.4 Discussion ... 37
2.4.1 Impact of heightened pCO_2 on bloom development ... 37
2.4.2 Effect of acidification on concentrations of dimethylated compounds ... 38
2.4.3 Impact of acidification on microbial uptake of DMSP and its fates ... 39
2.5 Conclusions ... 41
2.6 Acknowledgements ... 42

Chapitre 3 Experimental assessment of the sensitivity of an estuarine phytoplankton fall bloom to acidification and warming 43

Résumé 43
Abstract 44
3.1 Introduction 45
3.2 Materials and methods 47
3.2.1 Mesocosm setup 47
3.2.2 Setting 47
3.2.3 Seawater analyses 49
3.2.4 Statistical analyses 52
3.3 Results 54
3.3.1 Seawater chemistry 54
3.3.2 Dissolved inorganic nutrient concentrations 55
3.3.3 Phytoplankton biomass 55
3.3.4 Phytoplankton size-class 61
3.3.5 Phytoplankton taxonomy 62
3.3.6 Primary production 63
3.4 Discussion 66
3.4.1 General characteristics of the bloom 66
3.4.2 Phase I (diatom bloom development) 67
3.4.3 Phase II (declining phase of the bloom) 69
3.4.4 Effect of the treatments on primary production over the full experiment 70
3.4.5 Implications and limitations 71
3.5 Conclusion 72
3.6 Acknowledgements 72

Chapitre 4 Contrasting effects of acidification and warming on dimethylsulfide concentrations during a temperate estuarine fall bloom mesocosm experiment 74

Résumé 74
Abstract 75
4.1 Introduction 76
4.2 Materials and methods 79
4.2.1 Mesocosm setup 79
4.2.2 Experimental approach 80
4.2.3 Seawater analyses 80
4.2.4 Statistical analyses 83
4.3 Results 84
4.3.1 Physical and chemical conditions during the experiments 84
4.3.2 Phytoplankton, bacterial abundance and production 86
4.3.3 $DMSP_t$ and DMS 88
4.4 Discussion 94
4.4.1 General characteristics 94
4.4.2 DMSP dynamics 94
4.4.3 DMS dynamics 95
4.4.4 Limitations 98
4.5 Conclusions 99
4.6 Acknowledgements 100

Chapitre 5 Conclusion générale 101

5.1 Synthèse 102
5.2 Perspectives 105

Bibliographie 108

Annexes 126

Liste des tableaux

Tableau 1.1 Changements relatifs des concentrations de DMS (%) lors d'expériences d'acidification réalisées en mésocosmes ou microcosmes. ΔpH représente la diminution de pH_T appliquée dans chaque expérience. ND : *No data available*. Tableau modifié de Hussherr et al. (2017). 11

Table 2.1 Average values of pH_T (total hydrogen ion concentration scale), pCO_2 and total alkalinity (TA) per treatment for each day the carbonate chemistry parameters were measured. Average values are presented with ± standard errors. 24

Table 3.1 Day of maximum Chl *a* concentration, the associated average pH_T (total hydrogen ion concentration scale), and average pCO_2 over each individually defined phase. Phase I is defined from day 0 until day of maximum Chl *a* for each mesocosm, while Phase II is defined from the day after maximum Chl *a* until day 13. Average temperature over day 0 to day 13 is also presented for each mesocosm. Average values are presented with ± standard errors. 53

Table 3.2 Results of the generalized least squares models (gls) tests for the effects of temperature. pCO_2. and their interaction during Phase I (day 0 to day of maximum Chl *a* concentration). Separate analysis with pCO_2 as a continuous factor were performed when temperature had a significant effect. Chl *a* concentration, nanophytoplankton abundance, picoeukaryote abundance, picocyanobacteria abundance, particulate and dissolved primary production, and Chl *a*-normalized particulate and dissolved primary production. Significant results are in bold. ***p < 0.05**..... 57

Table 3.3 Results of the generalized least squares models (gls) tests for the effects of temperature, pCO_2 and their interaction. Separate analysis with pCO_2 as a continuous factor were performed when temperature had a significant effect. Accumulation rate of Chl *a* (day 0 to maximum Chl *a* concentration), maximum Chl *a* concentration, growth rate of nanophytoplankton (day 0 to maximum nanophytoplankton abundance), and maximum nanophytoplankton abundance. Significant results are in bold. ***p < 0.05**..... 59

Table 3.4 Results of the generalized least squares models (gls) tests for the effects of temperature, pCO_2, and their interaction during Phase II (day after maximum Chl *a* to day 13). Separate analysis with pCO_2 as a continuous factor were performed when temperature had a significant effect. Chl *a* concentration, nanophytoplankton abundance, picoeukaryote abundance, picocyanobacteria abundance, particulate and dissolved primary production, and Chl *a*-normalized particulate and dissolved primary production. Significant results are in bold. ***p < 0.05, **p < 0.01, ***p < 0.001**.... 60

Table 3.5 Results of the generalized least squares models (gls) tests for the effects of temperature, pCO_2 and their interaction. Separate analysis with pCO_2 as a continuous factor were performed when temperature had a significant effect. Maximum particulate and dissolved primary production, and time-integration over the full duration of the experiment (day 0 to day 13). Natural logarithm transformation is indicated in parentheses when necessary, significant results are in bold. ***p < 0.05, **p < 0.01**. 66

Table 4.1 Results of the generalized least squares models (gls) tests for the effects of temperature, pCO_2, and their interaction over the duration of the experiment (day 0 to day 13). Separate analyses with pCO_2 as a continuous factor were performed when temperature had a significant effect. Averages of bacterial abundance and production, $DMSP_t$, DMS, Chl *a*-normalized $DMSP_t$ and DMS concentrations, and DMS:$DMSP_t$ ratios are presented. Natural logarithm transformation is indicated when necessary. Significant results are in bold. ***p<0.05, **p<0.01, ***p<0.001**..... 88

Table 4.2 Results of the generalized least squares models (gls) tests for the effects of temperature, pCO_2, and their interaction on the maximum values of the parameters measured during the experiment. Separate analyses with pCO_2 as a continuous factor were performed when temperature had a significant effect. Maxima of $DMSP_t$, and DMS concentrations are presented. Significant results are in bold. ***p<0.05, **p<0.01, ***p<0.001**..... 91

Liste des figures

Figure 1.1 Proportion entre les trois espèces principales du CID en fonction du pH de l'eau de mer, adaptée de Hofmann and Schellnhuber (2010). 2

Figure 1.2 Série temporelle des concentrations atmosphériques de CO_2 mesurées à l'observatoire de Mauna Loa (rouge), la pCO_2 in situ à la Station Aloha (vert) et le pH correspondant (bleu). Figure reproduite de la *National Oceanic and Atmospheric Administration (NOAA),* données adaptées de Dore et al., (2009). 4

Figure 1.3 (a) Série temporelle des concentrations atmosphériques de CO_2 mesurées à l'observatoire de Mauna Loa (rouge) et au Pôle Sud (noir), (b) simulations CMIP5 entre 1950 et 2100 pour différents scénarios d'émissions de CO_2 (*Representative Concentration Pathway; RCP*), (c) moyenne globale du pH océanique selon les deux scénarios identifiés. Figure modifiée de IPCC (2014). 5

Figure 1.4 Carte de l'estuaire et du golfe du Saint-Laurent, Canada. Figure tirée de Savenkoff et al. (2017). 14

Figure 2.1 Sampling site on June 17, 2013, identified by a red star, located in the Lower St. Lawrence Estuary, near Rimouski, Québec, Canada (48° 50' 29" N 68° 31' 45" W)..... 20

Figure 2.2 Temporal variations in (a) pH_T, (b) pCO_2 in each treatment (1 × pCO_2, 2 × pCO_2, and 3 × pCO_2; see legend for symbol attribution). Daily averages are presented (mean ± standard error). 28

Figure 2.3 Temporal variations in (a) nitrate, (b) soluble reactive phosphate (SRP), and (c) silicic acid in each treatment (1 × pCO_2, 2 × pCO_2, and 3 × pCO_2; see legend for symbol attribution). Daily averages are presented (mean ± standard error). Tukey HSD between treatments on a given day are indicated by grouping letters (a, b)..... 29

Figure 2.4 Temporal variations in (a) chlorophyll *a*, (b) bacterial abundance, (c) particulate primary production (P_P), and (d) dissolved primary production (P_D) in each treatment (1 × pCO_2, 2 × pCO_2, and 3 × pCO_2; see legend for symbol attribution). Daily averages are presented (mean ± standard error). Tukey HSD between treatments on a given day are indicated by grouping letters (a, b, c).. 31

Figure 2.5 Relative abundance of 9 groups of protists at the beginning of the experiment (day 0), on day 6, and at the end of the experiment (day 12) in each treatment (1 × pCO_2, 2 × pCO_2, and 3 × pCO_2). The group « others » includes Chlorophyceae, Dictyochophyecae, Euglenophyceae, heterotrophic groups, and Ciliates. The bar plot on day 0 represents the initial community assemblage before acidification. For symbol attribution to protist groups, see legend. 32

Figure 2.6 Temporal variations in (a) total DMSP concentrations ($DMSP_t$), (b) dissolved DMSP concentrations ($DMSP_d$), and (c) DMS concentrations in each treatment (1 × pCO_2, 2 × pCO_2, and 3 × pCO_2; see legend for symbol attribution). Daily averages are presented (mean ± standard error). Tukey HSD between treatments on a given day are indicated by grouping letters (a, b)..... 34

Figure 2.7 Temporal variations of (a) microbial $DMSP_d$ loss rate constant (k_{DMSPd} in day^{-1}), (b) particulate yield (%), (c) microbial assimilation efficiency of ^{35}S-$DMSP_d$ into macromolecules (%), (d) particular untransformed ^{35}S, and (e) microbial DMS yield (%) in each treatment (1 × pCO_2, 2 × pCO_2, and 3 × pCO_2; see legend for symbol attribution). Daily averages are presented (mean ± standard error). Tukey HSD between treatments on a given day are indicated by grouping letters (a, b, c)..... 36

Figure 3.1 Schematic drawing including mesocosm dimensions and placement within the containers (Aquabiotech Inc, Québec, Canada). The whole setup includes a second container holding 6 more mesocosms not depicted here. 48

Figure 3.2 Changes in incident photosynthetic active radiation (PAR) at the top of the mesocosms level during the experiment as measurement by a Satlantic HyperOCR hyperspectral radiometer and integrated into the 400–700 nm range. Local sunrise and sunset times (EDT) are indicated with the corresponding days of the experiment. 49

Figure 3.3 Temporal variations over the course of the experiment for: (a) pH_T, (b) pCO_2, (c) temperature, (d) nitrate, (e) silicic acid, (f) soluble reactive phosphate. For symbol attribution to treatments, see legend. 54

Figure 3.4 Temporal variations, and averages ± SE during Phase I (day 0 to day of maximum Chl *a* concentration) and Phase II (day after maximum Chl *a* concentration to day 13) for: (a-c) chlorophyll *a*, (d-f) nanophytoplankton, (g-i) picoeukaryotes, (j-l) picocyanobacteria. For symbol attribution to treatments, see legend. 56

Figure 3.5 (a) Accumulation rate of Chl *a* (day 0 to maximum Chl *a* concentration), (b) maximum Chl *a* concentrations, (c) growth rate of nanophytoplankton (day 0 to maximum nanophytoplankton abundance), and (d) maximum nanophytoplankton abundance during the experiment. For symbol attribution to treatments, see legends. 58

Figure 3.6 Relative abundance of 10 groups of protists at the beginning of the experiment (day -4), on the day of maximum Chl a concentrations in each mesocosm, and at the end of the experiment (day 13) for (a) 10 °C and (b) 15 °C mesocosms. The group « others » include dinoflagellates, Chlorophyceae, Dictyochophyecae, Euglenophyceae, heterotrophic groups, and unidentified cells. Each bar plot represents a mesocosm at a given time. The bar plot on day -4 represents the initial community assemblage before temperature manipulation and acidification, and is therefore the same for each temperature treatment. For symbol attribution to treatments, see legend. 62

Figure 3.7 Temporal variations, time-integrated or averaged ± SE during Phase I (day 0 to day of maximum Chl *a* concentration) and Phase II (day after maximum Chl *a* concentration to day 13) for: (a-c) particulate primary production, (d-f) dissolved primary production, (g-i) Chl *a*-normalized particulate primary production, (j-l) Chl *a*-normalized dissolved primary production. For symbol attribution to treatments, see legend. 64

Figure 3.8 (a) Maximum particulate primary production, (b) time-integrated particulate primary production (c) maximum dissolved primary production, and (d) time-integrated dissolved primary production over the full course of the experiment (day 0 to day 13). For symbol attribution to treatments, see legend. 65

Figure 4.1 Temporal variations over the course of the experiment for: (a) temperature, (b) pH_T, (c) pCO_2. For symbol attribution to treatments, see legend. 85

Figure 4.2 Temporal variations, and averages over the course of the experiment (day 0 to day 13) for: (a–b) chlorophyll *a*, (c–d) free-living bacteria abundance, (e–f) bacterial production. For symbol attribution to treatments, see legend. 87

Figure 4.3 Temporal variations, and averages over the course of the experiment (day 0 to day 13) for: (a–b) $DMSP_t$, (c–d) DMS, (e–f) the natural logarithm of the DMS:$DMSP_t$ ratio. For symbol attribution to treatments, see legend. 89

Figure 4.4 (a) Maximum $DMSP_t$ concentrations, (b) maximum DMS concentrations reached over the full course of the experiment (day 0 to day 13). For symbol attribution to treatments, see legend. 90

Figure 4.5 Averages over the course of the experiment (day 0 to day 13) for: (a) $DMSP_t$:Chl *a* ratio, (b) DMS:Chl *a* ratio. For symbol attribution to treatments, see legend. 92

Figure 4.6 Linear regression between DMS concentrations and bacterial production during the experiment. 93

Liste des abréviations et des sigles

AO (OA)	Acidification océanique (ocean acidification)
A_T (TA)	Alcalinité totale (total alkalinity)
BP	Bacterial production
Chl *a*	Chlorophylle *a* (chlorophyll *a*)
CO_2	Dioxyde de carbone (carbon dioxide)
CO_3^{2-}	Ion carbonate
DCMU	3-(3,4-dichlorophenyl)-1,1-dimethylurea
Ddd+	DMSP-dependent DMS-releasing
DMS	Diméthylsulfure (dimethylsulfide)
DMSO	Diméthylsulfoxyde (dimethylsulfoxide)
DMSP	Diméthylsulfoniopropionate (dimethylsulfoniopropionate)
$DMSP_d$	DMSP dissous (dissolved DMSP)
$DMSP_p$	DMSP particulaire (particulate DMSP)
DNVS	Dissolved non-volatiles
DOC	Dissolved organic carbon
DOM	Dissolved organic matter
EMSL (LSLE)	Estuaire maritime du Saint-Laurent (Lower St. Lawrence Estuary)
GF/F	Glass microfiber filter
GIEC	Groupe d'experts Intergouvernemental sur l'Évolution du Climat
GLS	General least squares
GSL	Golfe du Saint-Laurent
H_2SO_4	Acide sulfurique (sulfuric acid)
HCl	Hydrochloric acid
HCO_3^-	Ion bicarbonate
$HgCl_2$	Mercury(II) chloride
HNA	High nucleic acid
ISMER	Institut des sciences de la mer
k_{DMSPd}	Microbial $DMSP_d$ loss rate constant
LNA	Low nucleic acid
M1-12	Mesocosms 1–12
MCM (CCM)	Mécanisme de concentration de carbone (Carbon concentration mechanism)
MeSH	Méthanethiol (methanethiol)
$NaHCO_3$	Sodium bicarbonate
NaOH	Sodium hydroxide
NCN (CCN)	Noyau de condensation de nuage (cloud condensation nuclei)

NO_2^-	Nitrite
NO_3^-	Nitrate
NOAA	National Oceanic and Atmospheric Administration
PAR	Photosynthetically active radiation
pCO_2	Pression partielle de CO_2 (CO_2 partial pressure)
P_D	Dissolved primary production
P_P	Particulate primary production
PFPD	Pulse flame photometric detector
pH_T	pH sur l'échelle de concentration totale d'ions hydrogène (pH on the total hydrogen ion concentration scale)
PnT	Purge and Trap
POC	Particulate organic matter
RCP	Representative carbon pathway
$Si(OH)_4$	Silicic acid
SO_4^{2-}	Sulfate
SRP	Soluble reactive phosphate
SST	Sea surface temperature
SVDF	Small-volume gravity drip filtration
TCA	Trichloroacetic acid
TEP	Transparent exopolymer
UVA	Ultraviolet A radiation
UVB	Ultraviolet B radiation

“La lutte elle-même vers les sommets
suffit à remplir un cœur d’homme.
Il faut imaginer Sisyphe heureux”

Albert Camus

“*This is an adventure”*

Steve Zissou

Remerciements

L'accomplissement d'une thèse de doctorat n'est certes pas réalisable du revers de la main, pas plus qu'elle ne soit le fruit du labeur d'une seule personne. Je tiens tout d'abord à remercier mon directeur de thèse Maurice Levasseur pour m'avoir guidé, scientifiquement et personnellement, avec enthousiasme et perspicacité au long de ce processus. Je tiens également à remercier mon codirecteur Michael Scarratt, pour son expertise et son inébranlable personnalité face aux périls de mes expériences.

Je tiens également à remercier les membres de mon comité d'encadrement, les professeurs Jean-Éric Tremblay et Alfonso Mucci, pour leur engouement et leurs apports judicieux à cette thèse. De plus, je voudrais remercier les professeurs Frédéric Maps, Marcel Babin et Steve Archer d'avoir accepté de participer à l'évaluation de cette thèse et sa soutenance.

Ma sincère gratitude à mon directeur, au FRQNT, au CRSNG, au département de biologie de l'Université Laval, à Québec-Océan et à la Fondation Madeli-Aide pour le support financier sans qui tout ceci n'aurait été possible.

Bien entendu, je me dois de remercier également les membres de notre laboratoire : Martine Lizotte pour sa bonne humeur qui n'a d'égal que son savoir généreusement partagé, Margaux Gourdal pour son support moral dans l'écriture, Virginie Galindo pour m'avoir initié au terrain en 2011, auquel j'ai heureusement survécu, et Rachel Hussherr pour avoir été une assistante tout feu tout flamme en 2013 et 2014.

Les nombreuses rencontres momentanées faites au fil des terrains auront d'ailleurs marqué ces années d'apprentissage. Aux merveilleux professionnels ayant croisé mon chemin : Michel Starr, Michel Gosselin, Sonia Michaud, Liliane St-Amand et Marjolaine Blais, un énorme merci pour les heures dédiées sur ce projet. Je voudrais également remercier et souhaiter bon succès à Marie-Amélie Blais, avec qui j'ai eu le plaisir de passer de très, très longues semaines pendant notre expérience en mésocosmes. Sans oublier les équipages du NGCC John P. Tully et NGCC Amundsen avec qui j'ai passé deux incroyables mois en mer.

Finalement, un merci spécial à mes improvisateurs, hockeyeurs, Madelinots et à mon entourage immédiat, Marie-Philippe, Véronique et Israël, ainsi qu'à mes parents, Adrien et Suzette, pour le support moral, financier et les réserves de subsistance. Merci pour votre patience, votre écoute et votre compréhension. Sans oublier Xena Paquette, fidèle présence anxiolytique.

Avant-propos

Cette thèse présente les résultats de mes recherches sous la direction du professeur Maurice Levasseur du département de biologie de l'Université Laval et du docteur Michael Scarratt de l'Institut Maurice-Lamontagne du Ministère des Pêches et Océans Canada. La collecte des données a été effectuée lors d'expériences en microcosmes en bassin extérieur à l'été 2013 à l'Institut Maurice-Lamontagne, Ste-Flavie, ainsi que lors d'une expérience en mésocosmes à l'automne 2014 à la Station Aquicole de Pointe-au-Père de l'Institut des sciences de la mer (ISMER), Rimouski. J'ai été responsable de la planification, de la réalisation de l'échantillonnage et de l'analyse des données recueillies lors de ces deux expériences.

Cette thèse comporte cinq chapitres dont une introduction et conclusion générale rédigées en français. Le corps de la thèse est composé de trois chapitres rédigés en anglais sous forme d'articles scientifiques en instance de publication, précédés de résumés en français. J'ai rédigé en tant que premier auteur les trois articles insérés dans cette thèse avec la contribution de mon directeur et des coauteurs identifiés pour chacun des articles.

Chapitre 1. Introduction générale

Chapitre 2. *Impact of ocean acidification on dimethylsulfide cycling: a peek into the microbial black box*. **Robin Bénard**, Martine Lizotte Maurice Levasseur, Michael Scarratt, Sonia Michaud, Michel Starr, Jean-Éric Tremblay, Ronald P. Kiene, and Sohiko Kameyama.
Cet article sera soumis à Microbial Ecology.

Chapitre 3. *Experimental assessment of the sensitivity of an estuarine phytoplankton fall bloom to acidification and warming.* **Robin Bénard**, Maurice Levasseur, Michael Scarratt, Marie-Amélie Blais, Alfonso Mucci, Gustavo Ferreyra, Michel Starr, Michel Gosselin, Jean-Éric Tremblay, and Martine Lizotte.
Publié dans Biogeosciences, 17 août 2018, https://doi.org/10.5194/bg-15-4883-2018

Chapitre 4. *Contrasting effects of acidification and warming on dimethylsulfide concentrations during a temperate estuarine fall bloom*. **Robin Bénard**, Maurice Levasseur, Michael Scarratt, Sonia Michaud, Michel Starr, Alfonso Mucci, Gustavo Ferreyra, Michel Gosselin, Jean-Éric Tremblay, Martine Lizotte, and Gui-Peng Yang.
Soumis à Biogeosciences, 22 août 2018, https://doi.org/10.5194/bg-2018-338

Chapitre 5. Conclusion générale

Les résultats de mes recherches ont également été présentés sous forme d'affiches scientifiques et de présentations orales lors de congrès locaux et internationaux.

Bénard, R., Levasseur, M., Scarratt, M. G., Starr, M., Mucci, A., Tremblay, J.-É., Kameyama, S., St-Amand, L., and Lizotte, M., 2012. *Impact of acidification on a natural planktonic community and DMS production in the St. Lawrence Estuary*. 10^{e} Réunion Scientifique Annuelle de Québec-Océan, Montréal, Canada.

Bénard, R., Levasseur, M., Scarratt, M. G., Starr, M., Mucci, A., Tremblay, J.-É., Michaud, S., and St-Amand, L., 2013. *Impacts of ocean acidification on phytoplanktonic communities of estuarine and coastal regions of Canada*. 11^{e} Réunion Scientifique Annuelle de Québec-Océan, Rivière-du-Loup, Canada.

Bénard, R., Levasseur, M., Scarratt, M. G., Starr, M., Mucci, A., Tremblay, J.-É., Michaud, S., and St-Amand, L., 2014. *Impact of acidification on DMS production in the St. Lawrence Estuary*. 2014 Ocean Sciences Meeting, Honolulu, United States.

Bénard, R., Levasseur, M., Scarratt, M. G., Blais, M-A., Mucci, A., Ferryra, G., Starr, M., Gosselin, M., and Tremblay, J.-É., 2014. *Testing the sensitivity of the St. Lawrence planktonic community to acidification and warming: a mesocosm study.* 12^{e} Réunion Scientifique Annuelle de Québec-Océan, Rivière-du-Loup, Canada.

Bénard, R., Levasseur, M., Scarratt, M. G., Blais, M-A., Mucci, A., Ferryra, G., Starr, M., Gosselin, M., and Tremblay, J.-É., 2015. *Impact de l'acidification et de l'augmentation de température sur la communauté planctonique du Saint-Laurent.* 83^{e} Congrès de l'Association francophone pour le savoir (ACFAS), Rimouski, Canada.

Bénard, R., Levasseur, M., Scarratt, M. G., Blais, M-A., Mucci, A., Ferryra, G., Starr, M., Gosselin, M., Tremblay, J.-É., Lizotte, M., 2016. *Acidification des océans : de l'enjeu global aux conséquences locales.* Forum Annuel de la Table de Concertation Régionale des Îles-de-la-Madeleine, Îles-de-la-Madeleine, Canada.

Chapitre 1 Introduction

L'augmentation des émissions anthropiques de gaz carbonique (CO_2) depuis la révolution industrielle a résulté en une accumulation des concentrations de CO_2 dans l'atmosphère et conséquemment en un accroissement de sa dissolution dans les océans. L'augmentation des concentrations de CO_2 anthropique dans les eaux de surface des océans a causé un déséquilibre de la chimie des carbonates, résultant en une augmentation des ions H^+ et en une diminution du pH. Ce phénomène, désigné d'acidification océanique (AO), suscite beaucoup d'inquiétude chez les scientifiques et décideurs. Plusieurs études ont déjà mis en évidence des effets de l'AO sur les organismes marins et les grands cycles biogéochimiques, notamment celui du soufre, sujet de mes recherches. Les émissions anthropiques de CO_2 occasionneront également un réchauffement des océans. Les organismes marins seront donc soumis à la fois à l'AO et au réchauffement des eaux de surface. Bien qu'inévitable, l'effet combiné de ces deux facteurs sur les écosystèmes marins demeure méconnu. Dans le cadre de cette thèse, je me suis donc intéressé aux effets combinés de l'acidification et du réchauffement sur les communautés planctoniques de l'estuaire maritime du Saint-Laurent et plus particulièrement sur leur capacité à produire le diméthylsulfure (DMS), un gaz d'origine planctonique au pouvoir refroidissant contribuant à l'équilibre du climat.

1.1 L'océan en changement

1.1.1 Acidification des océans

Les concentrations atmosphériques de CO_2 ont augmenté de 280 ppm en 1850 à 411 ppm en 2018 suite à l'activité humaine (NOAA, 2018). Les concentrations de CO_2 pourraient atteindre de 850 à 1370 ppm d'ici la fin du 21^e siècle selon les scénarios d'émissions élevés du Groupe d'experts Intergouvernemental sur l'Évolution du Climat (GIEC; IPCC, 2013). Ces augmentations seraient encore plus importantes si ce n'était de la présence des océans. En effet, environ 28 % des émissions anthropiques en CO_2 des 250 dernières années ont été absorbées par les océans (Sabine and Feely, 2007; Le Quéré et al., 2015). Cette absorption de CO_2 n'est cependant pas sans effet sur la chimie des océans et les organismes qui les habitent.

La loi de Henry stipule que la pression partielle moyenne de CO_2 dissous dans l'eau de mer doit s'équilibrer avec celle de l'atmosphère (Caldeira and Berner, 1999). Conséquemment, l'augmentation des concentrations atmosphériques de CO_2 se solde par une augmentation de la pression partielle de CO_2 (pCO_2) des eaux de surface océanique. La dissolution du CO_2 dans l'eau de mer engendre une série de réactions dépendantes de la pCO_2 initiale, de la température et du pH in situ (Dickson, 2010). En se dissolvant, le CO_2 forme un acide faible (H_2CO_3) qui se dissocie

pour produire des ions bicarbonate (HCO_3^-) et carbonate (CO_3^{2-}), ainsi que des ions hydrogène (H^+).

$$CO_2 + H_2O \leftrightarrow H_2CO_3 \leftrightarrow H^+ + HCO_3^- \leftrightarrow 2H^+ + CO_3^{2-} \quad (1.1)$$

L'ajout de CO_2 modifie l'équilibre entre ces réactions, produisant simultanément un accroissement des concentrations d'ions H^+ et menant à l'augmentation du carbone inorganique dissous (CID). Ce dernier paramètre peut être défini comme la somme des concentrations des espèces carbonés dans l'eau de mer (CO_2, HCO_3^-, CO_3^{2-}) et est principalement dominé par l'ion HCO_3^- (Fig. 1.1; Orr et al., 2005; Dickson, 2010; Hofmann and Schellnhuber, 2010).

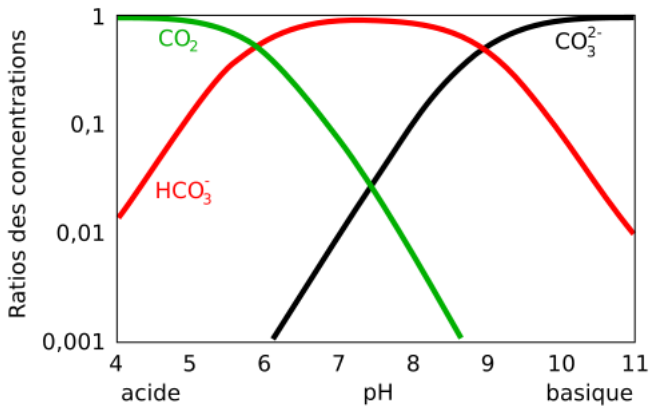

Figure 1.1 Proportion entre les trois espèces principales du CID en fonction du pH de l'eau de mer, adaptée de Hofmann and Schellnhuber (2010).

Une composante clé de la chimie des océans est l'alcalinité totale (A_T). Celle-ci peut être définie comme le nombre de moles d'ions hydrogène équivalant à l'excès d'accepteurs de protons versus les donneurs de protons dans un kilogramme d'eau de mer (Dickson, 1981). Les accepteurs de protons correspondent aux bases formées par les acides faibles (constante de dissociation $K < 10^{-4.5}$ à 25 °C), et les donneurs de protons correspondent aux acides avec des constantes de dissociations ($K > 10^{-4.5}$). Dans l'eau de mer elle peut être approximée par l'alcalinité pratique, soit l'expression suivante :

$$A_T \approx \left[HCO_3^-\right] + 2\left[CO_3^{2-}\right] + \left[B(OH)_4^-\right] + \left[OH^-\right] - \left[H^+\right] \quad (1.2)$$

La disponibilité des accepteurs de protons octroie un pouvoir tampon à l'eau de mer, diminuant les variations de pH occasionnées par la dissolution grandissante de CO_2. Le pH des eaux à l'alcalinité totale élevée est donc moins susceptible de varier grandement comparativement aux eaux de faible A_T. La réaction nette de la dissolution du CO_2 produit un nombre équivalent de donneurs et d'accepteurs de protons, ne modifiant pas l'alcalinité totale.

L'augmentation de l'acidité des océans due aux émissions anthropiques de CO_2 est souvent désignée comme « l'autre problème du CO_2 » (*The Other CO_2 Problem*; Caldeira and Wickett, 2003; Doney et al., 2009). La dissolution du CO_2 occasionne une augmentation du CID à alcalinité constante, provoquant un accroissement de la pCO_2, une diminution des concentrations de carbonate et davantage d'ions H^+. Le pH est utilisé pour quantifier l'acidité d'une solution et est défini par l'expression suivante (Dickson, 1993) :

$$pH=-\log_{10}[H^+] \tag{1.3}$$

où $[H^+]$ indique la concentration totale de l'ion hydrogène, incluant les formes complexes ioniques en solution (Dickson, 2010). L'accroissement des ions H^+ augmente donc l'acidité de l'eau de mer, rendant celle-ci moins alcaline (Caldeira and Wickett, 2003). Le pH peut être mesuré sur plusieurs échelles : celle du *National Bureau of Standards* (NBS), concentration totale d'ions hydrogène, concentration d'ions hydrogène libres et l'échelle d'eau de mer (Dickson, 2010). Le pH est généralement mesuré par spectrophotométrie via l'utilisation de colorants indicateurs ou par potentiométrie à l'aide d'électrodes calibrées (Dickson, 2010). Comme l'échelle NBS se base sur des mesures impliquant des solutions standards au faible potentiel ionique comparé à l'eau de mer, l'échelle de concentration totale d'ions hydrogène a été développée à l'aide de solutions standards d'eau de mer artificielle et inclut l'anion HSO_4^- dans son calcul (Hansson, 1973; Zeebe and Wolf-Gladrow, 2001; Dickson, 2010) :

$$pH=-\log_{10}\left(\left[H^+\right]+\left[HSO_4^-\right]\right) \tag{1.4}$$

L'absorption du CO_2 depuis le début du 20^e siècle a engendré une diminution du pH océanique de ~0,1, passant de ~8,2 à ~8,1 (Gattuso et al., 2015), une diminution qui pourrait atteindre ~0,7 unités en 2300 (Zeebe et al., 2008). Plusieurs épisodes d'acidification des océans ont eu lieu dans l'histoire terrestre, par exemple lors du maximum thermique du passage Paléocène-Éocène. Par contre, le pH océanique n'a oscillé que très peu au cours des 800 000 années précédant l'industrialisation, entre ~8,2 et ~8,3 entre les périodes glaciaires et interglaciaires (Zeebe and Ridgwell, 2011). De plus, le pH océanique de surface n'a probablement pas diminué sous ~8,1 au cours des deux derniers millions d'années (Hönisch et al., 2009).

Une acidification telle qu'elle se produit actuellement, par son amplitude et sa rapidité, n'a jamais eu lieu auparavant dans l'histoire de la Terre (Hönisch et al., 2012). Les mesures de séries temporelles, comme celle de *Hawaii Ocean Time-series* (HOT), ont permis de quantifier précisément la baisse graduelle du pH océanique, passant de 8,12 à 8,08 entre 1988 et 2007 (Fig. 1.2; Dore et al., 2009). L'acidification des océans est donc un phénomène en cours.

Le pH des eaux de surface peut cependant varier selon les régions et les saisons jusqu'à ± 0,3 unités (Raven et al., 2005). La variabilité du pH est dépendante de processus physiques à petite et grande échelle, mais aussi de processus biologiques. La température est le facteur principal influençant le pH, puisque la solubilité du CO_2 est inversement proportionnelle à la température (Zeebe and Wolf-Gladrow, 2001). Par conséquent, en région froide, il y a davantage de CO_2 qui se dissout, diminuant le pH. En régions côtières, les remontées d'eaux profondes riches en CO_2 peuvent également diminuer le pH des eaux de surface, tandis que les régions hautement productives sont susceptibles d'expérimenter des augmentations de pH sporadiques de l'ordre de 1 unité (Hinga, 2002). Dans ces milieux, les apports d'eau douce peuvent également diminuer le pH, en diminuant l'alcalinité totale et son pouvoir tampon (Millero, 2010; Cai et al., 2017). Les conditions de pH sont donc beaucoup plus variables en zones côtières que dans l'océan profond.

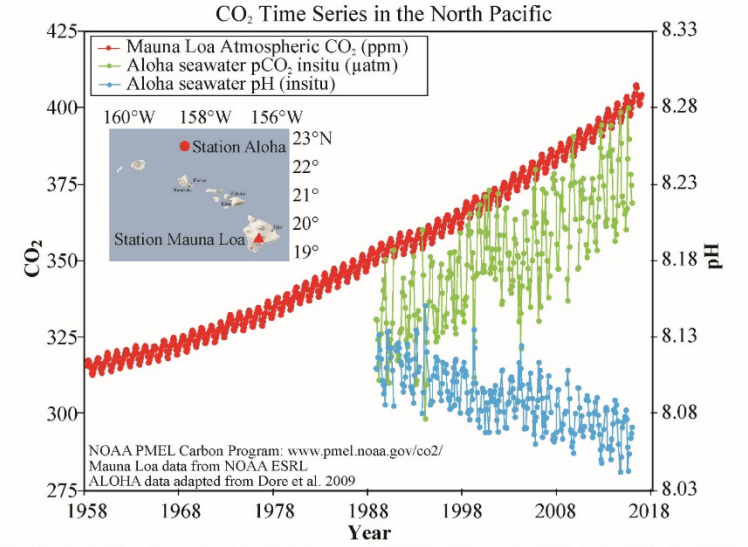

Figure 1.2 Série temporelle des concentrations atmosphériques de CO_2 mesurées à l'observatoire de Mauna Loa (rouge), la pCO_2 in situ à la Station Aloha (vert) et le pH correspondant (bleu). Figure reproduite de la *National Oceanic and Atmospheric Administration (NOAA),* données adaptées de Dore et al., (2009).

1.1.2 Variations attendues des concentrations atmosphériques de CO_2

Malgré l'absorption du CO_2 par les océans, les concentrations atmosphériques de CO_2 continuent d'augmenter. Au début des années 1990, le GIEC décida d'établir des scénarios estimant la production de gaz à effet de serre et son accumulation dans l'atmosphère en l'absence de politiques de mitigation (IPCC, 1995). Selon les quatre scénarios d'émissions du cinquième rapport du GIEC, les concentrations atmosphériques de CO_2 pourraient varier de ~400 µatm à ~1000 µatm d'ici à 2100, et pourraient atteindre 2000 µatm en 2300 (Fig. 1.3; IPCC, 2013, 2014).

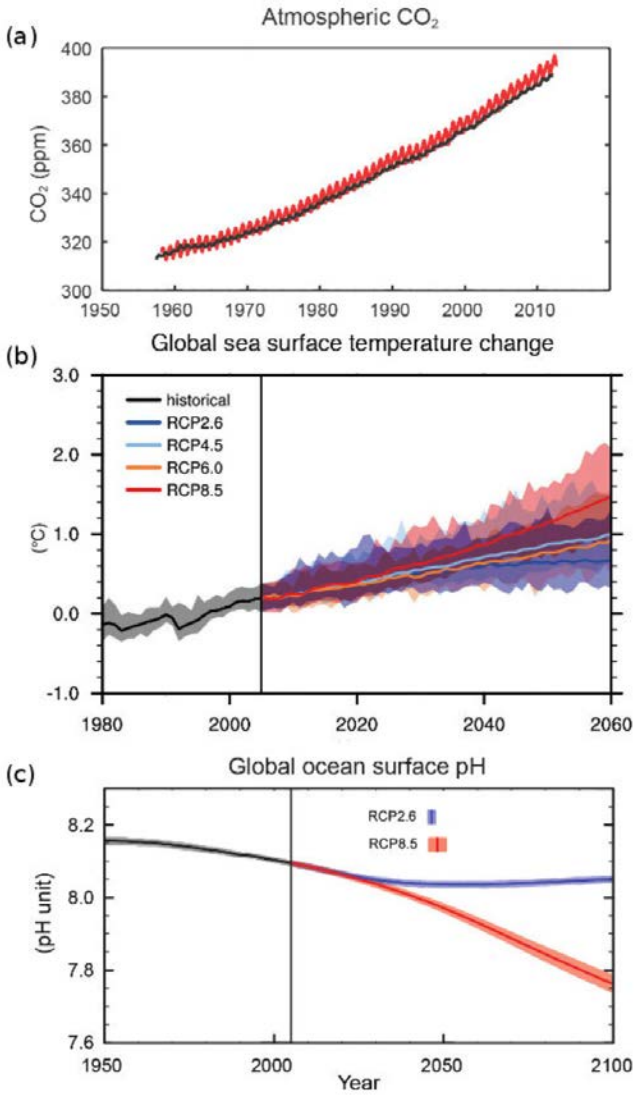

Figure 1.3 (a) Série temporelle des concentrations atmosphériques de CO_2 mesurées à l'observatoire de Mauna Loa (rouge) et au Pôle Sud (noir), (b) simulations CMIP5 entre 1950 et 2100 pour différents scénarios d'émissions de CO_2 (*Representative Concentration Pathway; RCP*), (c) moyenne globale du pH océanique selon les deux scénarios identifiés. Figure modifiée de IPCC (2014).

1.1.3 Impacts de l'acidification océanique sur les organismes marins

Depuis les deux dernières décennies, nous avons assisté à un nombre grandissant d'études sur les effets potentiels de l'acidification sur les organismes marins (revue par Kroeker et al., 2013). Les premières études ont porté essentiellement sur l'effet de l'acidification sur des cultures mono-spécifiques de phytoplancton marin (voir Riebesell and Tortell, 2011). Ces études ont mis en évidence une augmentation de la fixation du carbone chez plusieurs espèces phytoplanctoniques, réponse attendue puisque l'augmentation de la disponibilité du CO_2 dissous à faible pH favorise la RuBisCO, l'enzyme responsable de la fixation du carbone chez les organismes photosynthétiques (Riebesell et al., 2007; Rost et al., 2008). Toutefois, cet effet pourrait être limité puisque la plupart des groupes phytoplanctoniques utilisent des mécanismes de concentrations du carbone (MCC) afin de contrer la faible affinité de la RuBisCO pour le CO_2 (Giordano et al., 2005). L'efficacité des MCCs diffère entre les groupes taxonomiques, rendant difficile la prévision des effets de l'augmentation de la CO_2 sur les MCCs et la RuBisCO (Raven et al., 2014). Le phytoplancton de petite taille, comme les picoeucaryotes autotrophes, pourrait bénéficier davantage de l'augmentation en CO_2 puisque ces cellules ont la capacité de diffuser passivement le CO_2 à travers leur membrane cellulaire (Beardall et al., 2014). Cette capacité de diffusion est d'ailleurs inversement proportionnelle à la taille des cellules (Brussaard et al., 2013).

Parallèlement à l'augmentation du CID, la diminution du pH risque d'avoir des effets directs sur la physiologie du phytoplancton en affectant l'activité des enzymes intracellulaires (Beardall and Raven, 2004). Les expériences en monoculture n'ont cependant pas montré d'effets consistants d'une diminution de pH sur la croissance phytoplanctonique. Par exemple, des expériences menées avec le coccolithophore calcificateur *Emiliania huxleyi* ont montré une augmentation (Sciandra et al., 2003), une diminution (Iglesias-Rodriguez et al., 2008) ou une absence d'effets (Spielmeyer and Pohnert, 2012) du pH sur la croissance et la calcification chez cette espèce. Similairement, Berge et al. (2010) n'ont trouvé qu'une influence limitée des variations de pH sur la croissance de huit espèces phytoplanctoniques incluant des dinoflagellés, diatomées, cryptophytes et haptophytes. En plus des résultats divergents mis en évidence par les études menées sur différentes espèces, les interactions entre les espèces et la modification des assemblages phytoplanctoniques compliquent les prévisions des impacts de l'acidification au niveau des écosystèmes.

La mise en place ultérieure d'expériences en mésocosmes a permis d'étudier l'effet de l'acidification sur les communautés planctoniques (Riebesell et al., 2007, 2013). Ces études ont également généré des résultats très variables. Par exemple, la diminution du pH lors de trois expériences successives menées dans la mer du Nord (PeECE 2001, 2003 et 2005) n'a pas eu

d'effet sur la production primaire au cours des deux premières (Dellile et al., 2005; Egge et al., 2009) alors qu'une diminution a été observée lors de la troisième expérience (Egge et al., 2009). Des différences interannuelles dans les concentrations initiales en nutriments, de même que des assemblages phytoplanctoniques différents, ont été évoquées pour expliquer ces divergences. Lors d'une expérience en mésocosme menée au Svalbard, la diminution de pH a été accompagnée d'une augmentation de la production primaire, mais uniquement après l'ajout de nutriments et la stimulation d'une floraison phytoplanctonique (Engel et al., 2013). L'impact de l'acidification sur la structure des assemblages phytoplanctonique est également difficile à prédire. Puisque les cellules de petites tailles devraient théoriquement bénéficier de l'augmentation des concentrations de CO_2 (Beardall et al., 2014), l'acidification des océans est susceptible d'affecter la composition spécifique des assemblages phytoplanctoniques. Plusieurs expériences ont effectivement démontré un effet positif de l'acidification sur les petites cellules phytoplanctoniques (Yoshimura et al., 2010; Brussaard et al., 2013; Morán et al., 2015). Par contre, d'autres ont également mis en évidence une stimulation de plus grandes cellules comme les diatomées (e.g. Tortell et al., 2002). Bref, ces expériences ont généré des résultats parfois ambigus, souvent contradictoires, rendant jusqu'ici impossible l'établissement d'un consensus sur les effets de l'acidification sur les communautés phytoplanctoniques (Schulz et al., 2017). La composition initiale de la communauté phytoplanctonique et les concentrations initiales en nutriments peuvent entre autres expliquer les divergences entre les études.

1.1.4 Influence de la température sur l'effet de l'acidification

Tel que mentionné précédemment, les océans sont soumis à de multiples agents de stress. Par exemple, en plus du phénomène d'acidification, les océans se réchauffent et s'appauvrissent en éléments nutritifs (Harvey et al., 2013; Kroeker et al., 2013). Les résultats d'expériences où les effets du réchauffement et de l'acidification ont été testés séparément ne peuvent pas être combinés puisque ces facteurs sont susceptibles d'interagir de façon additive, synergétique ou antagoniste, souvent de manière imprévisible (Todgham and Stillman, 2013; Boyd et al., 2015; Riebesell and Gattuso, 2015; Gunderson et al., 2016). Il est donc essentiel de considérer les effets combinés de ces stress lors d'études visant à déterminer la réponse des océans aux changements globaux. Ainsi, les dernières années ont vu une augmentation progressive du nombre d'études dites à « multiples facteurs de stress » (Boyd et al., 2015).

Des expériences en laboratoire ont démontré qu'une acidification couplée à un réchauffement pouvait conduire à une augmentation de la photosynthèse et à une diminution de la richesse spécifique (Tatters et al., 2013). Similairement, des expériences en microcosmes menées dans la mer de Béring et l'Atlantique Nord ont montré une augmentation de la photosynthèse avec le

réchauffement à toutes les pCO_2 testées (Hare et al., 2007; Feng et al., 2009). L'augmentation de la photosynthèse due au réchauffement peut se traduire par un accroissement du carbone organique dissous plutôt que particulaire (Kim et al., 2011). Les résultats d'une étude en mésocosmes menée en mer Méditerranée ont mis en évidence un accroissement de l'abondance des picocyanobactéries en réponse à l'effet combinée du réchauffement et de l'acidification, sans effet significatif sur la production primaire (Maugendre et al., 2015). L'augmentation de la température a également engendré une augmentation de la biomasse phytoplanctonique et de la production primaire lors d'expériences en mer de Chine méridionale, mais ces augmentations étaient neutralisées à pCO_2 élevée (Gao et al., 2017). À l'inverse, en mer Baltique, une expérience en mésocosmes a résulté en une diminution de la biomasse avec le réchauffement des eaux, mais à une augmentation lorsque le réchauffement était combiné avec une augmentation de la pCO_2 (Sommer et al., 2015). Le nombre réduit d'études et la variabilité des réponses observées limitent notre capacité à prédire l'effet qu'auront ensemble le réchauffement et l'acidification sur les assemblages phytoplanctoniques et la production primaire.

1.2 La production océanique de DMS et son impact sur le climat

Outre son rôle sur le cycle du carbone, le phytoplancton est impliqué dans la production du diméthylsulfure (DMS), un gaz impliqué dans la physiologie du phytoplancton, le fonctionnement des écosystèmes marins et dans la régulation du climat. Le DMS est un composé organosulfuré produit par le phytoplancton généralement présent en sursaturation dans les eaux de surface océaniques (Barnard et al., 1982; Iverson et al., 1989; Kiene and Service, 1991; Cantin et al., 1996; Kettle et al., 1999). Une fois émis dans l'atmosphère, le DMS est rapidement oxydé en acide méthylsulfonique (MSA) et en acide sulfurique gazeux (H_2SO_4). Ce dernier gaz peut former des aérosols de sulfate hygroscopiques (SO_4^{2-}), diffusant la lumière incidente, ou agir comme noyau de condensation de nuages (NCN), augmentant l'albédo nuageuse et les propriétés radiatives de l'atmosphère (Charlson et al., 1987; Andreae and Crutzen, 1997; Liss and Lovelock, 2007; Woodhouse et al., 2013). Charlson, Lovelock, Andreae et Warren ont proposé en 1987 l'hypothèse CLAW (du nom des auteurs) stipulant l'existence d'une boucle de rétroaction entre la production de DMS par le phytoplancton et le budget radiatif de la Terre. Cette hypothèse a récemment été revisitée (Quinn and Bates, 2011). On reconnait maintenant que la formation des NCN nécessite des conditions particulières, incluant de faibles concentrations d'aérosols. Par conséquent, la contribution du DMS à la modification du budget radiatif terrestre serait plus importante dans les régions à faibles charges en particules atmosphériques (Carslaw et al., 2010; Quinn et al., 2017). Néanmoins, l'importance du DMS comme source de soufre n'est pas remise en question, les émissions de DMS constituant la plus grande source naturelle de soufre atmosphérique, avoisinant les 28.1 Tg annuellement (Lana et al., 2011). L'importance des flux océan-atmosphère de DMS

dépend des concentrations dans les eaux de surface (Malin and Kirst, 1997) et des facteurs contrôlant sa ventilation, i.e. le vent et la température (Nightingale et al., 2000). Dans les eaux de surface, la production de DMS varie dans le temps et l'espace en fonction de l'activité biologique et des facteurs physiques qui la contrôlent.

La principale source de DMS est le clivage enzymatique du diméthylsulfoniopropionate (DMSP), un métabolite produit par plusieurs groupes phytoplanctoniques (Cantoni and Anderson, 1956; Keller et al., 1989). Les quotas intracellulaires de DMSP varient de < 0,1 nmol L^{-1} à 400 nmol L^{-1} entre les groupes phytoplanctoniques, les haptophytes et dinoflagellés étant parmi les producteurs les plus prolifiques (Stefels et al., 2007). Le DMSP occupe plusieurs fonctions physiologiques chez le phytoplancton. Il est impliqué dans l'osmorégulation, la cryoprotection, la gestion des surplus d'énergie et fait partie d'une cascade d'antioxydants faisant également intervenir le DMS et le DMSO (voir revue par Simó, 2001; Stefels et al., 2007). Une partie du DMSP produit par le phytoplancton se retrouve en solution (DMSP dissous; $DMSP_d$) suite à l'exsudation par les cellules actives (Laroche et al., 1999), l'autolyse, la lyse virale et le broutage par le zooplancton (Stefels and Van Boeckel, 1993; Wolfe and Steinke, 1996; Malin et al., 1998). Le temps de résidence du $DMSP_d$ dans les eaux océaniques est court, de l'ordre de quelques heures, puisqu'il est consommé rapidement par les bactéries hétérotrophes qui l'utilisent comme source de carbone et de soufre. Le DMSP peut subvenir jusqu'à 15 % de la demande bactérienne en carbone et 100 % des besoins en soufre (Kiene et al., 2000; Simó et al., 2002). Une partie du $DMSP_d$ peut également être consommé par le phytoplancton (Malmstrom et al., 2005; Vila-Costa et al., 2006b; Ruiz-González et al., 2012), mais cette voie est considérée de moindre importance que la consommation bactérienne (Lavoie et al. 2018).

Le DMSP consommé par les bactéries peut emprunter l'une des quatre voies métaboliques suivantes : (1) clivage enzymatique en DMS, (2) déméthylation/déméthiolation en méthanethiol (MeSH), (3) transformation en composés sulfurés non-volatils et (4) accumulation intracellulaire sans métabolisation (Kiene et al., 1999, 2000; Kiene and Linn, 2000; Yoch, 2002; Reisch et al., 2011). L'importance relative de ces voies détermine le rendement bactérien en DMS, i.e. la quantité de DMS produit par rapport au DMSP consommé. Une récente revue de littérature a montré que le rendement microbien en DMS excède rarement 40 % dans les environnements marins et côtiers (Lizotte et al., 2017). Les bactéries hétérotrophes possèdent plusieurs familles de DMSP-lyases, les enzymes capables de cliver le DMSP en DMS (Ddd+ pour *DMSP-dependent DMS-releasing*), mais une seule famille de DMSP-lyase a jusqu'ici été identifiée chez les eucaryotes (Todd et al., 2007; Alcolombri et al., 2015; Johnston et al., 2016; Lei et al, 2018). La production de DMS est donc principalement attribuée aux bactéries hétérotrophes, mais l'influence phytoplanctonique peut être significative dans les communautés dominées par les dinoflagellés ou les haptophytes (Niki et al., 2000; Steinke et al., 2002; Lizotte et al., 2012).

Les puits de DMS incluent la photo-oxydation, la consommation bactérienne et la ventilation, ces processus variant selon l'intensité lumineuse, le vent et la profondeur de la couche de mélange de surface (Brimblecombe and Shooter, 1986; Simó and Pedros-Alió, 1999; Nightingale et al., 2000; Hatton et al., 2004; Simó, 2004). La production nette de DMS dans les eaux marines est donc dépendante de nombreux processus abiotiques et biotiques, ce qui la rend sensible aux changements globaux.

1.2.1 Impacts de l'acidification océanique sur le DMS

La majorité de ces expériences sur l'influence de l'AO sur la production de DMSP et de DMS ont montré une diminution de ces deux composés à faibles pH (Hopkins et al., 2010; Avgoustidi et al., 2012; Park et al., 2014; Webb et al., 2015). Lors de ces expériences, la diminution de la production du DMS et du DMSP est largement attribuée aux effets négatifs de l'acidification sur *Emiliania huxleyi*, l'espèce majoritairement responsable de la production de DMSP. Toutefois, l'acidification ne résulte pas systématique en une baisse de DMSP et de DMS. Par exemple, les résultats d'une expérience en mésocosme ont montré une augmentation des concentrations de DMSP accompagnée d'une diminution du DMS aux pCO_2 élevées (Archer et al., 2013). Dans ce cas, l'acidification agirait négativement sur la conversion du DMSP en DMS, tandis que l'augmentation de la biomasse de dinoflagellés, particulièrement l'abondance de l'espèce *Heterocapsa rotundata*, aurait stimulé la synthèse de DMSP. L'interaction entre les communautés productrices de DMSP et le broutage par le zooplancton a également été suggéré pour expliquer des diminutions de DMS observées suite à une baisse du pH (Park et al., 2014).

L'implémentation dans un modèle couplé océan-atmosphère de la relation négative pH-DMS rapportée par plusieurs études suggère que l'acidification des océans prévue pour 2100 résultera en une diminution de 18 ± 3 % des émissions de DMS (Six et al., 2013). Cette diminution pourrait mener à un réchauffement additionnel de 0.23–0.48 K selon le scénario A1B du GIEC, avec toutefois de fortes asymétries entre les régions (Schwinger et al., 2017). Cette prédiction dépend de la robustesse de la relation linéaire utilisée entre les concentrations de DMS et l'acidification. Toutefois, l'acidification ne résulte pas toujours en une baisse des concentrations de DMS, puisque certaines études ont révélé une absence d'effet et même une stimulation de la production nette de DMS sous acidification (Tableau 1.1; Vogt et al., 2008; Kim et al., 2010; Hopkins and Archer, 2014). Des différences régionales et saisonnières dans la composition de la communauté phytoplanctonique, l'influence du broutage par le zooplancton et l'activité des bactéries hétérotrophes sont les principaux processus identifiés pour expliquer ces divergences.

Tableau 1.1 Changements relatifs des concentrations de DMS (%) lors d'expériences d'acidification réalisées en mésocosmes ou microcosmes. ΔpH représente la diminution de pH_T appliquée dans chaque expérience. ND : *No data available*. Tableau modifié de Hussherr et al. (2017).

Localisation	ΔpH	ΔpCO_2 (µatm)	ΔDMS (%)	Référence
Baie de Baffin, Arctique	-0.75	500 - 3000	-80	Hussherr et al. (2017)
Mer Baltique	-0.4	350 - 1500	-34	Webb et al. (2016)
Raunefjorden, Norvège	-0.6	280 - 3000	-60	Webb et al. (2015)
Jangmok, Corée	-0.5	160 - 830	-82	Park et al. (2014)
Kongsfjorden, Norvège	-0.8	180 - 1420	-60	Archer et al. (2013)
Raunefjorden, Norvège	-0.2	300 - 750	-40	Avgoustidi et al. (2013)
Raunefjorden, Norvège	-0.3	300 - 750	-57	Hopkins et al. (2010)
Raunefjorden, Norvège	-0.5	300 - 750	0	Vogt et al. (2008)
Plateau européen du NW	-0.4	340 - 1000	225	Hopkins and Archer (2014)
Jangmok, Corée	ND	400–900	80	Kim et al. (2010)

1.2.2 Effets combinés de l'acidification océanique et du réchauffement sur la production de DMS

L'effet combiné de l'acidification et du réchauffement sur les assemblages planctoniques naturels et la production de DMS n'a fait l'objet que de deux études jusqu'à ce jour. Les deux études, réalisées en région côtière coréenne, ont mené encore là à des résultats divergents. La première a mis en évidence une augmentation de 80 % des concentrations intégrées de DMS sous pCO_2 élevée (900 ppm vs 400 ppm) et une réduction de 20 % de cet effet stimulant lorsque l'augmentation de la pCO_2 était accompagnée d'un réchauffement de 3 °C (Kim et al., 2010). Dans cette étude, l'absence d'un traitement où seulement la température était changée a empêché les auteurs de conclure sur l'effet spécifique de la température. Lors de la deuxième étude, les auteurs ont observé une diminution de 82 % des concentrations intégrées de DMS dans des conditions de pCO_2 élevée, une diminution semblant s'accroitre lorsque les eaux étaient réchauffées (Park et al., 2014). La relation négative entre la pCO_2 et les concentrations intégrées de DMS n'était cependant pas significative lorsque la température de l'eau était élevée de ~2 °C. Selon les auteurs des deux études, la présence d'assemblages phytoplanctoniques différents entre les deux expériences, de même que des pressions différentes de broutage, expliqueraient les résultats contrastés obtenus.

1.3 Approche scientifique

L'objectif général de ma thèse est de caractériser 1) l'influence de l'acidification océanique sur le développement des floraisons phytoplanctoniques, la production primaire et la production de DMS dans l'estuaire maritime du Saint-Laurent, et 2) de déterminer dans quelles mesures le réchauffement des eaux affectera l'influence de l'acidification sur ces processus. L'ensemble des données présentées sont issues d'une expérience en microcosmes réalisée à l'été 2013 à l'Institut Maurice-Lamontagne, à Ste-Flavie, suivie à l'automne 2014 d'une expérience de plus grande ampleur menée en mésocosmes à la Station Aquicole de l'ISMER, Rimouski.

1.3.1 Objectifs

L'objectif général du chapitre 2 est de caractériser l'influence de l'acidification sur le développement du bloom estival de diatomées et la production de DMS dans l'estuaire maritime du Saint-Laurent.

Objectif spécifique 2.1 : Quantifier l'effet de l'augmentation de la pCO_2 sur le métabolisme bactérien du DMSP.

L'objectif général du chapitre 3 est de déterminer l'influence combinée de l'acidification et du réchauffement sur la structure et la productivité de la communauté phytoplanctonique de l'estuaire maritime du Saint-Laurent.

Objectif spécifique 3.1 : Déterminer si le réchauffement des eaux aura un effet additif, antagoniste ou synergétique avec l'effet de l'acidification sur le développement de la floraison automnale de diatomée et la production primaire dans l'estuaire maritime du Saint-Laurent.

L'objectif général du chapitre 4 est de quantifier l'effet combiné de l'acidification et du réchauffement sur les concentrations de DMSP et de DMS associées au développement et déclin de la floraison automnale de diatomées dans l'estuaire maritime du Saint-Laurent.

Objectif spécifique 4.1 : Déterminer si le réchauffement des eaux aura un effet additif, antagoniste ou synergétique conjointement à l'effet de l'acidification sur la production nette de DMS.

1.4 Région d'étude

1.4.1 L'estuaire maritime du Saint-Laurent

Les expériences ont été réalisées avec des communautés naturelles de l'estuaire maritime du Saint-Laurent (EMSL). L'estuaire du Saint-Laurent, en excluant la portion fluviale, est traditionnellement divisé en deux parties : l'estuaire moyen allant de l'extrémité est de l'Île d'Orléans jusqu'à l'embouchure du fjord du Saguenay, et l'estuaire maritime en aval jusqu'à Pointe-des-Monts (El-Sabh and Silverberg, 1990). L'estuaire maritime est quant à lui la plus vaste portion du système (9350 km^2), la plus large (20–50 km), ainsi que la plus profonde (~300 m; d'Anglejan, 1990). L'EMSL est marqué par la présence du chenal Laurentien, une vallée glaciaire profonde s'étendant sur 1240 km entre Tadoussac et la limite est du plateau continental canadien. La tête du chenal Laurentien est un lieu de mélange de masses d'eau complexe fortement influencé par les marées (Gratton et al., 1988). La remontée des eaux profondes, riches en nutriments stimulent la productivité des eaux de surface qui s'écoulent vers le golfe du Saint-Laurent avec le courant de Gaspé (Coote and Yeats, 1979; Saucier and Chassé, 2000). Le cycle annuel de développement des communautés phytoplanctoniques de l'EMSL est marqué par deux floraisons de diatomées, une estivale et une automnale (Sevigny et al., 1979; Levasseur et al., 1984). La croissance des diatomées dans l'EMSL est éventuellement limitée par l'épuisement des nutriments en surface, principalement la silice et le nitrate (Levasseur et al., 1997).

Quatre masses d'eau convergent à la tête du chenal Laurentien, les eaux saumâtres de l'estuaire moyen, les eaux saumâtres provenant du fjord du Saguenay, la couche intermédiaire froide et les eaux profondes hypoxiques du EMSL (Mucci et al., 2011). Ces masses d'eaux, à l'exception des eaux de surface de la rivière Saguenay, sont actuellement sursaturés en CO_2 par rapport à l'atmosphère (Yang et al., 1996; Barth et al., 1999). Historiquement, le pH des eaux de surface de l'EMSL (< 75 m) a été réduit par moins de ~0,1 unité, cependant il peut varier rapidement dans le temps, pouvant passer de 7,85 à 7,93 en un seul cycle de marée (Mucci et al., 2017). De plus, des mesures de la pCO_2 des eaux de surface de l'EMSL entre 2003 et 2016 montrent que celles-ci varient spatialement entre 139 et 548 µatm et sont fortement influencées par l'activité biologique (Dinauer and Mucci, 2017). Quant aux eaux profondes de l'EMSL (170–335 m), elles se sont acidifiées de 0,2–0,3 unités sur une période de 73 ans pour atteindre un pH de 7,7–7,8 (Mucci et al., 2011). D'ailleurs, des remontées de ces eaux profondes pourraient rapidement réduire le pH de surface à ~7,62, une réduction qui pourrait être exacerbée par la contribution des eaux de faible pH de la rivière Saguenay (Mucci et al., 2017).

La température des eaux de surface du golfe du Saint-Laurent est corrélée avec la température ambiante avec un décalage d'un demi mois (Galbraith et al., 2012). Cette corrélation a permis de montrer que la température des eaux de surface du golfe avait augmenté de ~0,9 °C par siècle depuis 1873 (Galbraith et al., 2012). Des anomalies positives supplémentaires de 0,25–0,75 °C par rapport à la tendance au réchauffement ont cependant été mesurées pour la période 1985–2013 (Galbraith et al., 2016). Les températures les plus chaudes sont enregistrées au mois d'août dans le golfe et l'EMSL, la chaleur se dissipant graduellement dans la couche intermédiaire froide sous-jacente au cours de la période estivale (Cyr et al., 2011). L'ampleur du réchauffement attendu des eaux de surface dans l'EMSL est cependant incertaine. La présence de la couche intermédiaire froide et l'influence des processus physiques dans l'EMSL rendent difficiles les prédictions quant à son réchauffement.

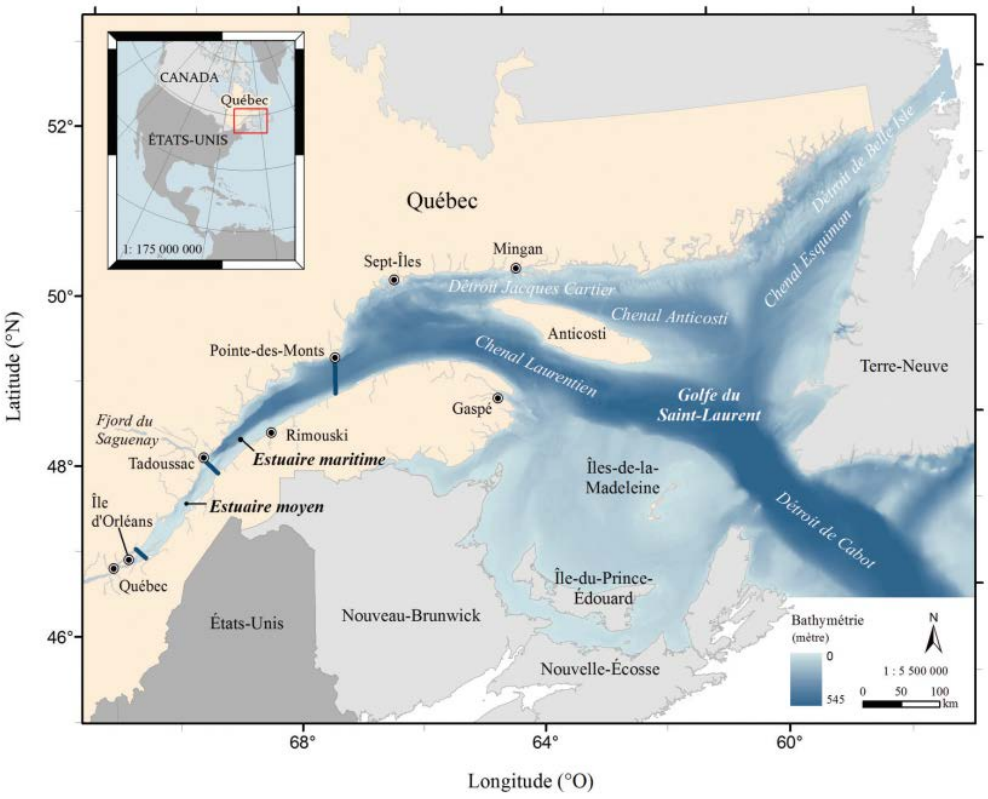

Figure 1.4 Carte de l'estuaire et du golfe du Saint-Laurent, Canada. Figure tirée de Savenkoff et al. (2017).

Chapitre 2 Impact of ocean acidification on dimethylsulfide cycling: a peek into the microbial black box

Résumé

L'impact potentiel de l'acidification sur les concentrations de diméthylsulfure (DMS), de diméthylsulfoniopropionate (DMSP) et les processus régissant le cycle de ces composés soufrés par des organismes microbiens a été étudié dans le cadre d'une expérience en microcosmes durant l'été 2013. Une communauté planctonique naturelle des eaux de surface de l'estuaire maritime du Saint-Laurent (EMSL) a été suivie pendant 12 jours sous trois cibles de pCO_2 : 1 × pCO_2 (775 µatm), 2 × pCO_2 (1850 µatm) et 3 × pCO_2 (2700 µatm). Les effets de l'augmentation de la pCO_2 ont été évalués sur la biomasse, la taxonomie et la productivité du phytoplancton, ainsi que sur les concentrations de DMSP et de DMS et sur le cycle microbien à l'aide de traceurs radioactifs (^{35}S-$DMSP_d$). Une floraison mixte de phytoplancton composée des diatomées *Chaetoceros* spp., *Skeletonema costatum* et *Thalassiosira* spp., ainsi que des flagellés non identifiés (2–20 µm) s'est développée dans tous les microcosmes. Les concentrations de chlorophylle *a* (Chl *a*) ont atteint un pic au jour 6, passant de 1,26 µg L^{-1} à 20 ± 4 µg L^{-1} et 17 ± 1 µg L^{-1}, à 1 × pCO_2 et 2 × pCO_2, respectivement. Cependant, le timing et l'ampleur du pic de biomasse ont été modifiés dans le traitement 3 × pCO_2, n'atteignant que 11 ± 4 µg L^{-1} au jour 8 de l'expérience. Les variations des concentrations de $DMSP_t$ étaient largement liées aux variations de Chl *a* (r_S = 0,77; p <0,001; n = 61) et les valeurs maximales de $DMSP_t$ ont été atteintes consécutivement au jour 8 dans le traitement 1 × pCO_2 (264 nmol L^{-1}), au jour 10 dans le 2 × pCO_2 (245 nmol L^{-1}), et au jour 12 dans le 3 × pCO_2 (192 nmol L^{-1}). Le DMSP dissous ($DMSP_d$) a augmenté irrégulièrement de 2 ± 1 nmol L^{-1} à une moyenne globale de 5,2 ± 0,8 nmol L^{-1} à la fin de l'expérience et les fluctuations de $DMSP_d$ étaient largement associées aux variations de $DMSP_t$ (r_S = 0,70; p < 0,001; n = 61). Dans l'ensemble, ni les concentrations de $DMSP_d$ ni l'efficacité de la prise microbienne du $DMSP_d$ (k_{DMSPd}) ne semblent être fortement affectées par l'augmentation du pCO_2, suggérant que l'acidification n'altère ni la disponibilité ni la prise microbienne de ce substrat. Cependant, nos résultats montrent une diminution moyenne du rendement bactérien en DMS de 34 % et 61 % dans les traitements 2 × pCO_2 et 3 × pCO_2. Doubler et tripler la pCO_2 a entraîné une baisse respective de 15 % et 40% des concentrations moyennes de DMS par rapport au contrôle. Les concentrations de DMS étaient positivement corrélées avec les rendements bactériens de DMS (r_S = 0,65; p < 0,001; n = 45), suggérant que dans les systèmes dominés par les diatomées, l'impact de l'acidification sur les concentrations de DMS peut être fortement lié aux altérations de la métabolisation microbienne du $DMSP_d$. Les résultats de cette étude fournissent la première preuve empirique de la sensibilité du métabolisme microbien du DMSP sous acidification.

Abstract

The potential impact of acidification on the concentrations of dimethylsulfide (DMS) and dimethylsulfoniopropionate (DMSP), as well as the processes governing the cycling of sulfur compounds by microbial organisms was investigated in a microcosm experiment during summer 2013. A natural planktonic community sourced from the surface waters of the Lower St. Lawrence Estuary (LSLE) was monitored over 12 days under three pCO2 targets: 1 × pCO_2 (775 µatm), 2 × pCO_2 (1850 µatm), and 3 × pCO_2 (2700 µatm). The effects of heightened pCO_2 were assessed on phytoplankton biomass, taxonomy and productivity, as well as on DMSP and DMS concentrations and microbial cycling via ^{35}S-$DMSP_d$ radioisotope uptake assays. A mixed phytoplankton bloom comprised of the diatoms *Chaetoceros* spp., *Skeletonema costatum*, and *Thalassiosira* spp., as well as unidentified flagellates (2–20 µm) developed over the course of the study period. Concentrations of chlorophyll *a* (Chl *a*) peaked on day 6 from an initial 1.26 µg L^{-1} to 20 ± 4 µg $L^{-1}$and 17 ± 1 µg L^{-1}, at 1 × pCO_2 and 2 × pCO_2, respectively. However, the timing and the magnitude of the biomass build-up were altered in the 3 × pCO_2 treatment reaching only 11 ± 4 µg L^{-1} by day 8 of the experiment. Variations in the concentrations of $DMSP_t$ were largely related to variations in Chl *a* (r_S = 0.77; $p < 0.001$; n = 61) and peak values of $DMSP_t$ were reached consecutively on day 8 in the 1 × pCO_2 treatment (264 nmol L^{-1}), on day 10 in the 2 × pCO_2 (245 nmol L^{-1}), and on day 12 in the 3 × pCO_2 (192 nmol L^{-1}). Dissolved DMSP ($DMSP_d$) increased irregularly from 2 ± 1 nmol L^{-1} to an overall average of 5.2 ± 0.8 nmol L^{-1} by the end of the experiment and fluctuations of $DMSP_d$ were broadly associated with variations in $DMSP_t$ (r_S = 0.70; $p < 0.001$; n = 61). As a whole, neither concentrations of $DMSP_d$ nor the microbial scavenging efficiency of $DMSP_d$ (k_{DMSPd}) seemed to be strongly affected by increasing pCO_2 suggesting that acidification did not alter the availability and the bacterial uptake of this substrate. However, our results show a reduction of the mean microbial yield of DMS by 34 % and 61 % in the 2 × pCO_2 and 3 × pCO_2 treatments. Doubling and tripling the pCO_2 respectively resulted in a 15 % and 40 % decline in average concentrations of DMS compared to the control. DMS concentrations were positively correlated with microbial yields of DMS (r_S = 0.65; $p < 0.001$; n = 45), suggesting that in diatom-dominated systems, the impact of OA on concentrations of DMS may be strongly linked with alterations of the microbial breakdown of $DMSP_d$. Findings from this study provide the first empirical evidence of the sensitivity of the microbial DMSP switch under OA.

2.1 Introduction

Marine microorganisms are integral to major biogeochemical cycles, fluxes and processes occurring in marine systems (Glöckner et al., 2012). Abundant and diverse, microbes produce, consume and emit various compounds that may be of critical importance to the regulation of the Earth's climate, including but not limited to, carbon dioxide (CO_2), methane (CH_4) and dimethylsulfide (DMS). Whilst atmospheric CO_2 and CH_4 act to amplify the Earth's positive radiative balance, the annual emission of ~28.1 Tg of sulfur (S) via oceanic DMS (Kettle and Andreae, 2000; Lana et al., 2011) is believed to represent a significant source (between 18 and 42 %) of global atmospheric aerosols (Chin and Jacob 1996; Gondwe et al., 2003; Kloster et al., 2006) that act to cool the climate to an extent that is still under debate (Quinn and Bates, 2011; Quinn et al., 2017). Sulfate (SO_4^{2-}) particles formed through the oxidation of DMS may scatter incoming solar radiation directly or indirectly by seeding nuclei upon which clouds may condense and grow, thereby modifying the Earth's albedo (Shaw, 1983; Charlson et al., 1987; Andreae and Crutzen, 1997). The sensitivity of cloud condensation nuclei to DMS-derived aerosols broadly depends on the presence of other major sources of atmospheric aerosols, including those derived from anthropogenic activities, as well as on the strength of DMS fluxes at the ocean-air interface (Carslaw et al., 2010; Woodhouse et al., 2013). By and large, microbial food webs in the oceans, including both autotrophic and heterotrophic organisms, are pivotal in shaping reservoirs of DMS that are available for emissions towards the atmosphere (reviews by Simó, 2001; Stefels et al., 2007).

DMS originates from the enzymatic breakdown of dimethylsulfoniopropionate (DMSP), a compatible solute biosynthesized to various intracellular concentrations by a wide span of phytoplankton groups (Keller et al., 1989, review by Stefels et al., 2007). While members of the classes Haptophyceae and Dinophyceae are considered as the most prolific of producers, certain members of the Bacillariophyceae (diatoms) and Chrysophyceae classes may also synthesize considerable amounts of DMSP (Stefels et al., 2007). The metabolic incentive behind the production of DMSP is believed to rest upon its efficiency to protect algal cells against environmental shifts in salinity, temperature, nutrients and various oxidants (Karsten et al., 1996; Kiene et al., 2000; Kirst et al., 1991; Stefels et al., 2000; Sunda et al., 2002). Most of the naturally occurring DMSP in seawater is found in its particulate form ($DMSP_p$), within algal cells, however it may be released into the water column as dissolved DMSP ($DMSP_d$) through various mechanisms that include active exudation, predation and diverse lytic processes (Stefels and Van Boeckel, 1993; Wolfe and Steinke, 1996; Malin et al., 1998; Stefels et al., 2000). Concentrations of $DMSP_d$ are notoriously difficult to gauge in natural systems due to this compound's inherent lability and considerable potential to supply carbon and reduced S to heterotrophic bacteria (Kiene and Linn, 2000) leading to rapid turnover (a few hours to days, see review table in Lizotte et al., 2017) of this compound in the oceans. Once

consumed by heterotrophic microorganisms, the fate of $DMSP_d$ can be trailed through four distinct metabolic routes using ^{35}S-$DMSP_d$ bioassays: (1) catabolism of $DMSP_d$ via the activity of DMSP-lyase enzymes yielding DMS; (2) demethylation–demethiolation of $DMSP_d$ yielding methyl-mercaptopropionate, methanethiol (MeSH) or inorganic sulfur; (3) production of dissolved non-volatile S compounds (DNVSs); (4) accumulation of DMSP intracellularly without metabolization (untransformed pool) (Kiene et al., 1999; Kiene and Linn, 2000; Kiene et al., 2000; Yoch, 2002; Reisch et al., 2011). A recent compilation of several ^{35}S-$DMSP_d$ tracer studies from various coastal and oceanic waters shows that microbial DMS yields rarely exceed 40% of consumed $DMSP_d$ (Lizotte et al., 2017) thereby putting a cap on the potential amount of DMS available for sea-to-air emissions through bacterial mediation of DMSP. Beyond the several DMSP-dependent DMS-releasing (Ddd+) enzymes that have been isolated in populations of heterotrophic bacteria, one family of DMSP-lyase, dubbed Alma, has been identified in eukaryotes such as *Emiliania huxleyi* and species of *Symbiodinium* displaying the potential for direct production of DMS by phytoplankton itself (Todd et al., 2007; Alcolombri et al., 2015; Johnston et al., 2016). To this day however, the relative importance of autotrophic and heterotrophic processes in supplying stocks of DMS in seawater remains unclear with provisional estimates fluctuating extensively (Lizotte et al., 2012). Moreover, studies have shown the uptake of ^{35}S-$DMSP_d$ by diatoms as well as cyanobacteria such as *Synechococcus* and *Prochlorococcus* (Vila-Costa et al., 2006b, Ruiz-González et al., 2012), a process that further diverts $DMSP_d$ away from the potential production of DMS. Ultimately the DMS that is produced may be withdrawn from seawater through bacterial degradation, photo-oxidation and finally only a minor portion (< 10 %) escapes to the atmosphere (Brimblecombe and Shooter, 1986; Bates et al., 1994; Kiene et al., 2000; Archer et al., 2002). As a result of the intrinsic coupling between microorganisms and the cycling of marine methylated compounds, ongoing and future disturbances in oceanic ecosystems related to anthropogenic forcing that may affect marine microbes may also impact the dynamics of the climate-relevant compound DMS.

Ocean acidification (OA), the decrease in oceanic pH, is one of the many consequences associated with the rise in anthropogenic CO_2. While atmospheric CO_2 concentrations have expanded from 280 to more than 400 ppm over the last 200 years, the oceans have absorbed ~28 % of those man-made emissions (Le Quéré et al., 2015). This oceanic uptake of CO_2 has already translated into a 0.11 unit decrease in the pH of surface waters (Gattuso et al., 2015), and modelling studies suggest that a further decrease of 0.3–0.4 units could be expected by the end of the century, while a drop by ~0.8 unit is foreseeable by 2300 (Caldeira and Wickett, 2005; Doney et al., 2009; Feely et al., 2009). By potentially impacting numerous microbial processes in the oceans, both autotrophic and heterotrophic (Piontek et al., 2010; Riebesell and Tortell, 2011), OA may possibly reshape reservoirs of methylated S compounds through differential alteration of production and consumption mechanisms. Experimental studies examining the effects of OA on natural planktonic assemblages and their production of DMSP and DMS reveal, in many cases, a negative impact of decreasing pH

on the net accumulation of these two compounds (see compilation Table in Hussherr et al., 2017), although uncertainties persist as to the underlying and manifold causes. In studies where natural communities were dominated by the DMSP-rich *E. huxleyi*, the adverse effect of OA on the growth of this calcifying organism may also have translated into a negative impact on the overall production of both DMSP and DMS (Hopkins et al., 2010; Avgoustidi et al., 2012; Webb et al., 2015). Other OA studies revealed that reductions in DMSP at low pH were intimately linked with heightened predation of DMSP-producing phytoplankton by grazers ensuing in a decline in concentrations of DMS (Kim et al., 2010; Park et al., 2014). However, contrasting outcomes in the dynamics of DMSP and DMS have also been observed with diminishing concentrations of DMS at high pCO_2 in spite of heightened or invariable responses in DMSP production to OA (Archer et al., 2013; Hussherr et al., 2017; Bénard et al., 2018a). In these studies, the distinct negative impact of OA on DMS concentrations had been hypothesized to be associated with the alteration of bacterial DMSP and DMS mediation without, however, direct empirical evidence of bacterial transformation rates to fully reinforce those assumptions leaving the bacterial 'black box' virtually sealed.

The main objective of this study was to experimentally assess the response of a summer planktonic community and its cycling of DMSP and DMS under OA, with a particular focus on bacterial DMSP catabolic processes. While the dependence of the concentration of DMS on bacterial metabolism had been investigated indirectly in OA experiments by comparing bacterial production rates to ratios of DMS:$DMSP_t$ or concentrations of DMS (Archer et al., 2013; Bénard et al., 2018a), to our knowledge the result presented here are the first to address the existing knowledge-gap by specifically determining the impact of OA on the microbial metabolism of DMSP using the ^{35}S-$DMSP_d$ tracer approach. With roughly 70 % of OA studies showing a decrease in DMS (Hussherr et al., 2017), the implementation of this negative pH-DMS relationship into coupled ocean-atmosphere models (Six et al., 2013; Schwinger et al., 2017) points towards amplification of warming in the future as OA persists. Conclusions from these modelling tools highlight the relevance of identifying the key processes controlling DMS concentrations under OA through targeted ground-truthing, especially since alterations in DMS have the potential to promote or alleviate climate change.

2.2 Materials and methods

2.2.1 Water collection and experimental setting

The incubations were conducted at the Maurice-Lamontagne Institute of the Department of Fisheries and Oceans Canada, Mont-Joli, Canada, from June 18 to July 1, 2013 (Fig. 2.1). Water was collected in the St-Lawrence Estuary (48° 50' 29" N 68° 31' 45" W) at 5 m depth using a 5 L

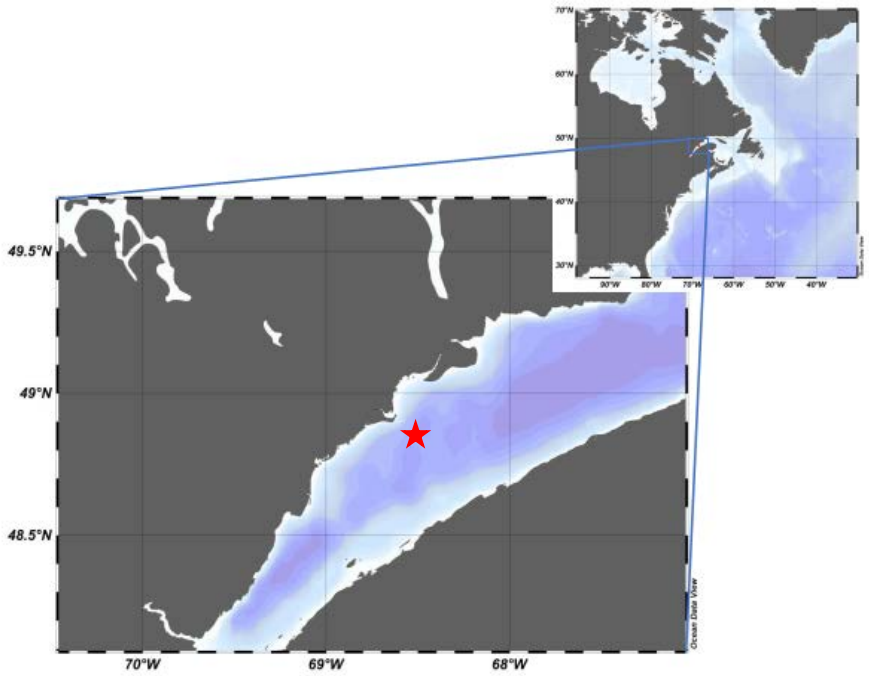

Figure 2.1 Sampling site on June 17, 2013, identified by a red star, located in the Lower St. Lawrence Estuary, near Rimouski, Québec, Canada (48° 50' 29" N 68° 31' 45" W).

Niskin bottle and filtered through a 250 µm mesh to remove large zooplankton on June 17. On June 18, water was incubated in 20 L collapsible bags (HyClone Labtainers^{TM}). Measured transmittance of the incubation bags was 77.5 % of incoming photosynthetically active radiation (PAR), 61.5 % UVA and 32.6 % UVB. The incubation bags were placed in an exterior incubator under a neutral mesh to reduce incoming radiation, roughly corresponding to the irradiance at sampling depth (~30 %; Le Fouest et al., 2006), as the photic zone in the LSLE is relatively shallow during that period (10–15 m; e.g. Levasseur et al., 1984). The incubator was kept at in situ temperature through the constant inflow of coastal surface waters. As water temperature naturally fluctuated during the 12-day experiment, it is not possible to completely exclude potential effects of these physical variables on the microbial processes under study. The use of the Tukey statistical test (see section 2.2.4) however allows simultaneous pairwise comparisons on a specific day, therefore disentangling the potential effect of naturally varying processes, such as temperature, over time.

2.2.2 Treatments and acidification protocol

A total of nine incubation bags were exposed to three treatments in triplicate with target pCO_2 of $1 \times pCO_2$ = 775 µatm (in situ control), $2 \times pCO_2$ = 1850 µatm, and $3 \times pCO_2$ = 2700 µatm. The pCO_2 in the $1 \times pCO_2$ was not artificially modified and corresponded to the in situ pCO_2. The

methods for acidification were based on recommendations from the *Guide to best practices in Ocean Acidification Research* (Riebesell et al., 2010). The technique of addition of a strong acid (HCl, 0.02 N) and bicarbonate ($NaHCO_3$, 0.3 N) was used as this procedure mimics OA by maintaining the total alkalinity constant through the acidification step. The volumes needed to reach the targeted pCO_2 were determined with the help of the MS Excel macro CO_2SYS (Pierrot et al., 2006) using the carbonic dissociation constants (K_1 and K_2) of Lueker et al. (2000), and the HSO_4^- association constants given by Dickson (1990). Both acid and bicarbonate solutions were added in the required amounts using syringes connected to the bags by a Luer-lock port. The acidification process was carried out on June 18 (day -1) following the filling of the bags on the same day. No further manipulation of the carbonate chemistry occurred after this initial acidification, implying that any drift or variations in pH and pCO_2 were related to biological activity (Table 2.1). The subsampling began the next day, ~16 hours after the initial acidification (day 0, June 19, 08:00).

2.2.3 Microcosm subsampling of chemical and biological parameters

The nine incubation bags were monitored for 13 days beginning after the initial acidification (day -1). Subsampling was carried out between 05:00 and 11:00 during days 0–12, although not all the variables were sampled every day. Water for pH, total alkalinity (TA), primary production, DMS concentrations, and ^{35}S-DMSP$_d$ bioassays was collected directly from the microcosms and processed immediately, except for TA samples that were analysed in the following month. Water for chlorophyll *a* (Chl *a*), nutrients, bacterial abundance, and phytoplankton taxonomy were collected in a brown bottle (Nalgene®, 1 L) and kept at 4 °C in the refrigerator until further subsampling within 6 hours of collection. Salinity samples were collected in 250 mL plastic bottles on days 0 and 12, and stored in the dark until analysis using a Guildline Autosal 8400B salinometer in the months following the experiment. At least half of the volume of the microcosms remained in the bags at the end of the experiment.

2.2.3.1 Carbonate chemistry

The carbonate chemistry parameters were determined on days 0, 2, 5, 7, 9, and 12. The pH was determined by carefully transferring water from the microcosm into a 125 mL plastic bottle without headspace and then allowed to equilibrate to 25.0 ± 0.1 °C in a thermostated bath. The pH samples were analysed within 2–3 hours of collection on a Hewlett-Packard UV-Visible diode array spectrophotometer (HP-8453A) and a 5 cm quartz cell with phenol red (PR; Robert-Baldo et al., 1985) and *m*-cresol purple (mCP; Clayton and Byrne, 1993) used as indicators. The pH on the total proton scale (pH_T) was calculated according to Byrne (1987), using the salinity of the sample and the HSO_4^- association constants given by Dickson (1990). The average relative error calculated on

the average relative standard deviation on replicated standard measurements and samples measurements was lower than 0.15 %. The TA samples were collected in pre-rinsed 250 mL glass bottles with the addition of a few crystals of $HgCl_2$, and sealed with Apiezon® Type-M high-vacuum grease and a ground-glass stopper. Determination of the TA was carried out by open-cell automated potentiometric titration (Titrilab 865, Radiometer®) using a pH combination electrode (pHC2001, Red Rod®) and a dilute HCl (0.025 N) titrant solution calibrated using Certified Reference Materials (CRM Batch#94,provided by A. G. Dickson, Scripps Institute of Oceanography, La Jolla, USA). The computed pH_T at 25 °C and the measured TA were used to calculate the carbonate chemistry parameters and respective pCO_2 at in situ temperature using CO_2SYS (Pierrot et al., 2006).

2.2.3.2 Nutrients

Water for the analyses of nutrient was filtered using Whatman® GD/X syringe filters (GF/F, 0.7 µm) and stored at -20 °C in acid-washed polyethylene tubes. The samples were analysed with a Bran and Luebbe Autoanalyzer III using a colorimetric method described by Hansen and Koroleff (2007). The analytical detection limit was 0.03 µmol L^{-1} for nitrate (NO_3^-) plus nitrite (NO_2^-), 0.02 µmol L^{-1} for NO_2^-, 0.1 µmol L^{-1} for silicic acid ($Si(OH)_4$), and 0.05 µmol L^{-1} for soluble reactive phosphate (SRP).

2.2.3.3 Plankton biomass, composition and enumeration

For Chl *a* determination, subsamples of 100 mL were filtered onto Whatman® GF/F filters (0.7 µm). Phytoplankton pigments were extracted by soaking the filters in a 90 % acetone solution at 4 °C in the dark for 24 h. Then, the solution was analysed by a 10-AU Turner Designs fluorometer using the acidification method (Parsons et al., 1984). The analytical detection limit for Chl *a* was 0.05 µg L^{-1}. Samples for microscopic identification and enumeration for eukaryotic cells > 2 µm were taken on days 0, 6, and 12. Samples of 200 mL were collected and preserved with acidic Lugol solution (Parsons et al., 1984), then stored in the dark until analysis. Cell identification was carried out in accordance with Lund et al. (1958) using an inverted microscope (Zeiss Axiovert 10) and taxonomic references of Tomas (1997) and Bérard-Therriault et al. (1999). For the enumeration of heterotrophic bacteria, samples were kept in 10 mL sterile cryogenic polypropylene vials fixed with glutaraldehyde Grade I (final concentration 0.1 %, Sigma-Aldrich; Marie et al., 2005). Samples were placed at 4 °C in the dark for 30 min, then flash-frozen in liquid nitrogen and kept at -80 °C until analysis. After defrosting to ambient temperature, the samples were stained with SYBR Green I (final concentration 0.1 %, Invitrogen Inc.) to which 600 µl of Tris-EDTA 10× buffer pH 8 (Laboratoire MAT; Belzile et al., 2008) and Fluoresbrite beads of 1 µm (Polysciences) were added

as an internal standard. The samples were then analysed using a FACS Calibur flow cytometer (Becton Dickinson) equipped with a 488 nm argon laser.

2.2.3.4 Primary production

Rates of primary production were determined using the ^{14}C-fixation method (Knap et al., 1996; Ferland et al., 2011). Two 250 mL polycarbonate bottles, one clear and one opaque, were filled directly from each microcosm bag before sunrise and amended with 250 µL $NaH^{14}CO_3$ (80 µCi mL^{-1}). To prevent active fixation of ^{14}C by phytoplankton in the dark bottles, 100 µl of 0.02 mol L^{-1}3-(3,4-dichlorophenyl)-1,1-dimethylurea (DCMU) was added (Legendre et al., 1983). The total initial radioactivity was determined in each bottle by subsampling 50 µL into 20 mL scintillation vial containing 10 mL of Ecolume^{TM} liquid scintillation cocktail and 50 µL of ethanolamine (Sigma). Bottles for the determination of primary production rates were placed in the same incubator as the microcosms, and incubated for 24 h. At the end of the incubation, 3 mL were subsampled for the determination of total primary production (P_T), 3 mL were filtered with a Whatman GD/X syringe filter (0.7 µm GF/F) to quantify the fixed carbon released in the dissolved organic carbon pool (P_D) and placed in 20 mL scintillation vials. The vials containing the P_T and P_D samples were acidified with 500 µL of HCl 6 N for 3 h under a fume hood, then neutralized with 500 µL of NaOH 6 N before adding 15 mL of Ecolume^{TM} liquid scintillation cocktail. Varying amounts of the remaining volume were filtered onto Whatman GF/F (0.7 µm) to determine the particulate primary production (P_P) by normalizing the measured radioactivity by the volume filtered. The filters were placed in 20 mL scintillation vials and acidified with 100 µL of HCl (0.05 N) and left to fume for 12 h before adding 15 mL of scintillation cocktail. The samples were analysed using a Tri-Carb 4910TR liquid scintillation counter (PerkinElmer). The rates of carbon fixation into particulate and dissolved fractions were calculated according to the equations of Knap et al. (1996).

Table 2.1 Average values of pH_T (total hydrogen ion concentration scale), pCO_2 and total alkalinity (TA) per treatment for each day the carbonate chemistry parameters were measured. Average values are presented with ± standard error.

	pH_T						pCO_2 (µatm)						TA (µmol kg^{-1})					
Day	0	2	5	7	9	12	0	2	5	7	9	12	0	2	5	7	9	12
Treatment																		
1 × pCO_2	7.72 ± 0.04	7.73 ± 0.04	8.01 ± 0.07	8.24 ± 0.07	8.31 ± 0.05	8.41 ± 0.06	776 ± 76	750 ± 83	381 ± 73	211 ± 44	169 ± 23	129 ± 21	1873 ± 3	1876 ± 3	1874 ± 2	1872 ± 3	1866 ± 3	1861 ± 4
2 × pCO_2	7.35 ± 0.01	7.40 ± 0.02	7.55 ± 0.03	7.68 ± 0.07	7.81 ± 0.09	7.89 ± 0.11	1855 ± 56	1660 ± 62	1169 ± 96	853 ± 137	633 ± 147	529 ± 147	1879 ± 2	1884 ± 4	1883 ± 2	1883 ± 1	1882 ± 1	1881 ± 2
3 × pCO_2	7.18 ± 0.01	7.19 ± 0.01	7.28 ± 0.01	7.37 ± 0.01	7.44 ± 0.03	7.46 ± 0.04	2728 ± 54	2723 ± 39	2162 ± 21	1767 ± 49	1488 ± 100	1427 ± 133	1879 ± 6	1882 ± 1	1882 ± 1	1881 ± 3	1883 ± 3	1884 ± 3

2.2.3.5 DMS and DMSP concentrations

Samples for the quantification of DMS were collected directly from the microcosms with a 60 mL syringe and kept at 4 °C in the dark until analysis within 2 hours of collection. Twenty-five mL of unfiltered DMS samples were directly injected into a purge and trap system (PnT) and pushed into a heated (70 °C) chamber bubbled with Ultrapure helium (50 ± 5 mL min^{-1}) by 1–5 mL of Mili-Q^{TM} water, then purged for 4 min. Gaseous DMS was trapped using a loop immersed in liquid nitrogen during the purging phase. The loop was then heated in a water bath to release the gas which was then analysed using a Varian 3800 Gas Chromatograph equipped with a pulsed flame photometric detector (PFPD, Varian 3800) and a detection limit of 0.9 nmol L^{-1} (Scarratt et al., 2000; Lizotte et al., 2012). DMS concentrations were calculated against microliter injections of DMS using a permeation tube (Certified Calibration by Kin-Tek Laboratories Inc.). For the quantification of $DMSP_d$, the small-volume gravity drip filtration technique (SVDF) was used as described in Kiene and Slezak (2006). Briefly, 20 mL of sample was gravity-filtered through a 47 mm Whatman® GF/F (0.7 µm) and the first 3.5 mL of filtrate was collected in 5 mL polyethylene tubes. For the quantification of $DMSP_t$, tubes were directly filled with 3.5 mL of sample. Both samples for $DMSP_d$ and $DMSP_t$, were preserved by adding 50 µL of a 50 % sulfuric acid solution (H_2SO_4) to the tubes before storing them at 4 °C in the dark until analysis in the days following collection. DMSP concentrations were determined after a mole to mole (1:1) conversion to DMS following hydrolysis with the addition of 1 mL of NaOH (5 N). The NaOH solution was injected first into the PnT, then the 3.5 mL sample was injected and pushed with water, before being bubbled and analysed as described above for the DMS.

2.2.3.6 Microbial ^{35}S-$DMSP_d$ uptake assays

For the determination of microbial $DMSP_d$ uptake and metabolism, samples of seawater were collected from the microcosm bags before sunrise, and amended with ^{35}S-$DMSP_d$ following the radiotracer methods described by Kiene and Linn (2000) with modifications by Slezak et al. (2007). The ^{35}S-DMSP was synthesized from L-[^{35}S]-methionine with an initial specific activity of 1175 Ci $mmol^{-1}$. We investigated several microbial DMSP transformations including the $DMSP_d$ loss rate constant (k_{DMSPd}), $DMSP_d$-to-DMS conversion efficiency (DMS yield), DMSP incorporation into particles > 0.2 µm (particulate yield), and the further incorporation of ^{35}S into macromolecules (a measure of the assimilation efficiency of sulfur) as well as the pool of untransformed ^{35}S-DMSP in cells (Kiene and Linn, 2000). Briefly, samples were taken from each microcosm in 71 mL HDPE Nalgene bottles, and trace amounts (< 5 pmol L^{-1}) of ^{35}S-$DMSP_d$ were added to obtain an initial radioactivity of ~1000 dpm mL^{-1}. Total initial activity was determined after gently mixing the bottles and subsampling 1 mL into 20 mL scintillation vials containing 10 mL of Ecolume^{TM} liquid

scintillation cocktail. To determine the k_{DMSPd}, the bottles were incubated in a thermostated bath at in situ temperature for 3 h during which time 1 mL was subsampled after 0, 30, 60, and 180 min, filtered using Whatman GD/X syringe filters (0.2 µm Nylon membrane) into a serum vial swiftly sealed with a rubber septum fitted with a well cup and a type-A/E glass filter soaked with 200 µL of stabilised H_2O_2 (3 %). The serum vials were placed on an orbital shaker at 100 rpm for ~6 h to trap the volatile ^{35}S-DMS after being injected with 200 µL of NaOH (5 N) through the stopper to cleave the remaining ^{35}S-DMSP$_d$ (Kiene and Linn, 2000). Then, the A/E filters were transferred into 20 mL scintillation vials containing 10 mL of Ecolume^{TM} liquid scintillation cocktail to determine the loss of DMSP$_d$ over time. The k_{DMSPd} was calculated as the slope of the natural logarithm of the fraction of remaining ^{35}S-DMSP$_d$ trapped as ^{35}S-DMS versus time. Blank abiotic controls were performed on day 4 and 12 by using 0.2 µm filtered seawater from a microcosm treated with ^{35}S-DMSP$_d$. The loss rates in those filtered controls were less than 1 % of the k_{DMSPd} of the live samples, indicating extracellular enzyme activity was not a significant process in DMSP$_d$ loss.

Determination of the different fates of consumed DMSP$_d$ was conducted in parallel incubations. Samples of 71 mL were collected in HDPE Nalgene bottles, injected with dimethyldisulfide (DMDS; 100 nmol L^{-1} final concentration), an inhibitor of DMS consumption (Simó et al., 2000; Galí et al., 2011), and tracer amounts of ^{35}S-DMSP$_d$ (< 5 pmol L^{-1}). The bottles were incubated at in situ temperature for 24 h until > 90 % of the ^{35}S-DMSP$_d$ was consumed (Slezak et al., 2007). After the incubation, 5 mL subsamples were taken to determine the volatile ^{35}S produced. The subsamples were placed in 100 mL serum vials containing 100 µL of sodium dodecyl sulfate (SDS), 200 nmol L^{-1} of unlabelled DMSP$_d$ to prevent the further metabolization of ^{35}S-DMSP$_d$, and 50 µL of Ellman's reagent to complex thiols such as MeSH, ensuring the majority of volatiles recovered were in the form of ^{35}S-DMS. Following the transfer of the subsamples, the serum vials were swiftly sealed with a rubber septum fitted with a well cup and a type-A/E glass filter soaked with 200 µL of stabilised H_2O_2 (3 %), and placed on an orbital shaker at 100 rpm for ~6 h to trap the volatile ^{35}S-DMS (Kiene and Linn, 2000). The filters were then placed in 20 mL scintillation vials containing 10 mL of Ecolume^{TM} liquid scintillation cocktail. After the ^{35}S-DMS was trapped, a new H_2O_2 soaked filter was placed in the well cup fixed to the septum of the serum vials before being sealed. Each serum vial was injected with 200 µL of NaOH (5 N) through the stopper to cleave the remaining ^{35}S-DMSP$_d$, allowing us to express the ^{35}S-DMS produced as a fraction of the consumed ^{35}S-DMSP$_d$ during the parallel incubation.

To quantify the particulate yield and the incorporation of ^{35}S-DMSP$_d$ into macromolecules, duplicate subsamples of 5 mL were taken from the 71 mL Nalgene bottles after the 24 h incubations and gently filtered by hand on 0.2 µm Nylon filters. The first filter was only rinsed with filtered seawater (particulate yield), while the second was also rinsed with trichloroacetic acid (TCA) to determine the assimilation efficiency into macromolecules (Kiene and Linn, 2000). The filters were then placed in

scintillation vials as described above. To estimate the pool of untransformed ^{35}S into particles, the fraction of ^{35}S found as macromolecules was subtracted from the particulate yield (Kiene and Linn, 2000). All the samples were counted on a Tri-Carb 4910TR liquid scintillation counter (PerkinElmer) in the weeks following collection. It should be noted that logistical constraints did not allow us to monitor microbial DMSP cycling dynamics prior to day 4 and that the transformation pathways of ^{35}S-$DMSP_d$ measured during this experiment are considered to be microbial processes, largely dominated by heterotrophic bacteria but not excluding low DMSP-producing phytoplankton and cyanobacteria that have also been shown to uptake $DMSP_d$ (Malmstrom et al., 2005; Vila-Costa et al., 2006b).

2.2.4 Statistical analyses

The statistical analyses were performed using RStudio, with the nlme package (R Core Team, 2016). Normality of the data was verified using a Shapiro-Wilk test ($p < 0.05$), and data were log- or rank-transformed when normality was rejected. The data were analysed using mixed model linear regressions, accounting for repeated measures covariance. Results from these models were used to test the effects of treatment ($1 \times pCO_2$, $2 \times CO_3$, and $3 \times pCO_2$), time, and the interaction of these factors over the duration of the experiment (Supplement Table 1). Post-hoc Tukey Honest Significant Difference (HSD) tests with Sidak corrections for multiple comparisons were performed to provide further assessment of the differences between treatments on selected days. Treatments were assigned to different letter groups (a, b, c) when significant differences were detected during daily pairwise comparisons (e.g. Supplement Table 2). In addition, non-parametric Spearman's rho correlation coefficients (r_S) were used to evaluate the strength and direction of association between two ranked variables.

2.3. Results

2.3.1 Physical and chemical conditions during the experiment

Table 2.1 summarises values of three carbonate system parameters (pH_T, pCO_2, TA) monitored or calculated for each treatment at day 0, 2, 5, 7, 9, 12. Over the duration of the experiment, TA remained constant in all treatments, varying by less than 1 % of the initial concentration. At the beginning of the experiment, the pH_T was 7.72 ± 0.04, 7.35 ± 0.01, and 7.18 ± 0.01 for the $1 \times pCO_2$, $2 \times pCO_2$, and $3 \times pCO_2$ treatments respectively (Fig 2.2a; Table 2.1). On day 0, the corresponding pCO_2 were 776 ± 76, 1855 ± 56, and 2728 ± 54 µatm for the $1 \times pCO_2$, $2 \times pCO_2$, and $3 \times pCO_2$ treatments (Fig. 2.2b). As expected the CO_2 uptake associated with photosynthetic microorganisms led to variations in pCO_2 and pH_T in all microcosms, a common phenomenon in

experiments allowing pH to drift naturally (Rost et al., 2008; Hussherr et al., 2017). The decrease in pCO_2 was stronger in the acidified treatments ~1300 µatm (2 × pCO_2, and 3 × pCO_2) as compared to the control ~650 µatm (1 × pCO_2) (Fig 2.2b; Table 2.1). Water salinity was 28.06 ± 0.02 on day 0 in all the microcosms and remained constant throughout the experiment, averaging 28.10 ± 0.04 on day 12. The temperature of the incubators naturally fluctuated throughout the experiment, with 7.5 °C on day 0, increasing to 8.4 °C on day 3–4, then decreasing to ~5 °C between days 7–12.

On day 0, NO_3^-, SRP, and $Si(OH)_4$ concentrations averaged 12.5 ± 0.7 µmol L^{-1}, 0.69 ± 0.07 µmol L^{-1}, and 19.84 ± 0.01 µmol L^{-1} respectively (Fig 2.3). During the incubation, the nutrients displayed the same general pattern, regardless of pCO_2 treatments. NO_3^- and SRP were rapidly drawn from the microcosms at the onset of the experiment, remaining near or below the detection limit from day 8 onward. $Si(OH)_4$ remained relatively stable until day 4, then decreased until day 12, although the concentrations were significantly lower in the 1 × pCO_2 between days 8 and 12, lessening to 3.9 ± 1.0 µmol L^{-1} compared to 7.0 ± 1.5 µmol L^{-1} and 9.0 ± 0.7 µmol L^{-1} for 2 × pCO_2 and 3 × pCO_2, respectively.

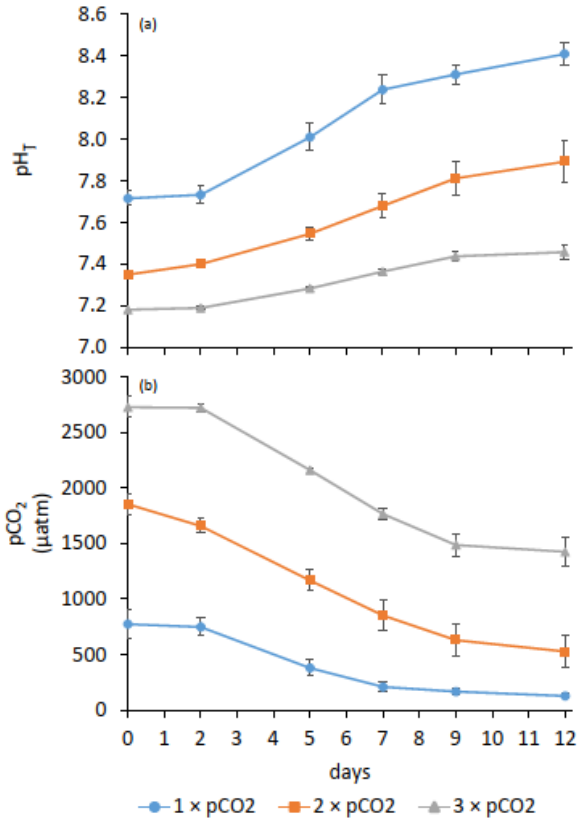

Figure 2.2 Temporal variations in (a) pH_T, (b) pCO_2 in each treatment (1 × pCO_2, 2 × pCO_2, and 3 × pCO_2; see legend for symbol attribution). Daily averages are presented (mean ± standard error).

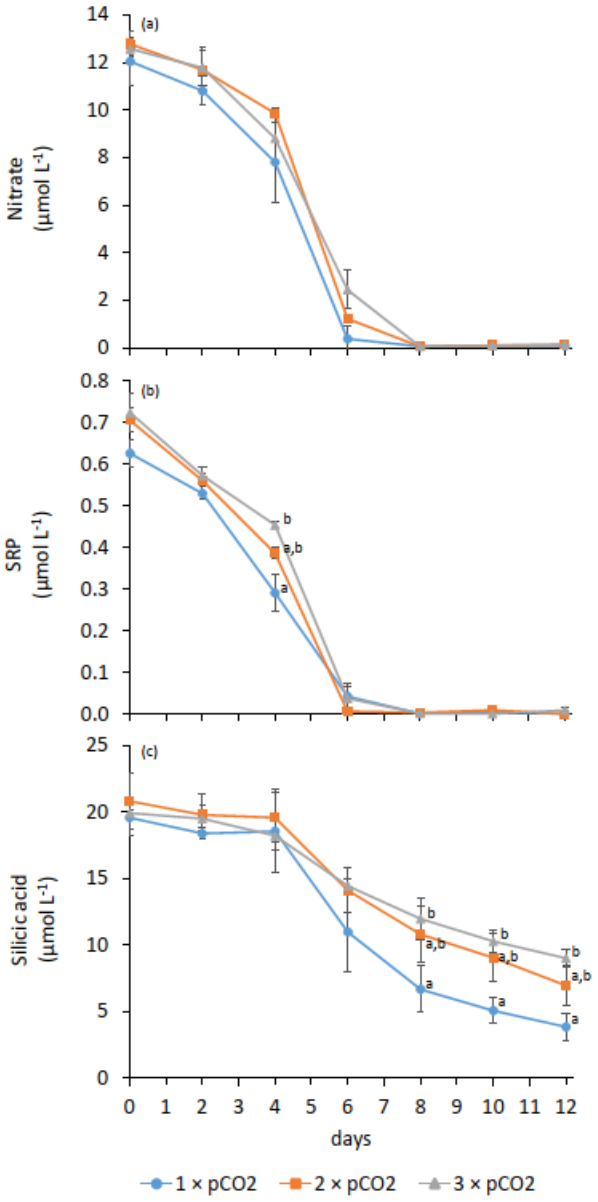

Figure 2.3 Temporal variations in (a) nitrate, (b) soluble reactive phosphate (SRP), and (c) silicic acid in each treatment (1 × pCO_2, 2 × pCO_2, and 3 × pCO_2; see legend for symbol attribution). Daily averages are presented (mean ± standard error). Tukey HSD between treatments on a given day are indicated by grouping letters (a, b).

2.3.2 Phytoplankton, bacterial abundance, and primary production

The average concentration of Chl *a* in all the microcosms on day 0 was 1.26 ± 0.2 µg L^{-1} and increased exponentially until day 6 to reach 20 ± 4 µg L^{-1} (1 × pCO_2) and 17 ± 1 µg L^{-1} (2 × pCO_2). In the 3 × pCO_2 treatment however, Chl *a* was significantly lower on day 6, with 10 ± 1 µg L^{-1}, and only reached its maximum concentration on days 8–10 (Fig. 2.4a). In the 1 × pCO_2 and 2 × pCO_2 treatments, the bloom was followed by a decrease in Chl *a* biomass, before reaching a plateau between 10 and 14 µg L^{-1} on days 8–12 irrespective of treatments.

The initial taxonomic composition of the planktonic community greater than 2 µm in size was identical in all the microcosms and was mostly composed of small unidentified flagellates (2 to < 10 µm; 51 % of total numerical abundance) and a mixed assemblage of cryptophytes (*Plagioselmis prolonga* var. n*ordica*; 7.4 %), choanoflagellates (2 to < 10 µm; 4 %), dinoflagellates (*Gymnodisium* spp., *Gyrodinium* spp.; 3.4 %), diatoms (*Chaetoceros* spp., and *Skeletonema costatum*; 2.5 %), and "others" (~24 %; comprised of heterotrophic groups, ciliates and undetermined cells 2 to < 20 µm; Fig. 2.5). By day 6, an important shift in relative abundance of taxonomic groups had taken place. The contribution of diatoms species, including *Chaetoceros* spp., *Skeletonema costatum*, and *Thalassiosira* spp., to total abundance of protists had reached 50, 25, and 17 % at 1 × pCO_2, 2 × pCO_2, and 3 × pCO_2, respectively. The relative abundance of unidentified flagellates was 28, 47 and 46 % while the group "others" contributed to 9, 17 and 21 % in the 1 × pCO_2, 2 × pCO_2, and 3 × pCO_2 treatments, respectively. By the last day of the experiment (day 12), diatoms were numerically dominant in all treatments, accounting for 60, 46, and 37 % of the total cell counts at 1 × pCO_2, 2 × pCO_2, and 3 × pCO_2 respectively.

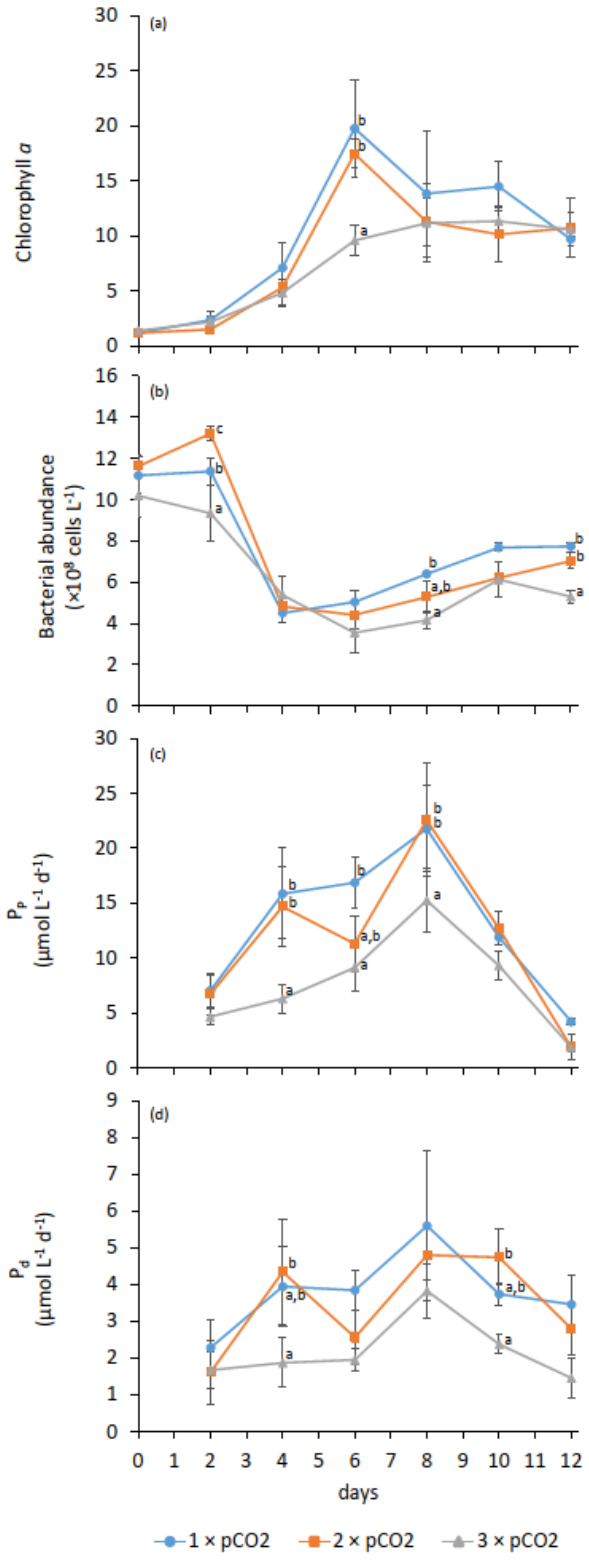

Figure 2.4 Temporal variations in (a) chlorophyll *a*, (b) bacterial abundance, (c) particulate primary production (P_P), and (d) dissolved primary production (P_D) in each treatment (1 × pCO_2, 2 × pCO_2, and 3 × pCO_2; see legend for symbol attribution). Daily averages are presented (mean ± standard error). Tukey HSD between treatments on a given day are indicated by grouping letters (a, b, c).

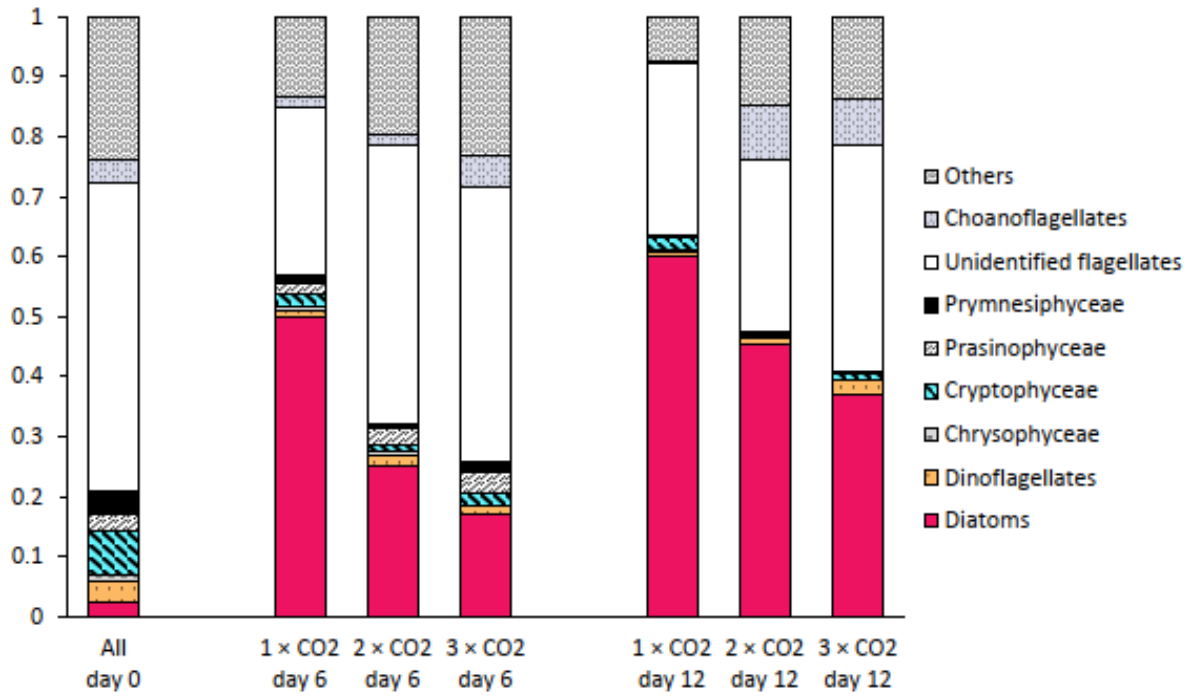

Figure 2.5 Relative abundance of 9 groups of protists at the beginning of the experiment (day 0), on day 6, and at the end of the experiment (day 12) in each treatment (1 × pCO_2, 2 × pCO_2, and 3 × pCO_2). The group « others » includes Chlorophyceae, Dictyochophyecae, Euglenophyceae, heterotrophic groups, and Ciliates. The bar plot on day 0 represents the initial community assemblage before acidification. For symbol attribution to protist groups, see legend.

The initial abundance of bacteria was 11 ± 1 × 10^8 cells L^{-1} on day 0, remaining relatively stable until day 2 before sharply decreasing to 4.9 ± 0.6 × 10^8 cells L^{-1} in all treatments on day 4 (Fig. 2.4b). Then, the bacterial abundance varied with an overall increasing trend until the last day of the experiment with 7.7 ± 0.2 × 10^8 cells L^{-1}, 7.0 ± 0.4 × 10^8 cells L^{-1}, and 5.3 ± 0.3 × 10^8 cells L^{-1} in the 1 × pCO_2, 2 × pCO_2, and 3 × pCO_2 treatments, respectively.

The P_P was low at the beginning of the experiment, averaging 6 ± 2 µmol C L^{-1} d^{-1} (Fig. 2.4c). Rates of P_p increased the fastest in the 1 × pCO_2, 2 × pCO_2 treatments, reaching maximum values of 22 ± 4 and 23 ± 5 µmol C L^{-1} d^{-1} on day 8 while P_P reached a maximum of 15 ± 3 µmol C L^{-1} d^{-1} in the 3 × pCO_2 treatment on the same day. Rates of P_P decreased during the following days to reach an overall average of 3 ± 1 µmol C L^{-1} d^{-1} on day 12, irrespective of treatment. Similarly, P_D was low at the beginning of the experiment with an average of 1.9 ± 0.7 µmol C L^{-1} d^{-1}. The maximum P_D values were attained on day 8, averaging 5 ± 1 µmol C L^{-1} d^{-1} across all treatments before diminishing to 3 ± 1 µmol C L^{-1} d^{-1} on day 12 (Fig. 2.4d). The proportion of dissolved to total primary

production (P_D:P_T ratio) was stable at ~20 % across all treatments from day 0 to 10, only increasing to ~50 % on the last day of the experiment.

2.3.3 $DMSP_t$ and DMS

Temporal patterns in the concentrations of $DMSP_t$ were similar in all three treatments (Fig. 2.6a). Initial average $DMSP_t$ concentration was 30 ± 6 nmol L^{-1}, and highest concentrations of $DMSP_t$ were reached sequentially by day 8 in the 1 × pCO_2 treatment (264 nmol L^{-1}), by day 10 in the 2 × pCO_2 (245 nmol L^{-1}), and on day 12 in the 3 × pCO_2 (192 nmol L^{-1}). No significant differences in concentrations of $DMSP_t$ were observed between the pCO_2 treatments other than on day 8. Overall, $DMSP_d$ concentrations showed no statistically different variations between treatments throughout the experiment. $DMSP_d$ was initially low, averaging 2 ± 1 nmol L^{-1} across treatments, decreased slightly on day 2, before increasing to 3.6 ± 0.7 nmol L^{-1} on day 4, and varying between 4–6 nmol L^{-1} until day 12 (Fig. 2.6b).

The DMS concentrations were low and stable in all treatments between days 0–3, averaging 1.6 ± 0.4 nmol L^{-1} during that time. From day 4 onward, DMS accumulated in all treatments until days 8, 9, and 10 in the 1 × pCO_2, 2 × pCO_2, and 3 × pCO_2 treatments, respectively reaching 22 ± 2 nmol L^{-1}, 19 ± 3 nmol L^{-1}, and 15 ± 3 nmol L^{-1}, then decreased or plateaued until day 12 (Fig. 2.6c). The highest daily DMS concentrations were always measured in the 1 × pCO_2 treatment, although not statistically differently than in the 2 × pCO_2 treatment, except on day 6. The lowest concentrations were always measured in the 3 × pCO_2 treatment, with significant differences observed with the other treatments on days 7–8 (Supplement Table 2). Calculated rates of DMS net change between day 3 and peak DMS per treatment were ~4.2, ~3.0, and ~1.9 nmol L^{-1} d^{-1}, for 1 × pCO_2, 2 × pCO_2, and 3 × pCO_2, respectively.

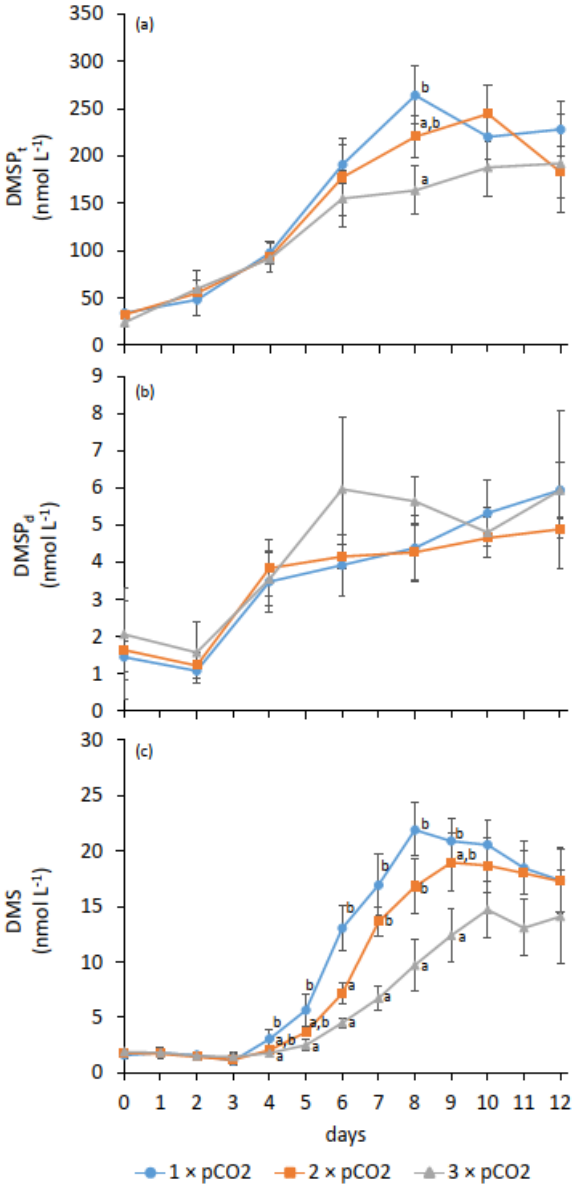

Figure 2.6 Temporal variations in (a) total DMSP concentrations ($DMSP_t$), (b) dissolved DMSP concentrations ($DMSP_d$), and (c) DMS concentrations in each treatment (1 × pCO_2, 2 × pCO_2, and 3 × pCO_2; see legend for symbol attribution). Daily averages are presented (mean ± standard error). Tukey HSD between treatments on a given day are indicated by grouping letters (a, b).

2.3.4 Microbial DMSP cycling

Measured ^{35}S-DMSP$_d$ loss rate constants, k_{DMSPd}, averaged 5.2 ± 1.5 day^{-1} on day 4 across treatments, then decreased to 2.6 ± 0.4 day^{-1} and 2.1 ± 0.4 day^{-1} in the 1 × pCO_2 and 2 × pCO_2 treatments on day 6 while remaining significantly higher in the 3 × pCO_2 treatment at 7.5 ± 1.4 day^{-1} (Fig. 2.7a). Values of k_{DMSPd} then ranged between 2.6 and 5.5 day^{-1} until day 12, irrespective of treatment. Between days 4 and 6, the ^{35}S-DMSP$_d$ present in particles > 0.2 µm (particulate yield) varied from 33 ± 6 % to 20 ± 8 % in all treatments (Fig. 2.7b). On day 8, the particulate yield was significantly higher in the 2 × pCO_2 and 3 × pCO_2 than in the 1 × pCO_2 treatment, with 32 ± 13 % and 34 ± 8 % versus 11 ± 2 %. During the last 2 days, the particulate yield increased from 22 ± 5 % to 38 ± 7 % across treatments. The incorporation of ^{35}S-DMSP$_d$ into macromolecules was higher in the 1 × pCO_2 treatment over days 4–6 with 10 ± 3 % while values for the rest of the experiment ranged from 3.5 to 6.7 % irrespective of treatments (Fig. 2.7c). Moreover, the untransformed fractions of ^{35}S-DMSP present in particles > 0.2 µm (total ^{35}S in particles – ^{35}S-incorporated in macromolecules) varied between 4 to 38 % throughout the experiment. Only on day 8 were the untransformed fractions of ^{35}S-DMSP$_d$ significantly higher in the two high pCO_2 treatments (27 % at 1 × pCO_2 and 30 % at 2 × pCO_2) as compared to the control (4 % at 1 × pCO_2; Fig 2.7d). The yields of DMS from DMSP$_d$, determined as the fraction of ^{35}S-DMSP$_d$ consumed and transformed into DMS, averaged 7 ± 4 % across treatments on day 4. The daily DMS yields were inversely proportionate to the CO_2 treatments between days 6 and 12, with the highest DMS yields at 1 × pCO_2 (~68 % on days 6–8), intermediate DMS yields at 2 × pCO_2 (~49 % on day 10), and the lowest maximum DMS yield at 3 × pCO_2 (~29 % on day 10; Fig. 2.7e).

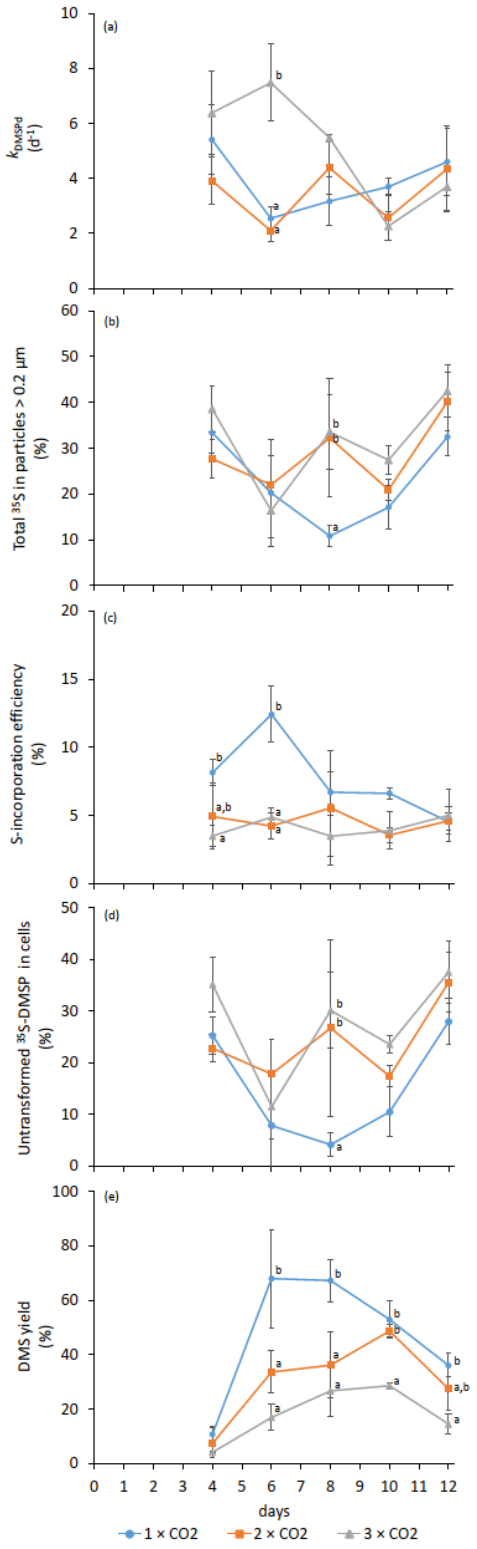

Figure 2.7 Temporal variations of (a) microbial $DMSP_d$ loss rate constant (k_{DMSPd} in day^{-1}), (b) particulate yield (%), (c) assimilation efficiency of ^{35}S-$DMSP_d$ into macromolecules (%),(d) particular untransformed ^{35}S, and (e) microbial DMS yield (%) in each treatment (1 × pCO_2, 2 × pCO_2, and 3 × pCO_2; see legend for symbol attribution). Daily averages are presented (mean ± standard error). Tukey HSD between treatments on a given day indicated by grouping letters (a, b, c).

2.4 Discussion

2.4.1 Impact of heightened pCO_2 on bloom development

In this study, a natural estuarine plankton community sourced during summer under pre-bloom conditions, that included high nutrient concentrations and low Chl *a* (Fig. 2.3 and 2.4), was exposed to three initial conditions of pCO_2, corresponding to in situ, double, and triple pCO_2 of the collected surface water. Following the acidification treatment, an increase in phytoplankton biomass occurred that translated into the exhaustion of NO_3^- and SRP in all microcosms (Fig. 2.3). While the initial mixed phytoplankton community was dominated by unidentified flagellates (51 %), the relative abundance of diatoms increased during the ensuing experiment, accounting respectively for 60, 46, and 37 % of the total community by the end of the experiment in the 1 × pCO_2, 2 × pCO_2, and 3 × pCO_2 treatments, respectively. A mixed assemblage of *Chaetoceros* spp., *Skeletonema costatum*, and *Thalassiosira* spp. was responsible for the increases in diatoms over the twelve-day experiment. This is typical of spring and early summer phytoplankton blooms in the LSLE that are characterized by the dominance of diatoms while the autumn succession favours the development of smaller groups including dinoflagellates and flagellates. Silicic acid, one of the co-limiting factors for the growth of diatoms in the LSLE (Levasseur et al., 1987, 1990), was not totally depleted by the end of the incubation period. However, the higher relative abundance of diatoms in the 1 × pCO_2 microcosms was accompanied by a significantly (Tukey HSD) sharper decrease in $Si(OH)_4$ concentrations (Fig. 2.3c) as compared to the triple pCO_2 treatment from day 8 onward, confirming the greater uptake of silicic acid by the diatoms in the non-acidified control. While the relative importance of diatoms increased across all treatments between day 0 and day 6, heightened pCO_2 dampened this signal from 50 % (1 × pCO_2), to 25 % (2 × pCO_2), and 17 % (3 × pCO_2), of the cell counts at 1 × pCO_2, 2 × pCO_2, and 3 × pCO_2 at mid-experiment, a pattern that was still visible at the end of the experiment (Fig. 2.5). Both laboratory and micro- or mesocosm experiments have shown that the growth of diatoms can be negatively impacted by increasing pCO_2 (Hare et al., 2007; Hopkins et al., 2010; Schulz et al. 2013; Gao and Campbell, 2014). The negative pCO_2 effect on the relative abundance of diatoms observed in this study may be indirectly related to other groups benefitting to a greater extent from the increase in available CO_2 (Hopkinson et al., 2011). As many diatoms operate highly efficient carbon concentrating mechanisms (Trimborn et al., 2009; Wu et al., 2010), they might not benefit as much from higher pCO_2 than smaller cells, thus potentially being outcompeted by cells relying more on CO_2 diffusion under high pCO_2 (Paulino et al., 2008; Brussard et al. 2013; Hama et al., 2016). The increase in pCO_2 also translated into differences in the timing and magnitude of maximum Chl *a* reached particularly in the triple pCO_2 treatment as compared to the in situ pCO_2 control (Fig. 2.4a) where Chl *a* peaked 2 days later and never exceeded 12 µg L^{-1} (3 × pCO_2) as compared to 20 ± 4 µg L^{-1} (1 × pCO_2). Significant differences in rates of P_P were also

observed (Tukey HSD test) between 1 × pCO_2 and 3 × pCO_2 during days 4 and 8 inclusively with lowest rates of P_P measured in the most acidified treatment (Fig. 2.4c). Although many studies have shown an increase in primary production under elevated pCO_2 (Riebesell et al., 2007; Egge et al., 2009; Engel et al., 2013), unabated or reduced primary productivity has also been reported (Gao et al., 2012b; Gao and Campbell, 2014; Maugendre et al., 2017). Most phytoplankton groups have developed carbon concentration mechanisms to cope with CO_2 deficiency, although the efficiencies of those mechanisms vary extensively between taxa (Raven et al., 2014). Therefore, it is challenging to predict how elevated pCO_2 might affect carbon fixation, given the numerous species present in an assemblage and their specific CO_2 affinities (Giordano et al., 2005). Furthermore, the decrease of pH is likely to influence the community structure, with repercussions on community production (Tatters et al., 2013; Eggers et al., 2014). Thus, in our experiment, the changes in community composition, along with a possible increase in microzooplankton grazing under high CO_2 (Rose et al., 2009; Neale et al., 2014) could have limited the primary production under elevated CO_2.

2.4.2 Effect of acidification on concentrations of dimethylated compounds

Patterns of $DMSP_t$ concentrations were very similar between treatments throughout most of the incubation period with a marginal decrease in $DMSP_t$ in the triple pCO_2 treatment relative to the in situ pCO_2 treatment on day 8 of the experiment. As a whole, concentrations of $DMSP_t$ were positively correlated with concentrations of Chl *a* ($r_S = 0.77$; $p < 0.001$; $n = 61$), suggesting that the greatest part of the variance in concentrations of $DMSP_t$ was associated with the variance in concentrations of Chl *a*. Similar results have already been shown, suggesting that OA will not strongly impact DMSP production, but could modulate DMS concentrations by altering the processes controlling the transformation of DMSP to DMS (Hopkins and Archer, 2014; Webb et al., 2015, 2016). Overall, concentrations of $DMSP_d$ fluctuated throughout the experiment (Fig. 2.6b), broadly following variations in $DMSP_t$ ($r_s = 0.70$; $p < 0.001$; $n = 61$) with no significant differences between pCO_2 treatments suggesting that the availability of $DMSP_d$ as a substrate for bacteria was not modulated by the acidification.

In stark contrast to pools of its precursor, DMS was significantly reduced under the 2 × pCO_2 treatment and even further under the 3 × pCO_2 (Fig 2.6c, Tukey HSD test) from day 4 onward. Averaged over the entire 12-d study period, doubling the pCO_2 resulted in a 15 % decline in mean concentrations of DMS, while tripling the pCO_2 decreased average DMS by 40 % as compared to in situ pCO_2. These results are consistent with previous results showing a decrease in DMS concentrations with increasing pCO_2 (Hopkins et al., 2010; Archer et al., 2013; Arnold et al., 2013; Park et al., 2014, Webb et al., 2015, 2016; Hussherr et al., 2017; Bénard et al., 2018a). Decreasing

trends in DMS concentrations following OA have largely been attributed to changes in the structure of communities, including shifts in species dominance, modulation of grazing pressure, but also to potential modifications in the microbial uptake of DMSP and ensuing metabolic fates (Archer et al., 2013; Webb et al., 2015; Hussherr et al., 2017; Bénard et al., 2018a). Despite the latter suite of processes being of central importance in modulating the amount of DMS available for sea-to-air transfer, up until now, only indirect evidence that OA may alter microbial dynamics of DMSP was available (Archer et al., 2013, Bénard et al., 2018a).

2.4.3 Impact of acidification on microbial uptake of DMSP and its fates

Bacteria are well known to efficiently scavenge $DMSP_d$ (Kiene et al., 1999; Kiene and Linn, 2000; Kiene et al., 2000; Vila-Costa et al., 2006a), and the determination of a loss rate constant (k_{DMSPd}) for added tracer amounts of ^{35}S-$DMSP_d$, allows the estimation of the rate of this scavenging efficiency. Throughout the experiment, k_{DMSPd} varied between 2–7 d^{-1} irrespective of treatment, with higher loss rate constants at 3 × pCO_2 detected on day 6 only. Overall, and with the exception of day 6, these results suggest that processes regulating the scavenging of $DMSP_d$ by microorganisms could be rather insensitive to acidification, at least in the estuarine context explored during this study. The range of k_{DMSPd} measured suggests turnover times of 3.5–12 hours, which, assuming steady-state conditions, would indicate the hourly renewal of 8–29 % of the $DMSP_d$ stock. Microbial loss rate constants were not found to be strongly related to bacterial abundance supporting the idea that bacterial community composition and production, may be more relevant in shaping k_{DMSPd} than the absolute number of bacteria (Malmstrom et al., 2005; Vila-Costa et al., 2007; Royer et al., 2010). However, in the absence of rates of bacterial production and without any identification and bacterial typing methods it is not possible to further explore these avenues. Overall, k_{DMSPd} values measured in this experiment are in agreement with rates reported from several oceanic and coastal regions (Lizotte et al., 2017), and appeared to be mostly unaffected by the manipulation of pCO_2, at least in the later stages of the experiment. However, as pCO_2 increased throughout the experiment following the initial acidification, it is uncertain that the bacterial $DMSP_d$ uptake would not have been altered further by a constant pH reduction, and if so, to what extent.

Once consumed by bacteria, ^{35}S-DMSP becomes part of an intracellular particulate fraction (Fig. 2.7b) and the fate of the S-moiety is thought to be linked to a “bacterial switch” (Simó, 2001), a regulatory pivot with opposing biogeochemical endpoints that exerts a control on the quantities of DMS ultimately produced through microbial mediation (Reisch et al., 2011). One possible fate for the S-moiety is its assimilation into TCA-insoluble material, most of which are protein operationally defined here as macromolecules (Gonzalez et al., 1999; Kiene et al., 1999). The S-incorporation

efficiency (or yield of macromolecules; Fig. 2.7c) was higher at 1 × pCO_2 as compared to 3 × pCO_2 on days 4 and 6, reaching 10 ± 3 %, while oscillating around 5 % for the rest of the experiment. Despite these two higher average values in the control microcosms, it remains unclear how acidification may specifically impact the assimilatory efficiency of sulfur by microbes seeing as the signal is not comprehensive over the full experiment, thus warranting further studies. The overall low S-assimilation efficiencies, less than 12 %, agree with previous studies suggesting that bacteria may afford to use DMSP solely as a carbon source, once their S requirements are met (Scarratt et al., 2000; Pinhassi et al., 2005; Lizotte et al., 2017). This would induce the switch towards the DMSP-cleavage pathway that produces acrylate used by bacteria as a carbon source, and DMS, which is released back into the medium (Kiene, 1990; Ledyard and Dacey, 1993; Yoch, 2002).

Results show for the first time, with the exception of day 4 when microbial DMS yields averaged 7 ± 4% across treatments, that $DMSP_d$-to-DMS conversion efficiencies were significantly different (Tukey HSD test) between in situ pCO_2 and triple pCO_2 (Fig. 2.7e) for the remainder of the experiment (days 6 to 12). These results suggest that OA may modify the fate of DMSP consumed by microorganisms by reducing the proportion of $DMSP_d$ that is converted into DMS. The significant positive correlation found between microbial yields of DMS and concentrations of DMS ($r_S = 0.65$; $p < 0.001$; $n = 45$), supports this idea and further suggests that in cosmopolitan diatom-dominated systems, OA may impact concentrations of DMS through the alteration of the microbial breakdown of $DMSP_d$. Bacterial ectoenzyme activity has been shown to be particularly sensitive to alterations in $[H^+]$ (Piontek et al., 2010), with potential consequences for the bacterial catabolism of DMSP and removal of DMS. Results from this study have vast implications seeing as even minor changes in the yields of DMS may significantly impact the gross production of DMS by bacteria. Microbial yields of DMS varied extensively during the experiment (Fig 2.7e), from 11 to 68 % (1 × pCO_2), from 8 to 49 % (2 × pCO_2), and from 4 to 29 % (3 × pCO_2). Several of these very high yields, especially in the control pCO_2, are some of the highest estimates reported in the literature, which rarely exceed ~40 % (see compilation table in Lizotte et al. 2017). While 65 % of the variance in net concentrations of DMS may be explained by the variance in yields of DMS in this study, the remaining variation could be related to other sources of DMS, including direct production through phytoplankton species possessing DMSP-lyases, as well as sinks of DMS including bacterial DMS consumption.

While DMS yields varied throughout the experiment, a noteworthy result from this study stems from the significant negative correlation ($r_s = -0.62$; $p < 0.001$; $n = 44$) found between these yields of DMS and the fraction of ^{35}S-$DMSP_d$ consumed by microbes and kept untransformed in the cells after 24 hours (Fig. 2.7d). While it is unclear how acidification may impact this untransformed pool of DMSP directly, with only day 8 exhibiting a significant increase of this untransformed fraction in the 3 × pCO_2 treatment as compared to the 1 × pCO_2 control (Fig. 2.7d), the negative association

between these potential metabolic fates is intriguing. Several studies show that bacteria are able to accumulate DMSP intracellularly over several hours without degrading it (Wolfe, 1996; Kiene et al., 1999; Kiene and Linn, 2000). In these studies, the accumulation of DMSP, much like other organic molecules such as betaines, has been shown to be more rapid in osmotically-stressed cells, suggesting that DMSP can be used as an osmotic solute by heterotrophic bacteria. In the very few ^{35}S-DMSP$_d$ tracer studies reporting on the specific partitioning of DMSP$_d$, about 15–20 % of added DMSP$_d$ was consumed by bacterial cells but not further metabolized even after 24 h of incubation (Kiene and Linn, 2000; Kiene et al., 2000; Tripp et al., 2008). Average fractions of untransformed ^{35}S-DMSP$_d$ in this study varied from 4 to 28 % in the 1 × pCO_2 treatment, from 17 to 36 % in the 2 × pCO_2, and from 12 to 38 % in the 3 × pCO_2 treatment (Fig. 2.7d) suggesting that a large portion of consumed DMSP$_d$ (more than a third on certain days in the acidified treatments) was stored untouched in the cells. While our results do not allow us to firmly conclude on the potential for these relatively large accumulations of DMSP$_d$ to be related to some type of adaptative mechanism in response to pH stress, they certainly warrant future investigation into the underlying metabolic processes responsible for the partitioning of DMSP within bacteria under OA.

2.5. Conclusions

To our knowledge, the results presented in this study provide the first peek into the microbially-mediated fates of DMSP under heightened pCO_2 derived from ^{35}S-DMSP radio-isotopic uptake assays. A natural plankton community sourced from the surface waters of the St-Lawrence estuary during summer 2013 was exposed to three initial pCO_2 targets, corresponding to in situ (775 µatm), double (1850 µatm), and triple pCO_2 (2700 µatm). Over the 12-day microcosm experiment, a mixed phytoplankton population, dominated by several species of diatoms and small unidentified flagellates, bloomed in all treatments resulting in an increase in concentrations of Chl *a* from an initial 1.26 µg L^{-1} to a peak of 20 ± 4 µg L^{-1} by day 6 in the 1 × pCO_2 control. While patterns of Chl *a* concentrations were similar in the 2 × pCO_2 treatment, the magnitude and timing of the biomass accumulation were different in the 3 × pCO_2 treatment, with a maximum of 11 ± 4 µg Chl *a* L^{-1} reached by day 8 of the experiment. Variations in the concentrations of DMSP$_t$ were broadly related to variations in Chl *a* ($r_S = 0.77$; $p < 0.001$; $n = 61$) and highest concentrations of DMSP$_t$ were reached sequentially on day 8 in the 1 × pCO_2 treatment (264 nmol L^{-1}), on day 10 in the 2 × pCO_2 (245 nmol L^{-1}), and on day 12 in the 3 × pCO_2 (192 nmol L^{-1}). Concentrations of DMSP$_d$ fluctuated throughout the experiment (Fig. 2.6b), largely associated with variations in DMSP$_t$ ($r_S = 0.70$; $p < 0.001$; $n = 61$) with no significant differences between pCO_2 treatments suggesting that acidification did not alter the availability of DMSP$_d$ as a substrate for bacteria. The microbial scavenging efficiency of DMSP$_d$ (*k*DMSP$_d$), as determined through ^{35}S-DMSP$_d$ uptake assays, appeared to be mostly unaffected by the acidification treatment, however the metabolic fate of

consumed $DMSP_d$ was impacted by heightened pCO_2. For the first time, results from this study show that, at peak bloom and onward (from day 6 to day 12), the microbial $DMSP_d$-to-DMS conversion efficiency, otherwise known as the DMS yield, was significantly reduced, by 61 %, in the $3 \times pCO_2$ treatment as compared to the control ($1 \times pCO_2$). Furthermore, concentrations of DMS were significantly curtailed under the acidification treatments: averaged over the entire 12-d study period, doubling the pCO_2 resulted in a 15 % decline in mean concentrations of DMS, while tripling the pCO_2 decreased average DMS by 40 % as compared to in situ pCO_2. Not surprisingly, a significant positive correlation was found between microbial yields of DMS and concentrations of DMS ($r_s = 0.65$; $p < 0.001$; $n = 45$), suggesting that the negative impact of OA on pools of DMS is intimately linked with modifications in the microbial partitioning of $DMSP_d$, particularly in diatom-dominated ecosystems. Although ambiguity persists on the specific impact acidification may have on all the many fates of DMSP consumed by bacteria, the negative association between DMS yields and the fraction of ^{35}S-$DMSP_d$ kept untransformed in the cells ($r_s = -0.62$; $p < 0.001$; $n = 44$), points towards the accumulation of DMSP as a potential protective mechanism in the face of heightened $[H^+]$. Further detailed studies, in various coastal and oceanic environments, are needed if the microbial black box is to be fully opened and explored under OA context.

2.6 Acknowledgements

The authors wish to thank the Maurice Lamontagne Institute and their staff for their support during the project. We also wish to acknowledge Rachel Hussherr and Liliane St-Amand, for their precious help over the duration of the experiment. This study was funded by a Team grant from the Fonds de la Recherche du Québec – Nature et Technologies (FRQNT-Équipe-165335), Fisheries and Oceans Canada, and the Canada Research Chair on Ocean Biogeochemistry and Climate. This a contribution to the research programme of Québec-Océan.

Chapitre 3 Experimental assessment of the sensitivity of an estuarine phytoplankton fall bloom to acidification and warming

Résumé

Nous avons étudié l'effet combiné de l'acidification et du réchauffement sur la dynamique de la floraison automnale du phytoplancton dans l'estuaire maritime du Saint-Laurent (EMSL), Canada. Douze mésocosmes de ~2600 L couvrant une large gamme de pH_T (pH sur l'échelle de concentration totale d'ions hydrogène) de 8.0 à 7.2 correspondant à une gamme de pCO_2 de 440 à 2900 µatm et deux températures (in situ et +5 °C) ont été monitorés durant 13 jours, capturant le développement et le déclin d'une prolifération de nanophytoplancton dominée par la diatomée *Skeletonema costatum*. Pendant la phase de croissance, l'augmentation de la pCO_2 n'a influencé ni l'ampleur ni le taux de croissance net de la prolifération nanophytoplanctonique, tandis que l'augmentation de la température de 5 °C a stimulé le taux d'accumulation de chlorophylle *a* (Chl *a*) de 76 % et le taux maximal de production primaire particulaire de 63 %. Pendant la phase de déclin de la floraison, le réchauffement a accéléré la perte de cellules de diatomées, parallèlement à une diminution progressive de l'abondance des picoeucaryotes photosynthétiques et à une prolifération de picocyanobactéries. L'augmentation de la pCO_2 et le réchauffement n'ont pas influencé l'abondance des picoeucaryotes alors que l'abondance des picocyanobactéries a été réduite par l'augmentation de la pCO_2 en combinaison avec le réchauffement dans la dernière phase de l'expérience. La production primaire nette intégrée dans la durée de l'expérience n'a pas été significativement affectée par les traitements de pCO_2 ou de températures. Dans l'ensemble, nos résultats suggèrent que le réchauffement, plutôt que l'acidification, est plus susceptible d'altérer le développement du phytoplancton de l'EMSL dans les années à venir. De futures études examinant un gradient plus large de températures devraient être menées sur une fenêtre saisonnière plus large afin de mieux prédire l'effet potentiel du réchauffement sur le développement des floraisons phytoplanctoniques dans l'EMSL et son impact sur le devenir de la production primaire.

Abstract

We investigated the combined effect of acidification and warming on the dynamics of the phytoplankton fall bloom in the Lower St. Lawrence Estuary (LSLE), Canada. Twelve 2600 L mesocosms were set to initially cover a wide range of pH_T (pH on the total proton scale) from 8.0 to 7.2 corresponding to a range of pCO_2 from 440 to 2900 µatm, and two temperatures (in situ and +5 °C). The 13-day experiment captured the development and decline of a nanophytoplankton bloom dominated by the chain-forming diatom *Skeletonema costatum*. During the development phase of the bloom, increasing pCO_2 influenced neither the magnitude nor the net growth rate of the nanophytoplankton bloom whereas increasing the temperature by 5 °C stimulated the chlorophyll *a* (Chl *a*) growth rate and maximal particulate primary production by 76 % and 63 %, respectively. During the declining phase of the bloom, warming accelerated the loss of diatom cells, paralleled by a gradual decrease in the abundance of photosynthetic picoeukaryotes and a bloom of picocyanobacteria. Increasing pCO_2 and warming did not influence the abundance of picoeukaryotes while picocyanobacteria abundance was reduced by the increase in pCO_2 when combined with warming in the latter phase of the experiment. Over the full duration of the experiment, the time-integrated net primary production was not significantly affected by the pCO_2 treatments or warming. Overall, our results suggest that warming, rather than acidification, is more likely to alter phytoplankton autumnal bloom development in the LSLE in the decades to come. Future studies examining a broader gradient of temperatures should be conducted over a larger seasonal window in order to better constrain the potential effect of warming on the development of blooms in the LSLE and its impact on the fate of primary production.

3.1 Introduction

Anthropogenic emissions have increased atmospheric carbon dioxide (CO_2) concentrations from their pre-industrial value of 280 to 412 ppm in 2017, and concentrations of 850–1370 ppm are expected by the end of the century under the business-as-usual scenario RCP 8.5 (IPCC, 2013). The global ocean has already absorbed about 28 % of these anthropogenic CO_2 emissions (Le Quéré et al., 2015), leading to a global pH decrease of 0.11 units (Gattuso et al., 2015), a phenomenon known as Ocean Acidification (OA). The surface ocean pH is expected to decrease by an additional 0.3–0.4 units under the RCP 8.5 scenario by 2100, and as much as 0.8 units by 2300 (Caldeira and Wickett, 2005; Doney et al., 2009; Feely et al., 2009). The accumulation of anthropogenic CO_2 in the atmosphere also results in an increase in the Earth's heat content that is primarily absorbed by the ocean (Wijffels et al., 2016), leading to an expected rise of sea surface temperatures of 3 to 5 °C by 2100 (IPCC, 2013). Whereas the effect of increasing atmospheric CO_2 partial pressures (pCO_2) on ocean chemistry is relatively well documented, the potential impacts of OA on marine organisms and how their response to OA will be modulated by the concurrent warming of the ocean surface waters are still the subject of much debate (Boyd and Hutchins, 2012; Gattuso et al., 2013).

Over the last decade, there has been increasing interest in the potential effects of OA on marine organisms (Kroeker et al., 2013). The first experiments were primarily conducted on single phytoplankton species (reviewed in Riebesell and Tortell, 2011), but subsequent mesocosm experiments highlighted the impact of OA on the structure and productivity of complex plankton assemblages (Riebesell et al., 2007, 2013). Due to their widely different initial and experimental conditions, these ecosystem-level experiments generated contrasting results (Schulz et al., 2017) but some general patterns nevertheless emerged. For example, diatoms generally benefit from higher pCO_2 through stimulated photosynthesis and growth rates since the increase in CO_2 concentrations compensates for the low affinity of RuBisCO towards CO_2 (Giordano et al., 2005; Gao and Campbell, 2014). Although most phytoplankton species have developed carbon concentration mechanisms (CCM) to compensate for the low affinity of RuBisCO towards CO_2, CCM efficiencies differ between taxa, rendering predictions of the impact of a CO_2 rise on the downregulation of CCM rather difficult (Raven et al., 2014). For example, some studies unexpectedly reported no significant or very modest stimulation of primary production under elevated CO_2 concentrations (Engel et al., 2005; Eberlein et al., 2017). OA can ultimately affect the structure of phytoplankton assemblages. Small cells such as photosynthetic picoeukaryotes can benefit directly from an increase in pCO_2 as CO_2 can passively diffuse through their boundary layer (Beardall et al., 2014), and the smallest organisms within this group could benefit most from the increase (Brussaard et al., 2013). Accordingly, OA experiments have typically favoured smaller

phytoplankton cells (Yoshimura et al., 2010; Brussaard et al., 2013; Morán et al., 2015), although the proliferation of larger cells has also been reported (Tortell et al., 2002). Hence, generic predictions of phytoplankton community responses to OA are challenging.

Few recent studies have investigated the combined effects of OA and warming on natural phytoplankton assemblages (Hare et al., 2007; Feng et al., 2009; Maugendre et al., 2015; Paul et al., 2015, 2016). Laboratory experiments have shown that OA and warming could together increase photosynthetic rates, but at the expense of species richness, the reduction of diversity predominantly imputable to warming (Tatters et al., 2013). Results of an experiment conducted with a natural planktonic community from the Mediterranean Sea showed no effect of a combined warming and decrease in pH on primary production, but higher picocyanobacteria abundances were observed in the warmer treatment (Maugendre et al., 2015). Shipboard microcosm incubations conducted in the northern South China Sea displayed higher phytoplankton biomass, daytime primary productivity and dark community respiration under warmer conditions, but these positive responses were cancelled at low pH (Gao et al., 2017). In contrast, a mesocosm experiment carried out with a fall planktonic community from the western Baltic Sea led to a decrease in phytoplankton biomass under warming alone, but combined warming and increased pCO_2 led to an increase in biomass (Sommer et al., 2015). Results from experiments where the impacts of pCO_2 and temperature are investigated individually may be misleading as multiple stressors can interact antagonistically or synergistically, sometimes in a nonlinear, unexpected fashion (Todgham and Stillman, 2013; Boyd et al., 2015; Riebesell and Gattuso, 2015; Gunderson et al., 2016).

The Lower St. Lawrence Estuary (LSLE) is a large (9350 km^2) segment of the greater St. Lawrence Estuary (d'Anglejan, 1990). From June to September, the LSLE is characterized by a dynamic succession in the phytoplankton community, mostly driven by changes in light and nutrient availability through variations in the intensity of vertical mixing (Levasseur et al., 1984). The spring and fall blooms are mostly comprised of diatoms, with simultaneous nitrate and silicic acid exhaustion ultimately limiting primary production (Levasseur et al., 1987; Roy et al., 1996). How OA and warming may affect these blooms and primary production has never been investigated in the LSLE. The OA problem is complex in estuarine and coastal waters where freshwater runoff, tidal mixing, and high biological activity contribute to variations in pCO_2 and pH on different time scales (Duarte et al., 2013). The surface mixed-layer pCO_2 in the LSLE varies spatially from 139 to 548 µatm and is strongly modulated by biological productivity (Dinauer and Mucci, 2017). Surface pH_T has been shown to vary from 7.85 to 7.93 in a single tidal cycle in the LSLE, nearly as much as the world's oceans have experienced in response to anthropogenic CO_2 uptake over the last century (Caldeira and Wickett, 2005; Mucci et al., 2017).

The main objective of this study was to experimentally assess the sensitivity of the LSLE phytoplankton fall assemblage to a large pCO_2 gradient at two temperatures (in situ and +5 °C). Whether lower trophic-level microorganisms thriving in a highly variable environment will show higher resistance or resilience to future anthropogenic forcings is still a matter of speculation.

3.2 Materials and methods

3.2.1 Mesocosm setup

The mesocosm system consists of two thermostated full-size shipping containers each holding six 2600 L mesocosms (Aquabiotech Inc., Québec, Canada). The mesocosms are cylindrical (2.67 m × 1.40 m) with a cone-shaped bottom (Fig. 3.1), within which mixing is achieved using a propeller fixed near the top of the enclosure. The mesocosms have opaque walls and all lie on the same plane level as not to shade each other. Light penetrates the mesocosms only through a sealed Plexiglas circular cover. The cover allows the transmission of 90 % of photosynthetically active radiation (PAR; 400–700 nm), 85–90 % of UVA (315–400 nm), and 50–85 % of solar UVB (280–315 nm).

The mesocosms are equipped with individual, independent temperature probes (AQBT-Temperature sensor, accuracy ± 0.2 °C). Temperature in the mesocosms was measured every 15 minutes during the experiment, and the control system triggered either a resistance heater (Process Technology TTA1.8215) located near the middle of the mesocosm or a pump-activated glycol refrigeration system to maintain the set temperature. The pH in each mesocosm was monitored every 15 minutes using Hach® PD1P1 probes (± 0.02 pH units) connected to Hach® SC200 controllers, and positive deviations from the target values activated peristaltic pumps linked to a reservoir of artificial seawater equilibrated with pure CO_2 prior to the onset of the experiment. This system maintained the pH of the seawater in the mesocosms within ± 0.02 pH units of the targeted values by lowering the pH during autotrophic growth but could not increase the pH during bloom senescence when the pCO_2 rose and pH decreased. Volume of acidified water added to the mesocosms was recorded throughout the experiment and did not amount to more than 2 % of the total volume of the mesocosm over the duration of the experiment.

3.2.2 Setting

The water was pumped from 5 m depth near Rimouski harbour (48° 28' 39.9" N, 68° 31' 03.0" W) on the 27th of September 2014 (indicated as day -5), and transported via a tank truck to the Station Aquicole of UQAR-ISMER. The experiment lasted until the 15th of October 2014 (day13).

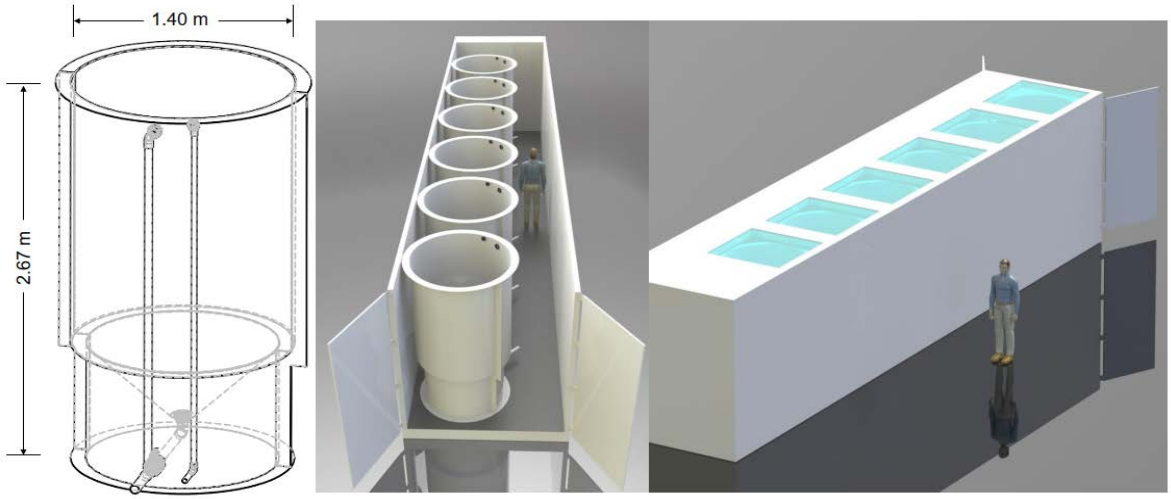

Figure 3.1 Schematic drawing including mesocosm dimensions and placement within the containers (Aquabiotech Inc, Québec, Canada). The whole setup includes a second container holding 6 more mesocosms not depicted here.

In situ conditions were: salinity = 26.52, temperature = 10 °C, nitrate (NO_3^-) = 12.8 ± 0.6 µmol L^{-1}, silicic acid ($Si(OH)_4$) = 16 ± 2 µmol L^{-1}, and soluble reactive phosphate (SRP) = 1.4 ± 0.3 µmol L^{-1}. On day -5, the water was filtered through a 250 µm mesh while simultaneously filling the 12 mesocosm tanks by gravity with a custom made 'octopus' tubing system. The initial pCO_2 was 623 ± 7 µatm and the in situ temperature of 10 °C was maintained in the twelve mesocosms for the first 24 h (day -4). After that period, the six mesocosms in one container were maintained at 10 °C while temperature was gradually increased to 15 °C during day -3 in the six mesocosms of the other container. To avoid subjecting the planktonic communities to excessive stress due to sudden changes in temperature and pH while setting the experiment, the mesocosms were left to acclimatize on day -2 before acidification was carried out over day -1. One mesocosm from each temperature-controlled container was not pH-controlled to assess the community response to the freely fluctuating pH. These two mesocosms were labelled "Drifters" as the initial in situ pH was allowed to fluctuate over time with the development of the phytoplankton bloom. The other mesocosms were set to cover a range of pH_T of ~8.0 to ~7.2 corresponding to a pCO_2 gradient of ~440 to ~2900 µatm after acidification was carried out. To attain initial targeted pH, CO_2-saturated artificial seawater was added to the mesocosms that needed a pH reduction while mesocosms M2 (8.0), M4 (7.8), M6 (Drifter), M9 (8.0), M11 (Drifter) and M12 (7.8) were openly mixed to allow the degassing of the supersaturated CO_2. Once the mesocosms had reached their target pH, the automatic system controlled the sporadic addition of CO_2-saturated water to prevent the pH from rising. Only the Drifters were not controlled throughout the experiment. Incident light was variable during our experiment, with only few sunny days (Fig. 3.2).

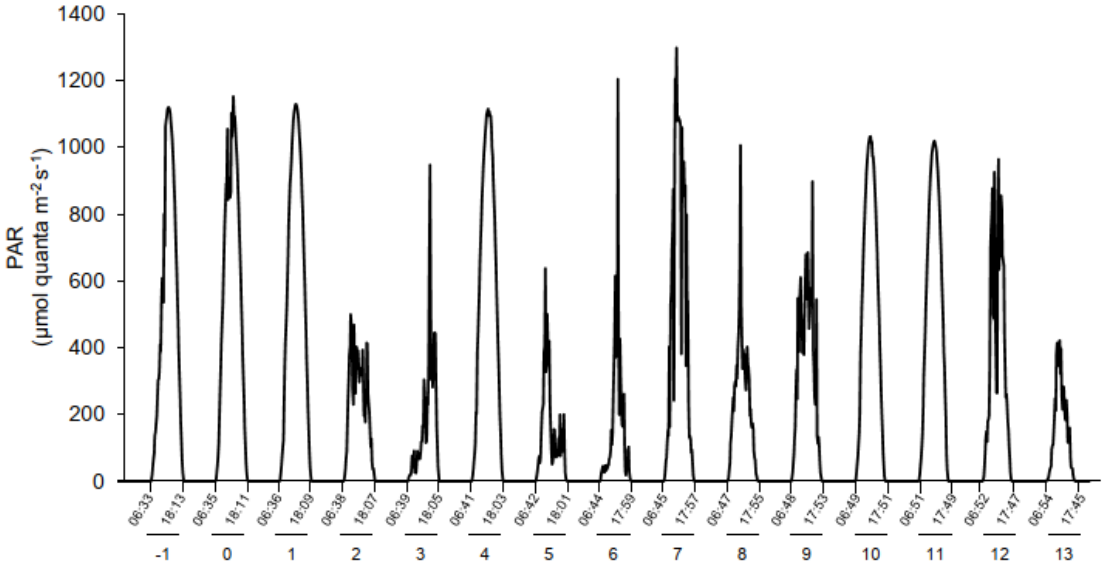

Figure 3.2 Changes in incident photosynthetic active radiation (PAR) at the top of the mesocosms level during the experiment as measurement by a Satlantic HyperOCR hyperspectral radiometer and integrated into the 400–700 nm range. Local sunrise and sunset times (EDT) are indicated with the corresponding days of the experiment.

3.2.3 Seawater analysis

The mesocosms were sampled between 05:00 and 08:00 a.m. every day. Seawater for carbonate chemistry, nutrients, and primary production were collected directly from the mesocosms as close to sunrise as possible. Seawater was also collected in 20 L carboys for the determination of chlorophyll *a* (Chl *a*), taxonomy, and other variables. The total volume sampled every day was 24 L or less. Samples for salinity were taken from the artificial seawater tanks and in the mesocosms on day -3, 3 and 13. The samples were collected in 250 mL plastic bottles and stored in the dark until analysis was performed using a Guildline Autosal 8400B Salinometer during the following months.

3.2.3.1 Carbonate chemistry

Carbonate chemistry parameters were determined using methods described in Mucci et al. (2017). Briefly, water samples for pH (every day) and total alkalinity (TA, every 3–4 days) measurements were, respectively, transferred from the mesocosms to 125 mL plastic bottles without headspace and 250 mL glass bottles. A few crystals of $HgCl_2$ were added to the glass bottles before sealing them with a ground-glass stopper and Apiezon® Type-M high-vacuum grease. The pH was determined within hours of collection, after thermal equilibration at 25.0 ± 0.1 °C, using a Hewlett-

Packard UV-Visible diode array spectrophotometer (HP-8453A) and a 5 cm quartz cell with phenol red (PR; Robert-Baldo et al., 1985) and *m*-cresol purple (mCP; Clayton and Byrne, 1993) as indicators. Measurements were carried out at the wavelength of maximum absorbance of the protonated (HL) and deprotonated (L) indicators. Comparable measurements were carried out using a TRIS buffer prepared at a practical salinity of 25 before and after each set of daily measurements (Millero, 1986).

The pH on the total proton concentration scale (pH_T) of the buffer solutions and samples at 25 °C was calculated according to the equation of Byrne (1987), using the salinity of each sample and the HSO_4^- association constants given by Dickson (1990). The TA was determined on site within one day of sampling by open-cell automated potentiometric titration (Titrilab 865, Radiometer®) with a pH combination electrode (pHC2001, Red Rod®) and a dilute (0.025 N) HCl titrant solution. The titrant was calibrated using Certified Reference Materials (CRM Batch#94, provided by A. G. Dickson, Scripps Institute of Oceanography, La Jolla, USA). The average relative error, based on the average relative standard deviation on replicate standard and sample analyses, was better than 0.15 %. The carbonate chemistry parameters at in situ temperature were then calculated using the computed pH_T at 25 °C in combination with the measured TA using CO_2SYS (Pierrot et al., 2006) and the carbonic acid dissociation constants of Cai and Wang (1998).

3.2.3.2 Nutrients

Samples for NO_3^-, $Si(OH)_4$, and SRP analyses were collected directly from the mesocosms every day, filtered through Whatman GF/F filters and stored at -20 °C in acid washed polyethylene tubes until analysis by a Bran and Luebbe Autoanalyzer III using the colorimetric methods described by Hansen and Koroleff (2007). The analytical detection limit was 0.03 µmol L^{-1} for NO_3^- plus nitrite (NO_2^-), 0.02 µmol L^{-1} for NO_2^-, 0.1 µmol L^{-1} for $Si(OH)_4$, and 0.05 µmol L^{-1} for SRP.

3.2.3.3 Plankton biomass, composition and enumeration

Duplicate subsamples (100 mL) for Chl *a* determination, used as a proxy for biomass, were filtered onto Whatman GF/F filters. Chl *a* concentrations were measured using a 10-AU Turner Designs fluorometer, following a 24 h extraction in 90 % acetone at 4 °C in the dark without grinding (acidification method: Parsons et al., 1984). The analytical detection limit for Chl *a* was 0.05 µg L^{-1}.

Pico- (0.2–2 µm) and nanophytoplankton (2–20 µm) cell abundances were determined daily by flow cytometry. Sterile cryogenic polypropylene vials were filled with 4.95 mL of seawater to which 50 µL of glutaraldehyde Grade I (final concentration = 0.1 %, Sigma Aldrich; Marie et al., 2005) were

added. Duplicate samples were flash frozen in liquid nitrogen after standing 15 minutes at room temperature in the dark. These samples were then stored at -80 °C until analysis. After thawing to ambient temperature, samples were analyzed using a FACS Calibur flow cytometer (Becton Dickinson) equipped with a 488 nm argon laser. The abundances of nanophytoplankton and picophytoplankton, which includes photosynthetic picoeukaryotes and picocyanobacteria, were determined by their autofluorescence characteristics and size (Marie et al., 2005). The biomass accumulation and nanophytoplankton growth rates were calculated by the following equation:

$$\mu = \ln (N_2/N_1) / (t_2-t_1) \quad (3.1)$$

where N_1 and N_2 are the biomass or cell concentrations at given times t_1 and t_2, respectively.

Microscopic identification and enumeration for eukaryotic cells larger than 2 µm was conducted on samples taken from each mesocosm on three days: day -4, the day when maximum Chl *a* was attained in each mesocosm, and day 13. Samples of 250 mL were collected and preserved with acidic Lugol solution (Parsons et al., 1984), then stored in the dark until analysis. Cell identification was carried out at the lowest possible taxonomic rank using an inverted microscope (Zeiss Axiovert 10) in accordance with Lund et al. (1958). The main taxonomic references used to identify the phytoplankton were Tomas (1997) and Bérard-Therriault et al. (1999).

3.2.3.4 Primary production

Primary production was determined daily using the ^{14}C-fixation incubation method (Knap et al., 1996; Ferland et al., 2011). One clear and one dark 250 mL polycarbonate bottle were filled from each mesocosm at dawn and spiked with 250 µL of $NaH^{14}CO_3$ (80 µCi mL^{-1}). One hundred µL of 3-(3,4-dichlorophenyl)-1,1-dimethylurea (DCMU) (0.02 mol L^{-1}) was added to the dark bottles to prevent active fixation of ^{14}C by phytoplankton (Legendre et al., 1983). The total amount of radioisotope in each bottle was determined by immediately pipetting 50 µL subsamples into a 20 mL scintillation vial containing 10 mL of scintillation cocktail (Ecolume™) and 50 µL of ethanolamine (Sigma). Bottles were placed in separate incubators, at either 10 °C or 15 °C, under reduced (30 %) ambient light for 24 h, which corresponds to the light transmittance at mid-mesocosm depth.

At the end of the incubation periods, 3 mL were transferred to a scintillation vial for determination of the total primary production (P_T), 3 mL were filtered through a syringe filter (GD/X 0.7 µm) to estimate daily photosynthetic carbon fixation released in the dissolved organic carbon pool (P_D). The remaining volume was filtered onto a Whatman GF/F filter to measure the particulate primary

production (P_P). Vials containing the P_T and P_D samples were acidified with 500 µL of HCl 6 N, allowed to sit for 3 h under a fume hood, then neutralized with 500 µL of NaOH 6 N. The vials containing the filters were acidified with 100 µL of 0.05 N HCl and left to fume for 12 h. Fifteen mL of scintillation cocktail were added to the vials and they were stored pending analysis using a Tri-Carb 4910TR liquid scintillation counter (PerkinElmer). Rates of carbon fixation into particulate and dissolved organic matter were calculated according to Knap et al. (1996) using the dissolved inorganic carbon concentration computed for each mesocosm at the beginning of the daily incubations and multiplied by a factor of 1.05 to correct for the lower uptake of ^{14}C compared to ^{12}C.

3.2.4 Statistical analyses

All statistical analyses were performed using R (nlme package). A general least squares (gls) model approach was used to test the linear effects of the two treatments (temperature, pCO_2), and of their interactions on the measured variables (Paul et al., 2016; Hussherr et al., 2017). The analysis was conducted independently on two different time periods: Phase I (day 0 to day of maximum Chl *a* concentration) was calculated individually for each mesocosm, whereas Phase II (day after maximum Chl *a* concentrations) corresponded to the declining phase of the bloom (Table 3.1). Averages (or time-integration in the case of primary production) of the response variables were calculated separately over the two phases and were plotted against pCO_2. Separate regressions were performed with pCO_2 as the continuous factor for each temperature when a temperature effect or interaction with pCO_2 was detected in the gls model. Otherwise, the model included data from both temperatures and the interaction with pCO_2. Normality of the residuals was determined using a Shapiro-Wilk test ($p > 0.05$) and data were transformed (natural logarithm or square root) if required. The gradient approach, instead of treatment replication, is particularly suitable when few experimental units are available such as in large volume mesocosm experiments (Havenhand et al., 2010; Kreyling et al., 2014). In addition, squared Pearson's correlation coefficients (r^2) with a significance level of 0.05 were used to evaluate correlations between key variables.

Table 3.1 Day of maximum Chl *a* concentration, the associated average pH_T (total hydrogen ion concentration scale), and average pCO_2 over each individually defined phase. Phase I is defined from day 0 until day of maximum Chl *a* for each mesocosm, while Phase II is defined from the day after maximum Chl *a* until day 13. Average temperature over day 0 to day 13 is also presented for each mesocosm. Average values are presented with ± standard errors.

		Phase I		Phase II		Day 0–13
Mesocosm	Day of max Chl *a*	pH_T	pCO_2 (µatm)	pH_T	pCO_2 (µatm)	Temperature (°C)
M1 (7.4 – 10 ℃)	4	7.32 ± 0.01	2231 ± 25	7.28 ± 0.02	2437 ± 92	10.06 ± 0.01
M2 (8.0 – 10 ℃)	4	7.84 ± 0.01	628 ± 16	7.74 ± 0.03	814 ± 65	10.00 ± 0.01
M3 (7.6 – 10 ℃)	7	7.54 ± 0.01	1294 ± 18	7.48 ± 0.02	1503 ± 64	10.07 ± 0.01
M4 (7.8 – 10 ℃)	4	7.71 ± 0.01	868 ± 13	7.66 ± 0.01	976 ± 29	10.04 ± 0.01
M5 (7.2 – 10 ℃)	7	7.17 ± 0.01	3122 ± 35	7.15 ± 0.01	3315 ± 94	10.03 ± 0.01
M6 (Drifter – 10 ℃)	4	7.93 ± 0.01	503 ± 15	8.22 ± 0.03	251 ± 25	10.02 ± 0.01
M7 (7.4 – 15 ℃)	4	7.38 ± 0.01	2004 ± 44	7.31 ± 0.02	2399 ± 120	15.00 ± 0.01
M8 (7.2 – 15 ℃)	2	7.21 ± 0.01	2961 ± 58	7.18 ± 0.01	3179 ± 74	15.01 ± 0.01
M9 (8.0 – 15 ℃)	2	7.85 ± 0.01	454 ± 13	7.79 ± 0.02	545 ± 25	15.03 ± 0.01
M10 (7.6 – 15 ℃)	2	7.54 ± 0.01	1364 ± 22	7.44 ± 0.02	1746 ± 106	14.94 ± 0.01
M11 (Drifter – 15 ℃)	1	8.07 ± 0.01	388 ± 90	8.59 ± 0.02	84 ± 7	14.96 ± 0.02
M12 (7.8 – 15 ℃)	2	7.67 ± 0.01	1001 ± 31	7.59 ± 0.01	1215 ± 44	14.98 ± 0.02

3.3. Results

3.3.1 Seawater chemistry

Water salinity was 26.52 ± 0.03 on day -4 in all mesocosms and remained constant throughout the experiment, averaging 26.54 ± 0.02 on day 13. The TA was practically invariant in the mesocosms, averaging 2057 ± 2 µmol kg_{sw}^{-1} on day -4 and 2058 ± 2 µmol kg_{sw}^{-1} on day 13. Following the filling of the mesocosms, the pH_T in all mesocosms decreased from an average of 7.84 to 7.53.

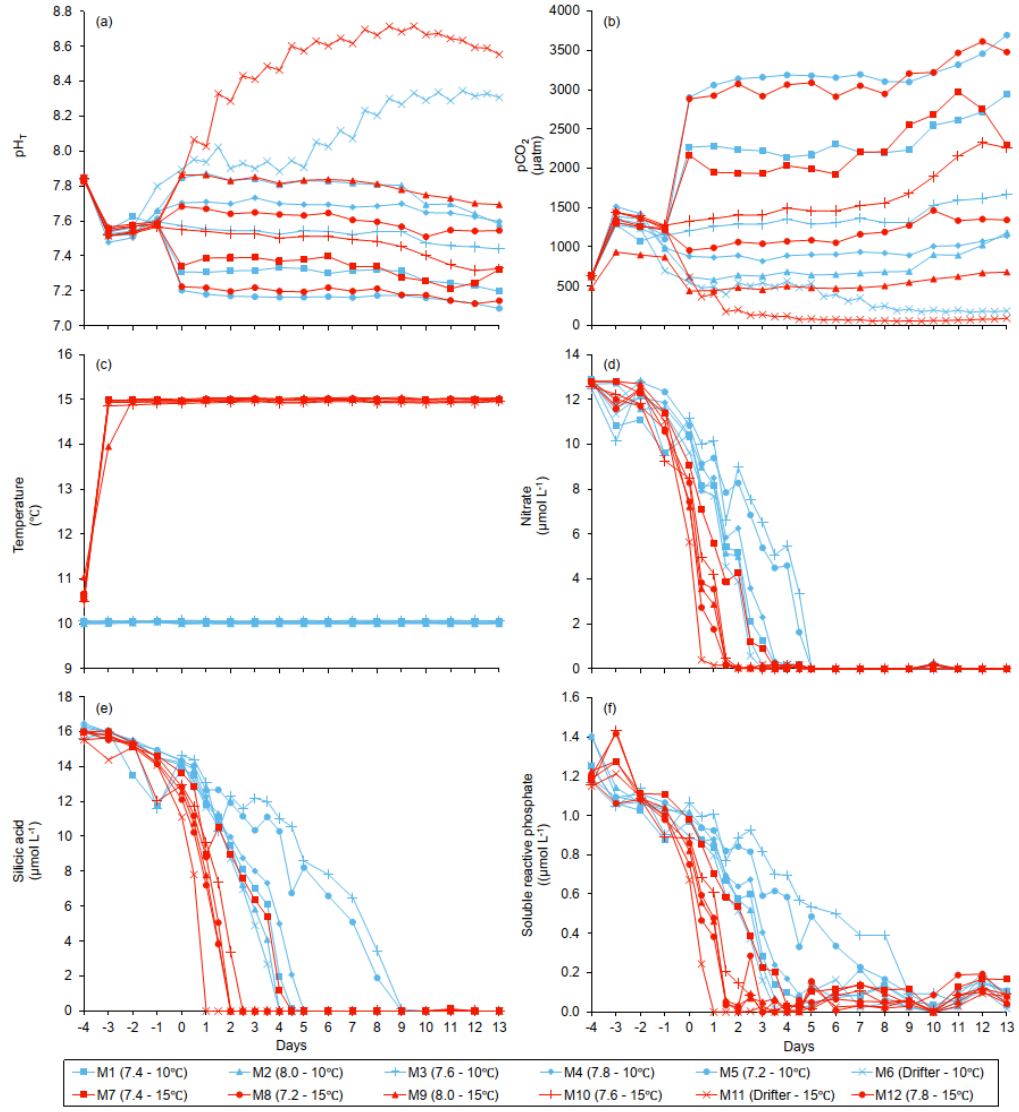

Figure 3.3 Temporal variations over the course of the experiment for: (a) pH_T, (b) pCO_2, (c) temperature, (d) nitrate, (e) silicic acid, (f) soluble reactive phosphate. For symbol attribution to treatments, see legend.

Throughout the rest of the experiment after treatments were applied, the pH remained relatively stable in the pH-controlled treatments, but decreased slightly during Phase II by an average of -0.14 ± 0.07 units relative to the target pH_T (Fig. 3.3a). Given a constant TA, pH variations were accompanied by variations in pCO_2, from an average of 1340 ± 150 µatm on day -3, and ranging from 564 to 2902 µatm at 10 °C, and from 363 to 2884 µatm at 15 °C on day 0 following the acidification (Fig. 3.3b; Table 3.1). The pH_T in the Drifters (M6 and M11) increased from 7.896 and 7.862 on day 0 at 10 °C and 15 °C, respectively, to 8.307 and 8.554 on day 13, reflecting the balance between CO_2 uptake and metabolic CO_2 production over the duration of the experiment.

3.3.2 Dissolved inorganic nutrient concentrations

Nutrient concentrations averaged 9.1 ± 0.5 µmol L^{-1} for NO_3^-, 13.4 ± 0.3 µmol L^{-1} for $Si(OH)_4$, and 0.91 ± 0.03 µmol L^{-1} for SRP on day 0 (Fig. 3.3d–f). Within individual mesocosms, concentrations of nitrate, silicic acid and soluble reactive phosphate displayed similar temporal patterns following the development of the phytoplankton bloom. Overall, NO_3^- depletion was reached within 5 days in all mesocosms at 10 °C, except for the Drifter which became nutrient-deplete by day 3. Nutrient depletion was reached slightly earlier within the 15 °C mesocosms, all of them displaying exhaustion within 3 days of the experiment. Accordingly, bloom development and primary production within each mesocosm were eventually limited by the supply of nutrients, irrespective of the temperature or pH treatment. Likewise, $Si(OH)_4$ fell below the detection limit between day 1 and 5 in all mesocosms except for those whose pH_T was set at 7.2 and 7.6 at 10 °C (M5 and M3) and in which $Si(OH)_4$ depletion occurred on day 9. Variations in SRP concentrations followed closely those of NO_3^- in all mesocosms except again for those set at pH 7.2 and 7.6 in which undetectable values were reached on day 9.

3.3.3 Phytoplankton biomass

Chl *a* concentrations were below 1 µg L^{-1} just after the filling of the mesocosms, and averaged 5.9 ± 0.6 µg L^{-1} on day 0 (Fig. 3.4a). They then quickly increased to reach maximum concentrations around 27 ± 2 µg L^{-1} on day 3 ± 2, and decreased progressively until the end of the experiment, reaching 11 ± 1 µg L^{-1} and 2.4 ± 0.2 µg L^{-1} at 10 °C and 15 °C on day 13. During Phase I, results from the gls model show no significant relationships between the mean Chl *a* concentrations and pCO_2, temperature, and the interaction of the two factors (Fig. 3.4b; Table 3.2). During this phase, the accumulation rate of Chl *a* was positively affected by temperature, increasing by ~76 %, but was not affected by the pCO_2 gradient at either temperature (Fig. 3.5a; Table 3.3). The maximum Chl *a* concentrations reached during the bloom were not affected by the two treatments (Fig. 3.5b; Table 3.3). During Phase II, we observed no significant effect of pCO_2, temperature, and the

interaction of those factors on the mean Chl *a* concentrations following the depletion of NO_3^- (Fig. 3.4c; Table 3.4).

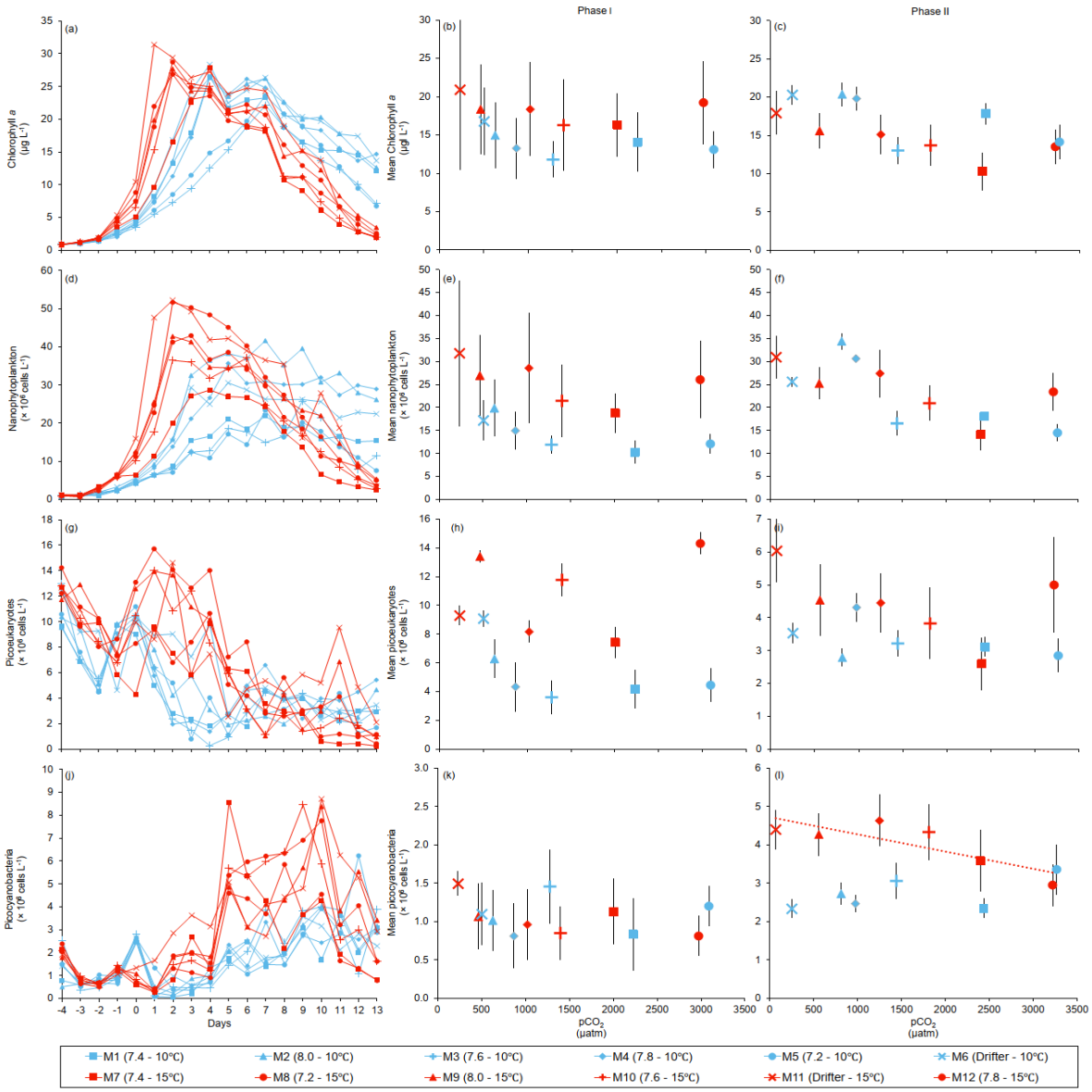

Figure 3.4 Temporal variations, and averages ± SE during Phase I (day 0 to day of maximum Chl *a* concentration) and Phase II (day after maximum Chl *a* concentration to day 13) for: (a-c) chlorophyll *a*, (d-f) nanophytoplankton, (g-i) picoeukaryotes, (j-l) picocyanobacteria. For symbol attribution to treatments, see legend.

Table 3.2 Results of the generalized least squares models (gls) tests for the effects of temperature. pCO_2. and their interaction during Phase I (day 0 to day of maximum Chl *a* concentration). Separate analysis with pCO_2 as a continuous factor were performed when temperature had a significant effect. Chl *a* concentration, nanophytoplankton abundance, picoeukaryote abundance, picocyanobacteria abundance, particulate and dissolved primary production, and Chl *a*-normalized particulate and dissolved primary production. Significant results are in bold. ***p < 0.05**.

Response Variable	Factor	df	t-value	p-value
Mean Chl *a* concentration ($\mu g\ L^{-1}$)	Temperature	8	2.004	0.080
	pCO_2	8	-0.464	0.655
	pCO_2 x Temperature	8	0.244	0.813
Mean nanophytoplankton abundance ($\times 10^6$ cells L^{-1})	Temperature	8	**2.725**	**0.026***
	pCO_2 (10°C)	4	-2.285	0.084
	pCO_2 (15°C)	4	-1.191	0.299
Mean picoeukaryote abundance ($\times 10^6$ cells L^{-1})	Temperature	8	1.056	0.322
	pCO_2	8	-1.159	0.280
	pCO_2 x Temperature	8	1.125	0.293
Mean picocyanobacteria abundance ($\times 10^6$ cells L^{-1})	Temperature	8	0.891	0.399
	pCO_2	8	0.991	0.351
	pCO_2 x Temperature	8	-1.166	0.277
Particulate primary production ($\mu mol\ C\ L^{-1}$)	Temperature	8	-0.124	0.905
	pCO_2	8	-1.011	0.342
	pCO_2 x Temperature	8	0.867	0.411
Dissolved primary production ($\mu mol\ C\ L^{-1}$)	Temperature	8	-1.429	0.191
	pCO_2	8	-0.569	0.585
	pCO_2 x Temperature	8	0.723	0.490
Chl *a*-normalized particulate primary production ($\mu mol\ C\ (\mu g\ Chl\ a)^{-1}\ d^{-1}$)	Temperature	8	1.689	0.130
	pCO_2	8	0.107	0.918
	pCO_2 x Temperature	8	-0.381	0.713
Chl *a*-normalized dissolved primary production ($\mu mol\ C\ (\mu g\ Chl\ a)^{-1}\ d^{-1}$)	Temperature	8	-1.046	0.326
	pCO_2	8	-0.381	0.713
	pCO_2 x Temperature	8	0.449	0.665

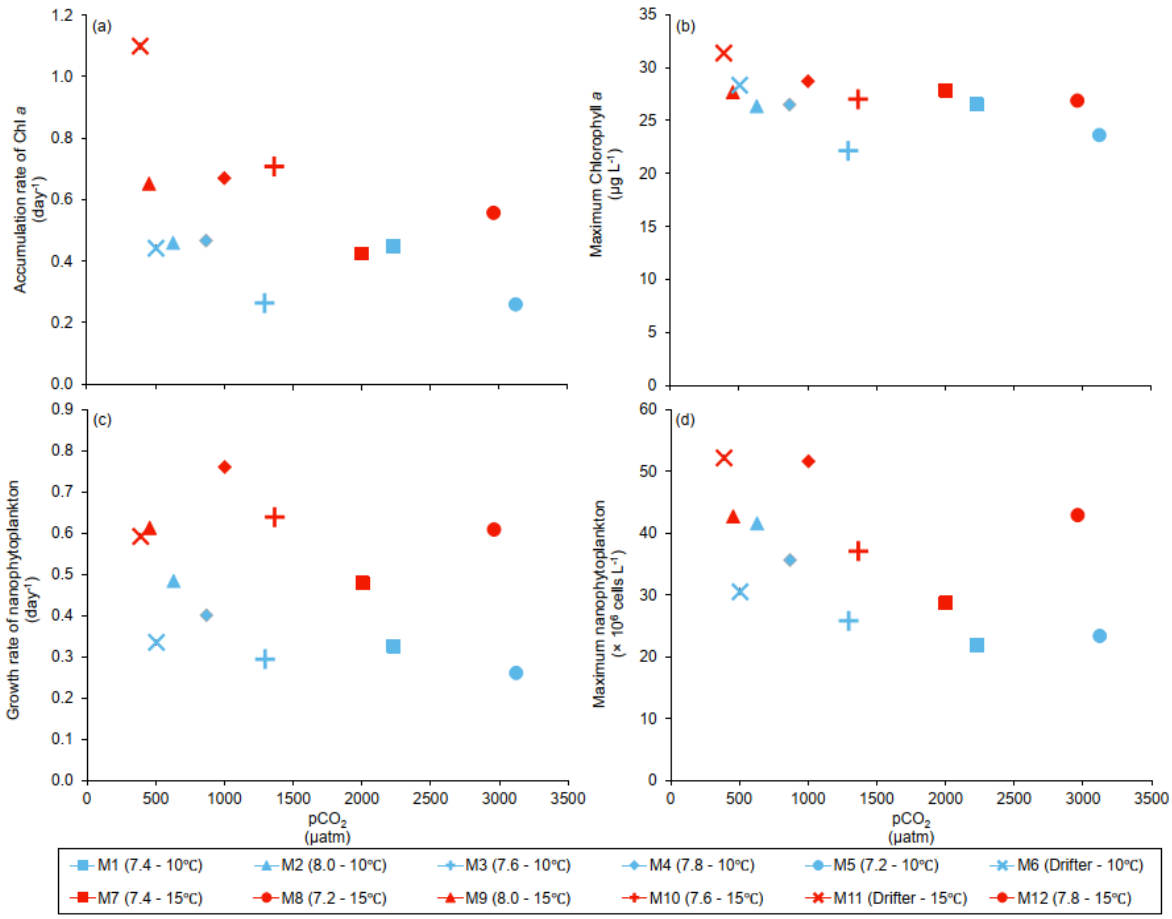

Figure 3.5 (a) Accumulation rate of Chl *a* (day 0 to maximum Chl *a* concentration), (b) maximum Chl *a* concentrations, (c) growth rate of nanophytoplankton (day 0 to maximum nanophytoplankton abundance), and (d) maximum nanophytoplankton abundance during the experiment. For symbol attribution to treatments, see legends.

Table 3.3 Results of the generalized least squares models (gls) tests for the effects of temperature, pCO_2 and their interaction. Separate analysis with pCO_2 as a continuous factor were performed when temperature had a significant effect. Accumulation rate of Chl *a* (day 0 to maximum Chl *a* concentration), maximum Chl *a* concentration, growth rate of nanophytoplankton (day 0 to maximum nanophytoplankton abundance), and maximum nanophytoplankton abundance. Significant results are in bold. ***p < 0.05**.

Response Variable	Factor	df	t-value	p-value
Accumulation rate of Chl *a* (day^{-1})	Temperature	8	**2.679**	**0.028***
	pCO_2 (10 °C)	4	-1.476	0.214
	pCO_2 (15 °C)	4	-1.759	0.154
Maximum Chl *a* concentration ($\mu g\ L^{-1}$)	Temperature	8	1.305	0.228
	pCO_2	8	-0.387	0.709
	pCO_2 × Temperature	8	0.022	0.983
Growth rate of nanophytoplankton (day^{-1})	Temperature	8	**2.534**	**0.035***
	pCO_2 (10 °C)	4	-0.882	0.403
	pCO_2 (15 °C)	4	0.601	0.564
Maximum nanophytoplankton abundance ($\times 10^6$ cells L^{-1})	Temperature	8	1.380	0.205
	pCO_2	8	-0.735	0.484
	pCO_2 × Temperature	8	0.302	0.770

Table 3.4 Results of the generalized least squares models (gls) tests for the effects of temperature, pCO_2, and their interaction during Phase II (day after maximum Chl *a* to day 13). Separate analysis with pCO_2 as a continuous factor were performed when temperature had a significant effect. Chl *a* concentration, nanophytoplankton abundance, picoeukaryote abundance, picocyanobacteria abundance, particulate and dissolved primary production, and Chl *a*-normalized particulate and dissolved primary production. Significant results are in bold. ***p < 0.05, **p < 0.01, ***p < 0.001.**

Response Variable	Factor	df	t-value	p-value
Mean Chl *a* concentration ($\mu g\ L^{-1}$)	Temperature	8	-1.539	0.162
	pCO_2	8	0.733	0.484
	pCO_2 x Temperature	8	0.156	0.880
Mean nanophytoplankton abundance ($\times 10^6$ cells L^{-1})	Temperature	8	-0.528	0.612
	pCO_2	8	1.264	0.242
	pCO_2 x Temperature	8	0.699	0.505
Mean picoeukaryotes abundance ($\times 10^6$ cells L^{-1})	Temperature	8	1.628	0.142
	pCO_2	8	0.226	0.827
	pCO_2 x Temperature	8	-0.521	0.617
Mean picocyanobacteria abundance ($\times 10^6$ cells L^{-1})	Temperature	8	**5.983**	**<0,001*****
	pCO_2 (10°C)	4	1.480	0.213
	pCO_2 (15°C)	4	**-3.051**	**0.038***
Particulate primary production ($\mu mol\ C\ L^{-1}$)	Temperature	8	-0.015	0.988
	pCO_2	8	-0.940	0.375
	pCO_2 x Temperature	8	0.460	0.658
Dissolved primary production ($\mu mol\ C\ L^{-1}$)	Temperature	8	1.894	0.095
	pCO_2	8	-1.145	0.285
	pCO_2 x Temperature	8	0.847	0.422
(Log) Chl *a*-normalized particulate primary production ($\mu mol\ C\ (\mu g\ Chl\ a)^{-1}\ d^{-1}$)	Temperature	8	-2.288	0.052
	pCO_2	8	-1.491	0.174
	pCO_2 x Temperature	8	1.105	0.301
(Log) Chl *a*-normalized dissolved primary production ($\mu mol\ C\ (\mu g\ Chl\ a)^{-1}\ d^{-1}$)	Temperature	8	**2.357**	**0.046***
	pCO_2 (10°C)	4	-2.573	0.062
	pCO_2 (15°C)	4	1.345	0.250

3.3.4 Phytoplankton size-class

Nanophytoplankton abundance varied from $8 \pm 1 \times 10^6$ cells L^{-1} on day 0 to an average maximum of $36 \pm 10 \times 10^6$ cells L^{-1} at the peak of the bloom (Fig. 3.4d). At both temperatures, nanophytoplankton abundance increased until at least days 2 or 4 and decreased or remained stable thereafter. The correlation between the nanophytoplankton abundance and Chl *a* ($r^2 = 0.75$, $p < 0.001$, df = 166) suggests that this phytoplankton size class was responsible for most of the biomass build-up throughout the experiment. As observed for the mean Chl *a* concentration, the mean abundance of nanophytoplankton was not significantly affected by the pCO_2 gradient at the two temperatures investigated during Phase I, but showed higher values at 15 °C ($26 \pm 2 \times 10^6$ cells L^{-1}) than at 10 °C ($14 \pm 1 \times 10^6$ cells L^{-1}) (Fig. 3.4e; Table 3.2). Likewise, the growth rate of nanophytoplankton during Phase I was not influenced by the pCO_2 gradient at the two temperatures but was significantly higher in the warm treatment (Fig. 3.5c; Table 3.3). During Phase II, no relationship was found between the mean nanophytoplankton abundance and the pCO_2 gradient, the temperature, and the pCO_2 × temperature interaction (Fig. 3.4f; Table 3.4).

Initial abundance of photosynthetic picoeukaryotes was $10 \pm 2 \times 10^6$ cells L^{-1}, accounting for more than 80 % of total plankton cells in the 0.2–20 µm size fraction. The abundance of this plankton size fraction decreased slightly through Phase I and their number remained relatively stable at $4 \pm 3 \times 10^6$ cells L^{-1} throughout Phase II (Fig. 3.4g). We found no relationship between the abundance of picoeukaryotes and the pCO_2 gradient at the two temperatures investigated during both Phases I and II, and no temperature effect was observed either (Fig. 3.4h–i; Tables 3.2 and 3.4).

Picocyanobacteria exhibited a different pattern than the nanophytoplankton and picoeukaryotes (Fig. 3.4j). Their abundance was initially low ($1.7 \pm 0.3 \times 10^6$ cells L^{-1} on day 0), remained relatively stable during Phase I, and increased rapidly during Phase II, accounting for ~50 % of the total picophytoplankton cell counts toward the end of the experiment. During Phase I, the mean picocyanobacteria abundance was not influenced by the pCO_2 gradient or temperature (Fig. 3.4k; Table 3.2). During Phase II, the mean picocyanobacteria abundance was not significantly affected by pCO_2 at in situ temperature. However, mean picocyanobacteria were higher at 15 °C, with the pCO_2 gradient responsible for a ~33% reduction of picocyanobacteria abundance from the Drifter to the more acidified treatment ($4.4 \pm 0.2 \times 10^6$ cells L^{-1} vs. $3.0 \pm 0.3 \times 10^6$ cells L^{-1}) (Fig. 3.4l; Table 3.4).

3.3.5 Phytoplankton taxonomy

The taxonomic composition of the planktonic assemblage larger than 2 µm was identical in all treatments at the beginning of the experiment, and was mainly composed of the cosmopolitan chain-forming centric diatom *Skeletonema costatum* (*S. costatum*) and the cryptophyte *Plagioselmis prolonga* var. *nordica* (Fig. 3.6). At the peak of the blooms (maximum Chl *a* concentrations), the species composition did not vary between the pCO_2 treatments nor the two temperatures tested.

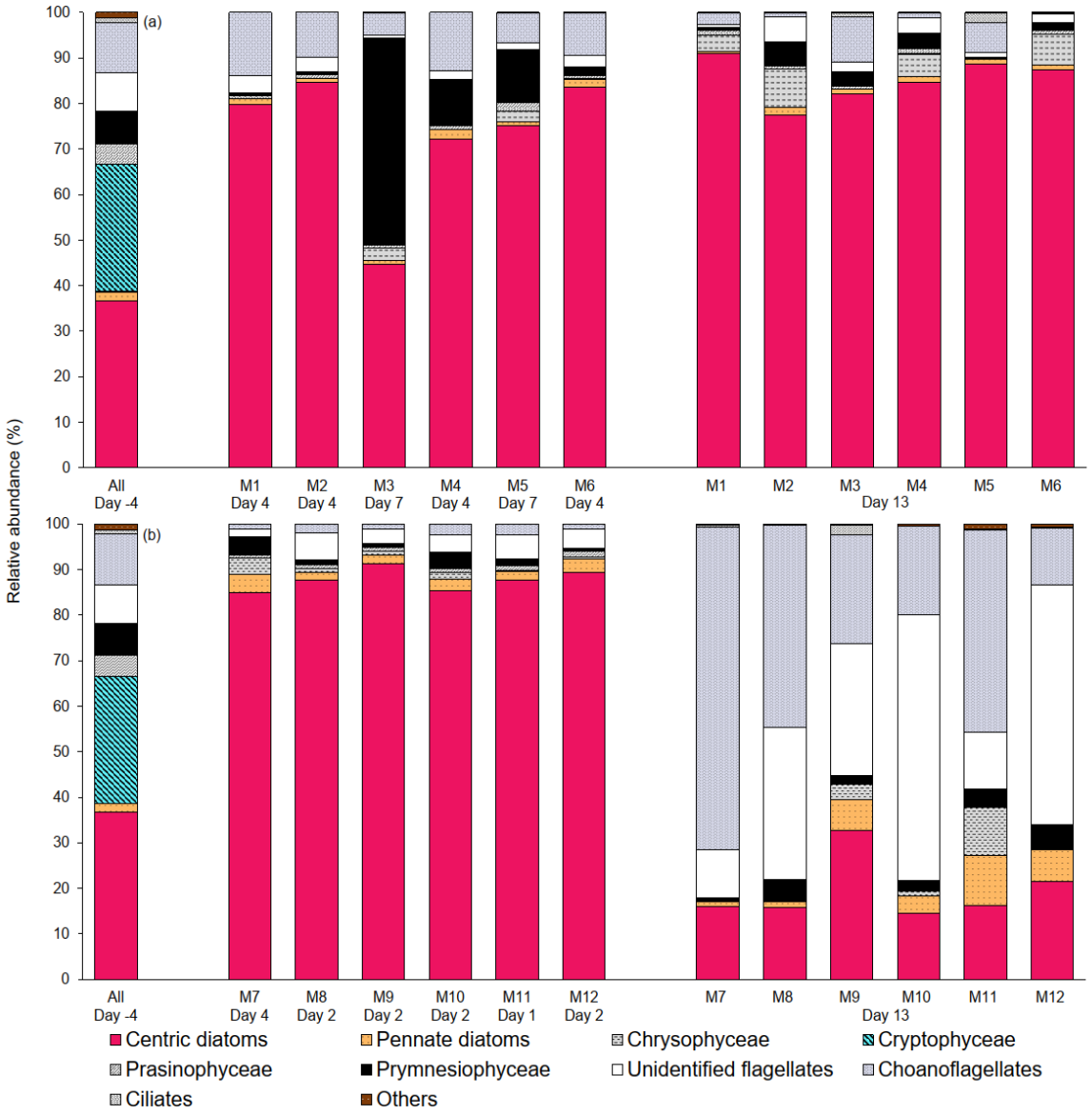

Figure 3.6 Relative abundance of 10 groups of protists at the beginning of the experiment (day -4), on the day of maximum Chl a concentrations in each mesocosm, and at the end of the experiment (day 13) for (a) 10 °C and (b) 15 °C mesocosms. The group « others » include dinoflagellates, Chlorophyceae, Dictyochophyecae, Euglenophyceae, heterotrophic groups, and unidentified cells. Each bar plot represents a mesocosm at a given time. The bar plot on day -4 represents the initial community assemblage before temperature manipulation and acidification, and is therefore the same for each temperature treatment. For symbol attribution to treatments, see legend.

S. costatum was the dominant species in all mesocosms (70–90 % of the total number of eukaryotic cells), except for one mesocosm (M3, pH 7.6 at 10 °C) where a mixed dominance of *Chrysochromulina* spp. (a prymnesiophyte of 2–5 µm) and *S. costatum* was observed (Fig. 3.6a). *S. costatum* accounted for 80–90 % of the total eukaryotic cell counts in all mesocosms at the end of the experiment carried out at 10 °C. At 15 °C, the composition of the assemblage had shifted toward a dominance of unidentified flagellates and choanoflagellates (2–20 µm) in all mesocosms with these two groups accounting for 55–80 % of the total cell counts while diatoms showed signs of loss of viability as indicated by the presence of empty frustules (Fig. 3.6b).

3.3.6 Primary production

P_P increased in all mesocosms during Phase I of the experiment, in parallel with the increase in Chl *a* (Fig. 3.7a). P_P maxima were attained on days 3–4, except for the 15 °C Drifter (M11) where P_P peaked on day 1. We found no significant effect of the pCO_2 gradient, temperature and the pCO_2 × temperature interaction on the time-integrated P_p during both Phases I and II (Fig. 3.7b–c; Tables 3.2 and 3.4). Similarly, the absence of significant treatment effects remained when normalizing P_P per concentrations of Chl *a* (Fig. 3.7g–i). Initial Chl *a*-normalized P_P values were 3.3 ± 0.5 µmol C (µg Chl *a*)$^{-1}$ d^{-1} and reached maxima between 3.7 ± 0.3 µmol C (µg Chl *a*)$^{-1}$ d^{-1} and 5.7 ± 0.6 µmol C (µg Chl *a*)$^{-1}$ d^{-1} at 10 °C and 15 °C, respectively. These values then decreased to 2.2 ± 0.6 µmol C (µg Chl *a*)$^{-1}$ d^{-1} and 0.9 ± 0.2 µmol C (µg Chl *a*)$^{-1}$ d^{-1} on the last day of the experiment. During Phase I, the mean Chl *a*-normalized P_P was not significantly affected by the pCO_2 gradient or warming, as observed for the mean Chl *a* concentrations and time-integrated P_P over that phase (Fig. 3.7h; Table 3.2). During Phase II, the log of the mean Chl *a*-normalized P_P was not significantly affected by the pCO_2 gradient, the temperature, or the interaction of these factors (Fig. 3.7i; Table 3.4).

P_D was low at the beginning of the experiment, averaging 1.5 ± 0.4 µmol C L^{-1} d^{-1}, increased progressively during Phase I to reach maximum values of 6–48 µmol C L^{-1} d^{-1} between days 4 and 8, and decreased thereafter (Fig. 3.7d). Time-integrated P_D was not significantly affected by the pCO_2 gradient, the temperature, and the pCO_2 × temperature interaction during the two phases (Fig. 3.7e–f; Tables 3.2 and 3.4). Chl *a*-normalized P_D was low on day 0, averaging 0.3 ± 0.1 µmol C (µg Chl *a*)$^{-1}$ d^{-1}, reached maximum values of 1.0 ± 0.2 µmol C (µg Chl *a*)$^{-1}$ d^{-1} and 1.6 ± 0.2 µmol C (µg Chl *a*)$^{-1}$ d^{-1} at 10 °C and 15 °C, then respectively decreased to 0.17 ± 0.05 µmol C (µg Chl *a*)$^{-1}$ d^{-1} and 0.6 ± 0.2 µmol C (µg Chl *a*)$^{-1}$ d^{-1} by the end of the experiment (Fig. 3.7j). During Phase I, the mean Chl *a*-normalized P_D was affected neither by the pCO_2 gradient, the temperature, nor by the interaction between those factors (Fig. 3.7k; Table 3.2).

During Phase II, the log of the mean Chl *a*-normalized P_D was not affected by pCO_2 at either temperature tested, but significantly increased with warming (Fig. 3.7l; Table 3.4).

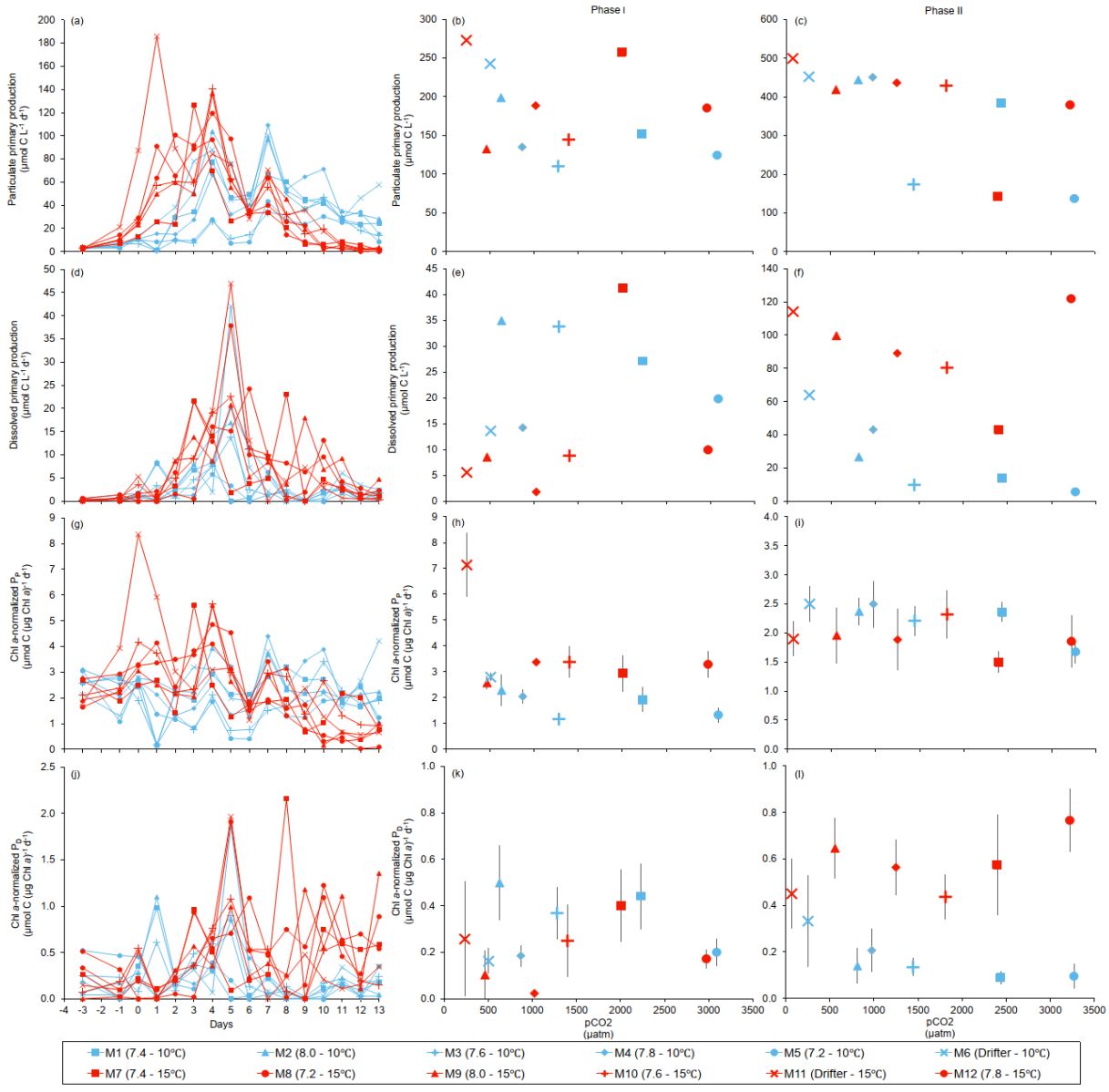

Figure 3.7 Temporal variations, time-integrated or averaged ± SE during Phase I (day 0 to day of maximum Chl *a* concentration) and Phase II (day after maximum Chl *a* concentration to day 13) for: (a-c) particulate primary production, (d-f) dissolved primary production, (g-i) Chl *a*-normalized particulate primary production, (j-l) Chl *a*-normalized dissolved primary production. For symbol attribution to treatments, see legend.

Figure 3.8 shows the influence of the treatments on maximum P_P and P_D as well as on the time-integrated P_P and P_D over the full length of the experiment. We found no effect of the pCO_2 gradient on the maximum P_P values at the two temperatures tested, but warming increased the maximum P_P values from 66 ± 13 µmol C L^{-1} d^{-1} to 126 ± 8 µmol C L^{-1} d^{-1} (Fig. 8a; Table 3.5). The time-integrated P_P over the full duration of the experiment was not affected by the pCO_2 gradient or the increase in temperature (Fig. 8b; Table 3.5). The maximum P_D values were significantly affected by the treatments (Fig 8c; Table3. 5). Maximum P_D decreased with increasing pCO_2 at in situ temperature but warming cancelled this effect (antagonistic effect). Nevertheless, the time-integrated P_D over the whole experiment did not vary significantly between treatments, although a decreasing tendency with increasing pCO_2 at 10 °C and an increasing tendency with warming can be seen in Fig. 3.8d (Table 3.5).

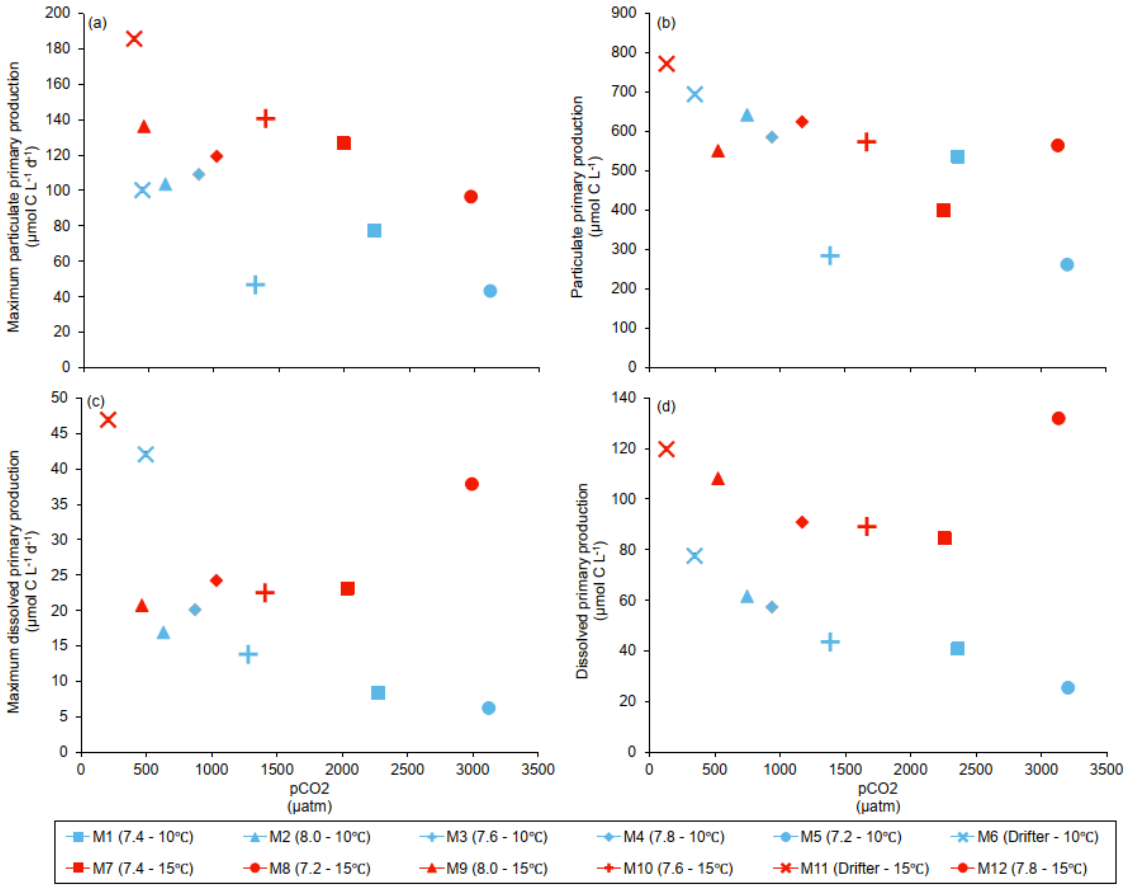

Figure 3.8 (a) Maximum particulate primary production, (b) time-integrated particulate primary production (c) maximum dissolved primary production, and (d) time-integrated dissolved primary production over the full course of the experiment (day 0 to day 13). For symbol attribution to treatments, see legend.

Table 3.5 Results of the generalized least squares models (gls) tests for the effects of temperature, pCO_2 and their interaction. Separate analysis with pCO_2 as a continuous factor were performed when temperature had a significant effect. Maximum particulate and dissolved primary production, and time-integration over the full duration of the experiment (day 0 to day 13). Natural logarithm transformation is indicated in parentheses when necessary, significant results are in bold. ***p < 0.05, **p < 0.01.**

Response Variable	Factor	df	t-value	p-value
Maximum particulate primary production ($\mu mol\ C\ L^{-1}\ d^{-1}$)	Temperature	8	**2.466**	**0.039***
	pCO_2 (10 °C)	4	-2.328	0.080
	pCO_2 (15 °C)	4	-2.394	0.075
Time-integrated particulate primary production ($\mu mol\ C\ L^{-1}\ d^{-1}$)	Temperature	8	-0.055	0.958
	pCO_2 (10 °C)	4	-1.300	0.230
	pCO_2 (15 °C)	4	0.801	0.446
(Log) Maximum dissolved primary production ($\mu mol\ C\ L^{-1}$)	Temperature	8	-0.659	0.528
	pCO_2	8	**-3.342**	**0.010****
	pCO_2 × Temperature	8	**2.858**	**0.021***
Time-integrated dissolved primary production ($\mu mol\ C\ L^{-1}$)	Temperature	8	1.687	0.130
	pCO_2	8	-2.153	0.063
	pCO_2 × Temperature	8	1.880	0.097

3.4. Discussion

3.4.1 General characteristics of the bloom

The onset of the experiment was marked by an increase of pCO_2 on the day following the filling of the mesocosms. This phenomenon often takes place at the beginning of such experiments when pumping tends to break phytoplankton cells and larger debris into smaller ones. We attribute the rapid fluctuations in pCO_2 to the release of organic matter following the filling of the mesocosms with a stimulating effect on heterotrophic respiration, and hence CO_2 production. Then, a phytoplankton bloom, numerically dominated by the centric diatom *S. costatum*, took place in all mesocosms, regardless of treatments (Fig. 3.6). *S. costatum* is a common phytoplankton species in the St. Lawrence Estuary and in coastal waters (Kim et al., 2004; Starr et al., 2004; Annane et al., 2015). The duration of the experiment (13 days) allowed us to capture both the development and declining phases of the bloom. The exponential growth phases lasted 1–4 days depending on the treatments, but maximal Chl *a* concentrations were reached only after 7 days in two of the twelve mesocosms (Fig. 3.4a; Table 3.1). The suite of measurements and statistical tests conducted did not provide any clues as to the underlying causes for the lower rates of biomass accumulation measured in these two mesocosms. Since statistical analyses conducted with or without these two apparent outliers gave similar results, they were not excluded from the analyses.

In situ nutrient conditions prior to the water collection were favourable for a bloom development. Based on previous studies, in situ phytoplankton growth was probably limited by light due to water turbidity and vertical mixing at the time of water collection (Levasseur et al. 1984). Grazing may also have played a role in keeping the in situ biomass of flagellates low prior to our sampling. However, a natural diatom fall bloom was observed in the days following the water collection in the adjacent region (Ferreyra, pers. comm.). The increased stability within the mesocosms, combined with the reduction of the grazing pressure (filtration on 250 µm) likely contributed to the rapid accumulation of phytoplankton biomass. During the development phase of the bloom, the concentration of all three monitored nutrients decreased, with NO_3^- and $Si(OH)_4$ reaching undetectable values. This nutrient co-depletion is consistent with results from previous studies suggesting a co-limitation of diatom blooms by these two nutrients in the St. Lawrence Estuary (Levasseur et al., 1987, 1990). Variations in P_P roughly followed changes in Chl *a*, and, as expected, the maximum Chl *a*-normalized P_P (5 ± 2 µmol C (µg Chl *a*)$^{-1}$ d^{-1}) was reached during the exponential growth phase in all mesocosms. Decreases in total phytoplankton abundances and P_P followed the bloom peaks and the timing of the NO_3^- and $Si(OH)_4$ depletions. A clear succession in phytoplankton size classes characterized the experiment. Nanophytoplankton cells were initially present in low abundance and became more numerous as the *S. costatum* diatom bloom developed. The correlation ($r^2 = 0.83$, $p < 0.001$, df=34) between the abundance of nanophytoplankton and *S. costatum* enumeration suggests that this cell size class can be used as a proxy of *S. costatum* counts in all mesocosms throughout the experiment. Nanophytoplankton cells accounted for 79 ± 7 % of total counts of cells < 20 µm on the day of the maximum Chl *a* concentration. Accordingly, nanophytoplankton exhibited the same temporal trend as Chl *a* concentrations. During Phase II, nanophytoplankton abundances remained roughly stable at in situ temperature but decreased at 15 °C towards the end of the experiment. Photosynthetic picoeukaryotes were originally abundant and decreased throughout the experiment whereas picocyanobacteria abundances increased during Phase II. This is a typical phytoplankton succession pattern for temperate systems where an initial diatom bloom growing essentially on allochthonous nitrate gives way to smaller species growing on regenerated forms of nitrogen (Taylor et al., 1993).

3.4.2 Phase I (diatom bloom development)

Our results show no significant effect of increasing pCO_2/decreasing pH on the mean abundance and net accumulation rate of the diatom-dominated nanophytoplankton assemblage during the development of the bloom (Figs. 3.4e and 3.5c). These results suggest that *S. costatum*, the species accounting for most of the biomass accumulation during the bloom, neither benefited from the higher pCO_2 nor was negatively impacted by the lowering of pH. Assuming that *S. costatum* was also responsible for most of the carbon fixation during the bloom development phase, the

absence of effect on P_P and Chl *a*-normalized P_p following increases in pCO_2 brings additional support to our conclusion. *S. costatum* operates a highly efficient CCM, minimizing the potential benefits of an increase of CO_2 (Trimborn et al., 2009). This may explain why the strain present in the LSLE did not benefit from the higher pCO_2 conditions. Likewise, a mesocosm experiment conducted in the coastal North Sea showed no significant effect of increasing pCO_2 on carbon fixation during the development of the spring diatom bloom (Eberlein et al., 2017).

In addition to the aforementioned insensitivity to increasing pCO_2, our results point towards a strong resistance of *S. costatum* to severe pH decline. During our study, surprisingly constant rates of Chl *a* accumulation and nanophytoplankton growth (Fig. 3.5a, c), as well as maximum P_P (Fig. 3.8a), were measured during the development phase of the bloom over a range of pH_T extending from 8.6 to 7.2 (Fig. 3.3a). In a recent effort to estimate the causes and amplitudes of short-term variations in pH_T in the LSLE, Mucci et al. (2017) showed that pH_T in surface waters was constrained within a range of 7.85 to 7.93 during a 50-h survey over two tidal cycles at the head of the Laurentian Channel. It is notable that even the upwelling of water from 100 m depth or of low-oxygen LSLE bottom water would not decrease pH_T beyond ~7.75 and ~7.62, respectively (Mucci et al., 2017 and references therein). Our results show that the phytoplankton assemblage responsible for the fall bloom may tolerate even greater pH_T excursions. In the LSLE, such conditions may arise when the contribution of the low pH_T (7.12) freshwaters of the Saguenay River to the LSLE surface waters is amplified during the spring freshet. However, considering that comparable studies conducted in different environments have reported negative effects of decreasing pH on diatom biomass accumulation (Hare et al., 2007; Hopkins et al., 2010; Schulz et al., 2013), it cannot be concluded that all diatom species thriving in the LSLE are insensitive to acidification.

In contrast to the pCO_2 treatment, warming affected the development of the bloom in several ways. Increasing temperature by 5 °C significantly increased the accumulation rate of Chl *a*, and the nanophytoplankton growth rate during Phase I of the bloom. The positive effects of warming on maximum P_P during the development phase of the bloom most likely reflect the sensitivity of photosynthesis to temperature (Eppley 1972; Geider 1987; Sommer and Lengfellner, 2008). It could also be related to optimal growth temperatures, which are often higher than in situ temperatures in marine phytoplankton (Thomas et al., 2012; Boyd et al., 2013). In support of this hypothesis, previous studies have reported optimal growth temperatures of 20–25 °C for *S. costatum*, which is 5–10 °C higher than the warmer treatment investigated in our study (Suzuki and Takahashi, 1995; Montagnes and Franklin, 2001). Extrapolating results from a mesocosm experiment to the field is not straightforward, as little is known of the projected warming of the upper waters of the LSLE in the next decades. In the Gulf of St. Lawrence, positive temperature anomalies in surface waters have varied from 0.25 to 0.75 °C per decade between 1985 and 2013 (Larouche and Galbraith,

2016). In the LSLE, warming of surface waters will likely result from a complex interplay between heat transfer at the air-water interface and variations in vertical mixing and upwelling of the cold intermediate layer at the head of the Estuary (Galbraith et al., 2014). Considering current uncertainties regarding future warming of the LSLE, studies should be conducted over a wider range of temperatures in order to better constrain the potential effect of warming on the development of the blooms in the LSLE.

Picoeukaryotes showed a more or less gradual decrease in abundance during Phase I, and our results show that this decline was not influenced by the increases in pCO_2 (Fig. 3.4g–h; Table 3.2). Picoeukaryotes are expected to benefit from high pCO_2 conditions even more so than diatoms as CO_2 can passively diffuse through their relatively thin boundary layer precluding the necessity of a costly uptake mechanism such as a CCM (Schulz et al., 2013). This hypothesis has been supported by several studies showing a stimulating effect of pCO_2 on picoeukaryote growth (Bach et al., 2016; Hama et al., 2016; Schulz et al., 2017 and references therein). On the other hand, in nature, the abundance of picoeukaryotes generally results from a delicate balance between cell division rates and cell losses through microzooplankton grazing and viral attacks. The few experiments, including the current study, reporting the absence or a modest effect of increasing pCO_2 on the abundance of eukaryotic picoplankton attribute their observations to an increase in nano- and microzooplankton grazing (Rose et al., 2009; Neale et al., 2014). During our experiment, the biomass of microzooplankton increased with increasing pCO_2 by ca. 200–300 % at the two temperatures tested (Ferreyra and Lemli, unpubl. data). Thus, it is possible that a positive effect of increasing pCO_2 and warming on picoeukaryote abundances might have been masked by higher picoeukaryote losses due to increased microzooplankton grazing.

3.4.3 Phase II (declining phase of the bloom)

The gradual decrease in nanophytoplankton abundances coincided with an increase in the abundance of picocyanobacteria (Fig. 3.4j). At in situ temperature, the picocyanobacteria abundance during Phase II was unaffected by the increase in pCO_2 over the full range investigated (Fig. 3.4l; Table 3.4). The lack of positive response of picocyanobacteria to elevated pCO_2 was somewhat surprising considering that they have less efficient CCMs than diatoms (Schultz et al., 2013). Accordingly, several studies have reported a stimulation of the net growth rate of picocyanobacteria under elevated pCO_2 in different environments (coastal Japan, Mediterranean Sea, and Raunejforden in Norway) and under different nutrient regimes, i.e. bloom and post-bloom conditions (Hama et al., 2016; Sala et al., 2016; Schulz et al., 2017). However, studies have also shown no direct effect of elevated pCO_2 on the net growth of picocyanobacteria during studies conducted in the Subtropical North Atlantic and the South Pacific (Law et al., 2012;

Lomas et al., 2012). In our study, picocyanobacteria abundance was even reduced when high CO_2 was combined with warming. Similar negative effects of CO_2 on picocyanobacteria (particularly *Synechococcus*) have also been observed under later stages of bloom development, i.e. nutrient depletion, either caused by competition or grazing (Paulino et al., 2008; Hopkins et al., 2010). A potential increase in grazing pressure, following the rise in heterotrophic nanoflagellates abundance (e.g. choanoflagellates; Fig. 3.6b) measured under high pCO_2 and warmer conditions, could explain the ostensible negative effect of increasing pCO_2 on picocyanobacteria abundance in our experiment. Despite the absence of grazing measurements during our study, our results support the hypothesis that the potential for increased picocyanobacteria population growth under elevated pCO_2 and temperature is partially dependent on different grazing pressures (Fu et al., 2007).

Neither warming nor acidification affected the net particulate carbon fixation during the declining phase of the bloom. In our study, the time-integrated P_P and Chl *a*-normalized P_P were not significantly affected by the increase in pCO_2 during Phase II at the two temperatures tested (Fig. 3.7; Table 3.4). This result is surprising since nitrogen-limited cells have been shown to be more sensitive to acidification, resulting in a reduction in carbon fixation rates due to higher respiration (Wu et al., 2010; Gao and Campbell, 2014; Raven et al., 2014). Although our measurements do not allow to discriminate between the contributions of the different phytoplankton size classes to carbon fixation, we can speculate that diatoms, which were still abundant during Phase II, contributed to a significant fraction of the primary production. If so, these results suggest that *S. costatum* remained insensitive to OA even under nutrient stress. However, in contrast to Phase I, increasing the temperature by 5 °C during Phase II significantly increased the Chl *a*-normalized P_D. The warming-induced increase in fixed carbon being release in the dissolved fraction likely stems from increased exudation by phytoplankton, or sloppy feeding / excretion following ingestion by grazers (Kim et al., 2011). The increase in fixed carbon released as dissolved organic carbon (DOC) measured during Phase II may also result from greater respiration by the nitrogen-limited diatoms during periods of darkness of the incubations, as dark phytoplankton respiration rates generally increase with temperature (Robarts and Zohary, 1987; Butrón et al., 2009). Moreover, the enclosures do not permit the sinking and export of particulates organic carbon (POC), allowing a further transformation into DOC by heterotrophic bacteria, a process that could be exacerbated under warming (Wohlers et al., 2009).

3.4.4 Effect of the treatments on primary production over the full experiment

As mentioned above, increasing pCO_2 had no effect on time-integrated P_P during the two phases of the bloom, and warming only affected the maximum P_P. As a result, primary production rates integrated over the whole duration of the experiment were not significantly different between the two

temperatures tested. Although not statistically significant, the time-integrated P_D over the full experiment displays a slight decrease with increasing pCO_2 at 10 °C and overall higher values in the warmer treatment (Fig. 3.8d; Table 3.5). Previous studies have reported increases of DOC exudation (Engel et al., 2013), but also decreasing DOC concentrations at elevated pCO_2 under nitrate limitation (Yoshimura et al., 2014). The increase in DOC exudation is attributed to a stimulation of photosynthesis resulting from its sensitivity to higher pCO_2 (Engel et al. 2013), but the causes for a decrease in DOC concentrations at high pCO_2 are less clear and potentially attributable to an increase in transparent exopolymer particle (TEP) production (Yoshimura et al, 2014). Elevated TEP production under high pCO_2 conditions has been measured both at the peak of a bloom in a mesocosm study (Engel et al., 2014), and in post-bloom nutrient depleted conditions (MacGilchrist et al., 2014). However, during our study, TEP production decreased under high pCO_2 (Gaaloul, 2017). Thus, the apparent decrease in P_D cannot be attributed to a greater conversion of exuded dissolved carbohydrate into TEP. The apparent rise in P_D under warming is consistent with previous studies reporting similar increases in phytoplankton dissolved carbon release with temperature (Morán et al., 2006; Engel et al., 2011). Although these apparent changes in P_D with increasing pCO_2 and warming require further investigations, they suggest that a larger proportion (~15 % of P_T at 15 °C compared to 10 % at 10 °C) of the newly fixed carbon could be exuded and become available for heterotrophic organisms under warmer conditions.

3.4.5 Implications and limitations

During our study, we chose to keep the pH constant during the whole experiment instead of allowing it to vary with changes in photosynthesis and respiration during the bloom phases. This approach differs from previous mesocosm experiments where generally CO_2 manipulations are seldom conducted after the initial targets are attained (Schulz et al. 2017 and therein). Keeping the pH and pCO_2 conditions stable during our study allowed us to precisely quantify the effect of the changing pH/pCO_2 on the processes taking place during the different phases of the bloom. Such control was not exercised in two of our mesocosms (i.e. the Drifters). In these two mesocosms, the pH_T increased from 7.9 to 8.3 at 10 °C, and from7.9 to 8.7 at 15 °C. Since the buffer capacity of acidified waters diminishes with increasing CO_2, the drift in pCO_2 and pH due to biological activity would have been even greater in the more acidified treatments (Delille et al., 2005; Riebesell et al., 2007). Hence, allowing the pH to drift in all mesocosms would have likely ended in an overlapping of the treatments where acidification effects would have been harder to detect. Thus, our experiment could be considered as an intermediate between strictly controlled small scale laboratory experiments and large scale pelagic mesocosm experiments in which the pCO_2 conditions are set initially and only readjusted periodically, if at all. By limiting pCO_2 decrease under high CO_2 drawdown due to photosynthesis during the development of the bloom phase, we

minimise confounding effects of pCO_2 potentially overlapping in association with high biological activity in the mesocosms. Hence, the experimental conditions could be considered as extreme examples of acidification conditions, due to the extent of pCO_2 values studied. However, the absence of OA effects on most biological parameters measured during our study, even under these extreme conditions, strengthens the argument that the phytoplankton community in LSLE is resistant to OA.

3.5. Conclusion

Our results reveal a remarkable resistance of the different phytoplankton size classes to the large range of pCO_2/pH investigated during our study. It is noteworthy that the plankton assemblage was submitted to decreases in pH far exceeding those that they are regularly exposed to in the LSLE. The resistance of *S. costatum* to the pCO_2 treatments suggests that the acidification of surface waters of the LSLE will not affect the development rate and the amplitude of fall blooms dominated by this species. Photosynthetic picoeukaryotes and picocyanobacteria thriving alongside the blooming diatoms were also insensitive to acidification. In contrast to the pCO_2 treatments, warming the water by 5 °C had multiple impacts on the development and decline of the bloom. The 5 °C warming hastened the development of the diatom bloom (albeit with no increase in total cells number) and increased the abundance of picocyanobacteria during Phase II despite a reduction under high pCO_2. These temperature-induced variations in the phytoplankton assemblage were accompanied by an increase in maximal P_P and suggest a potential increase in P_D under warming, although no significant changes in time-integrated P_P and P_D were observed over the phases or the full temporal scale of the experiment. Overall, our results indicate that warming could have more important impacts than acidification on phytoplankton bloom development in the LSLE in the next decades. Future studies should be conducted and specifically designed to better constrain the potential effects of warming on phytoplankton succession and primary production in the LSLE.

3.6 Acknowledgements

The authors wish to thank the Station Aquicole ISMER, especially Nathalie Morin and her staff, for their support during the project. We also wish to acknowledge Gilles Desmeules, Bruno Cayouette, Sylvain Blondeau, Claire Lix, Rachel Hussherr, Liliane St-Amand, Marjolaine Blais, Armelle Simo and Sonia Michaud for their help in setting up, sampling and processing samples during the experiment. The authors want to thank Jean-Pierre Gattuso for his constructive comments on an earlier draft of this manuscript. This study was funded by a Team grant from the Fonds de la Recherche du Québec – Nature et Technologies (FRQNT-Équipe-165335), the Canada Foundation

for Innovation, Fisheries and Oceans Canada, and the Canada Research Chair on Ocean Biogeochemistry and Climate. This is a contribution to the research programme of Québec-Océan.

Chapitre 4 Contrasting effects of acidification and warming on dimethylsulfide concentrations during a temperate estuarine fall bloom mesocosm experiment

Résumé

Les effets de l'acidification et du réchauffement sur les concentrations de diméthylsulfoniopropionate (DMSP) et de diméthylsulfure (DMS) ont été étudiés au cours d'une expérience en mésocosmes dans l'estuaire maritime du Saint-Laurent (EMSL). Douze mésocosmes couvrant une plage de pH_T (pH sur l'échelle de concentration totale d'ions hydrogène) de 8,0 à 7,2, correspondant à une gamme de pCO_2 de 440 à 2900 µatm et deux températures (in situ et +5 °C; 10 °C et 15 °C) ont été monitorés pendant 13 jours. Tous les mésocosmes ont été caractérisés par une floraison de diatomées dominée par *Skeletonema costatum*, suivi de son déclin à la suite de l'épuisement du nitrate et du silicium dissous. Ni l'acidification ni le réchauffement n'ont eu d'impact significatif sur l'abondance des bactéries au cours de l'expérience. Cependant, un réchauffement de 5 °C a entraîné une augmentation significative de la production bactérienne moyenne (BP) dans tous les mésocosmes à 15 °C par rapport à 10 °C, sans effet significatif de la pCO_2. Les variations des concentrations totales de DMSP ($DMSP_t$ = particulaire + DMSP dissous) ont suivi le développement de la floraison bien que la hausse du $DMSP_t$ ait persisté pendant quelques jours après les pics de Chl *a*. Les concentrations moyennes de $DMSP_t$ n'ont pas été affectées par l'acidification ou le réchauffement. Initialement faibles (< 1 nmol L^{-1}), les concentrations de DMS ont augmenté pour atteindre des valeurs de pointe allant de 30 à 130 nmol L^{-1} à la fin de l'expérience. L'augmentation de la pCO_2 a réduit les concentrations moyennes de DMS de 66 % et de 69 % à 10 °C et 15 °C, respectivement, pendant la durée de l'expérience. D'autre part, le réchauffement de 5 °C a augmenté les concentrations moyennes de DMS de 240 % par rapport à la température in situ, entraînant une compensation de l'impact négatif de la pCO_2. Les corrélations positives significatives calculées entre les taux de production bactérienne et les concentrations de DMS au cours de notre expérience suggèrent qu'une augmentation du métabolisme bactérien du DMSP associée à la température permettrait d'atténuer l'impact négatif de l'acidification sur la production nette de DMS dans l'EMSL et potentiellement dans l'océan global.

Abstract

The effects of ocean acidification and warming on the concentrations of dimethylsulfoniopropionate (DMSP) and dimethylsulfide (DMS) were investigated during a mesocosm experiment in the Lower St. Lawrence Estuary (LSLE). Twelve mesocosms covering a range of pH_T (pH on the total hydrogen ion concentration scale) from 8.0 to 7.2, corresponding to a range of CO_2 partial pressures (pCO_2) from 440 to 2900 µatm, at two temperatures (in situ and +5 °C; 10 °C and 15 °C) was monitored during 13 days. All mesocosms were characterized by the rapid development of a diatom bloom dominated by *Skeletonema costatum*, followed by its decline upon the exhaustion of nitrate and dissolved silicon. Neither the acidification nor the warming resulted in a significant impact on the abundance of bacteria over the experiment. However, warming the water by 5 °C resulted in a significant increase of the average bacterial production (BP) in all 15 °C mesocosms as compared to 10 °C, with no detectable effect of pCO_2 on BP. Variations in total DMSP ($DMSP_t$ = particulate + dissolved DMSP) concentrations tracked the development of the bloom although the rise in $DMSP_t$ persisted for a few days after the peaks in Chl *a*. Average concentrations of $DMSP_t$ were not affected by acidification or warming. Initially low concentrations of DMS (< 1 nmol L^{-1}) increased to reach peak values ranging from 30 to 130 nmol L^{-1} towards the end of the experiment. Increasing the pCO_2 reduced the averaged DMS concentrations by 66 % and 69 % at 10 °C and 15 °C, respectively, over the duration of the experiment. On the other hand, a 5 °C warming increased DMS concentrations by an average of 240 % as compared to in situ temperature, resulting in a positive offset of the adverse pCO_2 impact. Significant positive correlations found between bacterial production rates and concentrations of DMS throughout our experiment point towards temperature-associated enhancement of bacterial DMSP metabolism as a likely driver for the mitigating effect of warming on the negative impact of acidification on the net production of DMS in the LSLE and potentially the global ocean.

4.1 Introduction

Dimethylsulfide (DMS) is ubiquitous in productive estuarine, coastal and marine surface waters (Barnard et al., 1982; Iverson et al., 1989; Kiene and Service, 1991; Cantin et al., 1996; Kettle et al., 1999). With an estimated average 28.1 Tg of sulfur (S) being transferred to the atmosphere annually (Lana et al., 2011), DMS emissions constitute the largest natural source of tropospheric S (Lovelock et al., 1972; Andreae 1990; Bates et al., 1992). The oxidation of atmospheric DMS yields hygroscopic sulfate (SO_4^{2-}) aerosols that directly scatter incoming solar radiation and act as nuclei upon which cloud droplets can condense and grow, thereby potentially impacting cloud albedo and the radiative properties of the atmosphere (Charlson et al., 1987; Andreae and Crutzen 1997; Liss and Lovelock, 2007; Woodhouse et al., 2013). The scale of the impact of biogenic SO_4^{2-} particles on global climate, however, remains uncertain (Carslaw et al., 2010; Quinn and Bates, 2011, Quinn et al., 2017). The strength of DMS emissions depends on wind- and temperature-driven transfer processes (Nightingale et al., 2000) but mostly on its net production in the surface mixed layer of the ocean (Malin and Kirst, 1997). Net changes in the aqueous DMS inventory are largely governed by microbial food webs (see reviews by Simó, 2001; Stefels et al., 2007) whose productivity is potentially sensitive to modifications in the habitats that sustain them. Given the complexity of the biological cycling of DMS, understanding how climate change related stressors could impact the production of this climate-active gas is a worthy but formidable challenge.

DMS is produced, for the most part, from the enzymatic breakdown of dimethylsulfoniopropionate (DMSP) (Cantoni and Anderson, 1956), a metabolite produced by several groups of phytoplankton, with an extensive range in intracellular quotas between taxa (Keller et al., 1989; Stefels et al., 2007). Several species of the classes Haptophyceae and Dinophyceae are amongst the most prolific DMSP producers, but certain members of Bacillariophyceae (diatoms) and Chrysophyceae can also produce significant amounts of DMSP (Stefels et al., 2007). The biosynthesis of DMSP is highly constrained by abiotic factors and its up- or down-regulation may allow cells to cope with environmental shifts in temperature, salinity, nutrients and light intensity (Kirst et al., 1991; Karsten et al., 1996; Sunda et al., 2002), while its de novo synthesis and exudation may also serve as a sink for excess carbon (C) and S under unfavourable growth conditions (Stefels, 2000). Beyond active exudation in healthy cells (Laroche et al., 1999), cellular or particulate DMSP ($DMSP_p$) can be transferred to the water column as dissolved DMSP ($DMSP_d$) through viral lysis (Hill et al., 1998; Malin et al., 1998), autolysis (Nguyen et al., 1988; Stefels and Van Boeckel, 1993), and grazing by micro-, meso- and macrozooplankton (Dacey and Wakeham, 1986; Wolfe and Steinke, 1996). The turnover rate of $DMSP_d$ in the water column is generally very rapid (a few hours to days) as this compound represents sources of C and reduced S for the growth of microbial organisms (Kiene and Linn, 2000). Heterotrophic bacteria mediate most of the turnover of S-$DMSP_d$ through pathways that

constrain the overall production of DMS: (1) enzymatic cleavage of $DMSP_d$ that yields DMS; (2) demethylation/ demethiolation of $DMSP_d$ that yields methanethiol (MeSH); (3) production of dissolved non-volatile S compounds, including SO_4^{2-}, following oxidation of $DMSP_d$; (4) intracellular accumulation of $DMSP_d$ with no further metabolization (Kiene et al., 1999, 2000; Kiene and Linn, 2000; Yoch, 2002). A compilation of ^{35}S-$DMSP_d$ tracer studies conducted with natural microbial populations shows that microbial DMS yields rarely exceed 40% of consumed $DMSP_d$ in surface coastal and oceanic waters (see review table in Lizotte et al., 2017). Another potential fate of $DMSP_d$ is its uptake by non-DMSP producing eukaryotic phytoplankton such as certain diatoms (Vila-Costa et al., 2006b; Ruiz-González et al., 2012) and cyanobacteria such as *Synechococcus* and *Prochloroccocus* (Malmstrom et al., 2005; Vila-Costa et al., 2006b), but the overall turnover of $DMSP_d$ seems to be dominated by heterotrophic organisms.

Whereas the role of bacteria in the production of DMS via $DMSP_d$ is well recognized, an increasing number of studies have shown that the phytoplankton-mediated enzymatic conversion of total DMSP ($DMSP_t$) into DMS can also be significant when communities are dominated by DMSP-lyase producing phytoplankton groups such as Dinophyceae and Haptophyceae (Niki et al., 2000; Steinke et al., 2002; Stefels et al., 2007; Lizotte et al., 2012), particularly under high doses of solar radiation (Toole and Siegel, 2004; Toole et al., 2006, 2008; Vallina et al., 2008). Removal processes of DMS from surface waters include photo-oxidation, bacterial degradation and efflux across the air-sea interface, the individual intensity of which depends on several factors such as light intensity, wind velocity, the depth of the surface mixed layer and the gross production of DMS (Brimblecombe and Shooter, 1986; Simó and Pedros-Alió, 1999; Nightingale et al., 2000; Hatton et al., 2004; Simó, 2004). Overall, production and turnover of DMS and its precursor DMSP are unequivocally linked with microbial activity, both autotrophic and heterotrophic. The associated biological processes and interactions amongst these microorganisms have been shown to be sensitive to fluctuations in abiotic factors and may thus be further modulated by multiple drivers of climate change.

Since the pre-industrial era, atmospheric CO_2 concentrations have risen from 280 and reached 412 ppm in 2017. According to the business-as-usual scenario RCP 8.5 and global ocean circulation models, they are expected to reach 850–1370 ppm by 2100 (IPCC, 2013). The oceans have already absorbed about 28 % of the anthropogenic CO_2 emitted to the atmosphere (Le Quéré et al., 2015), leading to a pH decrease of 0.11 units in surface waters (Gattuso et al., 2015), a phenomenon called ocean acidification (OA). An additional decrease of pH by 0.3–0.4 units is expected by the end of this century, and could reach 0.8 units by 2300 (Caldeira and Wickett, 2005; Doney et al., 2009; Feely et al., 2009). In addition to the oceanic sink, a similar fraction of anthropogenic CO_2 emissions has been captured by terrestrial vegetation. while the anthropogenic CO_2 remaining (45% of total emissions) in the atmosphere (Le Quéré et al., 2013) has led to an estimated increased greenhouse effect of 0.3–0.6 W m^{-2} globally over the past 135 years

(Roemmich et al., 2015). Ninety percent of this excess heat has been absorbed by the ocean, increasing sea surface temperatures (SST) ~0.1 °C per decade since 1951 and could increase SST by 3–5 °C before 2100 (IPCC, 2013). Leading experts in the field of global change have called upon the scientific community to address critical knowledge gaps, among which, a top priority remains the assessment of the impact of multiple environmental stressors on marine microorganisms (Riebesell and Gattuso, 2015).

The sensitivity of natural planktonic assemblages to OA, along with their production of DMSP and DMS, has been investigated in several experimental studies (see review table in Hussherr et al., 2017). The majority of these experiments have shown a decrease in both DMSP and DMS concentrations with increasing pCO_2 (Hopkins et al., 2010; Avgoustidi et al., 2012; Park et al., 2014; Webb et al., 2015). The decrease in DMSP production has largely been attributed to the deleterious impact of decreasing pH on the coccolithophore *Emiliania huxleyi*, the dominant DMSP producer in several of these studies. Nevertheless, OA does not always result in a concomitant decrease in DMSP and DMS production. For example, the pCO_2-induced decrease in DMS reported by Archer et al. (2013) in Arctic waters was accompanied by an increase in DMSP concentrations, indicating that DMS production is at least partly dependent on the turnover of DMSP, rather than on the DMSP pool. A modeling study showed that the specific implementation of the negative effect of OA on DMS net production in a coupled ocean-atmosphere model reduces global DMS production by 18 ± 3 %, resulting in an additional warming of 0.23–0.48 K by 2100 under the A1B scenario (Six et al., 2013). Schwinger et al. (2017) further showed that the OA-induced decreases in oceanic DMS emissions could result in a transient global warming of 0.30 K, mostly resulting from a reduction of cloud albedo. These first attempts to model the potential effect of OA on climate through its impact on DMS oceanic production show that OA may significantly affect climate by reducing marine emissions of DMS but also highlight the importance of carefully assessing the robustness of the DMS-OA negative relationship. This is particularly relevant considering that some experiments reveal a neutral or positive effect of increasing pCO_2 on DMS net production (Vogt et al., 2008; Kim et al., 2010; Hopkins and Archer, 2014). Regional or seasonal differences in phytoplankton taxonomy, microzooplankton grazing, and bacterial activity have been proposed as key drivers of the discrepancies between these experimental results.

Whereas studies of the impact of OA on DMS cycling have gained momentum, the importance of assessing how combined drivers of change may impact the structure and the functioning of ocean ecosystems, using multifactorial approaches, is now increasingly recognized (Boyd et al., 2015; 2018; Riebesell and Gattuso, 2015; Gunderson et al., 2016). Thus far, only two mesocosm studies assessed the combined effect of OA and warming on DMS dynamics by natural plankton assemblages. The two studies, both conducted with coastal waters, led to contrasting results. The first study showed an 80 % increase in DMS concentrations under high pCO_2 conditions (900 ppm

vs. 400 ppm), and a reduction by 20 % of this stimulating effect when the increase in pCO_2 was accompanied by a 3 °C warming (Kim et al., 2010). However, the absence of a specific stand-alone warming treatment did not allow the authors to assess the sole impact of temperature on DMS net production. The second study showed decreasing DMS concentrations under both acidification and greenhouse conditions, with the lowest DMS concentrations measured under combined acidification and warming treatments (Park et al., 2014). The authors attributed these contrasting responses to differences in the phytoplankton assemblages, DMSP-related algal physiological characteristics, and microzooplankton grazing. Nevertheless, questions remain as to the combined effect of pCO_2 and warming on DMS net production since the temperature treatments were not conducted over the full range of pCO_2 tested (Kim et al., 2010; Park et al., 2014).

The combined influence of acidification and warming on the dynamics of the St. Lawrence Estuary phytoplankton fall bloom was investigated during a full factorial mesocosm experiment (Bénard et al., 2018b). During this experiment, a bloom of *Skeletonema costatum* developed in all mesocosms, independently of the pCO_2 gradient (from 440 to 2900 µatm) and temperatures tested (10 and 15 °C). The increase in pCO_2 had no influence on the bloom but warming accelerated the growth rate of the diatoms and hastened the decline of the bloom (Bénard et al., 2018b). Here, we report on the impacts of acidification and warming on DMSP and DMS concentrations with a focus on the dynamics of heterotrophic bacteria, a component of the marine food web known to affect the turnover of DMSP and DMS.

4.2 Materials and methods

4.2.1 Mesocosm setup

Mesocosm experiments were conducted at the ISMER marine research station of Rimouski (Québec, Canada). The twelve 2600 L cylindrical (2.67 m × 1.4 m), conical bottom, mesocosms were housed in two temperature-controlled, full-size shipping containers each containing six mesocosms (Aquabiotech Inc., Québec, Canada). Each mesocosm is mixed by a propeller secured near the top of the enclosure to ensure homogeneity of the water column. The mesocosms are sealed by a Plexiglas cover transmitting 50–85 % of solar UVB (280–315 nm), 85–90 % of UVA (315–400 nm), and 90 % of photosynthetically active radiation (PAR; 400–700 nm) of the natural incident light. Independent temperature probes (AQBT-Temperature sensor, accuracy ± 0.2 °C) were installed in each mesocosm, recording temperature every 15 minutes and either triggering a resistance heater (Process Technology TTA1.8215) or a glycol refrigeration system activated by an automated pump. The pH of the mesocosms was measured every 15 minutes by Hach® PD1P1 probes (± 0.02 pH units) linked to Hach® SC200 controllers. To maintain pH, two reservoirs of

artificial seawater were equilibrated with pure CO_2 before the start of the experiment and positive deviations from the target pH values in each mesocosm activated peristaltic pumps that injected the CO_2 supersaturated seawater into the mesocosm water. This control system was able to maintain the pH in the mesocosms within ± 0.02 pH units of the targeted values during the initial bloom development by lowering the pH, but it could not increase the pH during the declining phase of the bloom.

4.2.2 Experimental approach

Prior to the onset of the experiment, all the mesocosms were meticulously washed with diluted Virkon^{TM}, an anti-viral and anti-bacterial solution, according to the manufacturer's instructions (Antec International Limited), and thoroughly rinsed. To fill the mesocosms, water from ~5 m depth was collected near the Rimouski harbour (48° 28' 39.9" N, 68° 31' 03.0" W) on the 27th of September 2014 (day -5). Initial conditions were: practical salinity (S_P) = 26.52, temperature (t) = 10 °C, nitrate (NO_3^-) = 12.8 ± 0.6 µmol L^{-1}, silicic acid ($Si(OH)_4$) = 16 ± 2 µmol L^{-1}, and soluble reactive phosphate (SRP) = 1.4 ± 0.3 µmol L^{-1}. Following its collection, the water was screened through a 250 µm mesh while the mesocosms were simultaneously gravity-filled by a custom made "octopus" tubing system. The initial in situ temperature of 10 °C was maintained in all mesocosms for the first 24 h (day -4). On day -3, the six mesocosms in one of the containers were gradually heated to 15 °C while the mesocosms in the other container were maintained at 10 °C. No manipulations were performed on day -2 to avoid excessive stress, and acidification was carried out on day -1. The mesocosms were initially set to cover a gradient of pH_T (total proton concentration scale) of ~8.0 to 7.2 corresponding to a range of pCO_2 from 440 to 2900 µatm. Two mesocosms, one in each container (at each temperature), were not pH-controlled to assess the effect of freely fluctuating pH condition. These two mesocosms were called drifters since the in-situ pH was allowed to drift over time throughout the bloom development. To achieve the initially targeted pH_T, CO_2-saturated artificial seawater was added to mesocosms M1, M3, M5, M7, M8, M10 (pH_T 7.2–7.6) while mesocosms M2, M4, M6, M9, M11, M12 (pH_T 7.8–8.0 and the drifters) were openly mixed to allow CO_2 degassing. Then, the automatic system controlling the occasional addition of CO_2-satured artificial seawater maintained the pH equal or below the targeted pH, except for the drifters.

4.2.3 Seawater analysis

Daily sampling of the mesocosms was carried out between 05:00 and 08:00 every day (EDT). Samples for carbonate chemistry, nutrients, DMSP and DMS were collected directly from the mesocosms prior to filling of 20 L carboys from which seawater for the determination of

chlorophyll *a* (Chl *a*), bacterial abundance, and bacterial production was subsampled. Samples were collected directly from the mesocosms and the artificial seawater tank on days -3, 3 and 13 for practical salinity determinations. The samples were collected in 250 mL plastic bottles and stored in the dark until analysis was carried out on a Guildline Autosal 8400B salinometer in the months following the experiment.

4.2.3.1 Carbonate chemistry and nutrients

Analytical methods used to determine the carbonate parameters are described in detail in Bénard et al. (2018b). Briefly, pH was determined every day by transferring samples from the mesocosms to 125 mL plastic bottles without headspace. The samples were analyzed within hours of collection on a Hewlett-Packard UV-Visible diode array spectrophotometer (HP-8453A) and a 5 cm quartz cell using phenol red (PR; Robert-Baldo et al., 1985) and *m*–cresol purple (mCP; Clayton and Byrne, 1993) as indicators after equilibration to 25.0 ± 0.1 °C in a thermostated bath. The pH on the total proton scale (pH_T) was calculated according to Byrne (1987), with the salinity of the sample and the HSO_4^- association constants given by Dickson (1990). The reproducibility of pH measurements, based on replicate measurements of the same samples and values derived from both indicators, was on the order of 0.003. Total alkalinity (TA) samples were collected every 3–4 days in 250 mL glass bottles to which a few crystals of $HgCl_2$ were added before sealing with ground glass stoppers and Apiezon® Type-M high-vacuum grease. The TA determinations were carried out within one day of sampling by open-cell automated potentiometric titration (Titrilab 865, Radiometer®) with a pH combination electrode (pHC2001, Red Rod®) and a dilute (0.025 N) HCl titrant solution calibrated against Certified Reference Materials (CRM Batch#94, provided by A. G. Dickson, Scripps Institute of Oceanography, La Jolla, USA). The average relative error, calculated from the average relative standard deviation on replicate standards and sample analyses, was < 0.15 %. The computed pH_T at 25 °C, measured TA, silicic acid and SRP concentrations were used to calculate the in situ pH_T, pCO_2 and saturation state of the water in each mesocosm using CO_2SYS (Pierrot et al., 2006) and the carbonic acid dissociation constants of Cai and Wang (1998).

The samples for the determination of NO_3^-, $Si(OH)_4$, and SRP were filtered through Whatman GF/F filters, collected in acid washed polyethylene tubes and stored at -20 °C. Analysis was carried out using a Bran and Luebbe Autoanalyzer III using the colorimetric methods of Hansen and Koroleff (2007). The analytical detection limit was 0.03 µmol L^{-1} for NO_3^- plus nitrite (NO_2^-), 0.02 µmol L^{-1} for NO_2^-, 0.1 µmol L^{-1} for $Si(OH)_4$, and 0.05 µmol L^{-1} for SRP.

4.2.3.2 Biological variables

For Chl *a* determination, duplicate 100 mL samples were filtered onto Whatman GF/F filters. The filters were soaked in a 90 % acetone solution at 4 °C in the dark for 24 h, the solution was then analyzed by a 10-AU Turner Designs fluorometer (acidification method: Parsons et al., 1984). The analytical detection limit for Chl *a* was 0.05 µg L^{-1}.

Samples for the determination of free-living heterotrophic bacteria were kept in sterile cryogenic polypropylene vials and fixed with glutaraldehyde Grade I (final concentration = 0.5 %, Sigma Aldrich; Marie et al., 2005). Duplicate samples were placed at 4 °C in the dark for 30 min, then frozen at -80 °C until analysis by a FACS Calibur flow cytometer (Becton Dickinson) equipped with a 488 nm argon laser. Before enumeration, the samples were stained with SYBR Green I (0.1 % final concentration, Invitrogen Inc.) to which 600 µL of a Tris-EDTA 10 × buffer of pH 8 were added (Laboratoire MAT; Belzile et al., 2008). Fluoresbrite beads (diameter 1 µm, Polysciences) were also added to the sample as an internal standard. The green fluorescence of SYBR Green I was measured at 525 ± 5 nm. Bacterial abundance was determined as the sum of low and high nucleic (LNA and HNA) counts (Annane et al., 2015).

Bacterial production was estimated in each mesocosm except the Drifters on days 0, 2, 4, 6, 8, 10, 11 and 13 by measuring incorporation rates of tritiated thymidine (^{3}H-TdR), using an incubation and filtration protocol based on Fuhrman and Azam (1980, 1982). Twenty mL water subsamples were transferred from glass Erlenmeyers to five sterile glass vials; three as “measured” values and two as blanks. In all blank vials, 0.2 mL of formaldehyde 37 % were added, immediately after the sampling to stop all biological activities. Then, 1 mL of ^{3}H-TdR solution (4 µmol L^{-1}), prepared from commercial solution (63 Curie $mmol^{-1}$; 1 mCurie mL^{-1}, 10 µmol L^{-1} ^{3}H-TdR, MP Biomedicals), was added in all vials. Samples were incubated 2.5 h at experimental temperatures (10 or 15 °C), and then 0.2 mL of formaldehyde 37 % were immediately added in the three “measure” vials. Bacteria were then collected by filtration (diameter 25 mm; 0.2 µm porosity) and filters were treated according to Fuhrman and Azam (1980, 1982). The incorporation of ^{3}H-TdR was measured using a scintillation counter (Beckman LS5801) and results were expressed in dpm. Blank values were subtracted from “measured” values to remove background radioactivity.The ^{3}H-TdR incorporation rates were converted in mole of ^{3}H-TdR incorporated per unit of volume and time, before converting to rate of carbon production using the carbon conversion factor of Bell (1993).

4.2.3.3 DMSP and DMS concentrations

For the quantification of $DMSP_t$, duplicate 3.5 mL samples of seawater were collected into 5 mL polyethylene tubes. Samples were preserved by adding 50 µL of a 50 % sulfuric acid solution (H_2SO_4) to the tubes before storage at 4 °C in the dark until analysis in the following months. Samples for the quantification of $DMSP_d$ were taken daily, but a technical problem during storage and transport of the samples led to a loss of all samples. To quantify $DMSP_t$, 1 mL of NaOH (5 M) was injected into a purge and trap (PnT) system prior to the 3.5 mL sample to hydrolyze DMSP into DMS following a mole-to-mole conversion. Ultrapure helium was used to bubble the heated chamber (70 °C; 50 ± 5 mL min^{-1}; 4 min) trapping the gas sample in a loop immersed in liquid nitrogen. The loop was then heated in a water bath to release the trapped sample and analyzed using a Varian 3800 Gas Chromatograph equipped with a pulsed flame photometric detector (PFPD, Varian 3800) and a detection limit of 0.9 nmol L^{-1} (Scarratt et al., 2000; Lizotte et al., 2012). DMSP concentrations were determined against a calibration curve using standardized DMSP samples prepared by diluting known concentrations of DMSP standard (Research Plus Inc.) into deionized water and analyzed following the same methodology.

Samples for the quantification of DMS were directly collected from the mesocosms into 20 mL glass vials with a butyl septa and aluminum crimp. The samples were kept in the dark at 4 °C until analysis was carried out within hours of collection by injecting the 20 mL sample in the PnT system described above, without the prior addition of NaOH. DMS concentrations were calculated against microliter injections of DMS diluted with ultrapure helium using a permeation tube (Certified Calibration by Kin-Tek Laboratories Inc.; Lizotte et al., 2012).

4.2.4 Statistical analyses

The statistical analyses were performed using the nlme package in R (R Core Team, 2016). The data were analyzed using a general least squares (gls) approach to test the linear effects of the two treatments (temperature, pCO_2), and their interaction on the variables (Paul et al., 2016; Hussherr et al., 2017; Bénard et al., 2018b). The analyses were conducted on the averages of the measured parameters over the whole duration of the experiment, and separate regressions for pCO_2 were performed for each temperature when the latter had a significant effect. The residuals were checked for normality using a Shapiro-Wilk test ($p > 0.05$) and data were transformed (square root or natural logarithm) if necessary. In addition, squared Pearson's correlation coefficients (r^2) with a significance level of 0.05 were used to evaluate correlations between key variables.

4.3 Results

4.3.1 Physical and chemical conditions during the experiments

The S_p was 26.52 ± 0.03 on day -4 in all mesocosms and remained constant throughout the experiment, averaging 26.54 ± 0.02 on day 13 (Bénard et al., 2018b). The temperature of the mesocosms in each container remained within ± 0.1 °C of the target temperature throughout the experiment and averaged 10.04 ± 0.02 °C for mesocosms M1 through M6, and 15.0 ± 0.1 °C for mesocosms M7 through M12 (Fig. 4.1a). The pH_T remained relatively stable throughout the experiment in the pH-controlled treatments, but decreased slightly as the experiment progressed, deviating by an average of -0.14 ± 0.07 units relative to the target pH_T on the last day (Fig. 4.1b). The pH variations corresponded to changes in pCO_2 from an average of 1340 ± 150 µatm on day -3, and ranged from 564 to 2902 µatm at 10 °C and from 363 to 2884 µatm at 15 °C on day 0 following the acidification (Fig. 4.1c). The in situ pH_T in the drifters (M6 and M11) increased from 7.896 and 7.862 on day 0, at 10 °C and 15 °C respectively, to 8.307 and 8.554 on day 13, reflecting the balance between CO_2 uptake and metabolic CO_2 production over the duration of the experiment. On the last day, pCO_2 in all mesocosms ranged from 186 to 3695 µatm at 10 °C and from 90 to 3480 µatm at 15 °C.

Nitrate (NO_3^-) and silicic acid ($Si(OH)_4$) concentrations averaged 9.1 ± 0.5 µmol L^{-1} and 13.4 ± 0.3 µmol L^{-1} on day 0, respectively (Bénard et al., 2018b). The two nutrients displayed a similar temporal depletion pattern following the development of the phytoplankton bloom. NO_3^- concentrations reached undetectable levels (< 0.03 µmol L^{-1}) in all mesocosms by day 5. Likewise, $Si(OH)_4$ fell below the detection limit (< 0.1 µmol L^{-1}) between day 1 and 5 in all mesocosms except for those whose pH_T was set at 7.2 and 7.6 at 10 °C (M5 and M3) and in which $Si(OH)_4$ depletion occurred on day 9.

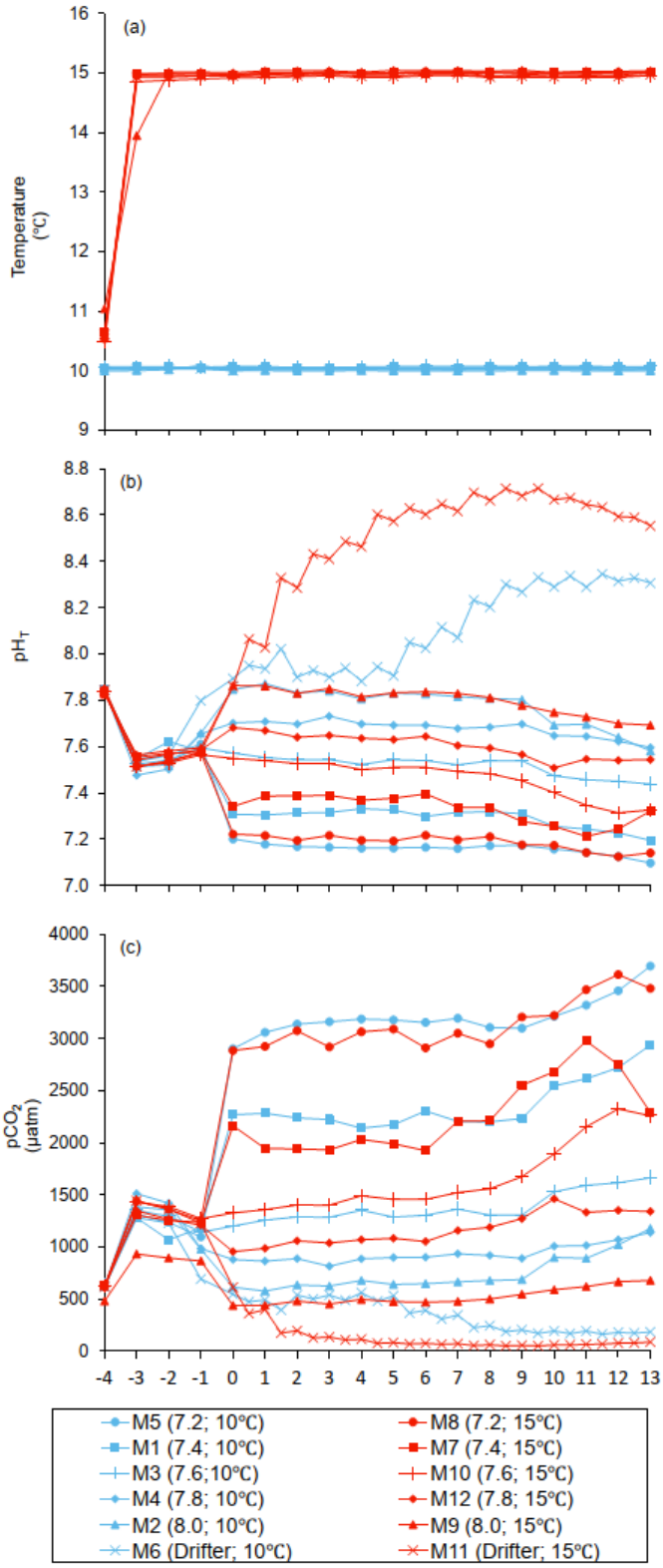

Figure 4.1 Temporal variations over the course of the experiment for: (a) temperature, (b) pH_T, (c) pCO_2. For symbol attribution to treatments, see legend.

4.3.2 Phytoplankton, bacterial abundance and production

Chl *a* concentrations were below 1 µg L^{-1} following the filling of the mesocosms (day -4), and had already increased to an average of 5.9 ± 0.6 µg L^{-1} on day 0 (Fig. 4.2a). At 10 °C, Chl *a* quickly increased to reach maximum concentrations around 27 ± 2 µg L^{-1} on day 3 ± 2, and decreased progressively until the end of the experiment. Increasing the temperature by 5 °C resulted in a more rapid development of the bloom and a speedier decrease of Chl *a* concentrations during the declining phase of the bloom. The maximum Chl *a* concentration reached at the peak of the bloom was, however, not significantly affected by the difference in temperature. We found no significant effect of the pCO_2 gradient on the mean Chl *a* concentrations measured over the days 0–13, nor during the development phase and the declining phase of the bloom as described in Bénard et al. (2018b) (Fig. 4.2a–b; Table 4.1).

The free-living bacterial abundance was ~1.2 × 10^9 cells L^{-1} on day -4, and increased rapidly to reach 3.1 ± 0.6 × 10^9 cells L^{-1} on day 0 (Fig. 4.2c). This initial increase in abundance probably resulted from the release of dissolved organic matter (DOM) during pumping of the seawater and filling of the mesocosms. The subsequent decrease in bacterial abundance during the development phase of the bloom suggests that the initial pool of DOM was fully utilized and that freshly released DOM was scarce. As expected, bacterial abundance increased during the declining phase of the bloom at 10 °C. Under warmer conditions, bacterial abundance decreased earlier during the initial bloom development than was observed at 10 °C, but was also marked by an earlier peak during the decline of the bloom, followed by a second, more variable peak in abundance. These variations in abundances probably reflect changes in the balance between bacterial growth and loss by grazing. When averaged over the experiment, we observed no effect of the treatments on the mean bacterial abundance (Fig. 4.2c–d; Table 4.1). At 10 °C, bacterial production was low at the beginning of the experiment and increased gradually during the development and declining phases of the bloom to reach peaks values of 9.3 ± 0.9 µg C L^{-1} d^{-1} (Fig. 4.2e). Bacterial production increased faster at 15 °C and reached maximal production rates of 19 ± 1 µg C L^{-1} d^{-1} on day 11. Results of the gls model show no effect of the pCO_2 gradient on bacterial production, but a positive effect of warming was observable throughout the experiment (Fig. 4.2f; Table 4.1).

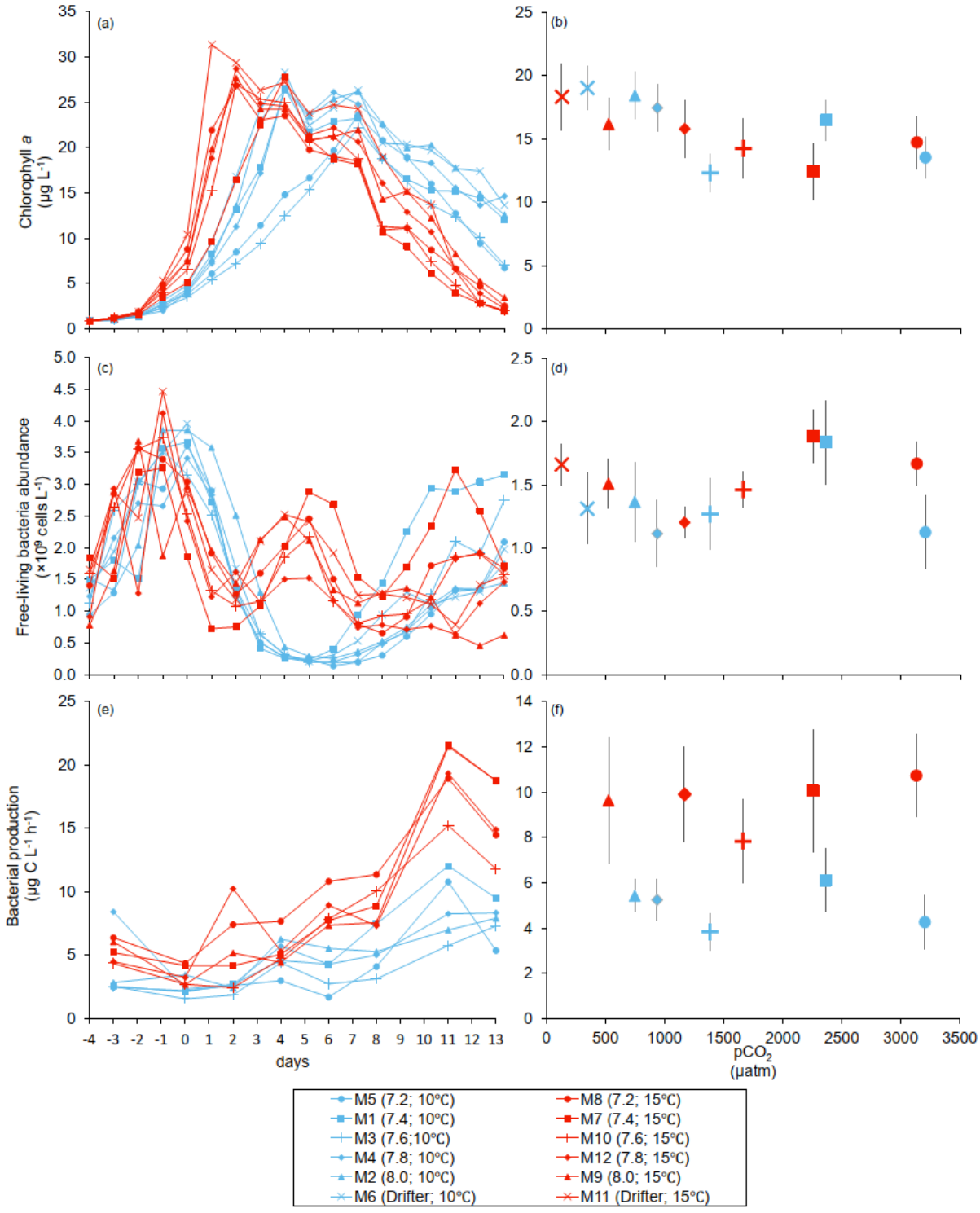

Figure 4.2 Temporal variations, and averages over the course of the experiment (day 0 to day 13) for: (a–b) chlorophyll *a*, (c–d) free-living bacteria abundance, (e–f) bacterial production. For symbol attribution to treatments, see legend.

Table 4.1 Results of the generalized least squares models (gls) tests for the effects of temperature, pCO_2, and their interaction over the duration of the experiment (day 0 to day 13). Separate analyses with pCO_2 as a continuous factor were performed when temperature had a significant effect. Averages of bacterial abundance and production, $DMSP_t$, DMS, Chl *a*-normalized $DMSP_t$ and DMS concentrations, and DMS:$DMSP_t$ ratios are presented. Natural logarithm transformation is indicated when necessary. Significant results are in bold. ***p<0.05, **p<0.01, ***p<0.001**.

Response Variable	Factor	df	t-value	p-value
Free-living bacterial abundance ($\times 10^9$ cells L^{-1})	Temperature	8	0.635	0.543
	pCO_2	8	-0.083	0.936
	pCO_2 x Temperature	8	0.221	0.830
Bacterial production ($\mu g\ C\ L^{-1}\ d^{-1}$)	Temperature	6	**2.454**	**0.050***
	pCO_2 (10°C)	3	-0.272	0.803
	pCO_2 (15°C)	3	0.746	0.510
$DMSP_t$ (nmol L^{-1})	Temperature	8	0.509	0.625
	pCO_2	8	-0.767	0.465
	pCO_2 x Temperature	8	0.134	0.897
DMS (nmol L^{-1})	Temperature	8	**6.822**	**<0.001****
	pCO_2 (10°C)	4	**-4.483**	**0.011***
	pCO_2 (15°C)	4	**-3.799**	**0.019***
$DMSP_t$:Chl *a* ratio (nmol (µg Chl *a*)$^{-1}$)	Temperature	8	**2.627**	**0.030***
	pCO_2	8	0.123	0.908
	pCO_2 x Temperature	8	0.621	0.568
DMS:Chl *a* ratio (nmol (µg Chl *a*)$^{-1}$)	Temperature	8	**5.225**	**<0.001****
	pCO_2 (10°C)	4	-1.373	0.242
	pCO_2 (15°C)	4	-2.227	0.090
Log(DMS:$DMSP_t$)	Temperature	8	**5.131**	**<0.001****
	pCO_2 (10°C)	4	-1.844	0.139
	pCO_2 (15°C)	4	**-3.138**	**0.035***

4.3.3 $DMSP_t$ and DMS

At in situ temperature, $DMSP_t$ concentrations averaged 9 ± 2 nmol L^{-1} on day 0 and increased regularly in all mesocosms up to day 10 before they plateaued or slightly decreased over the last 2–3 days (Fig. 4.3a). These results reveal that DMSP accumulation persisted for several days after the bloom peaks, to reach a maximum value between days 8–13 of 366 ± 22 nmol L^{-1}.

At 15 °C, $DMSP_t$ concentrations similarly increased after the maximum Chl *a* concentrations were reached, but increased faster than at in situ temperature. The maximum $DMSP_t$ concentrations were 396 ± 19 nmol L^{-1} at 15 °C, a value that is not statistically different from the peak values measured at 10 °C (Fig 4.4a; Table 4.2).

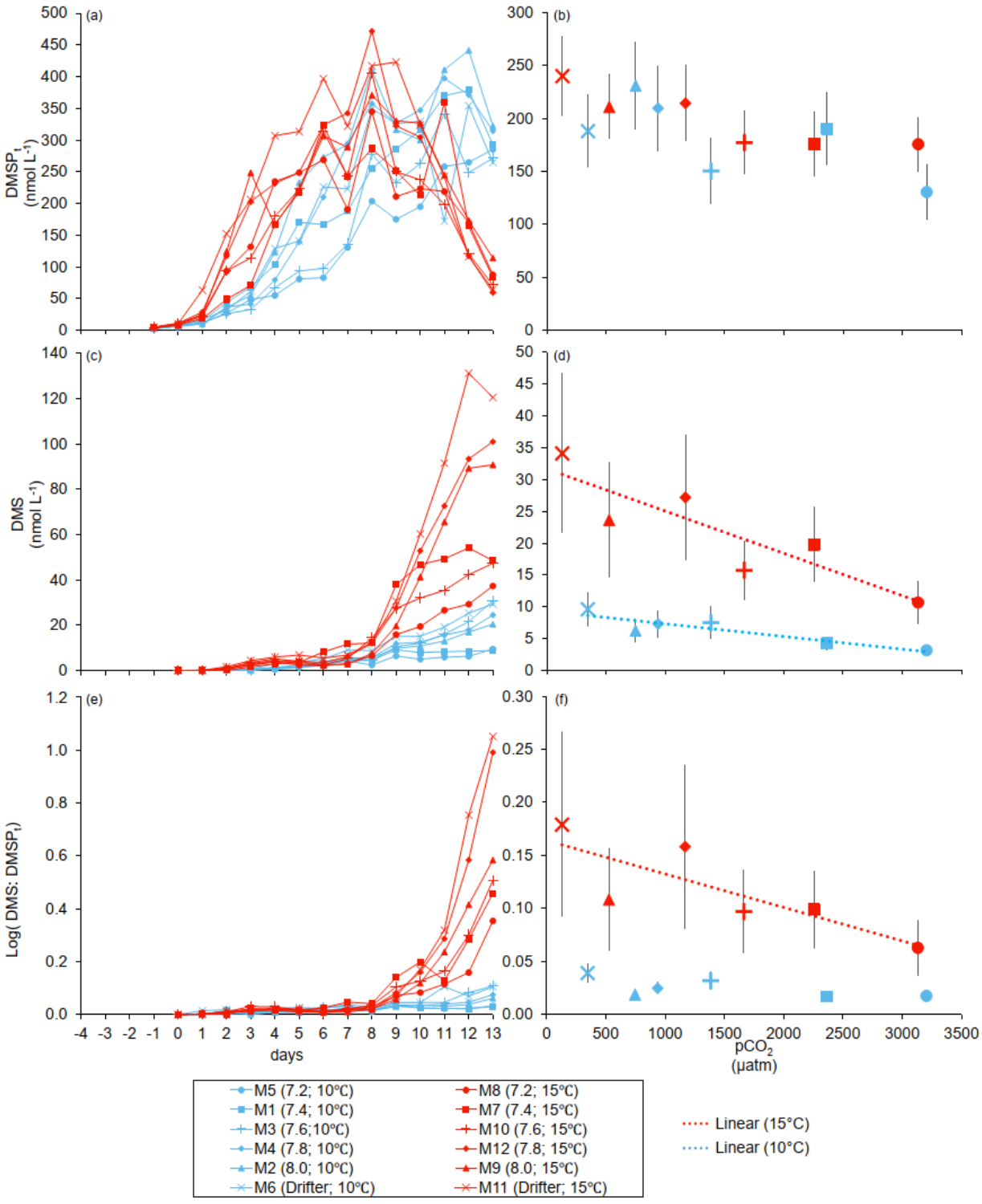

Figure 4.3 Temporal variations, and averages over the course of the experiment (day 0 to day 13) for: (a–b) $DMSP_t$, (c–d) DMS, (e–f) the natural logarithm of the DMS:$DMSP_t$ ratio. For symbol attribution to treatments, see legend.

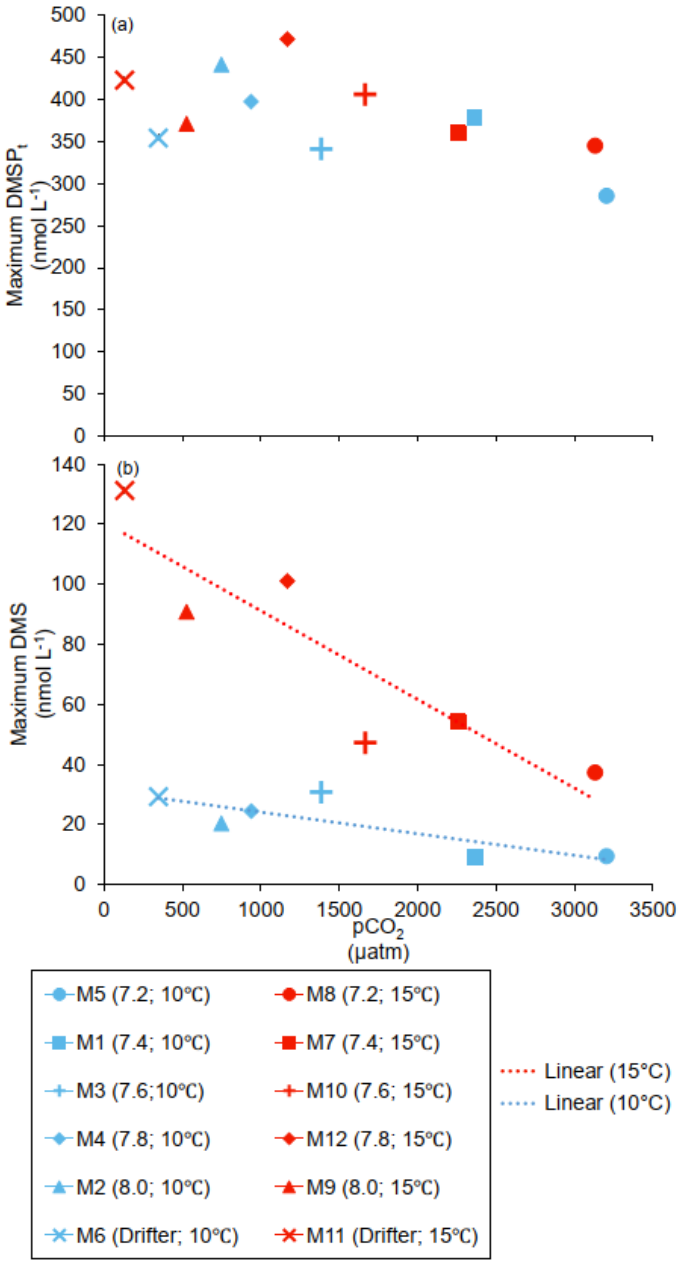

Figure 4.4 (a) Maximum $DMSP_t$ concentrations, (b) maximum DMS concentrations reached over the full course of the experiment (day 0 to day 13). For symbol attribution to treatments, see legend.

Table 4.2 Results of the generalized least squares models (gls) tests for the effects of temperature, pCO_2, and their interaction on the maximum values of the parameters measured during the experiment. Separate analyses with pCO_2 as a continuous factor were performed when temperature had a significant effect. Maxima of $DMSP_t$, and DMS concentrations are presented. Significant results are in bold. ***p<0.05, **p<0.01, ***p<0.001**.

Response Variable	Factor	df	t-value	p-value
$DMSP_t$ (nmol L^{-1})	Temperature	8	0.384	0.711
	pCO_2	8	-0.713	0.496
	pCO_2 x Temperature	8	0.300	0.772
DMS (nmol L^{-1})	Temperature	8	**6.403**	**<0.001*** **
	pCO_2 (10°C)	4	**-2.868**	**0.046***
	pCO_2 (15°C)	4	**-4.061**	**0.015***

A greater loss of DMSP took place in the last days of the experiment at 15 °C. By day 13, 79 ± 3 % of the peak $DMSP_t$ concentration was lost in the 15 °C mesocosms, while 19 ± 4 % of the peak $DMSP_t$ concentration was lost at 10 °C. When averaged over the duration of the experiment, the mean $DMSP_t$ concentrations were not significantly affected by the pCO_2 gradient, the temperatures or the interaction between these two factors (Fig. 4.3b; Table 4.1).

Over the 13 days, the $DMSP_t$:Chl *a* ratio averaged 11.4 ± 0.4 nmol (µg Chl *a*)$^{-1}$ at 10 °C and was not affected by increasing pCO_2 (Fig. 4.5a; Table 4.1). Due to the aforementioned mismatch between the peaks in Chl *a* and $DMSP_t$, the average $DMSP_t$:Chl *a* ratios were significantly higher at 15 °C, averaging 19 ± 1 nmol (µg Chl *a*)$^{-1}$ over the experiment (Fig. 4.5a; Table 4.1). However, we found no significant relationship between $DMSP_t$:Chl *a* and the pCO_2 gradient.

Initial DMS concentrations were below the detection limit on day 0 (< 0.9 nmol L^{-1}) and slowly increased during the first 7 days, while most of the build-up took place after day 8 in all treatments (Fig. 4.3b). The net accumulation of DMS was faster at 15 °C than at 10 °C, with higher daily DMS concentrations at 15 °C compared to 10 °C from day 3 until day 13. At the end of the experiment, DMS concentrations averaged 21 ± 4 nmol L^{-1} at 10 °C and 74 ± 14 nmol L^{-1} at 15 °C. Over the full duration of the experiment, we found significant negative effects of increasing pCO_2 on mean DMS concentrations at the two temperatures tested (Fig. 4.3d; Table 4.1). At 10 °C, we measured a ~67 % reduction of mean DMS concentrations from the drifter relative to the most acidified treatment (~345 ppm vs ~3200 ppm), with values decreasing from 10 ± 2 nmol L^{-1} to 3.2 ± 0.8 nmol L^{-1}. At 15 °C, the mean DMS concentrations decreased by roughly the same percentage (~69 %) as pCO_2 increased from the drifter to the most acidified treatment (~130 ppm vs ~3130 ppm). Nevertheless, the mean DMS concentrations were higher at 15 °C, ranging from

34 ± 13 nmol L^{-1} to 11 ± 3 nmol L^{-1}, an average increase of ~240 % compared to the DMS concentrations at 10 °C (Fig. 4.3d; Table 4.1). Similarly, the peak DMS concentrations decreased linearly with increasing pCO_2 at both temperatures and concentrations were always higher at 15 than at 10 °C for any given pCO_2 (Fig. 4.4b; Table 4.2).

The DMS:Chl *a* ratios remained below 1 nmol (µg Chl *a*)$^{-1}$ during the first 8 days in all mesocosms as DMS concentrations were low, but increased exponentially at 15 °C in the following days. At 10 °C, the DMS:Chl *a* ratio averaged 0.43 ± 0.7 nmol (µg Chl *a*)$^{-1}$ over the 13 days and was not affected by the pCO_2 gradient. At 15 °C, the DMS:Chl *a* ratios were not significantly affected by the pCO_2 gradient, but were significantly higher in the warmer treatment (Fig. 4.5b; Table 4.1).

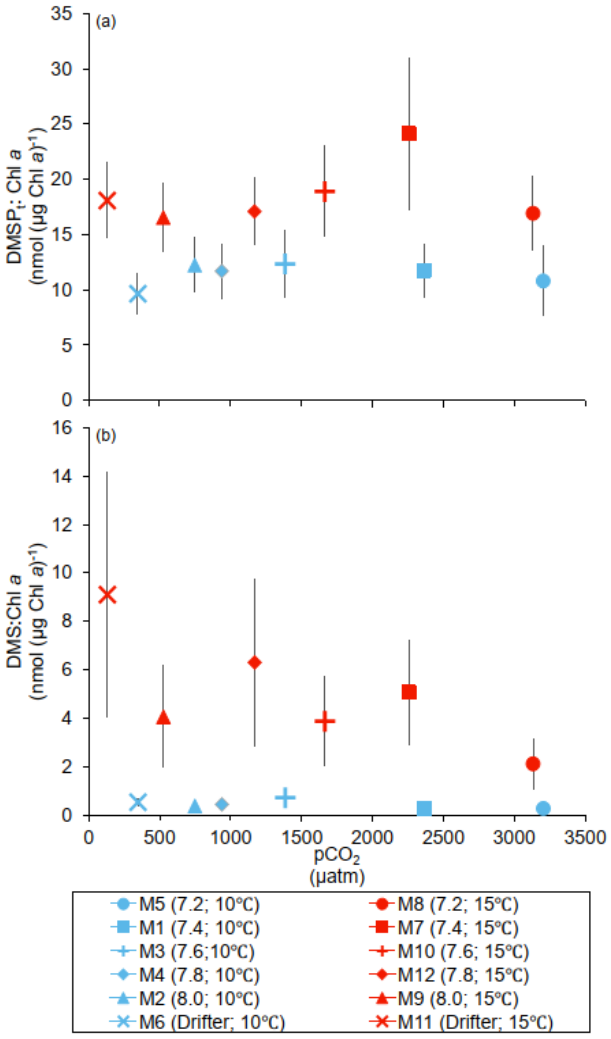

Figure 4.5 Averages over the course of the experiment (day 0 to day 13) for: (a) $DMSP_t$:Chl *a* ratio, (b) DMS:Chl *a* ratio. For symbol attribution to treatments, see legend.

The DMS:$DMSP_t$ ratio exhibited the same general pattern as the DMS, i.e. low and stable values during the first 8 days, and increasing values between days 8–13 (Fig. 4.3e). The natural logarithm of the DMS:$DMSP_t$ ratio was not affected by the pCO_2 gradient at 10 °C when averaged over the 13 days experiment, but a significant decrease of the DMS:$DMSP_t$ ratios was observed with increasing pCO_2 at 15 compared to 10 °C (Fig. 4.3f; Table 4.1). Moreover, there was a significant positive correlation between bacterial production and DMS concentrations, as 64 % of the variability of DMS concentrations is explained by variations in bacterial production ($r^2 = 0.64$, $p < 0.001$, $n = 70$; Fig. 4.6).

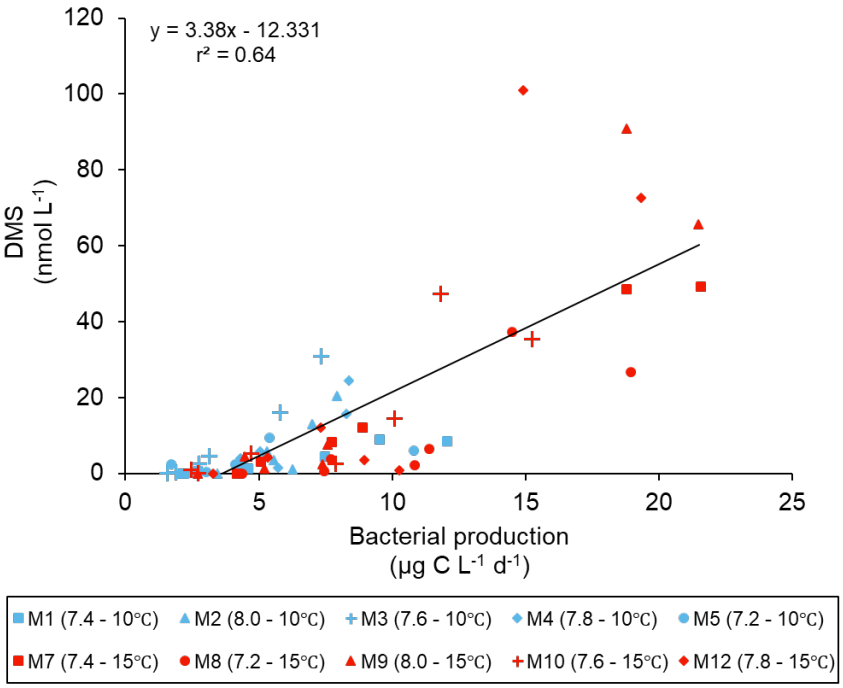

Figure 4.6 Linear regression between DMS concentrations and bacterial production during the experiment.

4.4. Discussion

4.4.1 General characteristics

As far as we know, this study is the first full factorial mesocosm experiment where all pCO_2 treatments (pH_T from 8.0 to 7.2) were replicated at two different temperatures (in situ and +5 °C), to assess the impact of ocean acidification and warming on the dynamics of DMSP and DMS concentrations during a phytoplankton bloom. A diatom bloom dominated by *Skeletonema costatum* developed in all mesocosms, regardless of the treatments. This chain-forming centric diatom is a cosmopolitan species in coastal and estuarine systems and a frequent bloomer in the Lower St. Lawrence Estuary (LSLE) (Kim et al., 2004; Starr et al., 2004; Annane et al., 2015). The 13 days where treatments were applied allowed us to capture the development and declining phases of the bloom. The impacts of the treatments on the dynamics of the bloom during these two phases are described in greater detail in Bénard et al. (2018b). Briefly, the acidification had no detectable effect on the development rate of the diatom bloom and on the maximum Chl *a* concentrations reached. However, increasing the water temperature by 5 °C increased the growth rate of the diatoms, shortening the development phase of the bloom, from 4–7 days at 10 °C to 1–4 days at 15 °C. However, these changes in the bloom timing did not alter the overall primary production throughout the experiment. Hereafter, we discuss how increasing pCO_2 (lowering the pH) affected DMSP and DMS concentrations and how a 5 °C increase in temperature altered the impacts of the pCO_2 gradient during the experiment.

4.4.2. DMSP dynamics

The buildup of the phytoplankton biomass during the bloom development was coupled with a rapid increase in $DMSP_t$ concentrations (Fig. 4.3a). Assuming that *S. costatum* was responsible for most of the DMSP production, our results indicate a low sensitivity of the DMSP synthesis pathway to acidification in this species. The net accumulation of $DMSP_t$ persisted several days after the peaks in Chl *a*, indicating a decoupling between DMSP synthesis, algal growth and nitrogen metabolism (Bénard et al., 2018b).

4.4.2.1 Effects of acidification on DMSP

At in situ temperature, the averaged $DMSP_t$ concentrations were not affected by the increase in pCO_2 (Fig. 4.3b; Table 4.1). The lack of significant changes in the $DMSP_t$:Chl *a* ratio as a function of the pCO_2 gradient also supports this conclusion (Fig. 4.5a; Table 4.1). This result is consistent with those of previous studies that showed a relatively weak effect of an increase in pCO_2 on DMSP

concentrations (Vogt et al., 2008; Lee et al., 2009; Avgoustidi et al., 2012; Archer et al., 2013; Webb et al., 2015). Furthermore, much like the patterns observed at 10 °C, there was no relationship between the concentrations of $DMSP_t$ and the pCO_2 gradient observable at 15 °C (Table 4.1).

4.4.2.2 Effects of warming on DMSP

In contrast to the absence of effects of acidification on DMSP, warming has been previously shown to affect DMSP concentrations in nature. Results from shipboard incubation experiments conducted in the North Atlantic have revealed an increase in particulate DMSP ($DMSP_p$) concentrations due to a 4 °C warming (Lee et al., 2009). During this last study, the higher $DMSP_p$ concentrations were attributed to a temperature-induced shift in community structure toward species with higher cellular DMSP content. During our study, the pCO_2 and temperature treatments did not alter the structure of the community (Bénard et al., 2018b). Most of the DMSP synthesis was likely linked to the numerically dominant diatoms, as all other algal groups identified contributed to less than 10 % of the total algal abundance (see Fig. 3.6 in chapter 3). Our results thus suggest that DMSP synthesis by *S. costatum* during the nitrate-replete growth phase was not significantly affected by warming. Rather, it is the accelerated growth rate of *S. costatum* that promoted the concurrent accumulation of biomass and $DMSP_t$, while the higher $DMSP_t$:Chl *a* ratio observable at 15 °C may be explained by the faster degradation of cells under warming. Several empty frustules were found during the last days of the experiment at 15 °C, suggesting a loss of integrity of the cells and potential increase of the release of intracellular dissolved organic matter, including DMSP. The increase in the abundance of bacteria and in bacterial production (Fig. 4.2c, e) during that period also suggest that more dissolved organic matter was produced during the decline of the bloom, as previously reported (Engel et al., 2004a, 2004b). During our experiment, transparent exopolymer particles (TEP) concentrations increased during this period (Gaaloul, 2017), adding to the evidence for heightened DOM production by the decaying bloom, with a potential increase in DMSP metabolization by heterotrophic bacteria under warming.

4.4.3 DMS dynamics

DMS concentrations remained very low during the development phase of the bloom (day 8) and increased in the latter days of the experiment. Most of the DMS accumulation in the mesocosms took place between days 8–13 and likely originated from DMSP that may have been released during cell lysis (Kwint and Kramer, 1995), or upon zooplankton grazing (Cantin et al., 1996). Unbalanced growth and photosynthesis of algal cells under nitrogen deficiency during that period may also be responsible for a greater production and active exudation of DMSP (Stefels et al., 2000; Kettles et al., 2014).

4.4.3.1 Effects of acidification on DMS

At in-situ temperature, we observed a significant linear decrease in DMS concentrations (both averaged over the full duration of the experiment and peak concentrations) with increasing pCO_2 (Figs. 4.3c, 4.4b; Tables 4.1 and 4.2). Several earlier mesocosm experiments have shown similar decreasing trends of DMS concentrations with increasing pCO_2 (Hopkins et al., 2010; Archer et al., 2013; Park et al., 2014; Webb et al., 2015, 2016). In these studies, the pCO_2-induced decreases in DMS were generally attributed to changes in the microbial community speciation and structure, or to microzooplankton grazing, although decreases in bacterial DMSP-to-DMS conversion or increases in DMS consumption have also been suggested (Archer et al., 2013; Hussherr et al., 2017). During our study, the decrease in DMS concentrations with increasing pCO_2 cannot be directly attributed to a decrease in $DMSP_t$ since this pool was not affected by the pCO_2 gradient (Figs. 4.3b, 4.4a; Tables 4.1 and 4.2). In Park et al. (2014), the increase in pCO_2 led to the reduction in the abundance of *Alexandrium* spp., an active DMSP and DMSP-lyase producer, and a concomitant reduction of the associated microzooplankton grazing. As *Alexandrium* spp. was less numerous, the associated attenuation of microzooplankton grazing resulted in a reduction of the mixing of DMSP and DMSP-lyase, leading to less DMSP-to-DMS conversion. Given the strong contribution of *S. costatum* to the bloom, a species with no reported DMSP-lyase, it can be assumed that most, if not all, of the DMS produced was driven by bacterial processes following DMSP release by the diatoms. Thus, the decrease in DMS concentrations in our study could have been the result of altered bacterial mediation; either through reduced bacterial production of DMS or heightened bacterial consumption of DMS. Whereas a reduction in bacterial uptake of DMSP is unlikely, given that the bacterial abundance and production were unaffected by the pCO_2 gradient (Table 4.1), the observed decrease in DMS concentrations could imply that at higher pCO_2 the bacterial yields of DMS are abated. The relative proportion of DMSP consumed by bacteria and further cleaved into DMS is closely tied to bacterial demand in carbon and sulfur as well as to the availability of DMSP relative to other sources of reduced sulfur in the environment (Levasseur et al., 1996; Kiene et al., 2000; Pinhassi et al., 2005). The absence of a significant pCO_2 effect on the concentrations of DMSP during this study may be interpreted as a pCO_2-related alteration of the microbially-mediated fate of consumed DMSP. Unfortunately, in the absence of detailed $^{35}S\text{-}DMSP_d$ bioassays, it is impossible to confirm the outcome of the DMSP metabolic pathways including the DMSP-to-DMS conversion efficiency in relation to the pCO_2 gradient as was described in Chapter 2. A few studies (Grossart et al., 2006; Engel et al., 2014; Webb et al., 2015;) have reported enhanced bacterial abundance and production at high pCO_2, especially for attached bacteria as opposed to free-living (Grossart et al., 2006). However, regardless of the temperature treatment, neither the abundance nor the activity of bacteria seemed to be significantly impacted by pCO_2 in this study. A pCO_2-induced increase in bacterial DMS turnover could also explain the decrease in DMS

concentrations, but several studies suggest that bacterial DMS consumption in natural systems is often tightly coupled to DMS production itself (Simó, 2001, 2004). Furthermore, while one laboratory study reported that non-limiting supplies of DMS may be used as a substrate by several members of Bacteroidetes (Green et al., 2011), another study showed that only a subset of the natural microbial population may turnover naturally-occurring levels of DMS (Vila-Costa et al., 2006b). Nevertheless, the sensitivity of these DMS-consuming bacteria to decreasing pH remains unknown. Likewise, whereas we cannot exclude a potential impact of pCO_2 on DMS turnover via bacterioplankton, it is plausible that the pCO_2 gradient may have affected a widespread physiological pathway among bacteria, specifically, the metabolic breakdown of DMSP (Chapter 2).

4.4.3.2 Effects of warming on DMS

A warming by 5 °C increased DMS concentrations at all pCO_2 tested, resulting in an offset of the negative pCO_2 impact when compared to the in situ temperature. This result differs from the observation of Kim et al. (2010) and Park et al. (2014) in two ways. First, our results show an increase in DMS concentrations in the warmer treatment while the two previous studies reported a decrease. Second, our results confirm that a temperature effect may be measured over a large range of pCO_2. It is noteworthy that the increase in DMS concentrations at the two temperatures tested varied from 110% at pH 8.0 up to 370% at pH 7.4. This highlights the scaling of the temperature effect over an extensive range of pCO_2 and the importance of simultaneously studying the impact of these two factors on DMS production. As observed at 10 °C, both the average and the peak DMS concentrations decreased linearly as pCO_2 increased in the warm treatment (Figs. 4.3d, 4.4b; Tables 4.1 and 4.2). Nevertheless, the pCO_2-induced decrease in DMS concentrations at 15 °C cannot be directly attributed to a decrease in $DMSP_t$ concentrations given that an increase in pCO_2 had no discernable effect on $DMSP_t$ concentrations. In contrast to our observations at the in situ temperature, where $DMSP_t$ continued to increase until day 12, $DMSP_t$ concentrations at 15 °C typically decreased from day 8 onward (Fig. 4.3a). This loss in $DMSP_t$ suggests that microbial consumption of DMSP exceeded DMSP algal synthesis. In light of the dominance of *S. costatum*, a phytoplankton taxon not known to exhibit DMSP-lyase activity, the bulk of microbial DMSP mediation was likely associated with heterotrophic bacteria. In support of this hypothesis, the bacterial production was ~2 times higher at 15 than at 10 °C between days 8–13 (19 ± 1 µg C L^{-1} d^{-1} vs 9.3 ± 0.9 µg C L^{-1} d^{-1}; Fig. 4.2), and we observed a significant correlation between the quantity of $DMSP_t$ lost during Phase II (day of the $DMSP_t$ peak concentration to day 13) and the quantity of DMS produced during the same period (coefficient of determination, $r^2 = 0.60$, $p < 0.01$, $n = 11$). Assuming that all the $DMSP_t$ lost was transformed into DMS by bacteria, we calculated that DMS yields could have varied by 0.5 to 32 % across the pCO_2 gradient (mean = 13 ± 11%). These very rough estimates of DMS yields are likely at the lower end since

measured DMS concentrations also reflect losses of DMS through photo-oxidation and bacterial consumption. Nevertheless, we cannot exclude the possibility of some passive uptake of DMSP by the picocyanobacterial population in the mesocosms, although this pathway is not considered to be significant in natural systems (Malmstrom et al., 2005; Vila-Costa et al., 2006a) and does not lead to the production of DMS. Moreover, our estimates do not account for the possible DMSP assimilation by grazers, reducing the $DMSP_d$ available for bacteria, and would lead to an increase in DMS yields. Our 'minimum community' DMS yield estimates agree with an expected range of microbial DMS yields in natural environments, from 2 % to 45 % (see review table in Lizotte et al., 2017). These gross but realistic estimates of heterotrophic bacterial DMSP-to-DMS conversions could explain the bulk of the DMS present in our study, a hypothesis also supported by the strong positive correlation ($r^2 = 0.64$, $p < 0.001$, $n = 70$; Fig. 4.6) between overall DMS concentrations and bacterial production rates. Combined, these findings reinforce the idea that bacterial metabolism, rather than bacterial stocks, may significantly affect the fate of DMSP (Malmstrom et al., 2004a, 2004b, 2005; Vila et al., 2004; Vila-Costa et al., 2007; Royer et al., 2010; Lizotte et al., 2017) and that drivers of environmental change, such as temperature and pH, that can alter bacterial activity and strongly impact the gross and net production of DMS. Specific measurements of bacterial DMSP uptake and DMS yields using $^{35}S\text{-}DMSP_d$ should be conducted to assess the impacts of pCO_2 and temperature on the microbial fate of DMSP.

4.4.4 Limitations

During our study, the pCO_2 changes were applied abruptly, over a day, from in situ values to pCO_2 levels exceeding the most pessimistic pCO_2 scenarios for the end of the century. Compared to our manipulation, ocean acidification will proceed at a much slower rate, potentially allowing species to adapt and evolve to these changing conditions (Stillman and Paganini, 2015; Schlüter et al., 2016). However, in the LSLE, the upwelling of low oxygenated waters can rapidly reduce the pH_T to ~7.62, or even lower with contributions of low pH_T (7.12) freshwaters from the Saguenay River during the spring freshet (Mucci et al., 2017). Thus, the swift and extensive pCO_2 range deployed in our experiment may seem improbable for the open ocean on the short term, but may not be inconceivable for this coastal region. However, the warming of 5 °C used in this mesocosm study possibly exceeds the upper limit of temperature increase for the end of the century in this region. In the adjacent Gulf of St. Lawrence (GSL), surface waters temperature (SST) correlates strongly with air temperature, allowing the estimation of past SST. This relationship showed that SST has increased in the GSL by 0.9 °C per century since 1873 (Galbraith et al., 2012), although additional positive anomalies of 0.25–0.75 °C per decade have been shown between 1985 and 2013 (Galbraith et al., 2016). In the LSLE, the highest temperatures occur at the end of summer / early fall, and gradually dissipate by heating the subjacent cold intermediate layer through vertical mixing

(Cyr et al., 2011). The extent of the projected warming in the LSLE is recondite, but will likely result from the multifaceted interactions between heat transfer from the air and physical factors controlling the water masses.

The results from our study could also be influenced by the absence of macrograzers in the mesocosms. An additional grazing pressure could limit the growth of the blooming species, reducing the amount of DMSP produced or could increase the release of $DMSP_d$ through sloppy feeding after the initial bloom (Lee et al., 2003). It is unclear how an increase in grazing pressure would have impacted the concentrations of DMS in our experiment. On the one hand, increased predation could have limited the net accumulation of $DMSP_p$, with a possible reduction in DMS production. On the other hand, increased grazing could have favoured the release of $DMSP_p$ as DMSPd, thus increasing the availability of this substrate for microbial uptake, mediation and possible conversion into DMS. Despite the absence of reported changes in community composition in our study, many OA mesocosm experiments have described changes in DMS concentrations associated with shifts in community structure in the past (Vogt et al., 2008; Hopkins et al.,2010; Kim et al., 2010, Park et al., 2014, Webb et al., 2015). Nonetheless, our results align with those of other OA studies (Archer et al., 2013; Hussherr et al., 2017), suggesting that the mediation of heterotrophic bacteria plays a major role in DMS cycling in the absence of reported phytoplanktonic DMSP-lyase, such as in a diatom dominated bloom in the LSLE.

4.5 Conclusions

The objective of this study was to quantify the combined impact of increases in pCO_2 and temperature on the dynamics of DMS during a fall diatom bloom in the St. Lawrence Estuary. Our mesocosm experiment allowed us to capture the development and declining phases of a bloom strongly dominated by the diatom *Skeletonema costatum* and the related changes in bacterial abundance and production. As expected, warming accelerated the development of the bloom, but also its decline. Both $DMSP_t$ and DMS concentrations increased during the development phase of the bloom, but peak concentrations were reached as the bloom was declining. Increasing pCO_2 had no discernable effect on the total amount of $DMSP_t$ produced at both temperatures tested. In contrast, increasing the pCO_2 to the value forecasted for the end of this century resulted in a linear decrease in DMS concentrations by 33 % and by as much as 69 % over the full pCO_2 gradient tested. These results are consistent with previous reports that acidification has a greater impact on the processes that control the conversion of DMSP to DMS than on the production of DMSP itself. The pCO_2-induced decrease in DMS concentrations observed in this study adds to the bulk of previous studies reporting a similar trend. In diatom dominated systems, such as the one under study in this experiment, heterotrophic processes underlying DMS production seem to be most

sensitive to modifications in pCO_2. Whereas predatory grazing and its associated impacts on DMS production cannot be ruled out entirely, the decreases in DMS concentrations in response to heightened pCO_2 are likely related to reductions in bacterial-mediated DMS production, a hypothesis partly supported by the significant positive correlations found between bacterial production rates and DMS concentrations. Whereas the DMS concentrations decreased significantly with increasing pCO_2 at both 10 °C and 15 °C, warming the mesocosms by 5 °C translated into a positive offset in concentrations of DMS over the whole range of pCO_2 tested. Higher DMSP release and increased bacterial productivity in the warm treatment partially explain the stimulating effect of temperature on DMS net production. Overall, results from this full factorial mesocosm experiment suggest that warming could mitigate the expected reduction in DMS production due to ocean acidification, even increasing the net DMS production with the potential to curtail radiative forcing.

4.6 Acknowledgements

The authors wish to thank the Station aquicole-ISMER, particularly Nathalie Morin and her staff, for their support during the mesocosm experiment. We also wish to acknowledge Gilles Desmeules, Bruno Cayouette, Sylvain Blondeau, Claire Lix, Rachel Hussherr, Liliane St-Amand, Marjolaine Blais, Armelle Galine Simo Matchim and Marie-Amélie Blais for their precious help over the duration of the experiment. This study was funded by a Team grant from the Fonds de recherche du Québec – Nature et technologies (FRQNT-Équipe-165335), the Canada Foundation for Innovation, the Canada Research Chair on Ocean Biogeochemistry and Climate, and by Fisheries and Oceans Canada. This is a contribution to the research program of Québec-Océan.

Chapitre 5 Conclusion générale

Cette thèse regroupe les résultats de deux expériences réalisées dans l'estuaire maritime du Saint-Laurent (EMSL). Les résultats de ses expériences ont permis de mieux cerner l'impact de l'acidification des eaux sur la communauté planctonique de cette partie de l'estuaire, les processus régissant sa production de DMS et la modulation de ces effets par le réchauffement prévu des eaux de surface. Dans le chapitre 2, mes premiers résultats mettent en évidence l'impact potentiel de l'acidification sur la communauté phytoplanctonique de l'EMSL. Dans cette expérience réalisée en microcosmes, j'ai observé que la floraison estivale de diatomées est généralement résistante à une acidification modérée, bien que l'abondance relative des diatomées, habituellement dominantes, soit réduite. Les effets négatifs de l'acidification surviennent principalement lorsque la communauté est soumise à une forte augmentation (facteur 3) des concentrations de pCO_2, engendrant une diminution de la production primaire. L'acidification des eaux résulte également en une diminution des concentrations de DMS. Des mesures du métabolisme microbien réalisées au cours de cette expérience montrent que la diminution du DMS à faible pH s'explique par une diminution de la conversion du DMSP en DMS par les bactéries, accompagnée d'une augmentation de la rétention du DMSP consommé et non transformé. Cette réponse bactérienne pourrait représenter une réaction au stress occasionné par la diminution du pH. Dans les chapitres 3 et 4, je me suis intéressé aux effets potentiellement interactifs du réchauffement des eaux et de leur acidification sur le développement des floraisons phytoplanctoniques (chapitre 3) et la production nette de DMS (chapitre 4). Lors de cette expérience, réalisée en mésocosmes, la communauté planctonique automnale de l'EMSL a été soumise à un gradient prononcé de pCO_2 à deux températures, soit la température in situ de 10 °C et à 15 °C. Le développement de la diatomée dominante lors de cette expérience, *Skeletonema costatum*, n'a pas été affecté par le gradient de pCO_2, et ce jusqu'à des valeurs de 3000 µatm. Contrairement à l'acidification, le réchauffement a eu un effet significatif sur le développement et le déclin de la floraison en accélérant les deux processus. Seuls les picocyanobactéries présentes lors du déclin de la floraison de diatomées ont démontré un effet antagoniste des augmentations de la pCO_2 et de la température. Mes mesures de production primaire ont cependant montré que l'acidification et le réchauffement n'avaient pas d'effet significatif sur la production primaire intégrée sur la toute la durée de la floraison. Lors de cette expérience en mésocosmes, l'augmentation de la pCO_2 s'est traduite par une diminution des concentrations en DMS, et ce aux deux températures testées (chapitre 4). Cette diminution du DMS en réponse à l'acidification concorde avec les observations effectuées lors de l'expérience réalisée sur la communauté estivale (chapitre 2) et la plupart des expériences similaires réalisées à ce jour dans différents environnements marins. Tel que mis en évidence au chapitre 2, l'effet négatif de l'acidification sur la production de DMS reporté ici semble résulter d'une altération du métabolisme bactérien. Cet effet négatif de l'acidification sur la production nette de DMS était par contre annulé

par le réchauffement, les concentrations de DMS étant supérieures à 15 °C qu'à 10 °C à toutes les pCO_2 testées. Ces résultats inédits suggèrent que le réchauffement des eaux de surface lié au réchauffement global pourrait contrer l'effet négatif de l'acidification sur la production nette de DMS dans l'EMSL et potentiellement dans l'océan mondial. Cette thèse représente une contribution majeure à la compréhension des processus de production bactérienne du DMS et leur altération face à l'acidification ainsi qu'une avancée concrète dans l'étude des effets combinés de l'acidification et du réchauffement des eaux de surface sur les communautés phytoplanctoniques de milieux estuariens.

5.1 Synthèse

Ma première expérience en microcosmes sur le développement de la floraison estivale phytoplanctonique de l'estuaire du Saint-Laurent soumise à des conditions d'acidification a permis d'effectuer le suivi d'une communauté exposée à des pCO_2 initiales in situ ($1 \times pCO_2 = 775$ µatm), doublées ($2 \times pCO_2 = 1850$ µatm) et triplées ($3 \times pCO_2 = 2700$ µatm). Au cours des 12 jours de cette expérience, un assemblage mixte de phytoplancton s'est développé dans chaque microcosme. La communauté était composée de plusieurs diatomées, dont *Chaetoceros* spp., *Skeletonema costatum*, et *Thalassiosira* spp, ainsi que de petites cellules flagellées. L'accumulation de biomasse était similaire entre le contrôle et le traitement $2 \times pCO_2$, atteignant respectivement 20 ± 4 µg Chl *a* L^{-1} et 17 ± 1 µg Chl *a* L^{-1}, tandis que le traitement $3 \times pCO_2$ n'a atteint que 11 ± 4 µg Chl *a* L^{-1} avec un délai de deux jours par rapport aux deux autres traitements. Cette différence entre les traitements était également observable sur les mesures de production primaire, des taux significativement plus faibles de production étant mesurés à $3 \times pCO_2$ comparativement à $1 \times pCO_2$. Ces résultats suggèrent que l'effet négatif de la pCO_2 sur la production primaire et la biomasse sont attribuables à une diminution de l'abondance relative des diatomées (de 60 % dans le traitement $1 \times pCO_2$ à 37 % dans le traitement $3 \times pCO_2$) qui sont généralement responsables de la production primaire lors des floraisons estivales dans l'EMSL. Cet effet négatif est par contre inattendu puisque les diatomées, dû à la faible affinité de la RuBisCO pour le CO_2, devraient théoriquement bénéficier de l'enrichissement en pCO_2. Étant donné la diversité de l'assemblage planctonique présent lors de cette expérience, il est possible que les diatomées aient dû faire face à une forte compétition et à une pression de broutage accrue par le microzooplancton, laquelle tend à augmenter leur sensibilité à l'acidification.

Les mesures du métabolisme bactérien du DMSP sous conditions d'acidification rapportées ici constituent une première. Mes résultats montrent que l'efficacité de la prise bactérienne du DMSP est peu affectée par les conditions de pCO_2, mais il en va autrement pour ce qui est de l'utilisation qu'en font les bactéries. Les mesures effectuées grâce au $^{35}S\text{-}DMSP_d$ révèlent une réduction de

l'efficacité de conversion microbienne du DMSP en DMS, passant de 47 % à 31 % et 18 % respectivement à 1 × pCO_2, 2 × pCO_2 et 3 × pCO_2. Ce changement marqué dans l'efficacité de conversion microbienne du DMSP en DMS explique en partie les diminutions de 15 % et de 40 % des concentrations moyennes de DMS mesurées dans le traitement intermédiaire et le plus acidifié par rapport au contrôle. Dans des conditions où la production de DMS est principalement médiée par les bactéries, telles que lors des floraisons de diatomées, une baisse de la métabolisation du DMSP en DMS serait le principal facteur modulant ces concentrations (r_S = 0,65; $p < 0,001$; n = 45). Incidemment, mes résultats suggèrent que les bactéries pourraient accumuler le DMSP sans le métaboliser, potentiellement afin de pallier les augmentations de $[H^+]$, diminuant de ce fait leur production de DMS; les deux processus étant inversement corrélés (r_S = -0,62; $p < 0,001$; n = 44). Les résultats de ce chapitre constituent une avancée dans l'étude des processus de production du DMS en condition d'acidification, quantifiant pour la première fois la baisse de l'efficacité bactérienne de conversion du DMSP en DMS et identifiant un possible mécanisme expliquant cette diminution.

La résistance de la communauté planctonique estivale face à une acidification modérée et les effets modestes décelés dans le cas d'une acidification sévère nous ont poussés à revoir notre méthodologie pour l'expérience présentée dans les chapitres 3 et 4. L'utilisation d'un gradient de pH (et de pCO_2 correspondantes) nous a permis de monitorer les changements dans la communauté planctonique et d'identifier la présence de réponses linéaires face à ce gradient. De plus, l'utilisation combinée de deux températures avec le gradient de pCO_2 nous a permis d'identifier la présence d'effets additifs, synergétiques ou antagonistes avec la pCO_2. Dans cette expérience, une floraison automnale de *Skeletonema costatum* a dominé tous les traitements, atteignant une biomasse maximale de 27 ± 2 µg L^{-1} indépendamment de la pCO_2. L'absence d'effets négatifs sur le développement de *S. costatum* suggère que les floraisons dominées par cette espèce dans l'EMSL ne seront pas influencées par l'acidification. L'augmentation de la température a cependant eu un effet stimulateur sur le développement et le déclin de la floraison. Un réchauffement de 5 °C a accéléré l'accroissement de la biomasse, les concentrations maximales de chlorophylle *a* étant atteintes entre les jours 1–4 plutôt que 4–7, à 15 °C et à 10 °C respectivement. Les picocyanobactéries qui ont succédées à *S. costatum* lors du déclin de leur floraison ont quant à elles été stimulées par l'augmentation de la température malgré un effet négatif de l'augmentation de la pCO_2, variant de 4,4 ± 0,2 à 3,0 ± 0,3 × 10^6 cellules L^{-1} à 15 °C entre les deux traitements extrêmes de pCO_2. Comparativement, l'abondance des picocyanobactéries était plutôt de 2,7 ± 0,4 × 10^6 cellules L^{-1} à 10 °C pendant cette phase de déclin de la floraison de diatomées. Le développement rapide des diatomées a été accompagné par une hausse momentanée de la production primaire, mais comme le déclin a également été précipité, il n'y a pas eu d'effet global de la température sur la production primaire intégrée sur la durée de l'expérience. Toutefois, nos résultats indiquent que les valeurs maximales journalières de

production primaire pourraient être plus élevées dans des eaux de surface plus chaudes. Conséquemment, les résultats de ce chapitre ont montré que le réchauffement des eaux de surface est susceptible d'avoir un impact plus marqué que l'acidification sur le développement de la floraison phytoplanctonique automnale et sa succession dans l'EMSL. La résistance des diatomées à l'acidification pourrait résulter de l'adaptation des espèces phytoplanctoniques présentes dans l'EMSL face aux importantes variations de pH pouvant avoir lieu en milieu estuarien. Les espèces présentent auraient donc la capacité de s'acclimater rapidement à de grandes variations de pH dues aux processus physiques en cours dans les estuaires comme les remontées d'eau profonde, le mélange vertical et les apports d'eau douce.

Dans le quatrième chapitre, j'ai démontré que le réchauffement des eaux de surface pouvait affecter de façon considérable l'effet négatif de l'acidification sur la production nette de DMS souvent reporté en milieux marins. Motivée par la relation négative mise en évidence entre les concentrations de DMS et la pCO_2 lors de ma première expérience en microcosmes, j'ai voulu tester la robustesse de cette relation dans le contexte du réchauffement global. Les concentrations de $DMSP_t$ et de DMS ont augmenté au cours du développement de la floraison de *S. costatum*, atteignant cependant leurs valeurs maximales 2–4 jours après le pic de Chl *a*. Les concentrations moyennes de $DMSP_t$ n'ont pas été influencées par les traitements de pCO_2, ni par le réchauffement. Similairement, les concentrations maximales de $DMSP_t$ n'ont pas varié selon les traitements, culminant à 380 ± 50 nmol L^{-1} dans tous les mésocosmes. En revanche, tel qu'observé lors de ma première expérience, les concentrations de DMS ont diminué linéairement en fonction de la pCO_2. Les concentrations de DMS ont diminué de ~66 % entre le traitement le moins acidifié et le traitement le plus acidifié. Lors de cette expérience, les concentrations de DMS étaient positivement corrélées avec la productivité bactérienne (r^2 = 0,64, $p < 0,001$, n = 70). Cette relation suggère que les bactéries étaient principalement responsables de la production du DMS dans les mésocosmes, tel qu'observé lors de ma première expérience. Tel qu'observée à 10 °C, l'augmentation de la pCO_2 a résulté en une diminution de ~69 % des concentrations de DMS à 15 °C. Cependant, l'effet interactif de la température avec la pCO_2 a engendré une augmentation considérable des concentrations moyennes de DMS, augmentant celles-ci de ~240 % à 15 °C par rapport à 10 °C. Cette hausse de production nette de DMS est partiellement explicable par un plus grand relargage du DMSP algal couplé à une augmentation de la productivité bactérienne. En effet, les variations de DMS entre le jour de $DMSP_t$ maximal et la fin de l'expérience sont principalement expliquées par la disparition du $DMSP_t$ pendant cette période (r^2 = 0,60, $p < 0,01$, n = 11), alors que la production bactérienne était deux fois plus élevée à 15 °C qu'à 10 °C (10 ± 1 µg C $L^{-1}d^{-1}$ vs 5 ± 1 µg C $L^{-1}d^{-1}$). Ces résultats démontrent le potentiel de mitigation de l'augmentation de la température sur la production nette de DMS par rapport à l'acidification. La diminution de l'efficacité bactérienne de conversion du DMSP en DMS en fonction de la pCO_2 serait toujours présente dans des eaux de surface plus chaudes et acides, mais l'effet stimulant du réchauffement sur le

métabolisme bactérien supplanterait cet effet négatif de l'acidification et pourrait même engendrer une augmentation de la production nette de DMS.

Pour conclure, cette thèse met en évidence la complexité des processus mis en cause dans le développement des floraisons planctoniques de l'EMSL et la production de DMS dans un contexte de changements globaux. Mes résultats ont montré que la métabolisation bactérienne du DMSP pouvait être sensible à l'acidification, une sensibilité précédemment suggérée, mais jusqu'ici non mesurée. Mes résultats indiquent également que les bactéries consomment autant de DMSP en conditions plus acides, toutefois sans le transformer. Les floraisons phytoplanctoniques de l'EMSL sont généralement résistantes à des variations élevées de pCO_2, puisque peu d'effets significatifs ont été décelés lors du développement de deux floraisons, estivale et automnale, et de la production primaire associée. Cette résistance pourrait refléter leur capacité d'acclimatation rapide au milieu estuarien où des variations de pH importantes (~0,08 unité) et brusques (~50 heures) prennent place dues aux apports d'eau douce, aux remontées d'eau profonde et au mélange vertical. Finalement, nos résultats ont montré que le réchauffement, plutôt que l'acidification, est plus susceptible d'altérer le fonctionnement de l'écosystème de l'estuaire maritime du Saint-Laurent en précipitant la croissance et le déclin du phytoplancton. Similairement, l'augmentation de la température a stimulé la production nette de DMS malgré de fortes diminutions causées par l'acidification. Cette thèse soulève donc de nombreuses interrogations quant au métabolisme bactérien et son utilisation du DMSP sous acidification, mais également en ce qui a trait à la sensibilité de l'EMSL aux variations de température, un phénomène possiblement plus important que l'acidification dans ce contexte côtier.

5.2 Perspectives

Les résultats de mes recherches ont permis de faire des avancées significatives sur les impacts potentiels de l'acidification des océans sur le développement des floraisons phytoplanctoniques et la production de DMS. Bien que réalisées en milieu estuarien, plusieurs de mes observations, notamment celles touchant l'effet combiné de l'acidification et du réchauffement sur le métabolisme bactérien du DMSP, s'appliquent à l'océan global. Comme c'est toujours le cas en science, mes travaux suscitent des questionnements qui mériteraient d'être considérés lors de recherches ultérieures.

Mes résultats présentés dans le chapitre 2 ont montré la sensibilité à l'acidification de l'efficacité de la conversion bactérienne du DMSP en DMS. Il serait toutefois important d'effectuer davantage d'études à l'aide du biotraceur $^{35}S\text{-}DMSP_d$ dans des contextes océaniques variés afin de vérifier la robustesse de cette relation. Par exemple, l'influence de l'intensité lumineuse sur la production

bactérienne de DMS a déjà été démontré par le passé (Slezak et al., 2007; Ruiz-Gonzalez et al., 2012). Il serait donc opportun d'effectuer des expériences où différentes communautés planctoniques seraient soumises aux trois stress acidification, réchauffement et lumière. De plus, les méthodes utilisées lors de notre expérience en microcosmes ne nous ont pas permis d'identifier les espèces responsables ni les enzymes spécifiques responsables de la conversion du DMSP en DMS. Il existe plusieurs familles d'enzymes capables de catalyser le DMSP pour produire du DMS, chacune ayant des efficacités variables (Lei et al., 2018). Il serait essentiel d'identifier les DMSP-lyases lors d'expériences similaires afin de catégoriser les familles d'enzymes pouvant être sensibles ou non à l'acidification, puisque certaines espèces de bactéries peuvent posséder plusieurs familles d'enzymes. D'ailleurs, il serait aussi utile de caractériser les espèces microbiennes de l'EMSL pouvant catalyser le DMSP afin d'utiliser nos expériences comme analogues et améliorer nos prédictions quant à la production de DMS sous acidification.

Les résultats présentés au chapitre 2 identifient un mécanisme potentiel de rétention du DMSP chez les bactéries en réponse à l'acidification. La capacité des bactéries d'accumuler du DMSP sans le métaboliser a déjà été démontrée (Kiene et al., 1999; Kiene and Linn, 2000; Kiene et al., 2000; Yoch, 2002; Reisch et al., 2011), mais pas en réponse à l'acidification. Malgré l'importance accordée aux bactéries lors de notre étude, une partie du ^{35}S-DMSP particulaire pourrait également avoir été assimilée par les diatomées ou les cyanobactéries dont la capacité à assimiler le DMSP dissous a été démontrée (Vila-Costa et al., 2006b; Ruiz-Gonzalez et al., 2012). Afin de pallier ces incertitudes, il serait nécessaire de quantifier précisément le devenir du ^{35}S-DMSP en utilisant des méthodes complémentaires comme la chromatographie en phase liquide à haute performance (*High-performance liquid chromatography; HPLC*; Kiene and Linn, 2000) et la microautoradiographie combinée à l'hybridation fluorescente in situ (*microautordiograhpy and fluoresce in situ hybridization; Micro-FISH*; Malmstrom et al., 2004b) afin de corroborer nos hypothèses.

Dans les chapitres 3 et 4, j'ai présenté les résultats d'une expérience où une communauté naturelle planctonique de l'EMSL était soumise à un gradient de pCO_2 et à deux températures (10 et 15 °C). La communauté phytoplanctonique de l'EMSL a démontré une résistance surprenante à l'acidification et ce sur une large gamme de pCO_2 (~100–3000 µatm). Cette résistance à de grandes variations de pCO_2 indique que les espèces présentes s'acclimatent rapidement à de faibles pH. Par contre, l'effet du réchauffement sur le développement de la floraison a été marqué. Il serait intéressant dans l'avenir de soumettre les communautés planctoniques à un gradient de température afin de mieux cerner l'impact du réchauffement sur leur dynamique. De plus, compte tenu de nos conclusions, il serait également important de mieux quantifier l'impact de l'acidification et du réchauffement sur les assemblages zooplanctoniques (micro et meso) et leur broutage. Lors de ces expériences, l'ajout de mesozooplancton (ex : copépodes), dont le broutage peut être

important lors des floraisons de diatomées, permettrait de reproduire plus fidèlement l'écosystème planctonique de l'EMSL. Dans le chapitre 4, j'ai constaté à nouveau l'impact négatif de l'acidification sur les concentrations de DMS, un phénomène que j'avais déjà attribué à une diminution de l'efficacité de conversion bactérienne du DMSP en DMS. Cependant, il serait important de quantifier également l'impact de l'acidification et du réchauffement sur la consommation bactérienne du DMS. Jusqu'ici, peu d'études se sont attardées à la quantification de la consommation bactérienne de DMS (Groene, 1995; Wolfe et al., 1999; Vila-Costa et al., 2006a; Valle et al., 2009). De façon générale, ces études montrent que la consommation bactérienne du DMS augmente avec la production brute de DMS. Un déséquilibre entre production et consommation pourrait néanmoins expliquer en partie la diminution observée des concentrations de DMS en fonction de la diminution du pH. De plus, tel que mentionné précédent, davantage d'attention devrait être portée à la pression et au contrôle possiblement effectué par le zooplancton dans nos expériences, puisque celui-ci pourrait avoir un effet non seulement sur les communautés algales mais également sur la production de DMS en condition d'acidification (Aberle et al., 2013; Tanaka et al., 2013; Park et al., 2014).

Finalement, mes résultats montrent que le réchauffement des eaux de surface pourrait avoir un effet marqué sur la phénologie des floraisons phytoplanctonique et leur capacité à produire du DMS. À l'instar de mon étude, plusieurs autres études menées dans des écosystèmes différents, ont mis en évidence une diminution marquée de la production nette de DMS en situation d'acidification. Mes résultats suggèrent que le réchauffement qui prendra place en parallèle à l'acidification est susceptible de contrer entièrement cet effet négatif. Une augmentation notable (~240 %) de la production nette de DMS pourrait même être observée lors d'une floraison phytoplanctonique. L'implémentation des relations négatives pH-DMS dans les modèles actuels suggère que l'acidification océanique diminuera les émissions de DMS, engendrant une augmentation additionnelle de température d'ici 2100 (Six et al., 2013; Schwinger et al., 2017). L'intégration dans ces modèles climatiques de relations pH-température-DMS issues d'expériences multifactorielles comme la nôtre permettra certainement d'améliorer les prédictions sur la climatologie du DMS dans un contexte de changements globaux.

Bibliographie

Aberle, N., Schulz, K. G., Stuhr, A., Malzahn, A. M., Ludwig, A. and Riebesell, U.: High tolerance of microzooplankton to ocean acidification in an Arctic coastal plankton community, Biogeosciences, 10(3), 1471–1481, doi:10.5194/bg-10-1471-2013, 2013.

Alcolombri, U., Ben-Dor, S., Feldmesser, E., Levin, Y., Tawfik, D. S. and Vardi, A.: Identification of the algal dimethyl sulfide-releasing enzyme: A missing link in the marine sulfur cycle, Science, 348(6242), 1466–1469, doi:10.1126/science.aab1586, 2015.

Andreae, M. O.: Ocean-atmosphere interactions in the global biogeochemical sulfur cycle, Mar. Chem., 30, 1–3, 1990.

Andreae, M. O. and Crutzen, P. J.: Atmospheric aerosols: Biogeochemical sources and role in atmospheric chemistry, Science, 276(5315), 1052–1058, doi:10.1126/science.276.5315.1052, 1997.

Annane, S., St-Amand, L., Starr, M., Pelletier, E., and Ferreyra, G. A.: Contribution of transparent exopolymeric particles (TEP) to estuarine particulate organic carbon pool, Mar. Ecol. Prog. Ser., 529, 17–34, doi:10.3354/meps11294, 2015.

Archer, S. D., Gilbert, F. J., Nightingale, P. D., Zubkov, M. V., Taylor, A. H., Smith, G. C. and Burkill, P. H.: Transformation of dimethylsulphoniopropionate to dimethyl sulphide during summer in the North Sea with an examination of key processes via a modelling approach, Deep. Res. Part II Top. Stud. Oceanogr., 49(15), 3067–3101, doi:10.1016/S0967-0645(02)00072-3, 2002.

Archer, S. D., Kimmance, S. A., Stephens, J. A., Hopkins, F. E., Bellerby, R. G. J., Schulz, K. G., Piontek, J., and Engel, A.: Contrasting responses of DMS and DMSP to ocean acidification in Arctic waters, Biogeosciences, 10(3), 1893–1908, doi:10.5194/bg-10-1893-2013, 2013.

Arnold, H. E., Kerrison, P. and Steinke, M.: Interacting effects of ocean acidification and warming on growth and DMS-production in the haptophyte coccolithophore *Emiliania huxleyi*, Glob. Chang. Biol., 19(4), 1007–1016, doi:10.1111/gcb.12105, 2013.

Avgoustidi, V., Nightingale, P. D., Joint, I., Steinke, M., Turner, S. M., Hopkins, F. E., and Liss, P. S.: Decreased marine dimethyl sulfide production under elevated CO_2 levels in mesocosm and in vitro studies, Environ. Chem., 9(4), 399, doi:10.1071/EN11125, 2012.

Bach, L. T., Taucher, J., Boxhammer, T., Ludwig, A., Aberle-Malzahn, N., Abrahamsson, K., Almén, A. K., Asplund, M. E., Audritz, S., Boersma, M., Breitbarth, E., Bridges, C., Brussaard, C., Brutemark, A., Clemmesen, C., Collins, S., Crawfurd, K., Dahlke, F., Deckelnick, M., Dittmar, T., Doose, R., Dupont, S., Eberlein, T., Endres, S., Engel, A., Engström-Öst, J., Febiri, S., Fleischer, D., Fritsche, P., Gledhill, M., Göttler, G., Granberg, M., Grossart, H. P., Grifos, A., Hoffmann, L., Karlsson, A., Klages, M., John, U., Jutfelt, F., Köster, I., Lange, J., Leo, E., Lischka, S., Lohbeck, K., Lundve, B., Mark, F. C., Meyerhöfer, M., Nicolai, M., Pansch, C., Petersson, B., Reusch, T., De Moraes, K. R., Schartau, M., Scheinin, M., Schulz, K. G., Schwarz, U., Stenegren, M., Stiasny, M., Storch, D., Stuhr, A., Sswat, L., Svensson, M., Thor, P., Voss, M., Van De Waal, D., Wannicke, N., Wohlrab, S., Wulff, A., Achterberg, E. P., Algueró-Muñiz, M., Anderson, L. G., Bellworthy, J., Büdenbender, J., Czerny, J., Ericson, Y., Esposito, M., Fischer, M., Haunost, M., Hellemann, D., Horn, H. G., Hornick, T., Meyer, J., Sswat, M., Zark, M., and Riebesell, U.: Influence of ocean acidification on a natural winter-to-summer plankton succession: First insights from a long-term mesocosm study draw attention to periods of low nutrient concentrations, PLoS ONE, 11(8), 1–33, doi:10.1371/journal.pone.0159068, 2016.

Barnard, W.R., Andreae, M.O., Watkins, W.E., Bingemer, H., and Georgii, H.W.: The flux of dimethylsulfide from the oceans to the atmosphere. J. Geophys. Res., 87(C11), 8787–8793, 1982.

Barth, J.A.C., and Veizer, J. Carbon cycle in St Lawrence aquatic ecosystems at Cornwall (Ontario), Canada: seasonal and spatial variations. Chem. Geol. 159: 107–128, 1999.

Bates, T. S., Lamb, B. K., Guenther, A., Dignon, J., and Stoiber, R. E.: Sulfur emissions to the atmosphere from natural sources, J. Atmos. Chem., 14(1–4), 315–337, doi:10.1007/BF00115242, 1992.

Beardall, J. and Raven, John, A.: The potential effects of global climate change on microalgal photosynthesis, growth and ecology, Phycologia, 43(January), 26–40, doi:10.2216/i0031-8884-43-1-26.1, 2004.

Beardall, J., Stojkovic, S., and Gao, K.: Interactive effects of nutrient supply and other environmental factors on the sensitivity of marine primary producers to ultraviolet radiation: Implications for the impacts of global change, Aquat. Biol., 22, 5–23, doi:10.3354/ab00582, 2014.

Bell, R. T.: Estimating production of heterotrophic bacterioplankton via incorporation of tritiated thymidine, in: Handbook of methods in aquatic microbial ecology, Eds: Kemp, P. F., Sherr, B. F., Sherr, E. B., and Cole, J., Lewis Publisher, Boca Raton, 495–503, 1993.

Belzile, C., Brugel, S., Nozais, C., Gratton, Y. and Demers, S.: Variations of the abundance and nucleic acid content of heterotrophic bacteria in Beaufort Shelf waters during winter and spring, J. Mar. Syst., 74(3–4), 946–956, doi:10.1016/j.jmarsys.2007.12.010, 2008.

Bénard, R., Levasseur, M., Scarratt, M., Michaud, S., Starr, M., Mucci, A., Ferreyra, G., Gosselin, M., Tremblay, J.-É., Lizotte, M. and Yang, G.-P.: Contrasting effects of acidification and warming on dimethylsulfide concentrations during a temperate estuarine fall bloom mesocosm experiment, Biogeosciences Discuss., (August), 1–33, doi:10.5194/bg-2018-338, 2018a.

Bénard, R., Levasseur, M., Scarratt, M., Blais, M.-A., Mucci, A., Ferreyra, G., Starr, M., Gosselin, M., Tremblay, J.-É. and Lizotte, M.: Experimental assessment of the sensitivity of an estuarine phytoplankton fall bloom to acidification and warming, Biogeosciences, 15(16), 4883–4904, doi:10.5194/bg-15-4883-2018, 2018b.

Bérard-Therriault, L., Poulin, M., and Bossé, L.: Guide d'identification du phytoplancton marin de l'estuaire et du golfe du Saint-Laurent incluant également certains protozoaires., Canadian Special Publication of Fisheries and Aquatic Sciences, 128, 1–387, doi :10.1139/9780660960579, 1999.

Berge, T., Daugbjerg, N., Balling Andersen, B. and Hansen, P.: Effect of lowered pH on marine phytoplankton growth rates, Mar. Ecol. Prog. Ser., 416, 79–91, doi:10.3354/meps08780, 2010.

Boyd, P. W., and Hutchins, D. A.: Understanding the responses of ocean biota to a complex matrix of cumulative anthropogenic change, Mar. Ecol. Prog. Ser., 470, 125–135, doi:10.3354/meps10121, 2012.

Boyd, P. W., Rynearson, T. A., Armstrong, E. A., Fu, F., Hayashi, K., Hu, Z., Hutchins, D. A., Kudela, R. M., Litchman, E., Mulholland, M. R., Passow, U., Strzepek, R. F., Whittaker, K. A., Yu, E., and Thomas, M. K.: Marine Phytoplankton temperature versus growth responses from polar to tropical waters - outcome of a scientific community-wide study, PLoS ONE, 8(5), doi:10.1371/journal.pone.0063091, 2013.

Boyd, P. W., Lennartz, S. T., Glover, D. M., and Doney, S. C.: Biological ramifications of climate-change-mediated oceanic multi-stressors, Nat. Clim. Chang., 5(1), 71–79, doi:10.1038/nclimate2441, 2015.

Boyd, P. W., Collins, S., Dupont, S., Fabricius, K., Gattuso, J.-P., Havenhand, J., Hutchins, D. A., Riebesell, U., Rintoul, M. S., Vichi, M., Biswas, H., Ciotti, A., Gao, K., Gehlen, M., Hurd, C. L., Kurihara, H., McGraw, C. M., Navarro, J. M., Nilsson, G. E., Passow, U. and Pörtner, H.-O.: Experimental strategies to assess the biological ramifications of multiple drivers of global ocean change-A review, Glob. Chang. Biol., 24(6), 2239–2261, doi:10.1111/gcb.14102, 2018.

Brimblecombe, P., and Shooter, D.: Photo-oxidation of dimethylsulphide in aqueous solution, Mar. Chem., 19, 343–353, 1986.

Brussaard, C. P. D., Noordeloos, A. A. M., Witte, H., Collenteur, M. C. J., Schulz, K., Ludwig, A., and Riebesell, U.: Arctic microbial community dynamics influenced by elevated CO_2 levels, Biogeosciences, 10(2), 719–731, doi:10.5194/bg-10-719-2013, 2013.

Butrón, A., Iriarte, A., and Madariaga, I.: Size-fractionated phytoplankton biomass, primary production and respiration in the Nervión-Ibaizabal estuary: A comparison with other nearshore coastal and estuarine ecosystems from the Bay of Biscay, Cont. Shelf Res., 29(8), 1088–1102, doi:10.1016/j.csr.2008.11.013, 2009.

Byrne, R. H.: Standardization of standard buffers by visible spectrometry, Anal. Chem, 59, 1479–1481, doi:10.1021/ac00137a025, 1987.

Cai, W. J., and Wang, Y.: The chemistry, fluxes, and sources of carbon dioxide in the estuarine waters of the Satilla and Altamaha Rivers, Georgia, Limnol. Oceanogr., 43(4), 657–668, doi:10.4319/lo.1998.43.4.0657, 1998.

Cai, W. J., Huang, W. J., Luther, G. W., Pierrot, D., Li, M., Testa, J., Xue, M., Joesoef, A., Mann, R., Brodeur, J., Xu, Y. Y., Chen, B., Hussain, N., Waldbusser, G. G., Cornwell, J. and Michael Kemp, W.: Redox reactions and weak buffering capacity lead to acidification in the Chesapeake Bay, Nat. Commun., 8(1), 1–12, doi:10.1038/s41467-017-00417-7, 2017.

Caldeira, K., and Berner, R.: Seawater pH and Atmospheric Carbon Dioxide, Science, 286(5447), 2043a–2043, doi:10.1126/science.286.5447.2043a, 1999.

Caldeira, K. and Wickett, M. E.: Anthropogenic carbon and ocean pH, Nature, 425(September), 234–236, 2003.

Caldeira, K., and Wickett, M. E.: Ocean model predictions of chemistry changes from carbon dioxide emissions to the atmosphere and ocean, J. Geophys. Res., 110(C9), 1–12, doi:10.1029/2004JC002671, 2005.

Cantin, G., Levasseur, M., Gosselin, M., Michaud, S.: Role of zooplankton in the mesoscale distribution of surface dimethylsulfide concentrations in the Gulf of St. Lawrence, Canada, Mar. Ecol. Prog. Ser., 141, 103-117, 1996.

Cantoni, G. L. and Anderson, D. Enzymatic cleavage of dimethylpropiothetin by Polysiphonia Lanosa, J. Bio. Chem., 222, 171-177, 1956.

Carslaw, K. S., Boucher, O., Spracklen, D. V., Mann, G. W., Rae, J. G. L.,Woodward, S., and Kulmala, M.: A review of natural aerosol interactions and feedbacks within the Earth system, Atmos. Chem. Phys., 10, 1701–1737, doi:10.5194/acp-10-1701- 2010, 2010.

Charlson, R., Lovelock, J., Andreae, M., and Warren, S.: Oceanic phytoplankton, atmospheric sulphur, cloud albedo and climate, Nature, 326, 656–661, 1987.

Chin, M. and Jacob, D. J.: Anthropogenic and natural contributions to tropospheric sulfate: A global model analysis, J. Geophys. Res. Atmos., 101(D13), 18691–18699, doi:10.1029/96JD01222, 1996.

Clayton, T. D., and Byrne, R. H.: Spectrophotometric seawater pH measurements: total hydrogen ion concentration scale calibration of m-cresol purple and at-sea results, Deep. Res. Part I, 40(10), 2115–2129, doi:10.1016/0967-0637(93)90048-8, 1993.

Coote, A., and Yeats, P. A.: Distribution of Nutrients in the Gulf of St. Lawrence, J. Fish. Res. Board Can., 36(2), 123–131, doi:10.1139/f79-021, 1979.

Cyr, F., Bourgault, D., and Galbraith, P. S.: Interior versus boundary mixing of a cold intermediate layer, J. Geophys. Res. Ocean., 116(12), 1–12, doi:10.1029/2011JC007359, 2011.

d'Anglejan, B.: Recent sediments and sediment transport processes in the St. Lawrence Estuary, in: Oceanography of a large-scale estuarine system, Eds: El-Sabh, M. I., and Silverberg, N., Springer-Verlag, New York, USA, 109–129, doi: 10.1002/9781118663783.ch6, 1990.

Dacey, J. W. H., and Wakeham, S. G.: Oceanic dimethylsulfide: production during zooplankton grazing, Science, 233, 1314–1316, 1986.

Delille, B., Harlay, J., Zondervan, I., Jacquet, S., Chou, L., Wollast, R., Bellerby, R. G. J., Frankignoulle, M., Borges, A. V., Riebesell, U. and Gattuso, J. P.: Response of primary production

and calcification to changes of pCO_2 during experimental blooms of the coccolithophorid *Emiliania huxleyi*, Global Biogeochem. Cycles, 19(2), 1–14, doi:10.1029/2004GB002318, 2005.

Devine, L., Plourde, S., Starr, M., St-Pierre, J., St-Amand, L., Joly, P. and Galbraith, P. S.: Chemical and biological oceanographic conditions in the Estuary and Gulf of St. Lawrence during 2014, DFO Can. Sci. Advis. Sec. Res., Doc. 2015/(December), v + 46 pp [online] Available from: http://www.dfo-mpo.gc.ca/csas-sccs/, 2015.

Dickson, A. G.: An exact definition of total alkalinity and a procedure for the estimation of alkalinity and total inorganic carbon from titration data, Deep Sea Res. Part A. Oceanogr. Res. Pap., 28(6), 609–623, doi:10.1016/0198-0149(81)90121-7, 1981.

Dickson, A. G.: Standard potential of the reaction: AgCl(s) + 1 2H2(g) = Ag(s) + HCl(aq) and the standard acidity constant of the ion HSO_4^- in synthetic sea water from 273.15 to 318.15 K, J. Chem. Thermodyn., 22(2), 113–127, doi:10.1016/0021-9614(90)90074-Z, 1990.

Dickson, A. G.: The measurement of sea water pH, Mar. Chem., 44(2–4), 131–142, doi:10.1016/0304-4203(93)90198-W, 1993.

Dickson, A. G.: The carbon dioxide system in sea water: equilibrium chemistry and measurements, in Guide for Best Practices in Ocean Acidification Research and Data Reporting, edited by U. Riebesell and V. J. Fabry, Publications Office of the European Union, Luxembourg, pp. 17–40, 2010.

Dinauer, A., and Mucci, A.: Spatial variability in surface-water pCO_2 and gas exchange in the world's largest semi-enclosed estuarine system: St. Lawrence Estuary (Canada), Biogeosciences, 14(13), 3221–3237, doi:10.5194/bg-14-3221-2017, 2017.

Doney, S. C., Fabry, V. J., Feely, R. A., and Kleypas, J. A.: Ocean acidification: The other CO_2 problem, Ann. Rev. Mar. Sci., 1(1), 169–192, doi:10.1146/annurev.marine.010908.163834, 2009.

Dore, J. E., Lukas, R., Sadler, D. W., Church, M. J. and Karl, D. M.: Physical and biogeochemical modulation of ocean acidification in the central North Pacific, Proc. Natl. Acad. Sci., 106(30), 12235–12240, doi:10.1073/pnas.0906044106, 2009.

Duarte, C. M., Hendriks, I. E., Moore, T. S., Olsen, Y. S., Steckbauer, A., Ramajo, L., Carstensen, J., Trotter, J. A., and McCulloch, M.: Is ocean acidification an open-ocean syndrome? Understanding anthropogenic impacts on seawater pH, Estuaries Coasts, 36(2), 221–236, doi:10.1007/s12237-013-9594-3, 2013.

Eberlein, T., Wohlrab, S., Rost, B., John, U., Bach, L. T., Riebesell, U., and Van De Waal, D. B.: Effects of ocean acidification on primary production in a coastal North Sea phytoplankton community, PLoS ONE, 12(3), e0172594, doi:10.1371/journal.pone.0172594, 2017.

Egge, J. K., Thingstad, T. F., Larsen, A., Engel, A., Wohlers, J., Bellerby, R. G. J. and Riebesell, U.: Primary production during nutrient-induced blooms at elevated CO_2 concentrations, Biogeosciences, 6(5), 877–885, doi:10.5194/bg-6-877-2009, 2009.

Eggers, S. L., Lewandowska, A. M., Barcelos e Ramos, J., Blanco-Ameijeiras, S., Gallo, F. and Matthiessen, B.: Community composition has greater impact on the functioning of marine phytoplankton communities than ocean acidification, Glob. Chang. Biol., 20(3), 713–723, doi:10.1111/gcb.12421, 2014.

El-Sabh, M. I. and Silverberg, N.: The St. Lawrence Estuary: Introduction, in Oceanography of a large-scale estuarine system, edited by M. I. El-Sabh and N. Silverberg, pp. 1–9, Springer-Verlag, New York., 1990.

Engel, A., Delille, B., Jacquet, S., Riebesell, U., Rochelle-Newall, E., Terbrüggen, A., and Zondervan, I.: Transparent exopolymer particles and dissolved organic carbon production by *Emiliania huxleyi* exposed to different CO_2 concentrations: A mesocosm experiment, Aquat. Microb. Ecol., 34(1), 93–104, doi:10.3354/ame034093, 2004a.

Engel, A., Thoms, S., Riebesell, U., Rochelle-Newall, E., and Zondervan, I.: Polysaccharide aggregation as a potential sink of marine dissolved organic carbon, Nature, 428(6986), 929–932, doi:10.1038/nature02453, 2004b.

Engel, A., Zondervan, I., Aerts, K., Beaufort, L., Benthien, A., Chou, L., Delille, B., Gattuso, J.-P., Harlay, J., Heeman, C., Hoffmann, L., Jacquet, S., Nejstgaard, J., Pizay, M.-D., Rochelle-Newall, E., Schneider, U., Terbrueggen A.., and Riebesell, U.: Testing the direct effect of CO_2 concentration on a bloom of the coccolithophorid *Emiliania huxleyi* in mesocosm experiments, Limnol. Oceanogr., 50(2), 493–507, doi:10.4319/lo.2005.50.2.0493, 2005.

Engel, A., Händel, N., Wohlers, J., Lunau, M., Grossart, H.-P., Sommer, U., and Riebesell, U.: Effects of sea surface warming on the production and composition of dissolved organic matter during phytoplankton blooms: Results from a mesocosm study, J. Plankton Res., 33(3), 357–372, doi:10.1093/plankt/fbq122, 2011.

Engel, A., Borchard, C., Piontek, J., Schulz, K. G., Riebesell, U., and Bellerby, R.: CO_2 increases ^{14}C primary production in an Arctic plankton community, Biogeosciences, 10(3), 1291–1308, doi:10.5194/bg-10-1291-2013, 2013.

Engel, A., Piontek, J., Grossart, H.-P., Riebesell, U., Schulz, K. G., and Sperling, M.: Impact of CO_2 enrichment on organic matter dynamics during nutrient induced coastal phytoplankton blooms, J. Plankton Res., 36(3), 641–657, doi:10.1093/plankt/fbt125, 2014.

Eppley, R. W.: Temperature and phytoplankton growth in the sea, Fish. Bull., 70(4), 1063–1085, 1972.

Feely, R. A., Doney, S. C., and Cooley, S. R.: Ocean acidification: present conditions and future changes in a high-CO_2 world, Oceanography, 22(4), 36–47, doi:10.5670/oceanog.2009.95, 2009.

Feng, Y., Hare, C. E., Leblanc, K., Rose, J. M., Zhang, Y., DiTullio, G. R., Lee, P. A., Wilhelm, S. W., Rowe, J. M., Sun, J., Nemcek, N., Gueguen, C., Passow, U., Benner, I., Brown, C., and Hutchins, D. A.: Effects of increased pCO_2 and temperature on the North Atlantic spring bloom. I. The phytoplankton community and biogeochemical response, Mar. Ecol. Prog. Ser., 388, 13–25, doi:10.3354/meps08133, 2009.

Ferland, J., Gosselin, M., and Starr, M.: Environmental control of summer primary production in the Hudson Bay system: The role of stratification, J. Mar. Syst., 88(3), 385–400, doi:10.1016/j.jmarsys.2011.03.015, 2011.

Fuhrman, J. A., and Azam, F.: Bacterioplankton secondary production estimates for coastal waters of British Columbia, Antarctica, and California, Appl. Environ. Microbiol., 39(6), 1085–1095, 1980.

Gaaloul, H.: Effets du changement global sur les particules exopolymériques transparentes au sein de l'estuaire maritime du Saint-Laurent, M.Sc. thesis, Université du Québec à Rimouski, Canada, 133 pp., 2017.

Galbraith, P. S., Chassé, J., Gilbert, D., Larouche, P., Brickman, D., Pettigrew, B., Devine, L, Gosselin, A., Pettipas, R. G., and Lafleur, C.: Physical oceanographic conditions in the Gulf of St. Lawrence in 2011, DFO Can. Sci. Advis. Sec. Res. Doc., 2012/023, iii + 85 pp, 2012.

Galbraith, P. S., Chassé, J., Gilbert, D., Larouche, P., Caverhill, C., Lefaivre, D., Brickman, D., Pettigrew, B., Devine, L., and Lafleur, C.: Physical oceanographic conditions in the Gulf of St. Lawrence in 2013, DFO Can. Sci. Advis. Sec. Res. Doc., 2014/062(November), vi + 84 pp, 2014.

Galbraith, P. S., Chassé, J., Caverhill, C., Nicot, P., Gilbert, D., Pettigrew, B., Lefaivre, D., Brickman, D., Devine, L., and Lafleur, C.: Physical oceanographic conditions in the Gulf of St. Lawrence in 2015, DFO Can. Sci. Advis. Sec. Res. Doc., 2016/056, v + 90 pp, 2016.

Galí, M., Saló, V., Almeda, R., Calbet, A. and Simó, R.: Stimulation of gross dimethylsulfide (DMS) production by solar radiation, Geophys. Res. Lett., 38(15), doi:10.1029/2011GL048051, 2011.

Gao, G., Jin, P., Liu, N., Li, F., Tong, S., Hutchins, D. A., and Gao, K.: The acclimation process of phytoplankton biomass, carbon fixation and respiration to the combined effects of elevated

temperature and pCO_2 in the northern South China Sea, Mar. Pollut. Bull., 118(1–2), 213–220, doi:10.1016/j.marpolbul.2017.02.063, 2017.

Gao, K., and Campbell, D. A.: Photophysiological responses of marine diatoms to elevated CO2 and decreased pH: A review, Funct. Plant Biol., 41(5), 449–459, doi:10.1071/FP13247, 2014.

Gao, K., Helbling, E. W., Häder, D. P. and Hutchins, D. A.: Responses of marine primary producers to interactions between ocean acidification, solar radiation, and warming, Mar. Ecol. Prog. Ser., 470, 167–189, doi:10.3354/meps10043, 2012.

Gattuso, J. P., Mach, K. J., and Morgan, G.: Ocean acidification and its impacts: An expert survey, Clim. Change, 117(4), 725–738, doi:10.1007/s10584-012-0591-5, 2013.

Gattuso, J.-P., Magnan, A., Bille, R., Cheung, W. W. L., Howes, E. L., Joos, F., Allemand, D., Bopp, L., Cooley, S. R., Eakin, C. M., Hoegh-Guldberg, O., Kelly, R. P., Portner, H.-O., Rogers, a. D., Baxter, J. M., Laffoley, D., Osborn, D., Rankovic, A., Rochette, J., Sumaila, U. R., Treyer, S., and Turley, C.: Contrasting futures for ocean and society from different anthropogenic CO_2 emissions scenarios, Science, 349(6243), doi:10.1126/science.aac4722, 2015.

Geider, R. J.: Light and temperature dependence of the carbon to chlorophyll *a* ratio in microalgae and cyanobacteria: implications for physiology and growth of phytoplankton, New Phytol., 106(1), 1–34, doi:10.1111/j.1469-8137.1987.tb04788.x, 1987.

Giordano, M., Beardall, J., and Raven, J. A.: CO_2 concentrating mechanisms in algae: Mechanisms, environmental modulation., and evolution, Annu. Rev. Plant Biol., 56(1), 99–131, doi:10.1146/annurev.arplant.56.032604.144052, 2005.

Glöckner, F. O., Gasol, J. M., McDonough, N. and Calewaert, J.-B.: Marine microbial diversity and its role in ecosystem functioning and environmental change, Marine Board Position Paper 17, edited by J.B. Calewaert and N. McDonough N., Marine Board-ESF, Ostend, Belgium, May, 2012.

Gondwe, M., Krol, M., Gieskes, W., Klaassen, W. and de Baar, H.: The contribution of ocean-leaving DMS to the global atmospheric burdens of DMS, MSA, SO_2, and NSS $SO_4^=$, Global Biogeochem. Cycles, 17(4), doi:10.1029/2003GB002153, 2003.

Gonzalez, J. M., Kiene, R. P. and Moran, M. A.: Transformation of sulfur compounds by an abundant lineage of marine bacteria in the alpha-subclass of the class Proteobacteria, Appl. Environ. Microbiol., 65(9), 3810–3819, 1999.

Gratton, Y., Mertz, G. and Gagne, J. A.: Satellite observations of tidal upwelling and mixing in the St. Lawrence Estuary, J. Geophys. Res., 93(C6), 6947–6954, doi:10.1029/JC093iC06p06947, 1988.

Green, D.H., Shenoy, D. M., Hart, M. C., and Hatton, A. D.: Coupling of dimethylsulfide oxidation to biomass production by a marine Flavobacterium, Appl. Environ. Microbiol., 77(9), 3137–3140, doi:10.1128/AEM.02675-10, 2011.

Groene, T.: Biogenic production and consumption of dimethylsulfide (DMS) and dimethylsulfoniopropionate (DMSP) in the marine epipelagic zone: a review, J. Mar. Syst., 6(3), 191–209, doi:10.1016/0924-7963(94)00023-5, 1995.

Grossart, H.-P., Allgaier, M., Passow, U., and Riebesell, U.: Testing the effect of CO_2 concentration on the dynamics of marine heterotrophic bacterioplankton, Limnol. Oceanogr., 51(1), 1–11, doi:10.4319/lo.2006.51.1.0001, 2006.

Gunderson, A. R., Armstrong, E. J., and Stillman, J. H.: Multiple stressors in a changing World: The need for an improved perspective on physiological responses to the dynamic marine environment, Ann. Rev. Mar. Sci., 8(1), 357–378, doi:10.1146/annurev-marine-122414-033953, 2016.

Hama, T., Inoue, T., Suzuki, R., Kashiwazaki, H., Wada, S., Sasano, D., Kosugi, N., and Ishii, M.: Response of a phytoplankton community to nutrient addition under different CO_2 and pH conditions, J. Oceanogr., 72(2), 207–223, doi:10.1007/s10872-015-0322-4, 2016.

Hansen, H. P., and Koroleff, F.: Determination of nutrients, in: Methods of Seawater Analysis, 3, Eds: Grasshoff K., Kremling, K.., and Ehrhardt, M., Wiley-VCH Verlag GmbH, Weinheim, Germany, 159–228, doi:10.1002/9783527613984.ch10, 2007.

Hansson, I.: A new set of pH scales and standard buffers for sea water, Deep. Res. Part I, 20, 479–491, doi:10.1016/0011-7471(73)90101-0, 1973.

Hare, C. E., Leblanc, K., DiTullio, G. R., Kudela, R. M., Zhang, Y., Lee, P. A., Riseman, S., and Hutchins, D. A.: Consequences of increased temperature and CO_2 for phytoplankton community structure in the Bering Sea, Mar. Ecol. Prog. Ser., 352, 9–16, doi:10.3354/meps07182, 2007.

Harvey, B. P., Gwynn-Jones, D. and Moore, P. J.: Meta-analysis reveals complex marine biological responses to the interactive effects of ocean acidification and warming, Ecol. Evol., 3(4), 1016–1030, doi:10.1002/ece3.516, 2013.

Hatton, A. D., Darroch, L., and Malin, G.: The role of dimethylsulphoxide in the marine biogeochemical cycle of dimethylsulphide, Oceanogr. Mar. Biol. An Annu. Rev., 42, 29–56, 2004.

Havenhand, J., Dupont, S., and Quinn, G. P.: Designing ocean acidification experiments to maximise inference, in Guide to best practices for ocean acidification research and data reporting, Eds: Riebesell, U., Fabry, V. J., and Gattuso, J.-P., Publications Office of the European Union, Luxembourg, 67–80, 2010.

Hill, R. W., White, B. A., Cottrell, M. T., Dacey, J. W. H.: Virus-mediated total release of dimethylsulfoniopropionate from marine phytoplankton: a potential climate process, Aquat. Microb. Ecol., 14, 1–6, 1998.

Hinga, K. R.: Effects of pH on coastal marine phytoplankton, Mar. Ecol. Prog. Ser., 238, 281–300, doi:10.3354/meps238281, 2002.

Hofmann, M. and Schellnhuber, H. J.: Ocean acidification: A millennial challenge, Energy Environ. Sci., 3(12), 1883–1896, doi:10.1039/c000820f, 2010.

Hönisch, B., Hemming, N. G., Archer, D., Siddall, M. and McManus, J. F.: Atmospheric carbon dioxide concentration across the mid-pleistocene transition, Science, 324(5934), 1551–1554, doi:10.1126/science.1171477, 2009.

Hönisch, B., Ridgwell, A., Schmidt, D. N., Thomas, E., Gibbs, S. J., Sluijs, A., Zeebe, R., Kump, L., Martindale, R. C., Greene, S. E., Kiessling, W., Ries, J., Zachos, J. C., Royer, D. L., Barker, S., Marchitto, T. M., Moyer, R., Pelejero, C., Ziveri, P., Foster, G. L. and Williams, B.: The geological record of ocean acidification, Science, 335(6072), 1058–1063, doi:10.1126/science.1208277, 2012.

Hopkins, F. E., and Archer, S. D.: Consistent increase in dimethyl sulfide (DMS) in response to high CO_2 in five shipboard bioassays from contrasting NW European waters, Biogeosciences, 11(18), 4925–4940, doi:10.5194/bg-11-4925-2014, 2014.

Hopkins, F. E., Turner, S. M., Nightingale, P. D., Steinke, M., Bakker, D., and Liss, P. S.: Ocean acidification and marine trace gas emissions, Proc. Natl. Acad. Sci., 107(2), 760–765, doi:10.1073/pnas.0907163107, 2010.

Hopkinson, B. M., Dupont, C. L., Allen, A. E. and Morel, F. M. M.: Efficiency of the CO_2-concentrating mechanism of diatoms, Proc. Natl. Acad. Sci., 108(10), 3830–3837, doi:10.1073/pnas.1018062108, 2011.

Hussherr, R., Levasseur, M., Lizotte, M., Tremblay, J. É., Mol, J., Thomas, H., Gosselin, M., Starr, M., Miller, L. A., Jarniková, T., Schuback, N., and Mucci, A.: Impact of ocean acidification on Arctic phytoplankton blooms and dimethyl sulfide concentration under simulated ice-free and under-ice conditions, Biogeosciences, 14(9), 2407–2427, doi:10.5194/bg-14-2407-2017, 2017.

Iglesias-Rodriguez, M. D., Halloran, P. R., Rickaby, R. E. M., Hall, I. R., Colmenero-Hidalgo, E., Gittins, J. R., Green, D. R. H., Tyrrell, T., Gibbs, S. J., Von Dassow, P., Rehm, E., Armbrust, E. V. and Boessenkool, K. P.: Phytoplankton calcification in a high-CO_2 world, Science, 320(5874), 336–340, doi:10.1126/science.1154122, 2008.

IPCC: Climate Change 1994: Radiative Forcing of Climate Change and an Evaluation of the IPCC IS92 Emission Scenarios, Cambridge University Press Cambridge, UK and New York, NY, USA, pp. 339, 1995.

IPCC: Working Group I Contribution to the Fifth Assessment Report Climate Change 2013: The Physical Science Basis, Intergov. Panel Clim. Chang., 1535, doi:10.1017/CBO9781107415324., 2013.

IPCC: Climate Change 2014 Synthesis Report Summary Chapter for Policymakers, Ipcc, 31, doi:10.1017/CBO9781107415324, 2014.

Iverson, R. L., Nearhoof, F. L. and Andreae, M. O.: Production of dimethylsulfonium propionate and dimethylsulfide by phytoplankton in estuarine and coastal waters, Limnol. Oceanogr., 34(1), 53–67, doi:10.4319/lo.1989.34.1.0053, 1989.

Johnston, A. W. B., Green, R. T. and Todd, J. D.: Enzymatic breakage of dimethylsulfoniopropionate - a signature molecule for life at sea, Curr. Opin. Chem. Biol., 31(Figure 1), 58–65, doi:10.1016/j.cbpa.2016.01.011, 2016.

Karsten, U., Kück, K., Vogt, C., and Kirst, G. O.: Dimethylsulfoniopropionate production in phototrophic organisms and its physiological functions as a cryoprotectant, in: Biological and environmental chemistry of DMSP and related sulfonium compounds, Eds: Kiene, R. P., Visscher, P. T., Keller, M. D., and Kirst, G. O., Springer US, Boston, MA, 143–153, doi:10.1007/978-1-4613-0377-0, 1996.

Keller, M. D.: Dimethyl sulfide production and marine phytoplankton: the importance of species composition and cell size, Biol. Oceanogr., 6(5–6), 375–382, doi:10.1080/01965581.1988.10749540, 1989.

Kettle, A. J. and Andreae, M. O.: Flux of dimethylsulfide from the oceans: A comparison of updated data sets and flux models, J. Geophys. Res. Atmos., 105(D22), 26793–26808, doi:10.1029/2000JD900252, 2000.

Kettle, A. J., Andreae, M. O., Amouroux, D., Andreae, T. W., Bates, T. S., Berresheim, H., Bingemer, H., Boniforti, R., Curran, M. A. J., diTullio, G. R., Helas, G., Jones, G. B., Keller, I. M. D., Kiene, R. P., Leck, C., Levasseur, M., Maspero, M., Matrai, P., McTaggart, A. R., Mihalopoulos, N., Nguyen, B. C., Novo, A., Putaud, J. P., Rapsomanikis, S., Roberts, G., Schebeske, G.; Sharma, S., Simó, R., Staubes, R., Turner, S., and Uher, G.: A global database of sea surface dimethylsulfide (DMS) measurements and a procedure to predict sea surface DMS as a function of latitude, longitude, and month, Global Biogeochem. Cycles, 13, 399-444, 1999.

Kettles, N. L., Kopriva, S., and Malin, G.: Insights into the regulation of DMSP synthesis in the diatom Thalassiosira pseudonana through APR activity, proteomics and gene expression analyses on cells acclimating to changes in salinity, light and nitrogen, PLoS One, 9(4), doi:10.1371/journal.pone.0094795, 2014.

Kiene, R. P.: Dimethyl sulfide production from dimethylsulfoniopropionate in coastal seawater samples and bacterial cultures, Appl. Environ. Microbiol., 56(11), 3292–3297, 1990.

Kiene, R. P., Linn, L. J.: Distribution and turnover of dissolved DMSP and its relationship with bacterial production and dimethylsulfide in the Gulf of Mexico, Limnol. Oceanogr., 45, 849–861, 2000.

Kiene, R. P., and Service, S. K.: Decomposition of dissolved DMSP and DMS in estuarine waters: dependence on temperature and substrate concentration, Mar. Ecol. Prog. Ser., 76, 1–11, 1991.

Kiene, R. P. and Slezak, D.: Low dissolved DMSP concentrations in seawater revealed by small-volume gravity filtration and dialysis sampling, Limnol. Oceanogr. Methods, 4(4), 80–95, doi:10.4319/lom.2006.4.80, 2006.

Kiene, R. P., Linn, L. J., Gonzalez, J., Moran, M. A., and Bruton, J. A.: Dimethylsulfoniopropionate and methanethiol are important precursors of methionine and protein-sulfur in marine bacterioplankton, Appl Environ. Microbiol., 65, 4549–4558, 1999.

Kiene, R. P., Linn, L. J., and Bruton, J. A. New and important roles for DMSP in marine microbial communities, J. Sea. Res., 43, 209–224, 2000.

Kim, J. H., Kim, K. Y., Kang, E. J., Lee, K., Kim, J. M., Park, K. T., Shin, K., Hyun, B., and Jeong, H. J.: Enhancement of photosynthetic carbon assimilation efficiency by phytoplankton in the future coastal ocean, Biogeosciences, 10(11), 7525–7535, doi:10.5194/bg-10-7525-2013, 2013.

Kim, J. M., Lee, K., Yang, E. J., Shin, K., Noh, J. H., Park, K. T., Hyun, B., Jeong, H. J., Kim, J. H., Kim, K. Y., Kim, M., Kim, H. C., Jang, P. G. and Jang, M. C.: Enhanced production of oceanic dimethylsulfide resulting from CO_2-induced grazing activity in a high CO_2 world, Environ. Sci. Technol., 44(21), 8140–8143, doi:10.1021/es102028k, 2010.

Kim, J. M., Lee, K., Shin, K., Yang, E. J., Engel, A., Karl, D. M. and Kim, H. C.: Shifts in biogenic carbon flow from particulate to dissolved forms under high carbon dioxide and warm ocean conditions, Geophys. Res. Lett., 38(8), doi:10.1029/2011GL047346, 2011.

Kim, K. Y., Garbary, D. J., and Mclachlan, J. L.: Phytoplankton dynamics in Pomquet Harbour, Nova Scotia: a lagoon in the southern Gulf of St Lawrence, Phycologica, 43(3), 311–328, 2004.

Kirst, G. O., Thiel, C., Wolff, H., Nothnagel, J., Wanzek M., and Ulmke, R.: Dimethylsulfoniopropionate (DMSP) in ice-algae and its possible biological role, Mar. Chem., 35, 381–388, 1991.

Kloster, S., Feichter, J., Maier-Reimer, E., Six, K. D., Stier, P. and Wetzel, P.: DMS cycle in the marine ocean-atmosphere system - A global model study, Biogeosciences, 3(1), 29–51, doi:10.5194/bg-3-29-2006, 2006.

Knap, A., Michaels, A., Close, A. R., Ducklow, H., and Dickson, A. G.: Protocols for the Joint Global Ocean Flux Study (JGOFS) core measurements, JGOFS Rep No. 19, Reprint of the IOC Manuals and Guides No. 29, UNESCO, Bergen, Norway, doi:10013/epic.27912, 1996.

Kreyling, J., Jentsch, A. and Beier, C.: Beyond realism in climate change experiments: Gradient approaches identify thresholds and tipping points, Ecol. Lett., 17(1), 10–11, doi:10.1111/ele.12193, 2014.

Kroeker, K. J., Kordas, R. L., Crim, R., Hendriks, I. E., Ramajo, L., Singh, G. S., Duarte, C. M., and Gattuso, J. P.: Impacts of ocean acidification on marine organisms: Quantifying sensitivities and interaction with warming, Glob. Chang. Biol., 19(6), 1884–1896, doi:10.1111/gcb.12179, 2013.

Kwint, R. L., and Kramer, K. J.: Dimethylsulphide production by plankton communities, Mar. Ecol. Prog. Ser., 121(1–3), 227–238, doi:10.3354/meps121227, 1995.

Lana, A., Bell, T. G., Simó, R., Vallina, S. M., Ballabrera-Poy, J., Kettle, a. J., Dachs, J., Bopp, L., Saltzman, E. S., Stefels, J., Johnson, J. E., and Liss, P. S.: An updated climatology of surface dimethylsulfide concentrations and emission fluxes in the global ocean, Global Biogeochem. Cycles, 25(1), 1–17, doi:10.1029/2010GB003850, 2011.

Laroche, D., Vézina, A. F., Levasseur, M., Gosselin, M., Stefels, J., Keller, M. D., Matrai, P. A., and Kwint, R. L. J.: DMSP synthesis and exudation in phytoplankton: A modeling approach, Mar. Ecol. Prog. Ser., 180(May), 37–49, doi:10.3354/meps180037, 1999.

Larouche, P., and Galbraith, P. S.: Canadian coastal seas and Great Lakes sea surface temperature climatology and recent trends, Can. J. Remote Sens., 42(3), 243–258, doi:10.1080/07038992.2016.1166041, 2016.

Lavoie, M., Waller, J. C., Kiene, R. P. and Levasseur, M.: Polar marine diatoms likely take up a small fraction of dissolved dimethylsulfoniopropionate relative to bacteria in oligotrophic environments, Aquat. Microb. Ecol., 81(3), 213–218, doi:10.3354/ame01871, 2018.

Law, C. S., Breitbarth, E., Hoffmann, L. J., McGraw, C. M., Langlois, R. J., Laroche, J., Marriner, A., and Safi, K. A.: No stimulation of nitrogen fixation by non-filamentous diazoytrophs under elevated CO_2 in the South Pacific, Glob. Chang. Biol., 18, 3004–3014, 2012.

Ledyard, K. M. and Dacey, J. W. H.: Microbial cycling of DMSP and DMS in coastal and oligotrophic seawater, Limnol. Oceanogr., 41(1), 33–40, doi:10.4319/lo.1996.41.1.0033, 1996.

Le Fouest, V., Zakardjian, B., Saucier, F. J. and Çizmeli, S. A.: Application of SeaWIFS- and AVHRR-derived data for mesoscale and regional validation of a 3-D high-resolution physical-biological model of the Gulf of St. Lawrence (Canada), J. Mar. Syst., 60(1–2), 30–50, doi:10.1016/j.jmarsys.2005.11.008, 2006.

Lei, L., Alcolombri, U. and Tawfik, D. S.: Biochemical Profiling of DMSP Lyases, in Methods in Enzymology, pp. 269–289., 2018.

Le Quéré, C., Andres, R. J., Boden, T., Conway, T., Houghton, R. A., House, J. I., Marland, G., Peters, G. P., Van Der Werf, G. R., Ahlström, A., Andrew, R. M., Bopp, L., Canadell, J. G., Ciais, P., Doney, S. C., Enright, C., Friedlingstein, P., Huntingford, C., Jain, A. K., Jourdain, C., Kato, E., Keeling, R. F., Klein Goldewijk, K., Levis, S., Levy, P., Lomas, M., Poulter, B., Raupach, M. R., Schwinger, J., Sitch, S., Stocker, B. D., Viovy, N., Zaehle, S., and Zeng, N.: The global carbon budget 1959-2011, Earth Syst. Sci. Data, 5(1), 165–185, doi:10.5194/essd-5-165-2013, 2013.

Le Quéré, C., Moriarty, R., Andrew, R. M., Canadell, J. G., Sitch, S., Korsbakken, J. I., Friedlingstein, P., Peters, G. P., Andres, R. J., Boden, T. A., Houghton, R. A., House, J. I., Keeling, R. F., Tans, P., Arneth, A., Bakker, D. C. E., Barbero, L., Bopp, L., Chang, J., Chevallier, F., Chini, L. P., Ciais, P., Fader, M., Feely, R. A., Gkritzalis, T., Harris, I., Hauck, J., Ilyina, T., Jain, A. K., Kato, E., Kitidis, V., Klein Goldewijk, K., Koven, C., Landschützer, P., Lauvset, S. K., Lefèvre, N., Lenton, A., Lima, I. D., Metzl, N., Millero, F., Munro, D. R., Murata, A., S. Nabel, J. E. M., Nakaoka, S., Nojiri, Y., O'Brien, K., Olsen, A., Ono, T., Pérez, F. F., Pfeil, B., Pierrot, D., Poulter, B., Rehder, G., Rödenbeck, C., Saito, S., Schuster, U., Schwinger, J., Séférian, R., Steinhoff, T., Stocker, B. D., Sutton, A. J., Takahashi, T., Tilbrook, B., Van Der Laan-Luijkx, I. T., Van Der Werf, G. R., Van Heuven, S., Vandemark, D., Viovy, N., Wiltshire, A., Zaehle, S., and Zeng, N.: Global Carbon Budget 2015, Earth Syst. Sci. Data, 7(2), 349–396, doi:10.5194/essd-7-349-2015, 2015.

Lee, P. A., Saunders, P. A., De Mora, S. J., Deibel, D. and Levasseur, M.: Influence of copepod grazing on concentrations of dissolved dimethylsulfoxide and related sulfur compounds in the North Water, Northern Baffin Bay, Mar. Ecol. Prog. Ser., 255, 235–248, doi:10.3354/meps255235, 2003.

Lee, P. A., Rudisill, J. R., Neeley, A. R., Maucher, J. M., Hutchins, D. A., Feng, Y., Hare, C. E., Leblanc, K., Rose, J. M., Wilhelm, S. W., Rowe, J. M., and Giacomo, R.: Effects of increased pCO_2 and temperature on the North Atlantic spring bloom. III. Dimethylsulfoniopropionate, Mar. Ecol. Prog. Ser., 388, 41–49, doi:10.3354/meps08135, 2009.

Legendre, L., Demers, S., Yentsch, C. M., and Yentsch, C. S.: The ^{14}C method: Patterns of dark CO_2 fixation and DCMU correction to replace the dark bottle, Limnol. Oceanogr., 28(5), 996–1003, doi:10.4319/lo.1983.28.5.0996, 1983.

Levasseur, M. E., and Therriault, J.-C.: Phytoplankton biomass and nutrient dynamics in a tidally induced upwelling: the role of teh NO_3:SiO_4 ratio, Mar. Ecol. Prog. Ser., 39, 87–97, 1987.

Levasseur, M., Therriault, J.-C., and Legendre, L.: Hierarchical control of phytoplankton succession by physical factors, Mar. Ecol. Prog. Ser., 19, 211–222, doi:10.3354/meps019211, 1984.

Levasseur, M. E., Harrison, P. J., Heimdal, B. R., and Therriault, J.-C.: Simultaneous nitrogen and silicate deficiency of a phytoplankton community in a coastal jet-front, Mar. Biol., 104(2), 329–338, doi:10.1007/BF01313275, 1990.

Levasseur, M., Michaud, S., Egge, J., Cantin, G., Nejstgaard, J. C., Sanders, R., Fernandez, E., Solberg, P. T., Heimdal, B., and Gosselin, M.: Production of DMSP and DMS during a mesocosm study of an *Emiliania huxleyi* bloom: Influence of bacteria and *Calanus finmarchicus* grazing, Mar. Biol., 126(4), 609–618, doi:10.1007/BF00351328, 1996.

Liss, P. S. and Lovelock, J. E.: Climate change: The effect of DMS emissions, Environ. Chem., 4(6), 377–378, doi:10.1071/EN07072, 2007.

Liss, P. S., Hatton, A. D., Malin, G., Nightingale, P. D., and Turner, S. M.: Marine sulphur emissions, Philos. Trans. R. Soc. B Biol. Sci., 352(1350), 159–169, doi:10.1098/rstb.1997.0011, 1997.

Lizotte, M., Levasseur, M., Michaud, S., Scarratt, M. G., Merzouk, A., Gosselin, M., Pommier, J., Rivkin, R. B., and Kiene, R. P.: Macroscale patterns of the biological cycling of dimethylsulfoniopropionate (DMSP) and dimethylsulfide (DMS) in the Northwest Atlantic, Biogeochemistry, 110(1–3), 183–200, doi:10.1007/s10533-011-9698-4, 2012.

Lizotte, M., Levasseur, M., Law, C. S., Walker, C. F., Safi, K. A., Marriner, A. and Kiene, R. P.: Dimethylsulfoniopropionate (DMSP) and dimethyl sulfide (DMS) cycling across contrasting biological hotspots of the New Zealand subtropical front, Ocean Sci., 13(6), 961–982, doi:10.5194/os-13-961-2017, 2017.

Lomas, M. W., Hopkinson, B. M., Losh, J. L., Ryan, D. E., Shi, D. L., Xu, Y., and Morel, F. M. M.: Effect of ocean acidification on cyanobacteria in the subtropical North Atlantic, Aquat. Microb. Ecol., 66(3), 211–222, doi:10.3354/ame01576, 2012.

Lovelock, J. E., Maggs, R. J., and Rasmusse R. A.: Atmospheric dimethyl sulfide and natural sulfur cycle, Nature, 237(5356), 452-453, 1972.

Lueker, T. J., Dickson, A. G. and Keeling, C. D.: Ocean pCO_2 calculated from dissolved inorganic carbon, alkalinity, and equations for K_1 and K_2: validation based on laboratory measurements of CO_2 in gas and seawater at equilibrium, Mar. Chem., 70(1), 105–119, doi:10.1016/S0304-4203(00)00022-0, 2000.

Lund, J. W. G., Kipling, C., and Le Cren, E. D.: The inverted microscope method of estimating algal numbers and the statistical basis of estimates by counting, Hydrobiologia, 11, 143–170, 1958.

MacGilchrist, G. A., Shi, T., Tyrrell, T., Richier, S., Moore, C. M., Dumousseaud, C., and Achterberg, E. P.: Effect of enhanced pCO_2 levels on the production of dissolved organic carbon and transparent exopolymer particles in short-term bioassay experiments, Biogeosciences, 11(13), 3695–3706, doi:10.5194/bg-11-3695-2014, 2014.

Malin, G., and Kirst, G. O.: Algal production of dimethyl sulfide and its atmospheric role, J. Phycol., 33, 889-896, 1997.

Malin, G., Wilson, W. H., Bratbak, G., Liss, P. S., and Mann, N. H.: Elevated production of dimethylsulfide resulting from viral infection of cultures of *Phaeocystis pouchetii*, Limnol. Oceanogr., 43(6), 1389–1393, doi:10.4319/lo.1998.43.6.1389, 1998.

Malmstrom, R. R., Kiene, R. P., Cottrell, M. T., and Kirchman, D. L.: Contribution of SAR11 bacteria to dissolved dimethylsulfoniopropionate and amino acid uptake in the north Atlantic Ocean, Appl. Environ. Microbiol., 70(7), 4129–4135, doi:10.1128/AEM.70.7.4129, 2004a.

Malmstrom, R. R., Kiene, R. P., and Kirchman, D. L.: Identification and enumeration of bacteria assimilating dimethylsulfoniopropionate (DMSP) in the North Atlantic and Gulf of Mexico, Limnol. Oceanogr., 49, 597–606, doi: 10.4319/lo.2004.49.2.0597, 2004b.

Malmstrom, R. R., Kiene, R. P., Vila, M., and Kirchman, D. L.: Dimethylsulfoniopropionate (DMSP) assimilation by *Synechococcus* in the Gulf of Mexico and northwest Atlantic Ocean, Limnol. Oceanogr., 50(6), 1924–1931, doi:10.4319/lo.2005.50.6.1924, 2005.

Marie, D., Simon, N., and Vaulot, D.: Phytoplankton cell counting by flow cytometry, Algal Cult. Tech., 253–267, doi:10.1016/B978-012088426-1/50018-4, 2005.

Maugendre, L., Gattuso, J. P., Louis, J., De Kluijver, A., Marro, S., Soetaert, K., and Gazeau, F.: Effect of ocean warming and acidification on a plankton community in the NW Mediterranean Sea, ICES J. Mar. Sci., 72(6), 1744–1755, doi:10.1093/icesjms/fsu161, 2015.

Maugendre, L., Guieu, C., Gattuso, J. P. and Gazeau, F.: Ocean acidification in the Mediterranean Sea: Pelagic mesocosm experiments. A synthesis, Estuar. Coast. Shelf Sci., 186, 1–10, doi:10.1016/j.ecss.2017.01.006, 2017.

Millero, F. J.: The pH of estuarine waters, Limnol. Oceanogr., 31(4), 839–847, doi:10.4319/lo.1986.31.4.0839, 1986.

Millero, F. J.: Carbonate constants for estuarine waters, Mar. Freshw. Res., 61(2), 139–142, doi:10.1071/MF09254, 2010.

Mohapatra, B. R., Rellinger, A. N., Kieber, D. J. and Kiene, R. P.: Comparative functional characteristics of DMSP lyases extracted from polar and temperate *Phaeocystis* species, Aquat. Biol., 18(2), 185–195, doi:10.3354/ab00504, 2013.

Montagnes, D. J. S., and Franklin, M.: Effect of temperature on diatom volume, growth rate, and carbon and nitrogen content: Reconsidering some paradigms, Limnol. Oceanogr., 46(8), 2008–2018, doi:10.4319/lo.2001.46.8.2008, 2001.

Morán, X. A. G., Sebastián, M., Pedrós-Alió, C., and Estrada, M.: Response of Southern Ocean phytoplankton and bacterioplankton production to short-term experimental warming, Limnol. Oceanogr., 51(4), 1791–1800, doi:10.4319/lo.2006.51.4.1791, 2006.

Morán, X. A., Alonso-Sáez, L., Nogueira, E., Ducklow, H. W., González, N., López-Urrutia, Á., Díaz-Pérez, L., Calvo-Díaz, A., Arandia-Gorostidi, N., and Huete-Stauffer, T. M.: More, smaller bacteria in response to ocean's warming?, Proc. R. Soc, 282(1810), 1–9, doi:http://dx.doi.org/10.1098/rspb.2015.0371, 2015.

Mucci, A., Starr, M., Gilbert, D. and Sundby, B.: Acidification of Lower St. Lawrence estuary bottom waters, Atmos. - Ocean, 49(3), 206–218, doi:10.1080/07055900.2011.599265, 2011.

Mucci, A., Levasseur, M., Gratton, Y., Martias, C., Scarratt, M., Gilbert, D., Tremblay, J.-É., Ferreyra, G., and Lansard, B.: Tidally-induced variations of pH at the head of the Laurentian Channel, Can. J. Fish. Aquat. Sci., doi:10.1139/cjfas-2017-0007, 2017.

Neale, P. J., Sobrino, C., Segovia, M., Mercado, J. M., Leon, P., Cortés, M. D., Tuite, P., Picazo, A., Salles, S., Cabrerizo, M. J., Prasil, O., Montecino, V., and Reul, A.: Effect of CO_2, nutrients and light on coastal plankton. I. Abiotic conditions and biological responses, Aquat. Biol., 22, 25–41, doi:10.3354/ab00587, 2014.

Nguyen, B. C., Belviso, S., Mihalopoulos, N., Gostan, J., Nival., P.: Dimethyl sulfide production during natural phytoplankton blooms, Mar. Chem., 24, 133–141, 1988

Nightingale, P.D., Malin, G., Law, C.S., Watson, A.J., Liss, P.S., Liddicoat, M.I., Boutin, J., Upstill-Goddard, R.C.: In situ evaluation of air–sea gas exchange parameterizations using novel conservative and volatile tracers, Global Biogeochem. Cycles, 14 (1), 373–387, 2000.

Niki, T., Kunugi, M., and Otsuki, A.: DMSP-lyase activity in five marine phytoplankton species: Its potential importance in DMS production, Mar. Biol., 136(5), 759–764, doi:10.1007/s002279900235, 2000.

NOAA: PMEL Carbon Program, Mauna Loa data, retrieved from https://www.pmel.noaa.gov/co2/file/Hawaii+Carbon+Dioxide+Time-Series, 2018.

Orr, J. C., Fabry, V. J., Aumont, O., Bopp, L., Doney, S. C., Feely, R. A., Gnanadesikan, A., Gruber, N., Ishida, A., Joos, F., Key, R. M., Lindsay, K., Maier-Reimer, E., Matear, R., Monfray, P., Mouchet, A., Najjar, R. G., Plattner, G. K., Rodgers, K. B., Sabine, C. L., Sarmiento, J. L., Schlitzer, R., Slater, R. D., Totterdell, I. J., Weirig, M. F., Yamanaka, Y. and Yool, A.: Anthropogenic ocean acidification over the twenty-first century and its impact on calcifying organisms, Nature, 437(7059), 681–686, doi:10.1038/nature04095, 2005.

Park, K. T., Lee, K., Shin, K., Yang, E. J., Hyun, B., Kim, J. M., Noh, J. H., Kim, M., Kong, B., Choi, D. H., Choi, S. J., Jang, P. G., and Jeong, H. J.: Direct linkage between dimethyl sulfide production and microzooplankton grazing, resulting from prey composition change under high partial pressure of carbon dioxide conditions, Environ. Sci. Technol., 48(9), 4750–4756, doi:10.1021/es403351h, 2014.

Parsons, T. R., Maita, Y., and Lalli, C. M.: A manual of chemical and biological methods for seawater analysis, Permagon Press, New York, 1984.

Paul, C., Matthiessen, B., and Sommer, U.: Warming, but not enhanced CO_2 concentration, quantitatively and qualitatively affects phytoplankton biomass, Mar. Ecol. Prog. Ser., 528, 39–51, doi:10.3354/meps11264, 2015.

Paul, C., Sommer, U., Garzke, J., Moustaka-Gouni, M., Paul, A., and Matthiessen, B.: Effects of increased CO_2 concentration on nutrient limited coastal summer plankton depend on temperature, Limnol. Oceanogr., 61(3), 853–868, doi:10.1002/lno.10256, 2016.

Paulino, A. I., Egge, J. K. and Larsen, A.: Effects of increased atmospheric CO_2 on small and intermediate sized osmotrophs during a nutrient induced phytoplankton bloom, Biogeosciences, 5(3), 739–748, doi:10.5194/bg-5-739-2008, 2008.

Pierrot, D. E., Lewis, E., and Wallace, D. W. R.: MS Excel program developed for CO_2 system calculations, Carbon Dioxide Information Analysis Center, ONRL/CDIAC-105a, Oak Ridge National Laboratory, US Department of Energy, Oak Ridge, Tennessee, USA, 2006.

Pinhassi, J., Simó, R., González, J. M., Vila, M., Alonso-Sáez, L., Kiene, R. P., Moran, M. A., and Pedrós-Alió, C.: Dimethylsulfoniopropionate turnover is linked to the composition and dynamics of the bacterioplankton assemblage during a microcosm phytoplankton bloom, Appl. Environ. Microbiol., 71(12), 7650–7660, doi:10.1128/AEM.71.12.7650-7660.2005, 2005.

Piontek, J., Lunau, M., Händel, N., Borchard, C., Wurst, M. and Engel, A.: Acidification increases microbial polysaccharide degradation in the ocean, Biogeosciences, 7(5), 1615–1624, doi:10.5194/bg-7-1615-2010, 2010.

Quinn, P. K., and Bates, T. S.: The case against climate regulation via oceanic phytoplankton sulphur emissions., Nature, 480(7375), 51–6, doi:10.1038/nature10580, 2011.

Quinn, P. K., Coffman, D. J., Johnson, J. E., Upchurch, L. M., and Bates, T. S.: Small fraction of marine cloud condensation nuclei made up of sea spray aerosol, Nat. Geosci., 10(9), 674–679, doi:10.1038/ngeo3003, 2017.

R Core Team: R: A language and environment for statistical computing. R Foundation for Statistical Computing, Vienna, Austria. URL https://www.R-project.org/, 2016.

Raven, J., Caldeira, K., Elderfield, H., Hoegh-Guldberg, O., Liss, P., Riebesell, U., Shepherd, J., Turley, C., Watson, A., Heap, R., Banes, R. and Quinn, R.: Ocean acidification due to increasing atmospheric carbon dioxide, R. Soc. Policy Doc. 12/05, Document N, 68, 2005.

Raven, J. A., Beardall, J., and Giordano, M.: Energy costs of carbon dioxide concentrating mechanisms in aquatic organisms, Photosynth. Res., 121, 111–124, 2014.

Reisch, C. R., Stoudemayer, M. J., Varaljay, V. A., Amster, I. J., Moran, M. A. and Whitman, W. B.: Novel pathway for assimilation of dimethylsulphoniopropionate widespread in marine bacteria, Nature, 473(7346), 208–211, doi:10.1038/nature10078, 2011.

Riebesell, U., and Gattuso, J.-P.: Lessons learned from ocean acidification research, Nat. Clim. Chang., 5(1), 12–14, doi:10.1038/nclimate2456, 2015.

Riebesell, U., and Tortell, P. D.: Effects of ocean acidification on pelagic organism and ecosystems, in Ocean Acidification, Eds: Gattuso J.-P., and Hansson L., Oxford University Press, New York, 99–121, 2011.

Riebesell, U., Fabry, V. J., Hansson, L. and Gattuso, J.-P.: Guide to best practices for ocean acidification research and data reporting, Guid. to best Pract. Ocean Acidif. Res. data Report., pp. 260, doi:10.2777/66906, 2010.

Riebesell, U., Schulz, K. G., Bellerby, R. G. J., Botros, M., Fritsche, P., Meyerhöfer, M., Neill, C., Nondal, G., Oschlies, a, Wohlers, J., and Zöllner, E.: Enhanced biological carbon consumption in a high CO_2 ocean., Nature, 450(7169), 545–548, doi:10.1038/nature06267, 2007.

Riebesell, U., Czerny, J., Von Bröckel, K., Boxhammer, T., Büdenbender, J., Deckelnick, M., Fischer, M., Hoffmann, D., Krug, S. A., Lentz, U., Ludwig, A., Muche, R., and Schulz, K. G.: Technical Note: A mobile sea-going mesocosm system - New opportunities for ocean change research, Biogeosciences, 10(3), 1835–1847, doi:10.5194/bg-10-1835-2013, 2013.

Robarts, R. D., and Zohary, T.: Temperature effects on photosynthetic capacity, respiration., and growth rates of bloom-forming cyanobacteria, New Zeal. J. Mar. Freshw. Res., 21(3), 391–399, doi:10.1080/00288330.1987.9516235, 1987.

Robert-Baldo, G., Morris, M., and Byrne, R.: Spectrophotometric determination of seawater pH using phenol red, Anal. Chem., 3(57), 2564–2567, doi:10.1021/ac00290a030, 1985.

Roemmich, D., Church, J., Gilson, J., Monselesan, D., Sutton, P. and Wijffels, S.: Unabated planetary warming and its ocean structure since 2006, Nat. Clim. Chang., 5(3), 240–245, doi:10.1038/nclimate2513, 2015.

Rose, J. M., Feng, Y., Gobler, C. J., Gutierrez, R., Harel, C. E., Leblanc, K., and Hutchins, D. A.: Effects of increased pCO_2 and temperature on the North Atlantic spring bloom. II. Microzooplankton abundance and grazing, Mar. Ecol. Prog. Ser., 388, 27–40, doi:10.3354/meps08134, 2009.

Rost, B., Zondervan, I. and Wolf-Gladrow, D.: Sensitivity of phytoplankton to future changes in ocean carbonate chemistry: Current knowledge, contradictions and research directions, Mar. Ecol. Prog. Ser., 373, 227–237, doi:10.3354/meps07776, 2008.

Roy, S., Chanut, J.-P., Gosselin, M., and Sime-Ngando, T.: Characterization of phytoplankton communities in the Lower St. Lawrence Estuary using HPLC-detected pigments and cell microscopy, Mar. Ecol. Prog. Ser., 142, 55–73, doi:10.3354/meps142055, 1996.

Royer, S. J., Levasseur, M., Lizotte, M., Arychuk, M., Scarratt, M. G., Wong, C. S., Lovejoy, C., Robert, M., Johnson, K., Peña, A., Michaud, S. and Kiened, R. P.: Microbial dimethylsulfoniopropionate (DMSP) dynamics along a natural iron gradient in the northeast subarctic Pacific, Limnol. Oceanogr., 55(4), 1614–1626, doi:10.4319/lo.2010.55.4.1614, 2010.

Ruiz-González, C., Galí, M., Gasol, J. M. and Simó, R.: Sunlight effects on the DMSP-sulfur and leucine assimilation activities of polar heterotrophic bacterioplankton, Biogeochemistry, 110(1–3), 57–74, doi:10.1007/s10533-012-9699-y, 2012.

Sabine, C. L. and Feely, R. A.: The oceanic sink for carbon dioxide, in Greenhouse Gas Sinks, edited by D. Reay, N. Hewitt, J. Grace, and K. Smith, pp. 31–49, CABI Publishing, Oxfordshire., 2007.

Sala, M. M., Aparicio, F. L., Balagué, V., Boras, J. A., Borrull, E., Cardelús, C., Cros, L., Gomes, A., López-Sanz, A., Malits, A., Martinez, R. A., Mestre, M., Movilla, J., Sarmento, H., Vázquez-Domínguez, E., Vaqué, D., Pinhassi, J., Calbet, A., Calvo, E., Gasol, J. M., Pelejero, C., and Marrasé, C.: Contrasting effects of ocean acidification on the microbial food web under different trophic conditions, ICES J. Mar. Sci., 73(3), 670–679, doi:10.1093/icesjms/fsv130, 2016.

Saucier, F. J. and Chassé, J.: Tidal circulation and buoyancy effects in the St. Lawrence Estuary, Atmos. - Ocean, 38(4), 505–556, doi:10.1080/07055900.2000.9649658, 2000.

Savenkoff, C., Gagné, J. A., Gilbert, M., Castonguay, M., Chabot, D., Chassé, J., Comtois, S., Dutil, J.-D., Galbraith, P. S., Gosselin, J.-F., Grégoire, F., Larocque, R., Larouche, P., Lavoie, D., Lebeuf, M., Lesage, V., Maps, F., McQuinn, I. H., Mosnier, A., Nozères, C., Ouellet, P., Plourde, S., Sainte-Marie, B., Savard, L., Scarratt, M. and Starr, M.: Le concept d'approche écosystémique appliqué à l'estuaire maritime du Saint-Laurent (Canada), Environ. Rev., 25(1), 26–96, doi:10.1139/er-2015-0083, 2017.

Scarratt, M. G., Levasseur, M., Schultes, S., Michaud, S., Cantin, G., Vézina, A., Gosselin, M. and De Mora, S. J.: Production and consumption of dimethylsulfide (DMS) in North Atlantic waters, Mar. Ecol. Prog. Ser., 204, 13–26, doi:10.3354/meps204013, 2000.

Schlüter, L., Lohbeck, K. T., Gröger, J. P., Riebesell, U. and Reusch, T. B. H.: Long-term dynamics of adaptive evolution in a globally important phytoplankton species to ocean acidification, Sci. Adv., 2(7), e1501660–e1501660, doi:10.1126/sciadv.1501660, 2016.

Schulz, K. G., Bellerby, R. G. J., Brussaard, C. P. D., Büdenbender, J., Czerny, J., Engel, A., Fischer, M., Koch-Klavsen, S., Krug, S. A., Lischka, S., Ludwig, A., Meyerhöfer, M., Nondal, G., Silyakova, A., Stuhr, A., and Riebesell, U.: Temporal biomass dynamics of an Arctic plankton bloom in response to increasing levels of atmospheric carbon dioxide, Biogeosciences, 10(1), 161–180, doi:10.5194/bg-10-161-2013, 2013.

Schulz, K. G., Bach, L. T., Bellerby, R. G. J., Bermudez, R., Budenbender, J., Boxhammer, T., Czerny, J., Engel, A., Ludwig, A., Meyerhofer, M., Larsen, A., Paul, A., Sswat, M., and Riebesell, U.: Phytoplankton blooms at increasing levels of atmospheric carbon dioxide: experimental evidence for negative effects on prymnesiophytes and positive on small picoeukaryotes, Front. Mar. Sci., 4, 64, doi:10.3389/fmars.2017.00064, 2017.

Schwinger, J., Tjiputra, J., Goris, N., Six, K. D., Kirkevåg, A., Seland, Ø., Heinze, C. and Ilyina, T.: Amplification of global warming through pH dependence of DMS production simulated with a fully coupled Earth system model, Biogeosciences, 14(15), 3633–3648, doi:10.5194/bg-14-3633-2017, 2017.

Sciandra, A., Harlay, J., Lefèvre, D., Lemée, R., Rimmelin, P., Denis, M. and Gattuso, J. P.: Response of coccolithophorid Emiliania huxleyi to elevated partial pressure of CO_2 under nitrogen limitation, Mar. Ecol. Prog. Ser., 261, 111–122, doi:10.3354/meps261111, 2003.

Sevigny, J.-M., Sinclair, M., El-Sabh, M. I., Poulet, S. and Coote, A.: Summer plankton distributions associated with the physical and nutrient properties of the northwestern Gulf of St. Lawrence., J. Fish. Res. Board Canada, 36(2), 187–203, doi:10.1139/f79-029, 1979.

Shaw, G. E.: Bio-controlled thermostasis involving the sulfur cycle, Clim. Change, 5(3), 297–303, doi:10.1007/BF02423524, 1983.

Simó, R.: Production of atmospheric sulfur by oceanic plankton: Biogeochemical, ecological and evolutionary links, Trends Ecol. Evol., 16(6), 287–294, doi:10.1016/S0169-5347(01)02152-8, 2001.

Simó, R.: From cells to globe: approaching the dynamics of DMS(P) in the ocean at multiple scales, Can. J. Fish. Aquat. Sci., 61(5), 673–684, doi:10.1139/f04-030, 2004.

Simó, R., and Pedrós-Alió, C.: Role of vertical mixing in controlling the oceanic production of dimethyl sulphide, Nature, 402, 396–399, doi:10.1038/46516, 1999.

Simo, R., Pedros-Alió, C., Malin, G. and Grimalt, J. O.: Biological turnover of DMS, DMSP and DMSO in contrasting open-sea waters, Mar. Ecol. Prog. Ser., 203, 1–11, doi:10.3354/meps203001, 2000.

Simó, R., Archer, S. D., Pedrós-Alió, C., Gilpin, L. and Stelfox-Widdicombe, C. E.: Coupled dynamics of dimethylsulfoniopropionate and dimethylsulfide cycling and the microbial food web in surface waters of the North Atlantic, Limnol. Oceanogr., 47(1), 53–61, doi:10.4319/lo.2002.47.1.0053, 2002.

Six, K. D., Kloster, S., Ilyina, T., Archer, S. D., Zhang, K., and Maier-Reimer, E.: Global warming amplified by reduced sulphur fluxes as a result of ocean acidification, Nat. Clim. Chang., 3(11), 975–978, doi:10.1038/nclimate1981, 2013.

Slezak, D., Kiene, R. P., Toole, D. A., Simó, R. and Kieber, D. J.: Effects of solar radiation on the fate of dissolved DMSP and conversion to DMS in seawater, Aquat. Sci., 69(3), 377–393, doi:10.1007/s00027-007-0896-z, 2007.

Sommer, U., and Lengfellner, K.: Climate change and the timing, magnitude, and composition of the phytoplankton spring bloom, Glob. Chang. Biol., 14(6), 1199–1208, doi:10.1111/j.1365-2486.2008.01571.x, 2008.

Sommer, U., Paul, C., and Moustaka-Gouni, M.: Warming and ocean acidification effects on phytoplankton - From species shifts to size shifts within species in a mesocosm experiment, PLoS ONE, 10(5), 17, doi:10.1371/journal.pone.0125239, 2015.

Spielmeyer, A. and Pohnert, G.: Influence of temperature and elevated carbon dioxide on the production of dimethylsulfoniopropionate and glycine betaine by marine phytoplankton., Mar. Environ. Res., 73, 62–9, doi:10.1016/j.marenvres.2011.11.002, 2012.

Starr, M., St-Amand, L., Devine, L., Bérard-Therriault, L. and Galbraith, P. S.: State of phytoplankton in the Estuary and Gulf of St. Lawrence during 2003, CSAS Res. Doc., 2004/123, 35, 2004.

Stefels, J.: Physiological aspects of the production and conversion of DMSP in marine algae and higher plants, J. Sea Res., 43(3–4), 183–197, doi:10.1016/S1385-1101(00)00030-7, 2000.

Stefels, J., and Van Boekel, W. H. M.: Production of DMS from dissolved DMSP in axenic cultures of the marine phytoplankton species Phaeocystis sp., Mar. Ecol. Prog. Ser., 97(1), 11–18, doi:10.3354/meps097011, 1993.

Stefels, J., Steinke, M., Turner, S., Malin, G., and Belviso, S.: Environmental constraints on the production and removal of the climatically active gas dimethylsulphide (DMS) and implications for ecosystem modelling, Biogeochemistry, 83(1–3), 245–275, doi:10.1007/s10533-007-9091-5, 2007.

Steinke, M., Malin, G., Archer, S. D., Burkill, P. H. and Liss, P. S.: DMS production in a coccolithophorid bloom: Evidence for the importance of dinoflagellate DMSP lyases, Aquat. Microb. Ecol., 26(3), 259–270, doi:10.3354/ame026259, 2002.

Stillman, J. H. and Paganini, A. W.: Biochemical adaptation to ocean acidification, J. Exp. Biol., 218(12), 1946–1955, doi:10.1242/jeb.115584, 2015.

Sunda, W., Kieber, D. J., Kiene, R. P., and Huntsman, S.: An antioxidant function for DMSP and DMS in marine algae, Nature, 418(6895), 317-320, 2002.

Suzuki, Y., and Takahashi, M.: Growth responses of several diatom species isolated from various environments to temperature, J. Phycol., 31(6), 880–888, doi:10.1111/j.0022-3646.1995.00880.x, 1995.

Tanaka, T., Alliouane, S., Bellerby, R. G. B., Czerny, J., de Kluijver, A., Riebesell, U., Schulz, K. G., Silyakova, A. and Gattuso, J.-P.: Effect of increased pCO_2 on the planktonic metabolic balance during a mesocosm experiment in an Arctic fjord, Biogeosciences, 10(1), 315–325, doi:10.5194/bg-10-315-2013, 2013.

Tatters, A. O., Roleda, M. Y., Schnetzer, A., Fu, F., Hurd, C. L., Boyd, P. W., Caron, D. A., Lie, A. A. Y., Hoffmann, L. J., and Hutchins, D. A.: Short- and long-term conditioning of a temperate marine diatom community to acidification and warming., Philos. Trans. R. Soc. Lond. B. Biol. Sci., 368(1627), 20120437, doi:10.1098/rstb.2012.0437, 2013.

Taylor, A. H., Harbour, D. S., Harris, R. P., Burkill, P. H., and Edwards, E. S.: Seasonal succession in the pelagic ecosystem of the North Atlantic and the utilization of nitrogen, J. Plankton Res., 15(8), 875–891, doi:10.1093/plankt/15.8.875, 1993.

Thomas, M. K., Kremer, C. T., Klausmeier, C. a and Litchman, E.: A global pattern of thermal adaptation in marine phytoplankton., Science, 338(6110), 1085–1088, doi:10.1126/science.1224836, 2012.

Todd, J. D., Rogers, R., You, G. L., Wexler, M., Bond, P. L., Sun, L., Curson, A. R. J., Malin, G., Steinke, M. and Johnston, A. W. B.: Structural and regulatory genes required to make the gas dimethyl sulfide in bacteria, Science, 315(5812), 666–669, doi:10.1126/science.1135370, 2007.

Todgham, A. E., and Stillman, J. H.: Physiological responses to shifts in multiple environmental stressors: Relevance in a changing world, Integr. Comp. Biol., 53(4), 539–544, doi:10.1093/icb/ict086, 2013.

Tomas, C. R. (ed): Identifying Marine Phytoplankton, Academic Press: San Diego, 858 pp., 1997.

Toole, D. A., and Siegel, D. A.: Light-driven cycling of dimethylsulfide (DMS) in the Sargasso Sea: closing the loop, Geophys. Res. Lett., 31(9), 1–4, doi:10.1029/2004GL019581, 2004.

Tortell, P. D., DiTullio, G. R., Sigman, D. M., and Morel, F. M. M.: CO_2 effects on taxonomic composition and nutrient utilization in an Equatorial Pacific phytoplankton assemblage, Mar. Ecol. Prog. Ser., 236, 37–43, doi:10.3354/meps236037, 2002.

Toole, D. A., Slezak, D., Kiene, R. P., Kieber, D. J., and Siegel, D. A.: Effects of solar radiation on dimethylsulfide cycling in the western Atlantic Ocean, Deep. Res. Part I Oceanogr. Res. Pap., 53(1), 136–153, doi:10.1016/j.dsr.2005.09.003, 2006.

Toole, D. A., Siegel, D. A. and Doney, S. C.: A light-driven, one-dimensional dimethylsulfide biogeochemical cycling model for the Sargasso Sea, J. Geophys. Res. Biogeosciences, 113(2), 1–20, doi:10.1029/2007JG000426, 2008.

Trimborn, S., Wolf-Gladrow, D., Richter, K. U., and Rost, B.: The effect of pCO_2 on carbon acquisition and intracellular assimilation in four marine diatoms, J. Exp. Mar. Bio. Ecol., 376(1), 26–36, doi:10.1016/j.jembe.2009.05.017, 2009.

Tripp, H. J., Kitner, J. B., Schwalbach, M. S., Dacey, J. W. H., Wilhelm, L. J. and Giovannoni, S. J.: SAR11 marine bacteria require exogenous reduced sulphur for growth, Nature, 452(7188), 741–744, doi:10.1038/nature06776, 2008.

Valle, D. A. del, Kieber, D. J., Toole, D. A., Brinkley, J. and Kiene, R. P.: Biological consumption of dimethylsulfide (DMS) and its importance in DMS dynamics in the Ross Sea, Antarctica, Limnol. Oceanogr., 54(3), 785–798, doi:10.4319/lo.2009.54.3.0785, 2009.

Vallina, S. M., Simó, R., Anderson, T. R., Gabric, A., Cropp, R., and Pacheco, J. M.: A dynamic model of oceanic sulfur (DMOS) applied to the Sargasso Sea: Simulating the dimethylsulfide (DMS) summer paradox, J. Geophys. Res. Biogeosciences, 113(1), doi:10.1029/2007JG000415, 2008.

Vila, M., Simó, R., Kiene, R. P., Pinhassi, J., González, J. M., Moran, M. A., and Pedrós-Alió, C.: Use of microautoradiography combined with fluorescence in situ hybridization to determine dimethylsulfoniopropionate incorporation by marine bacterioplankton taxa, Appl. Environ. Microbiol., 70, 4648– 4657, https://doi.org/10.1128/AEM.70.8.4648-4657.2004, 2004.

Vila-Costa, M., Simó, R., Harada, H., Gasol, J. M., Slezak, D., and Kiene, R. P.: Dimethylsulfoniopropionate Uptake by Marine Phytoplankton, Science, 314, 652–654, 2006a.

Vila-Costa, M., Del Valle, D. A., González, J. M., Slezak, D., Kiene, R. P., Sánchez, O., and Simó, R.: Phylogenetic identification and metabolism of marine dimethylsulfide consuming bacteria, Environ. Microbiol., 8, 2189–2200, https://doi.org/10.1111/j.1462-2920.2006.01102.x, 2006b.

Vila-Costa, M., Pinhassi, J., Alonso, C., Pernthaler, J., and Simó, R.: An annual cycle of dimethylsulfoniopropionate sulfur and leucine assimilating bacterioplankton in the coastal NW Mediterranean, Environ. Microbiol., 9, 2451–2463, https://doi.org/10.1111/j.1462-2920.2007.01363.x, 2007.

Vogt, M., Steinke, M., Turner, S., Paulino, a., Meyerhöfer, M., Riebesell, U., Le Quéré, C. and Liss, P.: Dynamics of dimethylsulphoniopropionate and dimethylsulphide under different CO_2 concentrations during a mesocosm experiment, Biogeosciences, 5(2), 407–419, doi:10.5194/bg-5-407-2008, 2008.

Webb, A. L., Leedham-Elvidge, E., Hughes, C., Hopkins, F. E., Malin, G., Bach, L. T., Schulz, K., Crawfurd, K., Brussaard, C. P. D., Stuhr, A., Riebesell, U., and Liss, P. S.: Effect of ocean acidification and elevated fCO_2 on trace gas production by a Baltic Sea summer phytoplankton community, Biogeosciences, 13(15), 4595–4613, doi:10.5194/bg-13-4595-2016, 2016.

Webb, A., Malin, G., Hopkins, F., Ho, K. L., Riebesell, U., Schulz, K., Larsen, A., and Liss, P.: Ocean acidification has different effects on the production of DMS and DMSP measured in cultures of *Emiliania huxleyi* and a mesocosm study: a comparison of laboratory monocultures and community interactions, Environ. Chem., 13(2), 314–329, doi:/10.1071/EN14268, 2015.

Wijffels, S., Roemmich, D., Monselesan, D., Church, J., and Gilson, J.: Ocean temperatures chronicle the ongoing warming of Earth, Nat. Clim. Chang., 6(2), 116–118, doi:10.1038/nclimate2924, 2016.

Wohlers, J., Engel, A., Zollner, E., Breithaupt, P., Jurgens, K., Hoppe, H.-G., Sommer, U. and Riebesell, U.: Changes in biogenic carbon flow in response to sea surface warming, Proc. Natl. Acad. Sci., 106(17), 7067–7072, doi:10.1073/pnas.0812743106, 2009.

Wolfe, G. V., Levasseur, M., Cantin, G. and Michaud, S.: Microbial consumption and production of dimethyl sulfide (DMS) in the Labrador Sea, Aquat. Microb. Ecol., 18(2), 197–205, doi:10.3354/ame018197, 1999.

Wolfe, G. V., and Steinke, M.: Grazing-activated production of dimethyl sulfide (DMS) by two clones of *Emiliania huxleyi*, Limnol. Oceanogr., 41(6), 1151–1160, doi:10.4319/lo.1996.41.6.1151, 1996.

Wolfe, G. V.: Accumulation of dissolved DMSP by marine bacteria and its degradation via bacterivory, in Biological and Environmental Chemistry of DMSP and Related Sulfonium Compounds, edited by R. P. Kiene, P. Visscher, M. D. Keller, and G. O. Kirst, pp. 277–291, New York. [online] Available from: http://link.springer.com/chapter/10.1007/978-1-4613-0377-0_24, 1996.

Woodhouse, M. T., Mann, G. W., Carslaw, K. S., and Boucher, O.: Sensitivity of cloud condensation nuclei to regional changes in dimethyl-sulphide emissions, Atmos. Chem. Phys., 13(5), 2723–2733, doi:10.5194/acp-13-2723-2013, 2013.

Wu, Y., Gao, K., and Riebesell, U.: CO_2-induced seawater acidification affects physiological performance of the marine diatom *Phaeodactylum tricornutum*, Biogeosciences, 7(9), 2915–2923, doi:10.5194/bg-7-2915-2010, 2010.

Yang, C., Telmer, K. and Veizer, J.: Chemical dynamics of the St.Lawrence riverine system: δD_{H2O}, and $\delta^{18}O_{H2O}$, $\delta^{13}C_{DIC}$, and $\delta^{34}S_{sulfate}$, and dissolved $^{87}Sr/^{86}Sr$, Geochim. Cosmochim. Acta, 60(5), 851–866, 1996.

Yoch, D. C.: Dimethylsulfoniopropionate: Its sources, role in the marine food web, and biological degradation to dimethylsulfide, Appl. Environ. Microbiol., 68(12), 5804–5815, doi:10.1128/AEM.68.12.5804-5815.2002, 2002.

Yoshimura, T., Nishioka, J., Suzuki, K., Hattori, H., Kiyosawa, H., and Watanabe, Y. W.: Impacts of elevated CO_2 on organic carbon dynamics in nutrient depleted Okhotsk Sea surface waters, J. Exp. Mar. Bio. Ecol., 395(1–2), 191–198, doi:10.1016/j.jembe.2010.09.001, 2010.

Yoshimura, T., Sugie, K., Endo, H., Suzuki, K., Nishioka, J., and Ono, T.: Organic matter production response to CO_2 increase in open subarctic plankton communities: Comparison of six microcosm experiments under iron-limited and -enriched bloom conditions, Deep Res. Part I Oceanogr. Res. Pap., 94, 1–14, doi:10.1016/j.dsr.2014.08.004, 2014.

Zeebe, R. E. and Ridgwell, a: Past changes of ocean carbonate chemistry, in Ocean acidification, edited by J. Gattuso and L. Hansson, pp. 21–40, Oxford University Press, Oxford., 2011.

Zeebe, R. E. and Wolf-Gladrow, D.: CO_2 in Seawater: Equilibrium, Kinetics, Isotopes, Vol. 65 (Elsevier Oceanography Series), Elsevier., pp. 360, 2001.

Zeebe, R. E., Zachos, J. C., Caldeira, K. and Tyrrell, T.: Oceans: Carbon emissions and acidification, Science, 321(5885), 51–52, doi:10.1126/science.1159124, 2008.

Annexes

Table S.1 Overview of the results of the mixed linear models testing for the effect of treatment (1 × pCO_2, 2 × CO_3, and 3 × pCO_2), time, and the interactions of these factors over the duration of the experiment on nitrate, silicic acid, soluble reactive phosphate (SRP), chlorophyll *a* (Chl *a*), bacterial abundance, particulate primary production (P_P), dissolved primary production (P_D), total dimethylsulfoniopropionate ($DMSP_t$), dissolved DMSP ($DMSP_d$), dimethylsulfide (DMS), $DMSP_d$ loss rate constant (k_{DMSPd}), ^{35}S-$DMSP_d$ fraction present in particles > 0.2 µm (particulate yield), ^{35}S-$DMSP_d$ incorporated into macromolecules, DMS yield. Transformations are indicated in parentheses when necessary. Results of the models are presented with the corresponding numerator and denominator degrees of freedom (df), F-value, and p-value. Significant results are indicated in bold, at the 0.05 significance level. Nitrate and SRP measurements are reported for days 0-6 only (values below detection limit beyond day 6).

Response variable	Factor	Num df	Den df	F-value	p-value
Nitrate	Treatment	2	6	4.073	0.076
(µmol L^{-1})	Time	3	18	465.203	**< 0.001**
	Treatment × Time	6	18	1.734	0.170
Silicic acid	Treatment	2	6	7.329	**0.025**
(µmol L^{-1})	Time	6	33	148.568	**< 0.001**
	Treatment × Time	12	33	2.535	**0.017**
SRP	Treatment	2	6	5.615	**0.042**
(µmol L^{-1})	Time	3	18	341.558	**< 0.001**
	Treatment × Time	6	18	2.532	0.059
(Log) Chl *a*	Treatment	2	6	4.319	0.069
(µg L^{-1})	Time	6	36	161.919	**< 0.001**
	Treatment × Time	12	36	2.121	**0.041**
Bacterial abundance	Treatment	2	6	12.346	**0.007**
(× 10^8 cells L^{-1})	Time	6	36	200.645	**< 0.001**
	Treatment × Time	12	36	6.497	**< 0.001**
P_P	Treatment	2	6	16.047	**0.004**
(µmol L^{-1} d^{-1})	Time	5	30	54.400	**< 0.001**
	Treatment × Time	10	30	2.292	**0.039**
P_D	Treatment	2	6	14.644	**0.005**
(µmol L^{-1} d^{-1})	Time	5	30	12.309	**< 0.001**
	Treatment × Time	10	30	1.492	0.191
$DMSP_t$	Treatment	2	6	9.420	**0.014**
(nmol L^{-1})	Time	6	34	75.181	**< 0.001**
	Treatment × Time	12	34	2.089	**0.046**
$DMSP_d$	Treatment	2	6	0.283	0.763
(nmol L^{-1})	Time	6	33	54.632	**< 0.001**
	Treatment × Time	12	33	1.784	0.093
(Log) DMS	Treatment	2	6	27.238	**< 0.001**
(nmol L^{-1})	Time	12	72	262.233	**< 0.001**
	Treatment × Time	24	72	4.016	**< 0.001**
k_{DMSPd}	Treatment	2	6	7.323	**0.025**
(d^{-1})	Time	4	22	6.948	**< 0.001**
	Treatment × Time	8	22	6.509	**< 0.001**
Particulate yield	Treatment	2	6	7.071	**0.026**
(%)	Time	4	24	13.020	**< 0.001**
	Treatment × Time	8	24	2.675	**0.030**

(Log) Macromolecule yield (%)	Treatment	2	6	13.315	**0.006**
	Time	4	23	1.921	0.141
	Treatment × Time	8	23	1.789	0.131
DMS yield (%)	Treatment	2	6	38.420	**< 0.001**
	Time	4	24	37.839	**< 0.001**
	Treatment × Time	8	24	5.282	**< 0.001**

Table S.2 Overview of a Tukey Honest Significant Difference (HSD) test for averages of DMS concentrations per treatment, per day. Average values are presented with lower and upper confidence intervals (CI). Daily pairwise comparisons are made between treatments. The treatments are assigned to the same group (e.g. a) if there is no significant difference between treatments on a given day. When there is a significant difference between two treatments for a given day, each treatment is assigned to a different group (a, b). A treatment can belong to two groups (e.g: 2 × pCO_2 on day 4), indicating that the treatment is not significantly different from either of the other two treatments (1 × pCO_2 ;group b or 3 × pCO_2 ; group a), although there is a significant difference between the 1 × pCO_2 and 3 × pCO_2 treatments.

Treatment	Day	Average	Lower CI	Upper CI	Groups
1 × pCO_2	0	1.6	1.1	2.2	a
2 × pCO_2	0	1.8	1.3	2.4	a
3 × pCO_2	0	1.9	1.4	2.6	a
1 × pCO_2	1	1.8	1.3	2.5	a
2 × pCO_2	1	1.7	1.3	2.4	a
3 × pCO_2	1	1.8	1.3	2.5	a
1 × pCO_2	2	1.6	1.2	2.2	a
2 × pCO_2	2	1.4	1.0	2.0	a
3 × pCO_2	2	1.5	1.1	2.1	a
1 × pCO_2	3	1.1	0.8	1.5	a
2 × pCO_2	3	1.2	0.8	1.6	a
3 × pCO_2	3	1.4	1.0	2.0	a
1 × pCO_2	4	3.0	2.2	4.2	b
2 × pCO_2	4	2.1	1.5	2.8	a, b
3 × pCO_2	4	1.8	1.3	2.5	a
1 × pCO_2	5	5.5	4.0	7.6	b
2 × pCO_2	5	3.7	2.7	5.1	a, b
3 × pCO_2	5	2.5	1.8	3.4	a
1 × pCO_2	6	12.9	9.4	17.8	b
2 × pCO_2	6	7.1	5.2	9.8	a
3 × pCO_2	6	4.5	3.3	6.2	a
1 × pCO_2	7	16.8	12.2	23.1	b
2 × pCO_2	7	13.6	9.8	18.7	b
3 × pCO_2	7	6.7	4.8	9.2	a
1 × pCO_2	8	21.8	15.8	30.0	b
2 × pCO_2	8	16.7	12.1	23.0	b
3 × pCO_2	8	9.5	6.9	13.1	a
1 × pCO_2	9	20.8	15.1	28.7	b

2 × pCO_2	9	18.8	13.7	26.0	a, b
3 × pCO_2	9	12.2	8.9	16.9	a
1 × pCO_2	10	20.5	14.9	28.2	a
2 × pCO_2	10	18.6	13.5	25.6	a
3 × pCO_2	10	14.6	10.6	20.1	a
1 × pCO_2	11	18.4	13.3	25.3	a
2 × pCO_2	11	17.9	13.0	24.7	a
3 × pCO_2	11	12.9	9.4	17.8	a
1 × pCO_2	12	17.2	12.5	23.7	a
2 × pCO_2	12	17.1	12.4	23.6	a
3 × pCO_2	12	13.6	9.9	18.8	a